AN INVESTIGATION OF THE PROPERTIES OF NUCLEAR LEVELS BY NUCLEAR ORIENTATION

A Thesis

submitted for the degree of Doctor of Philosophy

at Oxford University

by

P. Dagley, B.A.

Trinity College, Oxford

Hilary Term, 1959.

BODLEIAN LIBRARY OXFORD
DEPOSITED
THESIS
13 VII 59

ABSTRACT

of a dissertation presented for the degree of Doctor of Philosophy

by P. Dagley, B.A., Trinity College, Hilary Term, 1959.

entitled

An Investigation of the Properties

of Nuclear Levels by Nuclear Orientation

Nuclear alignment has been an established technique in nuclear physics for some years and the majority of the experiments have employed the methods suggested by Bleaney (1951) and by Rose (1949) and Gorter (1948). The former is simpler since it requires no external fields. For this method the nucleus must be the core of a paramagnetic ion which is included in a crystal with suitable internal fields. The alignment arises through anisotropic hyperfine structure ($S_{eff}=\frac{1}{2}$) or isotropic hyperfine structure with a finite splitting of the electronic levels caused by the crystalline field ($D \neq 0 S \geq 1$). Certain nuclear states will become predominantly populated at very low temperatures which can conveniently be produced by adiabatic demagnetisation of an ion incorporated in the same salt.

Paramagnetism arises through vacancies in the 3f and 4d electronic shell so that those nuclei studied fall in the iron-transition and rare-earth groups. The former can be conveniently incorporated with the salts of the Tutton series (double sulphates) or the double nitrates, both of which have been extensively studied. However, the Tutton salts

have two ions per unit cell giving rise to two alignment axes inclined at about 70° while for some of the iron group elements (e.g. Co^{++}, Mn^{++}) the double nitrates have two positions in the unit cell with different hyperfine constants.

Following the successful cooling of nickel-zinc fluosilicate by adiabatic demagnetisation (Hill, Meyer & Milner 1959) it was realised that this salt which has one ion per unit cell might be suitable for nuclear orientation and indeed have some advantages over the other salts. All the principal experiments described in this thesis have been performed with nickel-zinc fluosilicate.

The angular distribution of the gamma-radiation from an aligned nucleus is not in general isotropic, the anisotropy depending on the degree of alignment and decay characteristics of the isotope. Thus by measuring the anisotropy it is possible to deduce values for some of the nuclear parameters such as the angular momenta and magnetic moment of the levels involved.

The first experiment attempted was with Mn^{54} which had previously been studied (Grace et al 1954) in cerium magnesium nitrate but for which a complete interpretation was not possible because of the anomalous variation of anisotropy with temperature. The present experiment showed that high degrees of alignment could be obtained with nickel-zinc fluosilicate and in particular the variation of anisotropy was monotonic within the range of temperature achieved ($\frac{1}{T} \leqslant 100$). The decay scheme was known from the previous work (Grace 1954) to be 3 or 2(δ)2(γ)0 and by fitting the experimental results to the possible

theoretical curves the magnetic moment of Mn^{54} is found to be $\mu = 2.85 \pm 0.35$nm if I=3 and $\mu = 2.25 \pm 0.35$nm if I=2. No definite choice between the two possible spin values can be made but I=3 appears to be favoured from the shape of the curve. These values compare quite well with those ($\mu = 3.3 \pm 0.06$, I=3; $\mu = 2.2 \pm 0.04$, I=2) resulting from a paramagnetic resonance experiment reported during the course of this work (Jeffries 1958). The values predicted on the basis of the nuclear shell model, $\mu = 4.32$, I=3; $\mu = 4.65$, I=2, using empirical g-values ($g_p(\frac{7}{2}) = 1.44 (Mn^{53})$; $g_n(\frac{3}{2}) = -0.334 (Cr^{53})$), differ markedly from the experimental results but the discrepancy is less for I=3. This discrepancy probably arises from a coupling between the nucleons different from that described by the shell model. Such an "anomalous" coupling has already been noted for Mn^{55} which has a spin of $\frac{5}{2}$ rather than the expected value for an odd proton of $\frac{7}{2}$. The nuclear configurations for Mn^{54} and Mn^{56} are very similar - differing only by two neutrons - and therefore one might expect the spin and moment to be closely the same. The spin and moment for Mn^{56} have been measured as I=3, $\mu = 3.5$ (Childs et al 1958).

Following the successful experiment with Mn^{54}, Mn^{52} has been aligned in the same salt. For this isotope the beta-decay is followed by a cascade of three gamma-rays and it was found that each of these had a positive anisotropy of the same magnitude. Consideration of the possible spin sequences shows that all the observed facts can only be explained by the sequence $6^+ \rightarrow 4^+ \rightarrow 2^+ \rightarrow 0^+$ for the excited states of Cr^{52} involved, with the ground state of Mn^{52} either 6^+ or 7^+. The

magnetic moment is found to be $\mu = 2.0 \pm 0.5$nm if I=6 and j= 0; $\mu = 2.5 \pm 0.5$ if I=6, j= 1; and $\mu = 2.5 \pm 0.5$ if I=7.

It is not possible to choose between these values from the present experiment alone but the nuclear gyromagnetic ratio has been measured by Abraham et al (1957) to be $g = \mu/I = 0.514 \pm 0.02$. This value is only compatible with the present experiment if I=6 and the beta-transition is predominantly of the Gamow-Teller type j= 1. This assignment is also consistent with the beta-ray experiments of Ambler et al (1958) which show that both Fermi and Gamow-Teller modes occur.

A similar gamma-ray experiment using cerium magnesium nitrate carried out by Huiskamp (1957) also gives this decay scheme and a nuclear magnetic moment of $I = 2.8 \, ^{+0.8}_{-0.5}$nm for I=6, j= 1. The nuclear shell model favours a high value for the spin, i.e. 6 or 7, with Schmidt limits for the magnetic moments of $\mu = 3.309$ nm and $\mu = 3.86$nm respectively in reasonable agreement with the measured values.

Previously one of the conditions which an isotope had to satisfy was that its half-life must be sufficiently long to allow a crystal to be grown from active solution. This is about one day if the crystal grows easily and the shortest lived isotope studied so far has been Pr^{142}(19hr) in cerium magnesium nitrate. The feasibility of aligning an isotope produced by neutron irradiation in an inactive crystal has now been investigated, 2.6 hr. Mn^{56} having been chosen for the experiments. Previous work (Grace 1955) had shown that alignment can be obtained under these circumstances although radiation damage causes the magnitude to be less than that found for a crystal grown

from active solution. No attempt was made to derive any nuclear information from the results but it was found that if the damaged crystal is annealed the degree of alignment can be increased.

Mn^{56} has three principal gamma-rays, two of which are dipole-quadrupole mixtures each in cascade with the third, a pure quadrupole transition. By finding, experimentally, the value of A_2 in the angular distribution expansion, $I(\theta)=\sum_\nu A_\nu P_\nu(\cos\theta)$, for each gamma-ray and comparing the experimental and theoretical ratios of A_2 for the mixed gamma-ray to A_2 for the pure transition, the mixing ratios for possible spin sequences have been found. Comparing these with the values found by an angular correlation experiment on the same gamma rays by Gregory (see Dagley et al 1959), the spin assignments of 2^+ for the 2.98 Mev and 2.66 Mev levels in Fe^{56} have been made unique. Furthermore it is concluded that the ground state spin of Mn^{56} can only be 2 if the beta-decay is predominantly of the Fermi type, and on these grounds the value of 3 is preferred.

Because of irradiation damage it is not possible to find a value for the nuclear magnetic moment although it is shown that the lower limit must be μ=1.3nm. If it is assumed that displaced ions give an isotropic angular distribution, then the distribution can be written $I(\theta)=1+\lambda A_2 P_2(\cos\theta)+\lambda A_4 P_4(\cos\theta)$ where $(1-\lambda)$ is the fraction of the ions displaced from their lattice sites. Then using the measured values of spin and moment ($I=3, \mu=3.5$; Childs et al 1958) it is possible to fit curves to the experimental points and so deduce the extent of the damage. It is found that~50% of the ions are displaced ($\lambda=0.5$)

following an irradiation at 40°C (normal pile temperature for P.F=5) but when the same crystal was annealed at 80°C for two hours after irradiation λ=0.71 showing that only 29% of the ions remained displaced.

The decay scheme of Co^{58} had been determined by an alignment experiment (Daniels 1952) to be 2(β)2(γ)0 thus allowing both Fermi and Gamow-Teller types of transition. The fraction of Fermi transitions was later (Griffing & Wheatley 1956) found to be 0.11±0.04 but while demonstrating the non-conservation of parity, Ambler et al (1957) showed that if the two-component theory of the neutrino was valid then the transition must be pure Gamow-Teller. This discrepancy has been investigated in the present experiment by measuring the gamma-ray angular distribution for Co^{58} in nickel fluosilicate. For a uniaxial crystal the dependence of I(0°) on I(90°) is very sensitive to the beta-ray admixture and it is shown that the transition is pure Gamow-Teller, the fraction of transitions for which j=0 being -0.6 0.5% corrections having been made for the finite aperture of the counters, scattering and pulses due to other gamma-rays. This result makes it possible for all the beta-ray experiments to be explained by the two-component neutrino theory. The biaxial Tutton salt used by Griffing and Wheatley does not give such good sensitivity to the admixture as the fluosilicate and the analysis of the results is somewhat complicated. It is considered that the large Fermi admixture found from that experiment results from these causes.

The present measurement of the admixture is made independently of

a knowledge of the absolute temperature so that, the other parameters being known, it has been possible to derive a temperature scale for nickel-zinc fluosilicate from the measured anisotropy. A suitable thermodynamic temperature scale is not at present available so the Co^{58} results have been used to interpret all the other experiments.

The method of obtaining the population parameters, B_ν, from the Spin Hamiltonian is described in an appendix and values of these parameters for Co^{60}, Co^{58} and Mn($I=3, \mu=3.5$) are plotted as functions of temperature. Some approximate solutions for manganese with other values of spin and moment are tabulated. The Clebsch-Gordon coefficients relevant to these calculations are also tabulated.

REFERENCES

Abraham, M., Jeffries, C.D., Kedzie, R.W., and Liefson, D.S., 1957 Bull. Am. Phys. Soc. 2, 382

Ambler, E., Hayward, R.W., Hoppes, D.D., Hudson, R.P. and Wu, C.S., 1957, Phys. Rev. 106, 1361

Ambler, E., Hayward, R.W., Hoppes, D.D., and Hudson, R.P., 1958, Phys. Rev. 110, 787

Bleaney, B., 1951, Proc. Phys. Soc., 64, 315

Childs, W.J., Goodman, L.S., and Kieffer, L.J., 1958, Phys. Rev. Letters, 1, 296

Dagley, P., Grace, M.A., Gregory, J.L., and Hill, J.S., 1959, Proc. Roy. Soc. (to be published).

Daniels, J.M., Grace, M.A., Halban, H., Kurti, N., and Robinson, F.N.H., 1952, Phil. Mag. 43, 1297

Gorter, C.J., 1948, Physica 14, 504

Grace, M.A., Johnson, C.E., Kurti, N., Lemmer, H.R. and Robinson, F.N.H., 1952, Phil. Mag. 45, 1192

Grace, M.A., Johnson, C.E., Kurti, N., Scurlock, R.G., and Taylor, R.T., 1955, Comm. conf. Basses Temperatures, Paris.

Griffing, D.F., and Wheatley, J.C., 1956, Phys. Rev. 104, 389

Hill, J.S., Meyer, H. and Milner, J., 1959, (to be published)

Huiskamp, W.J., Diddens, A.N., Severiens, J.C., Miedema, A.R. and Steenland, M.J., 1957, Physica 23, 605

Jeffries, C.D., 1958, Private communication.

Rose, M.E., 1949, Phys. Rev. 75, 213

TABLE OF CONTENTS

ACKNOWLEDGEMENTS Page 1

CHAPTER 1. INTRODUCTION 2

1. Introduction 2

2. Nuclear Orientation 4

3. Methods for producing orientation 5
   a. The Hamiltonian 5
   b. External field polarisation 6
   c. Magnetic hyperfine structure polarisation 6
   d. Electric h.f.s. alignment 6
   e. Magnetic h.f.s. alignment 7

4. Bleaney (magnetic h.f.s.) alignment 7
   a. The hyperfine structure 7
   b. Isotropic hyperfine structure (The Manganese Mn^{++} ion) 8
   c. Anisotropic hyperfine structure (The Cobalt Co^{++} ion) 9
   d. The environment 11
   e. Adiabatic demagnetisation 12

5. The angular distribution of gamma-rays from aligned nuclei 13
   a. The detection of the alignment; a typical decay scheme 13
   b. Multipole radiation 14
   c. An isomeric transition 14
   d. The intervening transitions 16
   e. The angular distribution 18

6. The derivation of nuclear data 19

CHAPTER 2. EXPERIMENTAL CONSIDERATIONS 18

1. Introduction 23

2. The choice of crystal 24
   a. Tutton salts 24
   b. Double nitrates 25
   c. Fluosilicates 27

CHAPTER 2 (Continued) Page

3. Growing the crystals 29

4. The low temperature apparatus 32

5. The nuclear physics apparatus 33

6. The experimental procedure 37

7. Treatment of data: Corrections 39
   a. A composite spectrum 39
   b. Resolving time of apparatus 39
   c. Finite aperture of the counter 40
   d. Scattering 42
   e. Counting rate drift 44

8. The deduction of information 45
   a. From the observed intensities 45
   b. From the anisotropy 46
   c. From the correlation parameters 47
   d. The derivation of a temperature scale 47
   e. Other uses of nuclear alignment 48

CHAPTER 3 THE MAGNETIC MOMENT OF MANGANESE 54 50

1. Introduction 50

2. The decay scheme 50

3. The previous orientation experiments 53

4. The design of the present experiment 57

5. The alignment of Mn^{54} 58
   a. The experiments 58
   b. The source material 59
   c. The crystals 59
   d. The gamma-ray spectra 60
   e. The analysis of the composite spectrum 60
   f. Procedure 62
   g. The theoretical curves 66
   h. Corrections 75
   i. The results 76

6. The alignment of Co^{60} 77

7. Discussion 84

CHAPTER 4 THE NUCLEAR ALIGNMENT OF MANGANESE 52 Page 87

1. Introduction 87

2. Decay Scheme 88

3. Experimental 92
   a. The production of Mn^{52} 92
   b. The chemical separation 94
   c. The crystal 94
   d. The gamma-ray spectrum 95
   e. Procedure 97
   f. Scattering and aperture correction 97
   g. Results 101

4. Conclusions 101
   a. The spin sequence 101
   b. The angular distribution 104
   c. The magnetic moment 105

5. Other experiments 105
   a. Gamma-ray measurements with oriented nuclei 105
   b. Beta-ray measurements 109
   c. The spin and magnetic moment from paramagnetic resonance 109

6. Discussion 110

CHAPTER 5 THE DECAY OF MANGANESE 56 112

1. Introduction 112

2. The decay scheme 113

3. Irradiation damage 116

4. The design of the experiment 118

5. The angular correlation and scintillation spectrometer study 121

6. Experimental 122
   a. The composition of the crystal 122
   b. The irradiation parameters 123
   c. The presence of other activities 123
   d. The alignment experiment 126

CHAPTER 5 (Continued) Page

7. Analysis of results 129
a. The temperature scale 129
b. Correction for sodium activity 129
c. Decay correction 132
d. Correction for other gamma-rays 132
e. The results 137

8. Interpretation of data 144
a. Test of the angular distribution 144
b. The mixing ratios 147
c. Possibilities of spin 2 for Mn^{56} 151
d. The magnetic moment of Mn^{56} 153
e. The damage factor 154
f. Summary of conclusions 154

9. Discussion 156

CHAPTER 6 THE BETA TRANSITION IN COBALT 58 160

1. Introduction 160

2. The decay scheme 160

3. The parity experiments 163

4. The previous alignment experiments 166

5. Design of the present experiment 168

6. Experimental 170
a. The source material 170
b. The spectrum 172
c. The crystal 175
d. The counters 175
e. Precautions 176
f. Results 179

7. Corrections 184
a. The finite aperture of the counters 184
b. The effect of the 0.815 Mev and 1.62 Mev gamma rays 184
c. The Co^{60} contamination 186
d. Scattering 187
e. Uncertainties 188

CHAPTER 6 (Continued) Page

8. Conclusion 188

9. Discussion 189

10. Corollary - the derivation of a temperature scale 191

APPENDIX: THE EVALUATION OF THE ORIENTATION PARAMETERS FROM THE SPIN HAMILTONIAN 197

1. The problem 197
   a. Introduction 197
   b. The eigen functions 197
   c. The rules for using the spin operators 198
   d. The energy matrix 199
   e. The orientation parameters 200
   f. Clebsch-Gordon coefficients 200

2. Cobalt in $Zn\,Si\,F_6,6H_2O$ 202

3. Manganese in $Zn\,Si\,F_6,6H_2O$ 205

REFERENCES 215

ACKNOWLEDGEMENTS

The work described in this thesis was carried out at the Clarendon Laboratory during the tenure of a Research Studentship awarded by the Department of Scientific and Industrial Research. I wish to thank that body for its support and Professor Elsasser for allowing me to use the facilities of the Laboratory.

I would also like to thank my supervisor, Dr. M.A. Grace, for suggesting these experiments and for his advice, encouragement and inexhaustible enthusiasm which have made this thesis possible.

I am also grateful for the invaluable assistance of Mr. J.S. Hill who maintained the low temperature apparatus and to Drs. N. Kurti and R.G. Scurlock for their advice.

I wish to thank:-

Dr. P.F.D. Shaw for his help and advice with the chemistry

Dr. G.R. Satchler for numerous discussions in connection with the calculation of orientation parameters and theoretical deductions;

Mr. C.V. Sowter for his assistance with the Co^{58} experiments

Mr. J.M. Gregory for carrying out the Mn^{56} angular correlations

Mr. W. Stenard, Mr. G. Frater, Mr. T.H. Carr and the workshop staff for their skill and willing cooperation.

The Isotope Division, A.E.R.E. Harwell, and the Radiochemical Centre, Amersham for their cooperation in carrying out the many irradiations and to the Nuffield Cyclotron Group at Birmingham for the preparations of Mn^{52}.

Finally I would like to thank my wife for typing this thesis and for her encouragement.

CHAPTER 1

INTRODUCTION

1. Introduction

During the last few years much data has been accumulated on the various properties of nuclear levels and nuclear theory has been particularly successful through the shell model (Jensen, 1955) and collective approach (Bohr & Mottleson, 1955) in interpreting much of this information. However, much more accurate knowledge is required if we are to have a true understanding of the nucleus and not to be repeatedly disordered by the breakdown of cherished laws such as happened recently with the conservation of parity (Lee & Yang, 1956).

Nuclear orientation played an important part in putting parity in perspective (Wu, Ambler et al, 1957) and has contributed many other useful pieces of information. It seems, however, that because there are many limitations on the isotopes which can be studied by this method some have been neglected while the maximum information has not been obtained for some of those which can be studied.

In this thesis all the principal experiments have been carried out using crystals of nickel-zinc fluosilicate. This salt, although studied by paramagnetic resonance has been up to now neglected in spite of its having some advantages over the "well-worn" salts (Chapter 2) and the work described here was carried out to demonstrate its suitability.

Of the four isotopes studied, two (Co^{58}, Mn^{54}) had been aligned previously (Daniels 1952, Griffing 1956, Grace 1954, Bishop 1954).

Difficulties with the environment had left Mn^{54} uncompleted for several years and it was the fact that its alignment in cerium magnesium nitrate could not be understood that prompted the use of fluosilicates. Appropriately it was chosen as the first isotope to be incorporated in the fluosilicate while the absence of a temperature scale led to the alignment of Co^{60} also and both these experiments are described in Chapter 3.

Following the successful alignment of Mn^{54}, Mn^{52} presented no outstanding difficulties and its alignment is described in Chapter 4. The third isotope studied, Mn^{56}, has a half-life of only 2.58 hours. This work (Chapter 5) shows how nuclear orientation can be made to give useful results for such short-lived nuclei and indicates a possible use for the method in the study of the solid state.

The earliest experiments (Daniels 1952) with Co^{58} had not been sufficiently accurate to give the maximum information as regards the beta transition while the later work of Griffing (1956) was inconsistent with the beta-ray asymmetry measurements of Ambler (1957). An accurate experiment to determine the character of the transition is described in Chapter 6.

The rest of this chapter will be devoted to a theoretical discussion of the methods used in this work for the production and detection of nuclear orientation in order to show how the various nuclear properties enter into the relationships used, experimental considerations are dealt with in Chapter 2.

2. Nuclear Orientation

A nucleus of Spin I can have any one of 2 I+1 orientations with respect to a direction in space which by convention is called the z-axis. For each orientation the nucleus has a specific z-component of spin $I_z = M$ where $-I \leqslant M \leqslant I$.

If W_M is the probability of finding the nucleus in the substate M, then in the absence of any directional influence such as a magnetic field $W_M = \frac{1}{2I+1}$ and is independent of M.

If W_M can be made dependent on M the nucleus is said to be oriented. This can be achieved, for example, by the application of a large magnetic field H. The direction of the field defines the z-axis and energy of a nucleus in substate M is given by $E(M) = \frac{\mu}{I} \cdot \beta_N \underline{H} \cdot \underline{M}$ where μ is the nuclear magnetic moment and β_N the nuclear magneton. The relative populations of the substates when in thermal equilibrium are now dependent on the Boltzmann factor $\exp\{E(M)/kT\}$ and $W_M = \frac{\exp\{E(M)/kT\}}{\sum_M \exp\{E(M)/kT\}}$, where T is the absolute temperature and k the Boltzmann's constant, so that those sublevels with least magnetic energy will be preferentially populated. In order for the effect to be appreciable this direct method would require fields of about 10^5 gauss at temperatures of 0.01^0K.

Two cases of nuclear orientation occur; one in which $W_M = W_{-M}$ and the expectation value of M^2, $(\langle M^2 \rangle)$, is non-vanishing and the other for which $W_M > W_{M-1}$ for all M, i.e. $\langle M \rangle_{av}$ is not zero, (Steenberg 1953)[6]. The first case is usually termed alignment, the nuclear spins being equally

divided between the s and -s directions, while the second case is known as polarisation since there is a net magnetic moment in the +s direction.

3. Methods for producing orientation

3a. The Hamiltonian

The example of direct nuclear polarisation quoted above is not possible with present techniques using external fields because such large fields are required simultaneously with very low temperatures and these are not normally mutually compatible.

However, this difficulty is avoided if one chooses as the environment for the nuclei a single crystal of a paramagnetic salt where it is known that large electric and magnetic fields are present. The methods then available can best be discussed in terms of the Hamiltonian of Abragam and Pryce (1951) which describes the energy levels of an ion in a paramagnetic crystal.

$$\mathcal{H} = -\frac{\mu}{I}\beta_N \underline{H}.\underline{I} + \beta_B\{g_{\parallel} H_z S_z + g_{\perp}(H_x S_x + H_y S_y)\}$$
$$+\{A S_z I_z + B(S_x I_x + S_y I_y)\} + D\{S_z^2 - S(S+1)/3\} + P\{I_z^2 - I(I+1)/3\}$$
$$+ \frac{a}{6}\{S_1^4 + S_2^4 + S_3^4 - S(S+1)(3S^2+3S-1)/5\}$$

where μ = nuclear magnetic moment; β_N = nuclear magneton;

H = external magnetic field; β_B = Bohr magneton;

$g_{\parallel}, g_{\perp}$ = electronic g values parallel and perpendicular to the crystal axis.

S = effective electronic spin, i.e. such that the degeneracy is $2S+1$;

S_1, S_2, S_3 refer to the cubic field axes relative to which the z-axis (trigonal) is the 111 direction.

A, B = hyperfine structure constants

D = crystalline electric field splitting for a field with axial (e.g. trigonal) symmetry.

$Q = q^3 e \frac{\partial^2 V}{\partial z^2} \frac{1}{4I(2I-1)}$, with q = nuclear electric quadrupole moment and V = the crystalline electric potential.

The terms in g^4 is small and is only important for S-state ions.

3b. External field polarisation

The first term represents the direct coupling between the external field and the nuclear magnetic moment. This was given as an example in paragraph 2 and although the experimental difficulties are very great, orientation has been achieved by the method for a favourable case, In^{115}, where the magnetic moment is large, (Dabbs et al 1955).

3c. Magnetic hyperfine structure polarisation

Consider the second and third terms of the Hamiltonian. If a small external magnetic field ($\sim 10^2$-10^3 gauss) is applied a preferential population of the electron spins parallel to the field is produced (2nd term of Hamiltonian); then because of the hyperfine coupling (3rd term), the nuclear spins will also become polarised if the temperature is low enough. This method has been widely used (see for instance R.J. Blin-Stoyle & M.A. Grace, 1957) and is commonly known as the Gorter-Rose method (Gorter 1948; Rose 1949).

3d. Electric h.f.s. alignment

This was suggested by Pound (1949) and arises out of the last term of the Hamiltonian. Here the nuclear electric quadrupole moment interacts with the electric field gradient which is strong for certain

covalent bonds. If a uniaxial crystal is used all the field gradients have the same orientation and the nuclear spins will become aligned at sufficiently low temperatures. Alignment has been achieved for U^{233} in a diamagnetic uranyl salt using this method by Dabbs, Roberts and Parker (1956).

3e. Magnetic h.f.s. alignment

The fourth method was suggested by Bleaney (1951) and enters through the 3rd and 4th terms of the Hamiltonian. It has been employed for the present work and will be discussed in some detail. This method requires no external field and is therefore simpler than the Gorter-Rose method.

4. Bleaney (magnetic h.f.s.) alignment

4a. The hyperfine structure

The hyperfine structure arises through the interaction between the nuclear magnetic moment and the magnetic field set up by the electronic orbits. The interaction energy is given a relation of the form $E=\alpha\mu\mu_N r^{-3}$, where r is the electron coordinate and α a proportionality factor. Putting $\mu_N = I_N g_N \beta_N$ and $\mu \sim g\beta S$, $E_N = \alpha g g_N \beta_N \beta r^{-3} S.I = A S I$. The hyperfine structure is anisotropic if the electronic g value is anisotropic, the latter effect being caused by the contribution to the magnetic moment of the ion by the orbital motion which is affected by the crystalline field.

If there is a crystalline electric field, then the energy of the electronic system will depend on the orientation of the orbits with

respect to this field. The level splitting due to this is described by the D term. Alignment can arise in two ways.

4b. Isotropic h.f.s. (The Manganese Mn^{++} ion).

(i) If D is finite and $S > \frac{1}{2}$ there will be a splitting of the electronic levels, with the S state lowest for $D<0$. Thus in a single crystal the electron spins will be aligned with respect to the axis of symmetry and the hyperfine coupling will bring about nuclear alignment at sufficiently low temperatures.

The form of the level scheme is shown in figure 4 of the Appendix. At zero temperatures the nuclear spins are saturated, all $M = \pm I$ and alignment would be complete. If, however, $D>0$, the $\pm$ S state will lie highest and although alignment might be obtained under suitable conditions, the lowest spin state will always be a mixture of states M, M±1.

(ii) The Manganese ion Mn^{++} has five 3d electrons which half-fill the 3d shell and according to Hund's Rule give an S state for the free ion. Because there is no total orbital angular momentum, in a first order approximation, no effect of the crystalline field on the magnetic properties of the free ion are to be expected. The ground state has $S = \frac{5}{2}$ and has six-fold spin degeneracy (figure 1a). It has been shown that a small fine structure splitting exists and this is probably due to the distortion of the spherical electron density by a trigonal field (Pryce 1950; Abragam and Pryce 1951). Phenomenologically the results can be described by adding a term DS_z^2 to the Hamiltonian together with a term in S^4 to describe the effect of the cubic field

on an S- state ion

$$\mathcal{H} = D S_z^2 + A S_z I_z + \frac{A}{2}(S_+ I_- + S_- I_+) + \frac{a}{6}(S_1^4 + S_2^4 + S_3^4)$$

For Mn^{++} in zinc fluosilicate $D = -0.0134 \pm 0.0003$ cm^{-1}; $A_{55} = \pm 0.0091 \pm 0.0001$ cm^{-1} $a = +0.0009 \pm 0.0002$ cm^{-1} (Bleaney and Ingram 1951a).

D is slightly temperature dependent (figure 2) but the value at 1°K is not expected to be significantly different from the value measured at 20°K; it is independent of the isotope.

4e. Anisotropic h.f.s. (The Cobalt Co^{++} ion).

(i) The second case arises when the ion has an odd number of electrons and the electronic levels form Kramers doublets. Here the separations between doublets are usually so large that it is only necessary to consider the lowest giving $S_{eff} = \frac{1}{2}$. The alignment is then determined by the hyperfine structure alone and will only occur if this is anisotropic: the two extreme cases are A finite, B = 0 and A = 0, B finite. The B term gives mixing of levels having the same total quantum number $\underline{F} = \underline{S} + \underline{I}$ so that in the latter case none of the levels are pure in M_I. For the case when A and B are both finite and $A \gg B$ the degree of alignment is reduced by a factor approximately equal to $1 - (B/A)^2$ from the value expected if B = 0.

(ii) The Cobalt ion, Co^{++}, $(3d^7\,{}^4F)$ has a sevenfold orbital ground state which is split into a singlet and two triplets by the influence of a cubic field. A triplet state lies lowest and taking the spin angular momentum, $S = \frac{3}{2}$, into account, this level has twelve-fold degeneracy. The spin-orbit coupling combined with the influence of a tetragonal or trigonal field causes a splitting of the level into six

Figure 1

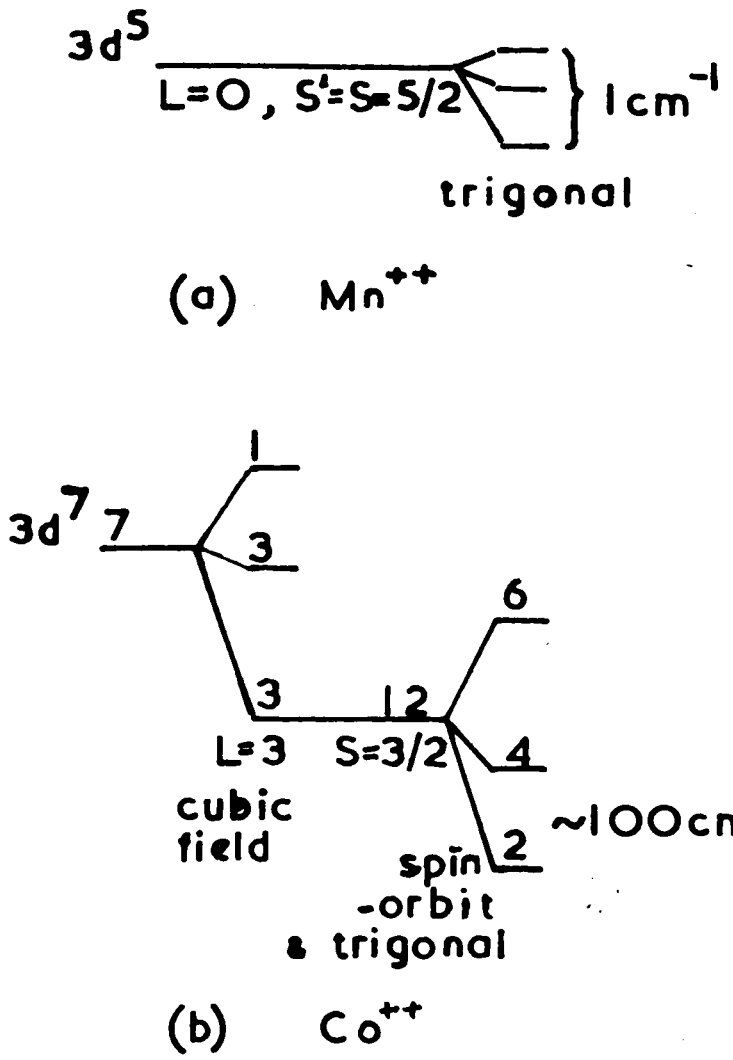


Figure 3

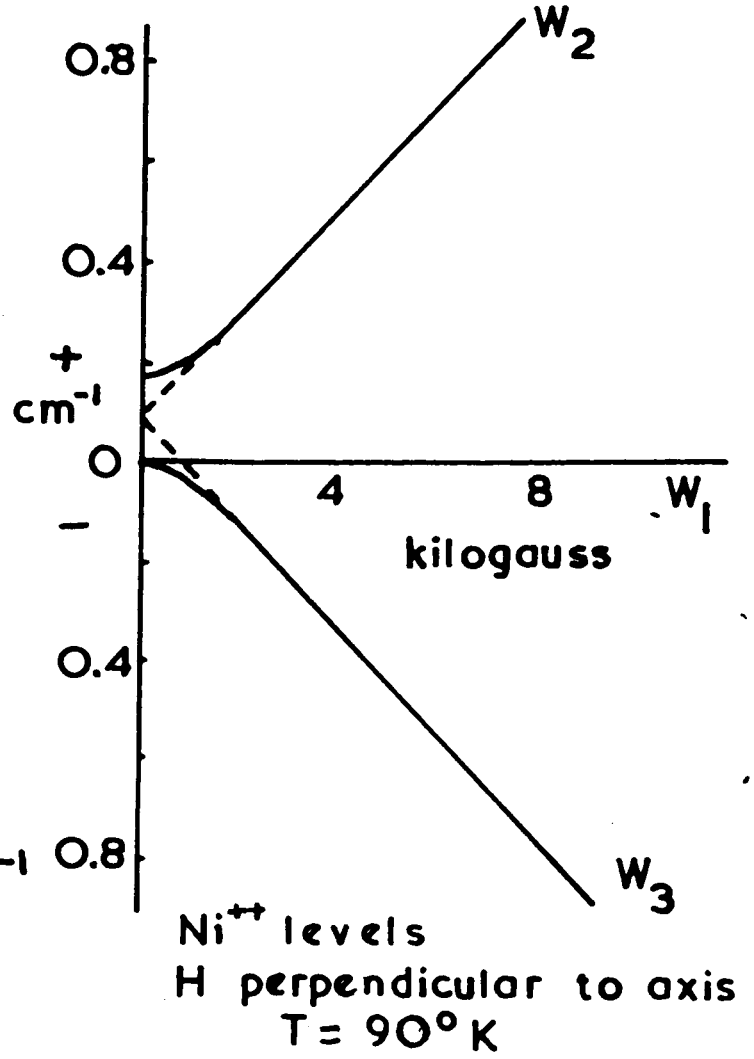
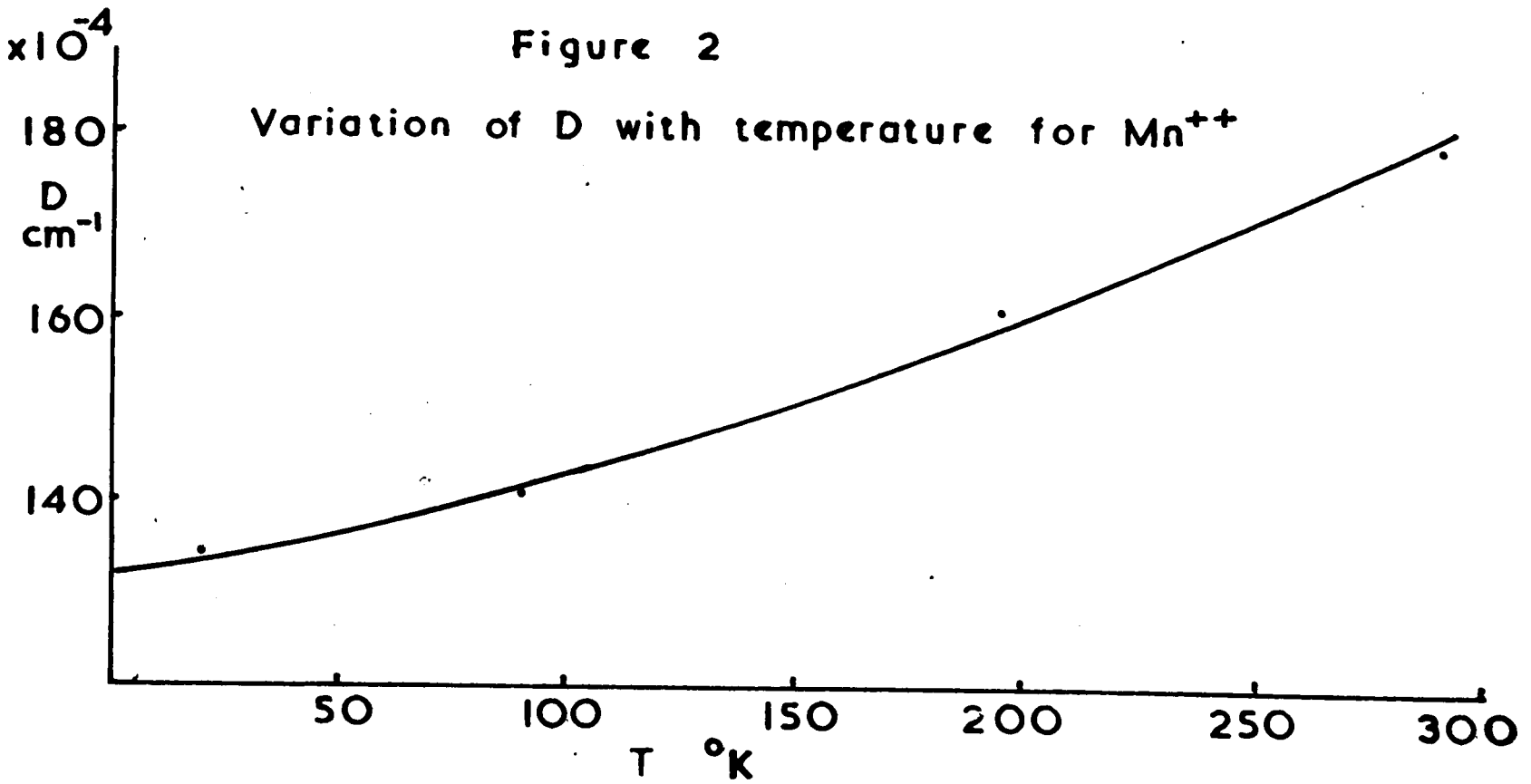


Figure 2

Variation of D with temperature for Mn^{++}



Kramer's doublets. (figure 1 b). The lowest of these is well separated from the rest so that the Hamiltonian is:

$\mathcal{H} = A.S_z I_z + \frac{1}{2}B(S_+ I_- + S_- I_+)$ with $S_{eff} = \frac{1}{2}$. The hyperfine constants in zinc fluosilicate have been measured for the stable isotope, Co^{59},

$A_{sq} = 0.0184 \pm 0.0004$ cm^{-1}, $B = 0.0047 \pm 0.0001$ cm^{-1}

For other isotopes $A = \frac{A_{sq}}{g_{sq}} \cdot g$, where $g = \mu/I$

4d. <u>The environment</u>

A single crystal or a number of aligned single crystals are required ideally with only one ion per unit cell, since the axis about which the nuclei process, which is determined by the crystallographic structure, is then parallel for all ions. The crystals must also be dilute since otherwise the alignment would be spoilt by the magnetic fields of neighbouring paramagnetic ions or exchange interactions between them. These magnetic fields are of the same order as the hyperfine structure, i.e. the field exerted on the electron shell of an ion by its own nucleus.

The salt must be one for which the parameters D, A and B for the ion concerned are suitable, i.e. as described in sections b and c, and possible salts are discussed in Chapter 2.

A rough criterion for successful alignment is that $A/kT \sim 1$

Thus for Mn^{54} in zinc fluosilicate, $A \sim -0.007$ cm^{-1} so $A/kT = 1$ if $T = 0.01^{\circ}K$ which is readily obtainable by adiabatic demagnetisation.

4e. Adiabatic demagnetisation

The mechanism by which low temperatures are produced by this method can be discussed in terms of a specific example, viz. the Ni^{++} ion. A fuller discussion is given by Ambler and Hudson (1955).

The cubical part of a crystalline field splits the orbital levels of the Ni^{++} ion so that a singlet lies lowest and the effective spin is the same as the actual spin $S = 1$. A trigonal field, e.g. nickel fluosilicate, splits this level into a singlet and a doublet, the separation between these levels being $\delta \sim 0.12$ cm^{-1} (Penrose & Stevens 1949) with the doublet lowest and all will be equally populated at 1°K If now a large external magnetic field is applied at 1°K, these levels separate out so that the spacing is now $g\beta H \gg \delta$ (fig. 3) and the lowest will become predominantly populated at the expense of the other two since $g\beta H \gg kT$. The system is ordered and thermodynamically entropy has been removed. This level system, i.e. the crystal, can now be thermally isolated from the surroundings (helium at 1°K) and the magnetic field removed. The levels will collapse to their zero field spacings but only the doublet will be appreciably populated. Since the specimen was isolated no entropy can be regained from the surroundings so that the spin system has in effect been reduced to a very low temperature. Some entropy will be regained from the lattice through the spin lattice interactions so that the loss of entropy is shared by all the ions and provided the magnetic field was large enough the final temperature will still be less than 1°K. Hill, Meyer and Milner (1959) have shown that temperatures of 0.01°K can be produced in this way if

the nickel salt is diluted with diamagnetic zinc (see Chapter 2).

If the doublet had been above the singlet then the lowest temperatures that could have been reached would have been of the order of the splitting between doublet and singlet, i.e. 0.12 $cm^{-1} \equiv 0.17^{\circ}K$.

5. The angular distribution of gamma-rays from aligned nuclei

5a. The detection of the alignment; a typical decay scheme

The preceding discussion has outlined the method used for aligning nuclei and it is now necessary to consider how the alignment may be detected in order to obtain nuclear information.

For stable nuclei the scattering of polarised particles serves as a method of detecting the orientation (Bernstein et al 1954) while for radioactive nuclei the angular distribution of the radiations is sensitive to the nuclear orientation (Spiers 1948, 1949).

Experiments have been performed in which alpha-particles (Dabbs et al, 1956) and beta-rays (Wu, Ambler et al 1957) from oriented nuclei have been detected but this leads to technical difficulties, when using very low temperatures, as the source is usually enclosed in the cryogenic equipment and for this reason the gamma-radiation has been more frequently used. However, because gamma-emitting states are very short-lived all nuclei so far studied decay by a beta-gamma cascade as represented by the typical decay scheme shown in figure 4a. It will be useful to consider the physical processes involved and it will be convenient to consider first a single isomeric transition.

5b. Multipole Radiation

An electromagnetic radiation field may be described by a series of spherical harmonics, $Y_{l,m}(\theta,\phi)$, with respect to some z-axis so that it can be considered as the sum of several components of different multipolarity l, m (Blatt & Weiskopf 1952). It can be shown (ibid) that a quantum of multipole radiation l,m carries with it an angular momentum l with z-component m, both measured in units of $\hbar$. The radiation can be either electric or magnetic in character, multipoles l,m of either type carrying away the same angular momentum but having different parities given by: $\pi(elec) = (-1)^l$; $\pi(mag) = (-1)^{l+1}$.

5c. An isomeric transition

If we consider a transition between two nuclear states ψ_2, ψ_3, the overall angular momentum of the system must remain constant so $\underline{I_2} = \underline{I_3} + \underline{l}$ and the selection rules are:

$$|I_2 - I_3| \leqslant l \leqslant I_2 + I_3 \quad ; \quad M_2 - M_3 = m \quad (\Delta M = 0, \pm 1)$$

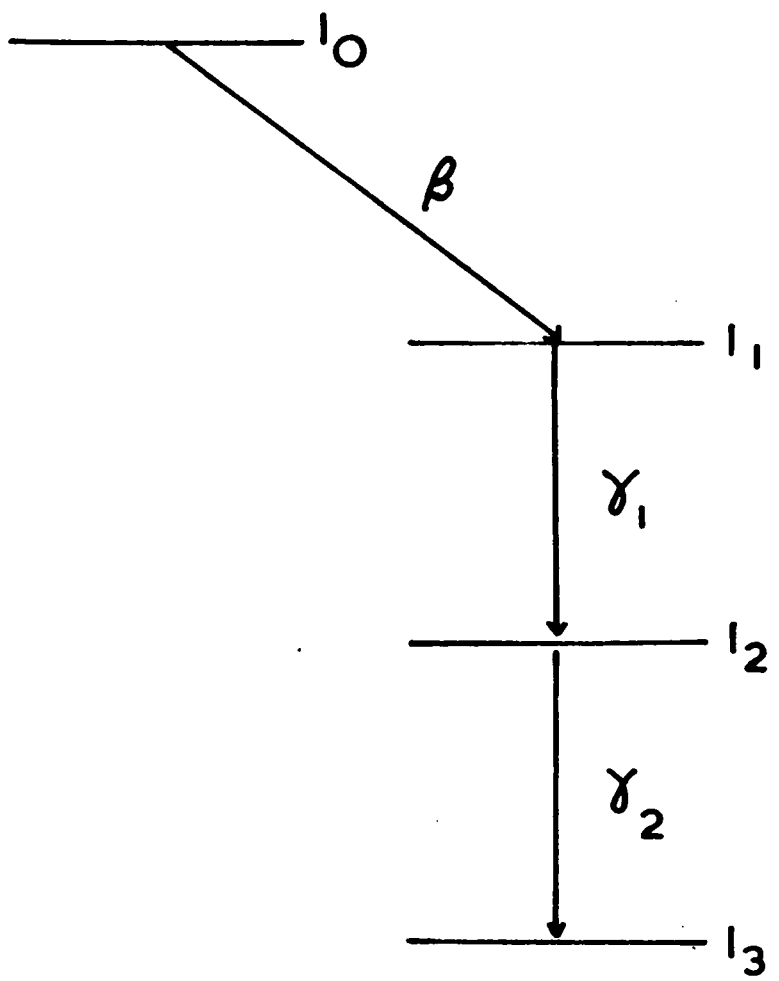
and $\pi_2 = \pi_3 \pi$ where π is the parity of the multipole.

The probability of a transition falls off rapidly with l so that for most cases it is necessary to consider only the lowest possible multipole $l = |I_2 - I|$. The energy emitted per second is given by the Poynting vector $S \equiv \frac{c}{4\pi} E \times H$ and its angular distribution for a pure multipole l, m is given by

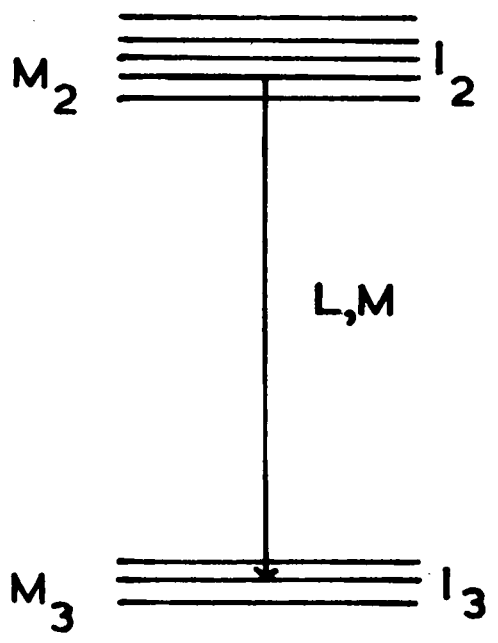
$$I_{l,m}(\theta,\phi) \propto \tfrac{1}{2}\left[1 - \frac{m(m+1)}{l(l+1)}\right] |Y_{l,m+1}|^2 + \tfrac{1}{2}\left[1 - \frac{m(m-1)}{l(l+1)}\right] |Y_{l,m-1}|^2 + \frac{m^2}{l(l+1)} |Y_{l,m}|^2$$

(Blatt & Weiskopf 1952).

Thus for a dipole, l = 1, there are two radiation patterns depending on whether m=0 or m=1. If m = 0, $I_1^0 \propto \sin^2\theta$ if m = 1 $I_1^{\pm 1} \propto 1 + \cos^2\theta$.



a. A Typical Decay Scheme



b. An Isomeric Transition

Figure 4

A single transition as illustrated in figure 4b, consists of several components between the discrete m-states. The components are not resolved because any splitting is much less than the natural line width and the composite angular distribution will depend on the initial populations of the substates $P(M_2)$, the relative transition probabilities $G(M_2M_3)$ for the components and individual angular distributions.

The populations depend on how the level was excited and the transition probabilities are given by the square of the Clebsch-Gordon coefficient (Condon & Shortley 1935) for the vector addition

$$\underline{I_2} = \underline{I_3} + \underline{L} \quad , \quad M_2 = M_3 + L$$

Hence $$I_L(\theta) = \sum_M P(M_2)\, G(M_2 M_3)\, I_L^M(\theta)$$

For equally populated M_2 states $I_L(\theta)$ is isotropic but if $P(M_2)$ depends on M_2 the distribution will be anisotropic. In the case of nuclear orientation the population of these states depends on the degree of orientation of the parent nucleus and on the intervening transitions which may or may not spoil the orientation.

5d. The Intervening transitions

(i) The population of the substates M_0 is given by $W_M = \frac{\exp\{E(M)/kT\}}{\sum_M \exp\{E(M)/kT\}}$

Each of these states decays by a β-process to one of the magnetic sub-states of the level I_1 in the daughter nucleus. Because of the selection rules for I and M only certain daughter M states will be affected. Thus if the decay is of the allowed type and obeys Fermi selection rules, then $\Delta I = 0, \Delta M = 0$ and only one M state is filled for each one decaying leaving the orientation unaffected. However, if the decay is of the Gamow-Teller type ($\Delta I = 0, \pm 1, \Delta M = 0, \pm 1$) more than

one M state of the daughter level is concerned and the disorientation produced is described by a parameter $U(I_0 I_1 j)$, giving the relative transition probabilities of the components. For Fermi transitions $U=1$ but $U<1$ for the Gamow-Teller case. If both selection rules are applicable then it is necessary to sum over the two modes giving $U=\lambda U^{F}+(1-\lambda)U^{G-T}$ where $\lambda = \frac{C_F^2|M_F|^2}{C_F^2|M_F|^2+C_{GT}^2|M_{GT}|^2}$ is the fraction of the transitions obeying Fermi selection rules, C is the coupling coefficient and M the matrix element for the decay. There is no interference term of the radiation is unobserved (Satchler 1953) because one is only interested in the populations of the final states and not in the radiation pattern.

(ii) An unobserved gamma transition may also produce some disorientation depending on whether $L=\Delta I$ or $L>\Delta I$, and this is described by a similar parameter $U(I,I_2,L_1)$ where L_1 is the multipolarity of the gamma-ray. In the case of mixed transitions involving gamma-rays of multipolarity L, L+1, we must again sum over the components giving $U=\frac{U(L)+\delta^2 U(L+1)}{1+\delta^2}$

where $\delta^2 = \frac{\text{Intensity of } L+1}{\text{Intensity of } L}$

Mixed transitions will occur when the transition probabilities of two multipoles of different characters are comparable. For instance, the probability falls off rapidly with increasing L (Mosakowski 1955) but magnetic transitions are less probable than electric transitions of the same order so in some cases it is possible

for magnetic dipole and electric quadrupole radiation to compete.

(iii) The observed transition has already been discussed. As with the unobserved transitions it is necessary to sum over all possible values of L but in this case the components will be coherent and interference terms occur. Because of the transitions probabilities it is only necessary to consider the two lowest possible multipoles, L and L+1 which satisfy the selection rules. The angular distribution is then $$I(\theta) = \frac{I_L(\theta) + \delta^2 I_{L+1}(\theta) + 2\delta I_{L,L+1}(\theta)}{1+\delta^2}$$

where δ^2 has the same meaning as before.

5e. The angular distribution

From the foregoing discussion it can be seen that the distribution must have the form

$$I(\theta) = \sum W_{M_0} U(\beta) U(\gamma) G(M_2 M_3) I_L{}^M(\theta)$$

It has been investigated theoretically by Spiers (1949) for single emission and later extended by Steenberg (1951, 1952, 1953) and Satchler (1953, 1954) to cases where several radiations are emitted in cascade. Steenberg shows that $I(\theta)$ can be expressed as a series of Legendre polynomials $P_\nu(\cos\theta)$ i.e. $I(\theta) = \sum A_\nu P_\nu(\cos\theta)$ with the restriction the ν is even. Gray and Satchler (1955) have further shown how to define the population functions W_M for the oriented parent nucleus so that the coefficients A_ν split up into factors each depending on one process only. Thus $A_\nu = B_\nu U_\nu U_\nu' F_\nu$ and use can be made of the extensive tabulations of the various angular momentum

addition coefficients

$$B_\nu(I_0,T) = \sum (2\nu+1)^{\frac{1}{2}} C^{I_0 I_0 \nu}_{M M 0} \; W(M)$$

normalised to give $B_0 = 1$ where $\nu \leqslant 2I$ and $C^{I_0 I_0 \nu}_{M M 0}$ is a Clebsch-Gordon coefficient which adds states of angular momentum I, ν to form a single state of angular momentum I, z -component M (Condon & Shortley 1935).

$U_\nu(I_0 I_1 j)$ and $U_\nu(I_1 I_2 L_1)$ are normalised Racah coefficients

$U_\nu = \left\{(2I_0+1)(2I_1+1)\right\}^{\frac{1}{2}}(-1)^{I_0+I_1-j} \; W(I_0 I_0 I_1 I_1 ; \nu j)$ and simply describe the relative transition probabilities for the components of the unobserved transitions. The Racah coefficients W(ABCD: EF) describe the addition of three angular momenta and are functions of Clebsch-Gordon coefficients. Their properties are discussed by Biedenharn, Blatt & Rose (1952) while numerical tables have been given by Simon, Van der Sluis and Biedenharn (1954)

$$F_\nu(LL'I_3I_2) = (-1)^{I_3-I_2-1}\left\{(2I_2+1)(2L+1)(2L'+1)\right\}^{\frac{1}{2}} C^{LL'\nu}_{1-1} \; W(I_2 I_2 LL'; \nu I_3)$$

and these functions are tabulated by Ferentz & Rosenzweig and Biedenharn and Rose (1953).

The properties of the various angular momentum addition coefficients allow ν max $\leqslant \min(2I_0, 2I_1, 2I_2, 2L)$.

6. The derivation of nuclear data

Summarising the angular distribution we have

$$I(\theta) = \sum_\nu B_\nu(I_0,T)\, U_\nu(I_0 I_1 j)\, U'_\nu(I_1 I_2 L_1)\, F_\nu(I_2 I_3 L_2)\, P_\nu(\cos\theta)$$

$$\nu \leqslant (2I_0, 2I_1, 2I_2, 2L_2) \quad ; \quad B_0 = U_0 = F_0 = 1$$

Each of the parameters B_ν, U_ν and F_ν depend on the properties of the nuclear levels involved in the decay.

B_ν depends on the spin of the parent nucleus and its magnetic moment, U_ν and F_ν depend on the spins of two levels and the angular momentum carried away by the radiation linking the two. Thus the measurement of the angular distribution for the gamma radiation from aligned nuclei can lead to a knowledge of some of the properties the nuclear levels but it is clear that since there are so many parameters it would be impossible to interpret the experimental data unless some are known beforehand.

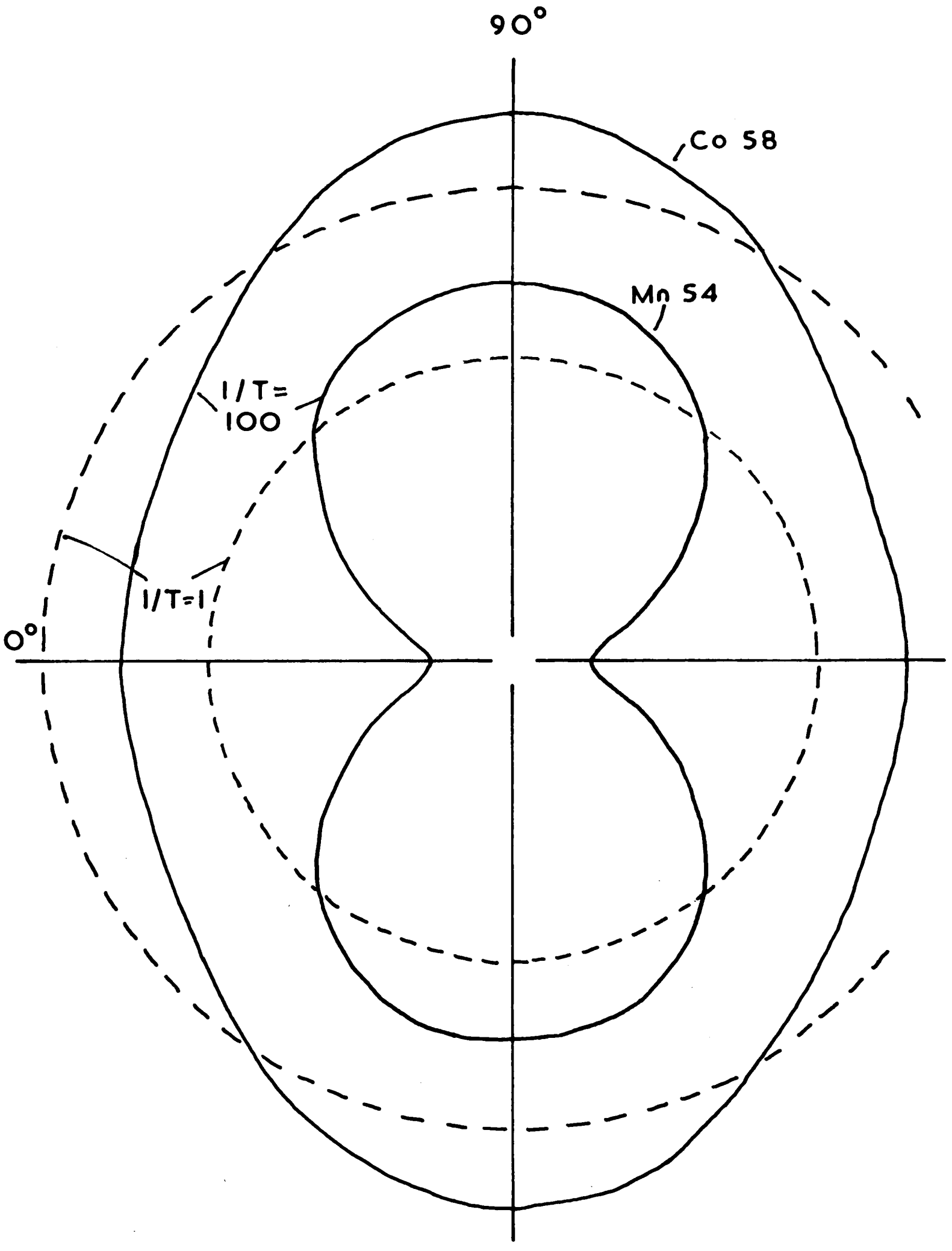
However, the number of terms involved is limited by the fact that dipole and quadrupole radiations are much more probable than higher multipoles so $\nu < 4$. Further, the distribution will be isotropic if any one of I_0, I_1 and I_2 are 0 or $\frac{1}{2}$. This latter fact places quite wide limitations on the nuclei which may be studied; already there is the restriction that the ion must be paramagnetic.

Since the distribution can be written

$$I(\theta) = 1 + A_2 P_2(\cos\theta) + A_4 P_4(\cos\theta)$$

it follows that measurements at two angles allows A_2 and A_4 to be found. P_2 and P_4 vary most slowly at 0° and 90° so these angles are usually selected for study.

So far it has been assumed that the lifetime of the intermediate states is so short that no perturbations can affect the relative populations of the M states and so alter the distribution. This effect arises through a precession of the nuclei under the disturbing force. The lifetimes, of course, are finite but for the magnetic dipole and electric quadrupole radiations considered here are of the order of



Polar Diagrams for Co 58 and Mn 54
Figure 5

$< 10^{-10}$ seconds and perturbations are not expected for $\tau < 10^{-10}$ seconds. As a step towards interpreting the data it is convenient to define an anisotropy ϵ, in terms of $I(0^\circ)$ and $I(90^\circ)$,

$$\epsilon = \frac{I(90^\circ) - I(0^\circ)}{I(90^\circ)}$$

For pure multipoles $\epsilon > 0$ for L=2 and $\epsilon < 0$ for L=1 for alignment along the axis, although a preceeding decay could reverse the sign.

The following chapters describe some examples of the uses of nuclear orientation.

If the decay scheme is known and the only unknown parameter is $B_\nu(I_o, T)$ then the magnetic moment of the nucleus can be found through the dependence of B_ν on the hyperfine parameter A. (Mn^{54}, Mn^{52}).

Alternatively if U_ν or F_ν is unknown then the angular momenta of the levels involved can be deduced together with the characteristics of the radiation. Thus for the beta-decay it is possible to measure the relative amounts of Fermi and Gamow-Teller components present (Co^{58}) while for gamma transitions the multipole admixture, i.e. δ, can be deduced (Mn^{56}).

CHAPTER 2

EXPERIMENTAL CONSIDERATIONS

1. Introduction

It has been seen in the previous chapter that in order to produce appreciable orientations it is necessary to use temperatures of the order of 0.01°K. The only practicable method for obtaining temperatures in this range is by the adiabatic demagnetisation of a paramagnetic salt (see Ambler and Hudson 1955).

The requirement of a magnetically dilute crystal in order that interactions do not spoil the alignment is also necessary for the cooling since cooling by adiabatic demagnetisation is, as we have seen, essentially an ordering (or alignment) of the ionic spin system. A single crystal or assembly of aligned single crystals is required for alignment in order that all the nuclei align in parallel directions. A single crystal is to be preferred because although composite specimens have been used it is not always certain that the whole is at a uniform temperature.

Two separate salts - one suitable for cooling and the other for alignment - can be held in thermal contact so that the alignment crystal is cooled externally. However, for this case the temperature reached depends on the quality of the thermal contact and at low temperatures it is very difficult to make this efficient. Further, the temperature homogeneity of the alignment crystal will depend on its thermal conductivity. Both these problems are overcome to a great

extent if a composite specimen is made up of a crystalline powder of the two salts cemented or pressed together but in the absence of an external field there would be no single preferred direction and the alignment could not be observed. If, however, the "cooling" and "alignment" ions both form salts of the same class which are isomorphous then they can be incorporated in the same crystal. There are no problems of external thermal contact in this case since the temperature of the alignment ions is determined by the temperature of the demagnetised spin system through the common lattice. If the radioactivity is uniformly distributed temperature inhomogeneities can only arise if the surface warms up more quickly than the interior.

Further, it is preferable for the crystal structure to have only one ion per unit cell so that the ions have parallel alignment axes.

2. The choice of crystal

For the elements of the iron group studied the salts which satisfy the necessary conditions are the Tutton salts (double sulphates), the double nitrates and the fluosilicates.

2a. The Tutton Salts

The Tutton salts have the general formula $M^{++}M_2^{+}(SO_4)_2.6H_2O$ and low temperatures can be reached by using copper as the cooling agent, e.g. $CuRb_2(SO_4)_2.6H_2O$. Further dilution to reduce spin-spin interactions between neighbouring Cu ions can be produced by replacing some of them by diamagnetic zinc or magnesium while the nucleus to be aligned need only be introduced as a trace e.g. (TrCo, 20% Cu 80% Zn) $Rb_2(SO_4)_2.6H_2O$. However, these salts have two ions per unit cell and

the axes of the two differently oriented magnetic complexes $M^{++}(H_2O)_6$ are not related to the monoclinic (a,b,c) axes of the crystal but are related to each other by reflection in the a-c plane. This gives rise to two axes of alignment inclined at an angle, 2α, to each other and not immediately located with respect to the crystal faces. The experimentally determined orientation of the axes, xyz, can be described on the approximation that for each magnetic complex there is an axis of tetragonal symmetry z. Then α is the angle of inclination of z to the a-c plane and the projection of z on the a-c plane is one of the susceptibility axes K_1 or K_2 depending whether χ_z is greater or less than $\chi_{x,y}$. ψ is then the angle between K_1 and c such that the angle between a and c is obtuse. Detailed investigation however (see Bowers & Owen 1955) show that the assumption of tetragonal symmetry for the environment of the paramagnetic ion is not good and that the magnitude, sign and direction of the distortions are temperature dependent. They also differ for salts of different composition.

Since it is impossible to separate the two angular distributions it is never possible to observe the maximum anisotropy and furthermore great reliance has to be placed on the measurement of the angles between the crystal axes and the alignment axes.

2b. <u>The Double Nitrates</u>

Experiments with double nitrates ($M^{+++}_2 M^{++}_3 (NO_3)_{12}.24H_2O$) by Daniels and Robinson (1953) have shown that by incorporating cerium ions as a cooling agent, viz. $Ce_2Mg_3(NO_3)_{12}.24H_2O$, temperatures of the order

of 0.003°K could easily be reached by demagnetisation from fields of about 10 kilogauss at 1°K. However, in this class of salt the divalent ions can be accommodated both at the face centres and at the body centre of the unit cube. Although this gives rise to a single axis of alignment parallel to the main crystal axis the two positions give rise to two different magnetic complex for Ce^{++} and Mn^{++}. Those two types have different degrees of anisotropy, i.e. departure from cubic symmetry, and the number of more anisotropic ones to less anisotropic appears to be about 1 : 1.6 but it is not known exactly (Bowers & Owen 1955).

The greatest drawback to the use of cerium magnesium nitrate for the iron group is the disturbance of the orientation found experimentally for Co^{60} (Ambler 1953), Mn^{54} (Grace 1954) and Mn^{52} (Huiskamp 1956, 1957) which made it impossible to give a complete interpretation of the results. For Co^{60} and Mn^{52} the anisotropy reaches a temperature independent maximum below $\frac{1}{T_\Theta} \sim 150$ while for Mn^{54} the anisotropy passed through a maximum at $\frac{1}{T_\Theta} \sim 100$ decreasing for lower temperatures.

It has been suggested (Johnson, 1955; Huiskamp, 1956, 1957) that this disturbance is due to interactions between the divalent and trivalent ions which affects the Spin Hamiltonian and in the case of Ce^{++} it could be that the sign of A is different for the two complexes. Such effects can be overcome by the use of an external magnetic field (Grace 1954).

The presence of some interaction is supported by a recent paramagnetic resonance experiment on Co in cerium-bismuth magnesium nitrate

(Gager et al 1958). They found that the resolution of the h.f.s. depended on the cerium concentration and they attributed this to a magnetic dipole interaction between the Ce^{++} and Ce^{+++} ions. It has also been found (Johnson, 1955) that if the Cobalt is included in a crystal of lanthanum magnesium nitrate cooled externally there is good agreement between theoretical and experimental anisotropies.

2c. The fluosilicates

The salts of this class have the general formula $M^{++}SiF_6.6H_2O$; the crystals have trigonal symmetry and grow in hexagonal pillars parallel to the trigonal axis. The crystal structure is illustrated in figure 1 which is taken from Wycoff (1951).

The unit cell is rhombohedral, with one molecule per unit cell. The divalent ion is surrounded by a nearly regular octohedron of six water molecules with a small trigonal distortion. The "parallel" and "perpendicular" axes of the magnetic complex coincide with those of the crystal and also with the susceptibility axes.

Bansie and Cooke (1950) have measured the specific heat of nickel fluosilicate and they found evidence for considerable exchange interactions. However, Hill et al (1959) have shown that, diluted with zinc, a non-paramagnetic isomorphous ion, it can be cooled by adiabatic demagnetisation from initial fields of 20 kilo oersted at 1°K to temperatures below 0.05°K. They also deduced a $T - T^*$ correlation from measurements of the entropy of magnetisation and specific heat of the crystal, which was 15% Ni and 85% Zn. The splitting of the doublet and singlet contributes to both these quantities and itself is dependent

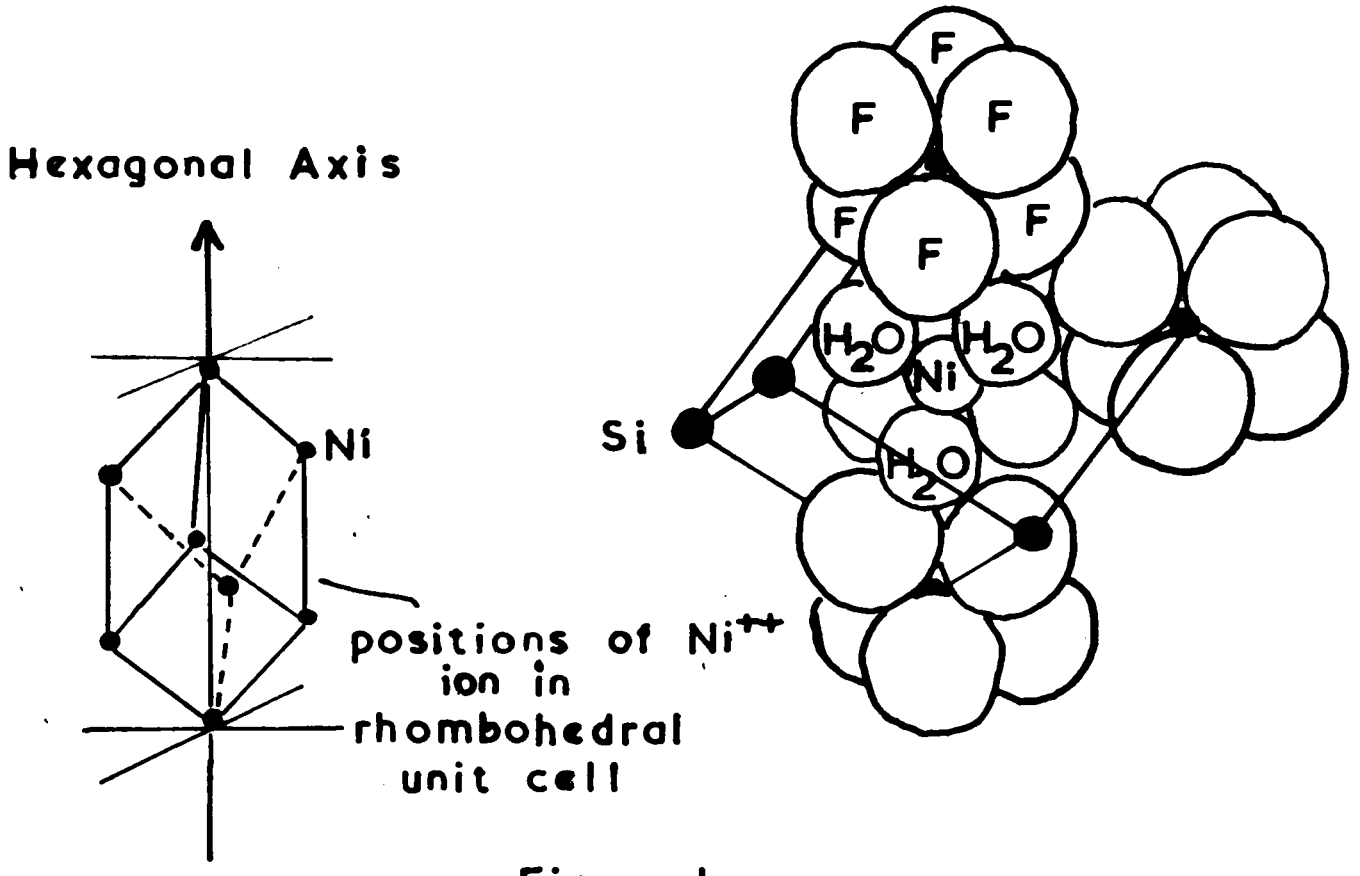


Figure 1

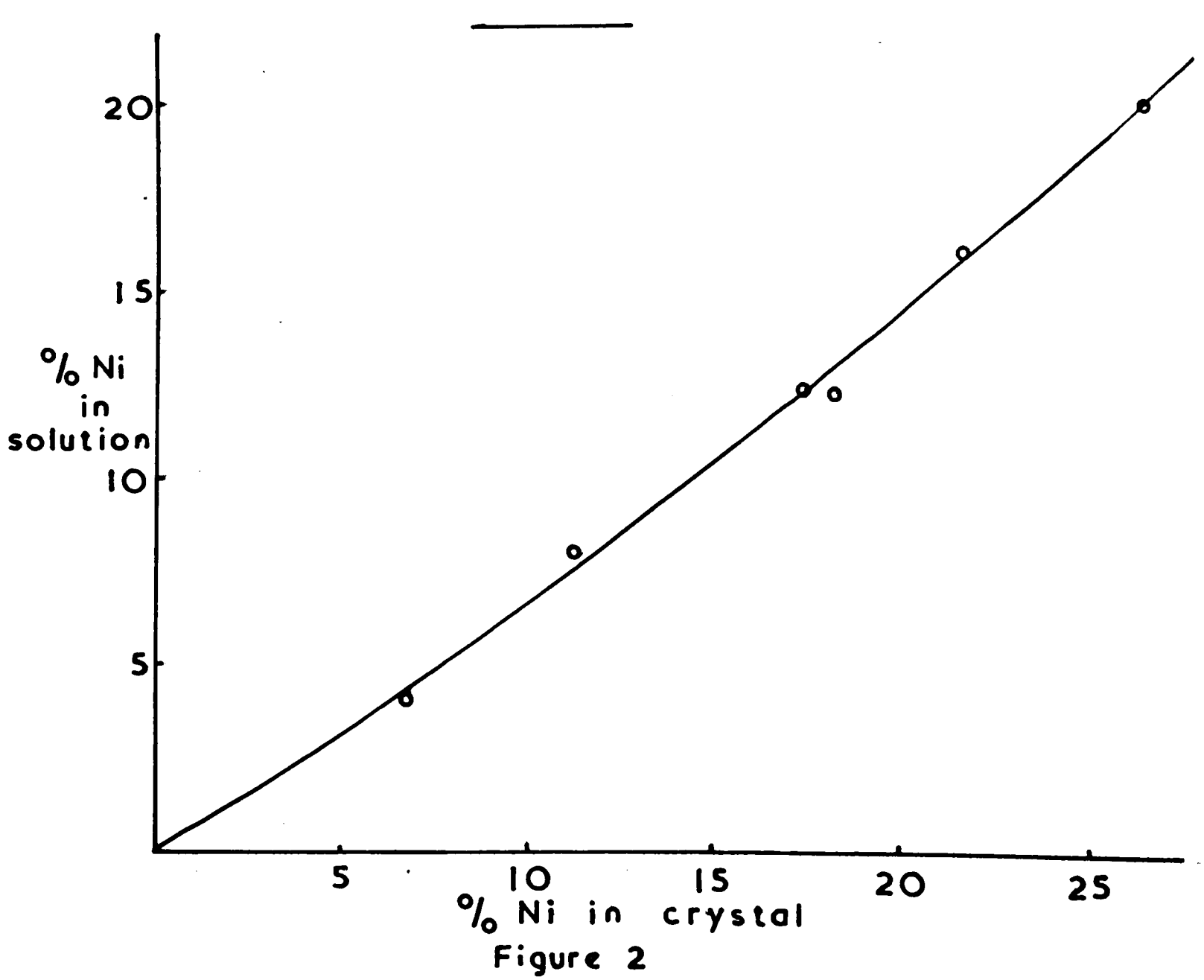


Figure 2

on the dilution of the crystal, presumably because the diluent changes the lattice dimensions slightly and alters the crystal field (Meyer 1957). This means that the T-T* correlation will depend on the concentration of the crystal.

The choice of concentration to be used is governed by two factors; Firstly, the interactions will be reduced by dilution and so lower temperatures can be reached and secondly, the specific heat depends linearly on the concentration. If the specific heat is made too small then the crystal will heat up too rapidly for observations to be made. There is also a limit to the dilution reached when the Ni-Ni interactions become of the same order as those caused by the random fields produced by the protons in the water of crystallisation.

Although crystals of the fluosilicates do not grow as readily as those of either the Tutton salts or the double nitrates, they have the advantage of one ion per unit cell and a single axis of alignment. For this reason they have been used throughout this work. It was intended to use crystals of the same concentration as Hill et al in order to have a temperature scale .

3. Growing the crystals

The concentration of the crystal will depend on the concentration of the growing solution, and the temperature. It has been found by analysing fluosilicate crystals grown from solutions of different concentrations that the nickel ion grows into the crystal more readily than the zinc. The results are shown in figure 2. On this basis a

solution containing only 10% Ni would be expected to produce a crystal having about the same concentration as that used by Hill, Meyer and Milner and therefore the T-T* correlation would be applicable.

Consequently the crystals used throughout this work were grown from 10% solutions and it was found convenient to start with 10 gms of solute. Fluorine attacks glass so all the vessels used for the fluosilicate chemistry were made of polythene. The technique is as follows: A small seed crystal was placed in a small pot and covered by a saturated solution containing a slight excess of hydrofluosilicic acid. The latter precaution is to prevent hydrolysis. The pot was placed in a dessicator at between $\frac{1}{2}$ - 0 atmospheres using concentrated sulphuric acid as the dehydrating agent. The dessicator was kept in a box to shield it from draughts and the temperature was maintained at 20°C to within about $\frac{1}{2}$°C.

It was necessary to clean the seed regularly to avoid small pieces adhering to the surface and growing with a different orientation. Fluosilicate crystals tend to twin parallel to the hexagonal axis and although this is no disadvantage for nuclear orientation it makes it more difficult to ensure that the crystal is clean and that there are no inclusions.

When growing the crystals for Mn^{56} a few milligrams of Manganese (55) carbonate were added to the growing solution. If the activity (Mn^{54}, Mn^{52}, Co^{58}) is to be grown into the crystal then it was usually obtained as a chloride in aqueous solution. This could be evaporated

down to dryness to remove excess chlorine and dissolved up in a small quantity of hydrofluosilicic acid before adding to the growing solution.

Crystals weighing up to 3 gms have been grown although the average size was 2 gms. The larger the crystal the greater the thermal capacity and hence a slower warming up rate.

A typical crystal is shown in figure 3.

All the crystals were analysed after the experiments were completed and the results are shown in Table I:-

TABLE I

Mn^{54}	A	8.0 ± 0.1% Ni
	B	10.8
	C	10.6
Co^{60}		8.6
Mn^{52}		9.25
Mn^{56}		9.45
Co^{58}		8.57

It is seen that none of the crystals has a concentration of 15% but are all closely the same as the concentration of the solution. This is probably due to the fact that the alignment crystals were grown from larger quantities of solution than those used to give figure 2. This means the $T-T^*$ correlation cannot be used but since all the crystals have approximately the same concentration a temperature scale derived from the alignment of Co^{58} (Chapter 6) has been used.

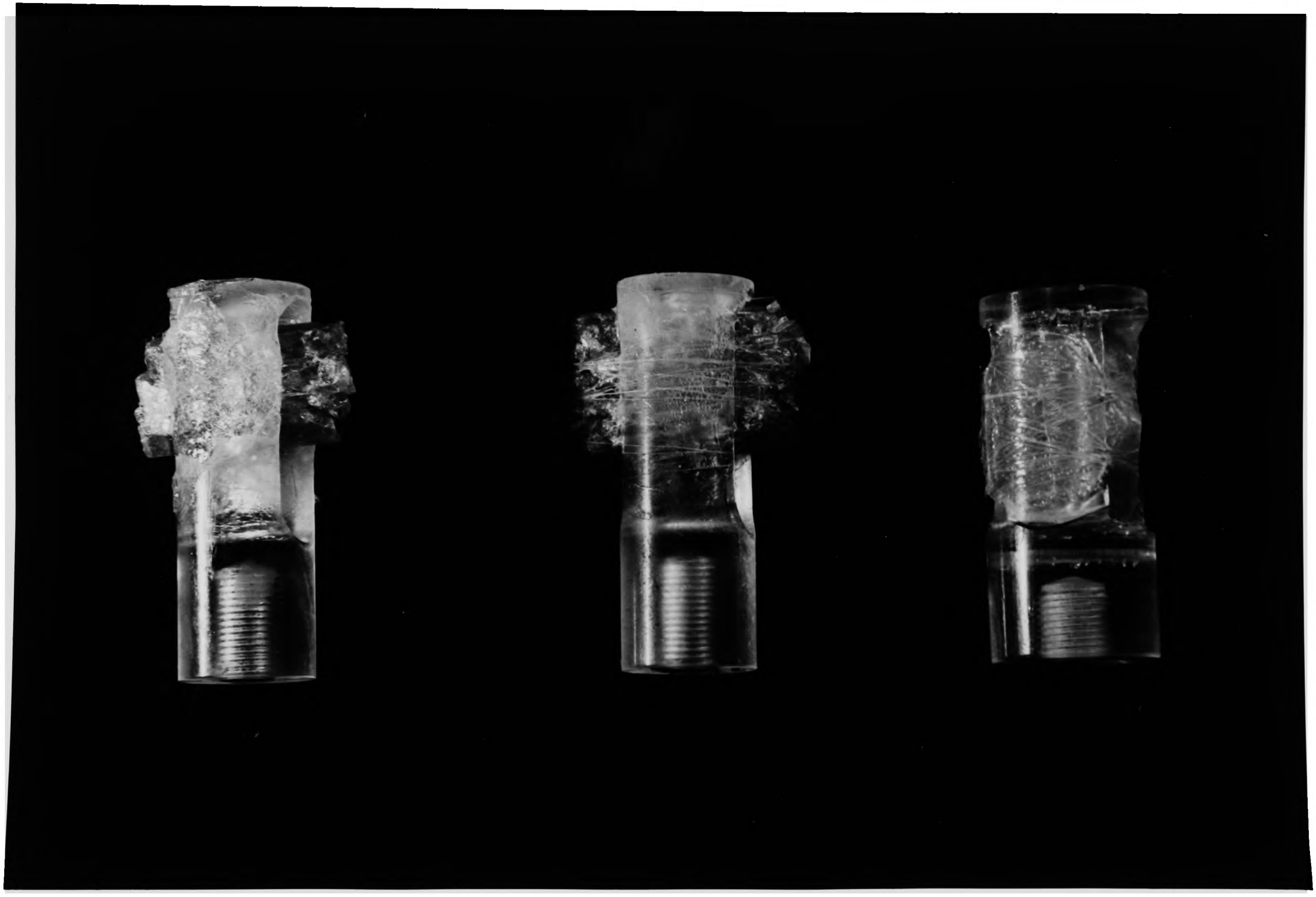


Figure 3

4. The Low Temperature Apparatus

The general layout and details of the "tail" of the apparatus are illustrated in the accompanying figures (4a,b,c).

The specimen is held in a perspex holder by perspex cement and fine nylon thread so that it is in no danger of being displaced. The holder is supported from a rigid glass spill in the inner jacket of the apparatus, which can be filled with helium exchange gas. The crystal axis is made horizontal, so that the geometry for both counters is similar, and is made to lie along a line marked on the magnet top which also defines the position of the axial counter. A pill of Manganese ammonium sulphate is pressed around the spill several centimetres away from the specimen. On cooling this pill reaches temperatures of the order of $0.1^{\circ}K$ and so acts as a heat sink for heat conducted down the spill and also helps to adsorb any remaining traces of exchange gas. The position of this pill is fixed so that it can be demagnetised simultaneously with the specimen and yet be far enough away not to interfere with the susceptibility measurements.

The inner space is surrounded by a bath of liquid helium kept at $\sim 1^{\circ}K$ by continual pumping. The outer jacket encloses a vacuum space for insulation and is itself kept at the temperature of liquid hydrogen contained in the metal dewar vessel.

Temperature changes are measured by the change in the mutual inductance of a coil produced by the change of the susceptibility of the specimen with temperature on the assumption that Curies' Law, $\chi = \frac{C}{T-\Delta}$ holds. The measuring coil is wound on a former which slides onto

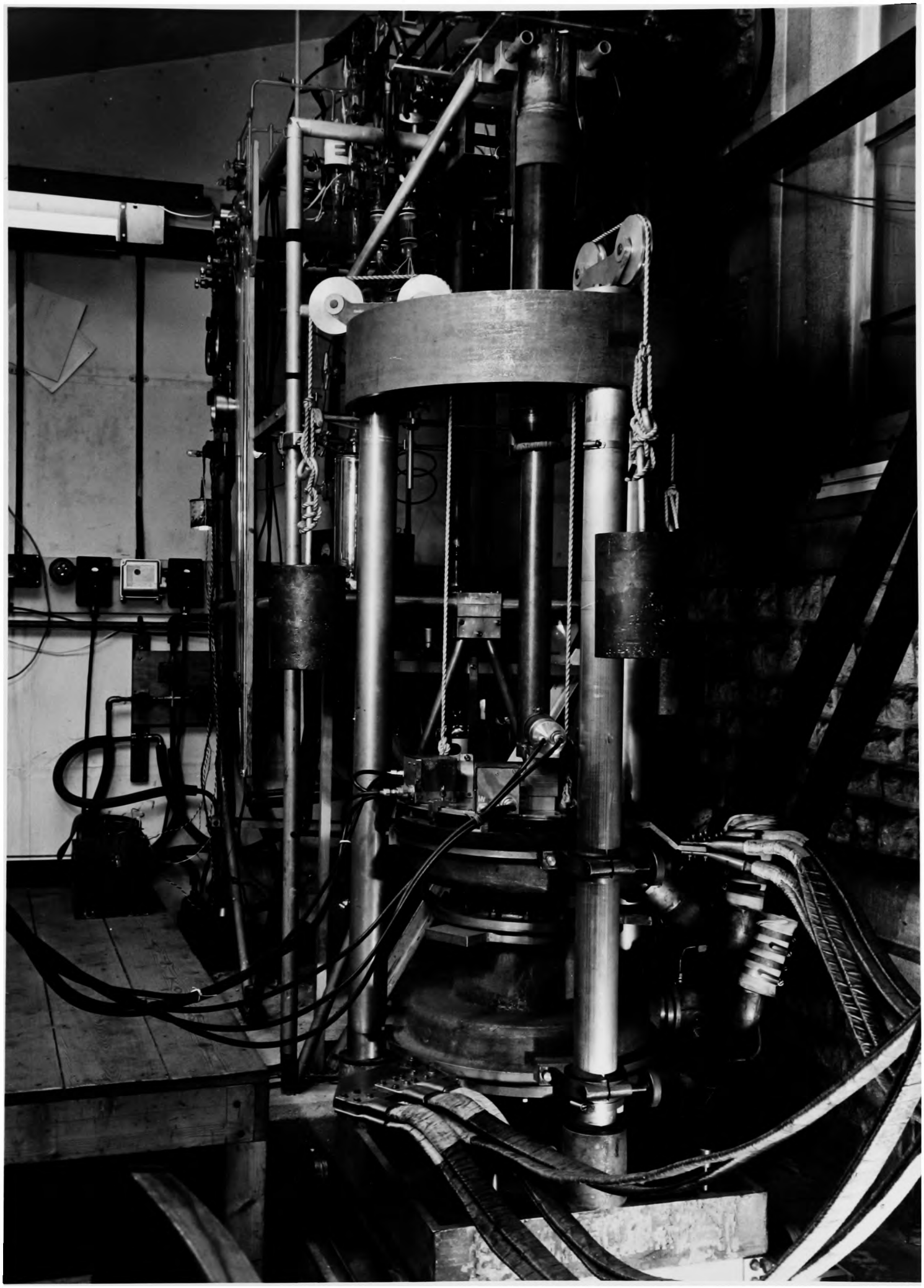


Figure 4a

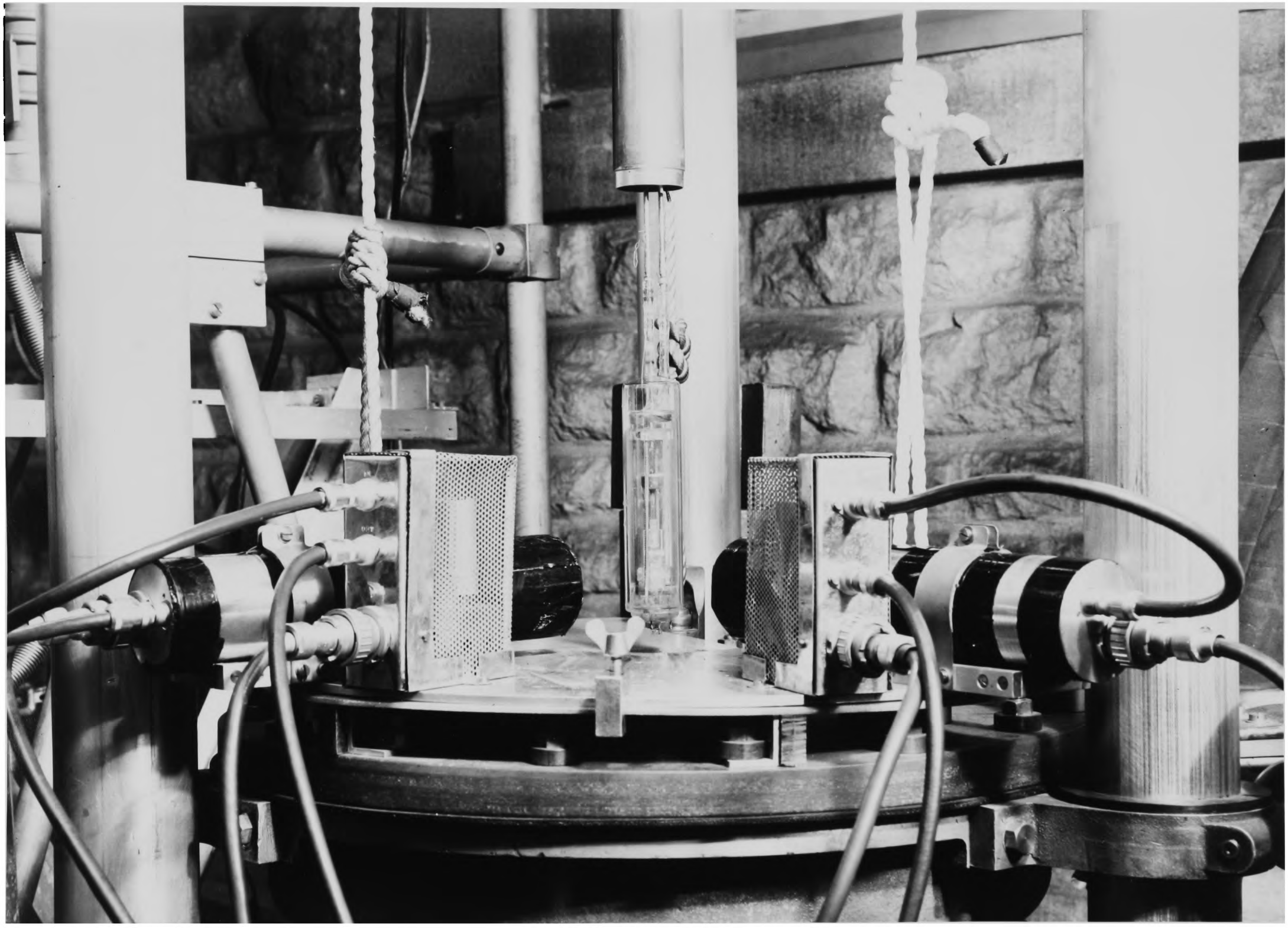


Figure 4b

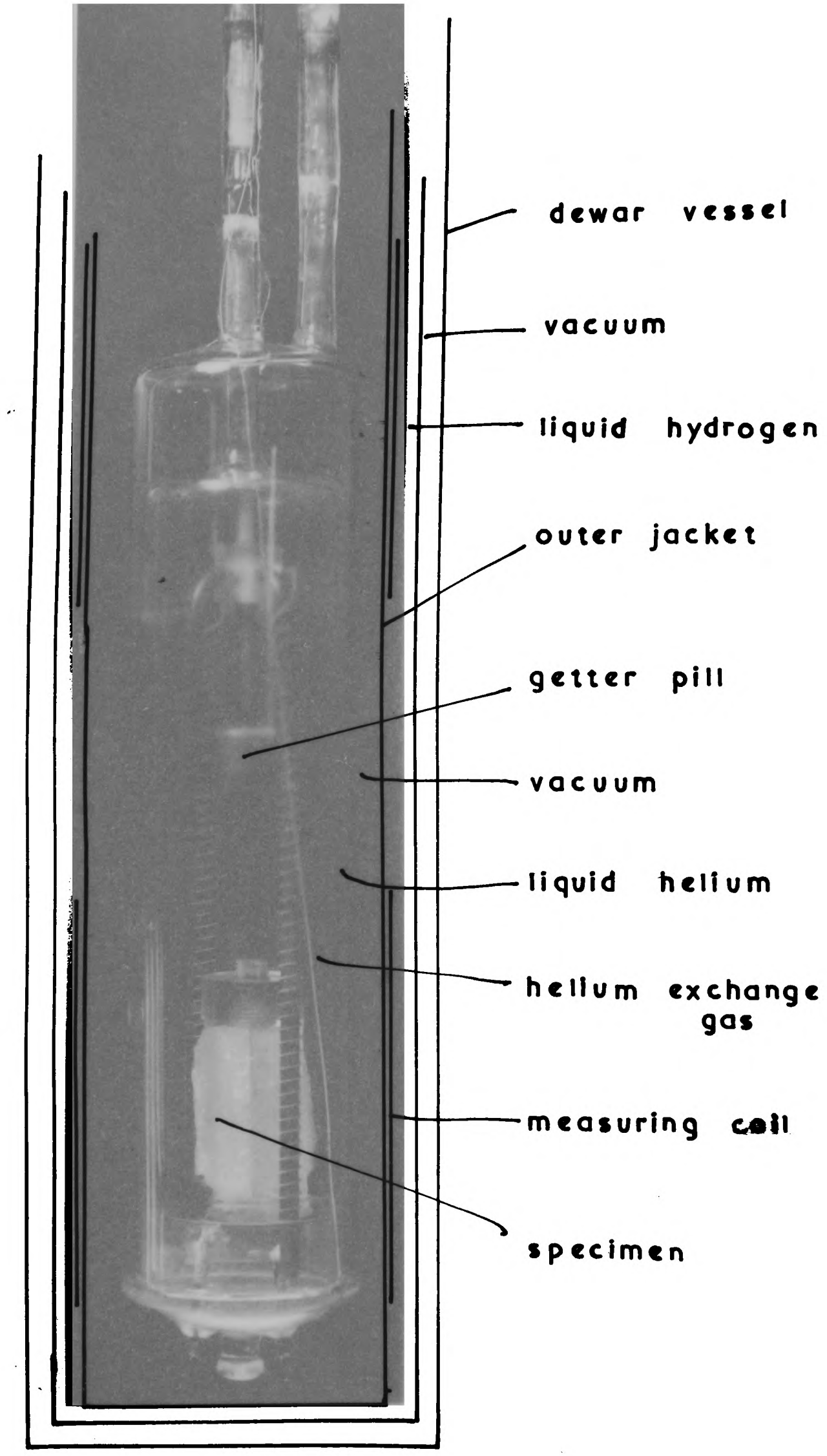

dewar vessel
vacuum
liquid hydrogen
outer jacket
getter pill
vacuum
liquid helium
helium exchange gas
measuring coil
specimen

Figure 4c

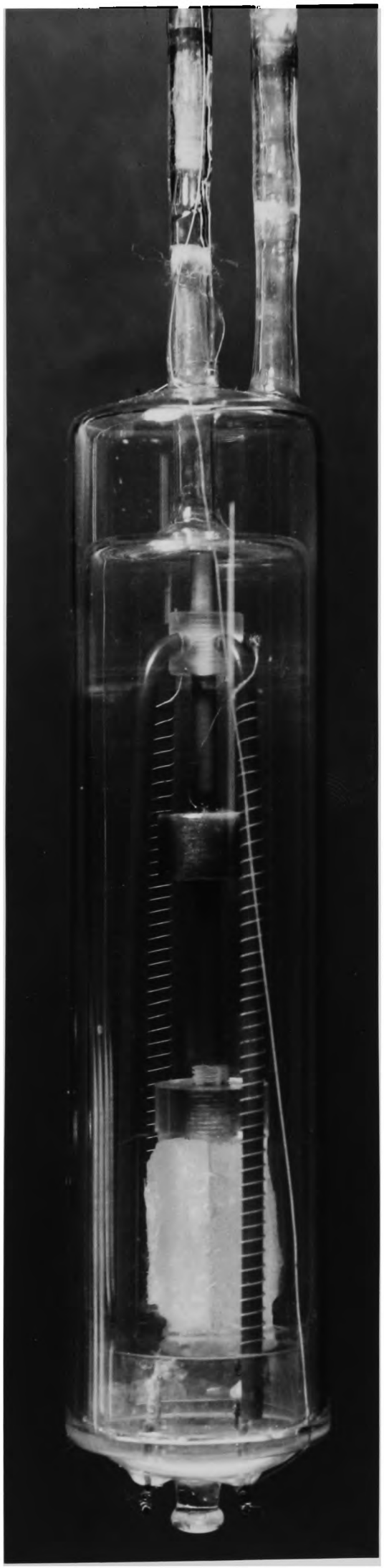


Figure 4c

the outer jacket. It consists of two primary windings in the same sense and two secondary windings wound in opposite senses. A calibration is made between 4°K and 1°K against the vapour pressure of liquid helium; Curies' Law is valid for this region. The upper half of the coil compensates for such things as the susceptibility of the cryostat and the "getter" pill is placed in the null portion of the sensitivity curve so its susceptibility should not interfere with the measurements.

The change in mutual inductance is measured by the throw of a ballistic galvanometer, , which is proportional to the susceptibility. Thus $\delta \propto \frac{C}{T^*-\Delta}$ and T^*, the magnetic temperature, can be found from the calibration graph. In calculating the absolute temperature, T, from T^*, one must allow for the demagnetising effect of the specimen and this is difficult when the specimens are not ellipsoidal. Further the susceptibility, and hence T^*, at a given temperature will depend on the composition of a mixed crystal.

The magnetising field is provided by a Bitter type, air-cored, water-cooled solenoid which has been described by Milner (1957). Current is taken from a 2 megawatt generator and fields of up to 35 kilo oersted have been used.

5. Nuclear Physics Apparatus

The gamma-rays from the aligned nuclei are detected by scintillation counters. 2" x 2" cylindrical sodium iodide phosphors are used to give a linear response to energy; they are held in optical contact

with photomultipliers (EMI type 6097F) using a clear silicone grease. Crystals of fairly good resolution are required and in practice those used have given about 9% for the 0.661 Mev photopeak of Cs^{137}. The electrons may be deviated from their path between the dynodes by stray magnetic fields causing a variable loss in gain. In order to reduce the possibility of this happening the photomultiplier cases were made from mu-metal.

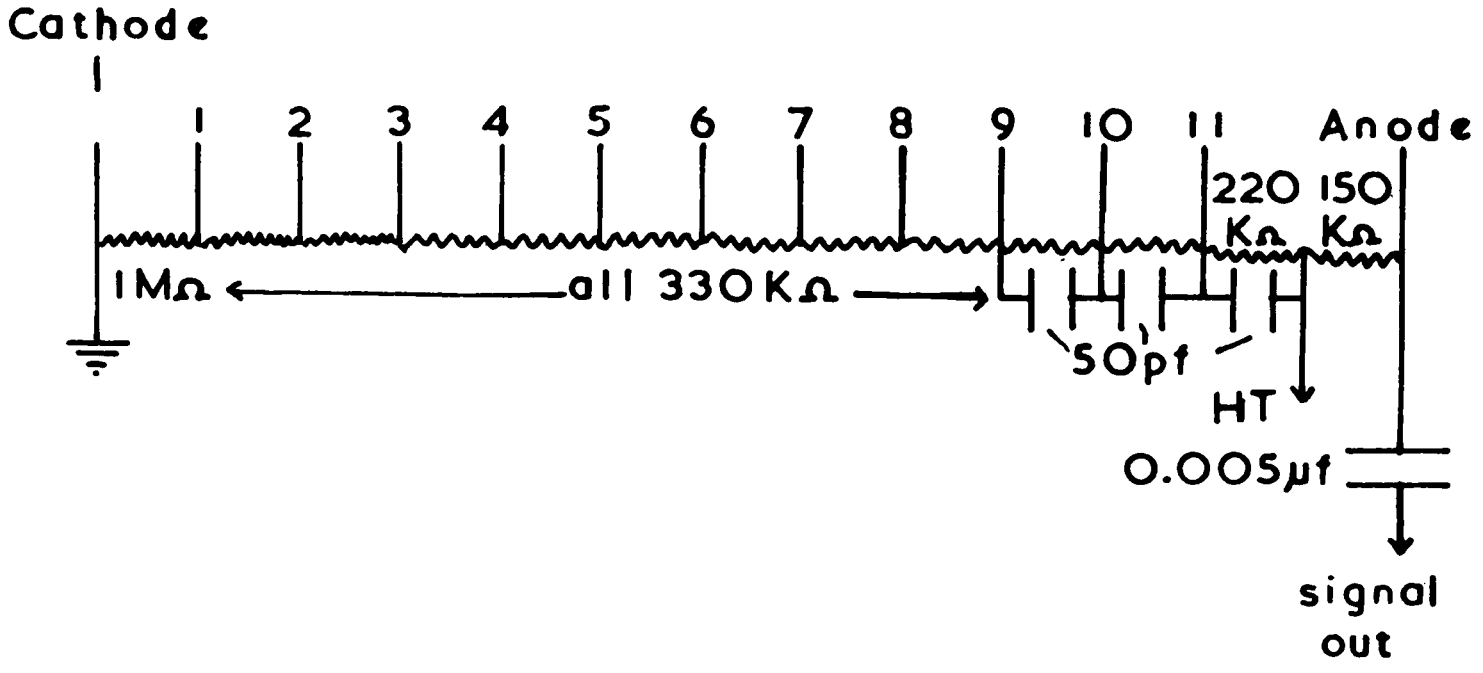
Both counters are mounted on one "dural" plate to facilitate handling, with small pegs for immediate and accurate location. With respect to the cryostat. The power supplies are obtained from a commercial 2kV power unit, the manufacturers' specifications giving a long term overall stability of ± 2% and a short term stability of about ½%. Tests over a period of two or three hours using a standard potentiometer show that the stability is within 1 in 10,000. The high voltage supplies are fed to the photomultipliers through a potential dividing unit enabling the voltage to be varied between 500 and 2000 volts. The interdynode voltages are maintained using a chain of high stability resistors (figure 5). The output pulse from the counter is passed through a cathode follower before being carried to the main amplifier. Amplifier stability is governed by neon stabilisation and feedback and gives a gain stability of ½% for a 10% mains variation. The long term stability due to all causes is not worse than 1%. Additional precautions are taken by passing the mains supplies for all the electronic equipment through an electronically controlled variac limiting the variations to about ½%. By these various measures

the overall gain of the counting equipment can be kept very steady so that the principal error in the counting rate arises from the statistical decay of the source.

The proportional output of the amplifier is fed into a pair of discriminators, each followed by a pair of scalers in tandem. The settings of the discriminators was such that the scalers recorded the total number of counts just above and just below the photopeak of the gamma ray being studied. This method allows the anisotropy of both sets of pulses to be calculated and enables corrections for other gamma rays of higher energy to be made directly. A block diagram of the apparatus is drawn in Figure 6.

Tests were carried out before each experiment to see that there are no fluctuations or drifts in the counting rate. These stability tests were made after the equipment had been adjusted for the experiment and took the form of a long series of counts. These were divided up into sets of ten for which the standard deviation is approximately $\sigma = \frac{\text{range}}{\sqrt{10}}$ and this can be compared with the statistical error, $\sqrt{N}$. The comparison of mean values for succeeding sets gives the overall stability.

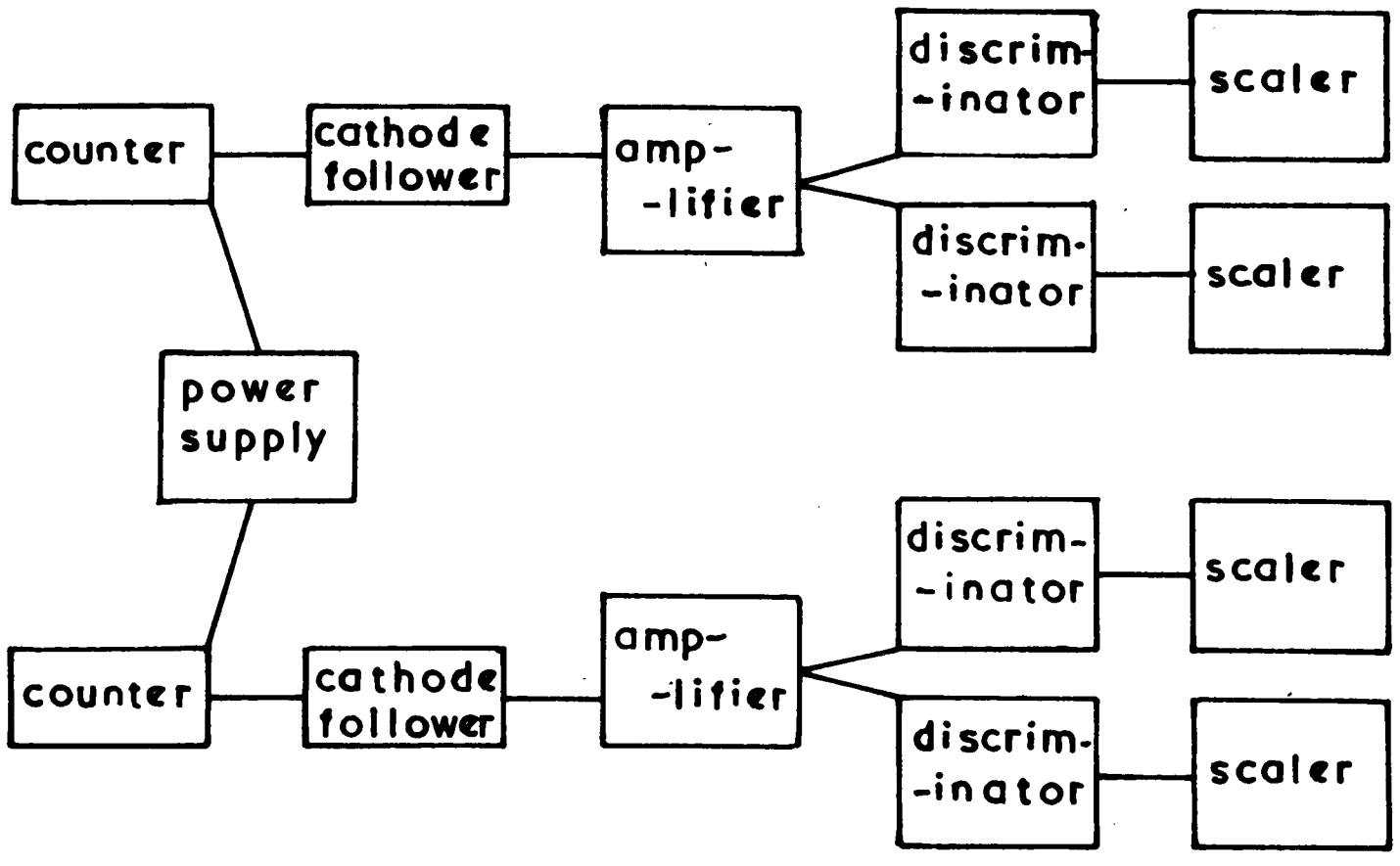
The counters are adjusted so that each has approximately the same gain and the source counter distance will be approximately the same for equal counting rates on both counters. This means that the same corrections are applicable and therefore the normalised intensities of the two counters carry equal weight.



Photomultiplier Circuit

Figure 5

Figure 6



Block Diagram of Electronic Apparatus

6. The experimental procedure

The magnet is raised round the "tail" of the dewar so that the crystal is in the maximum field position. The specimen is magnetised with a pressure of a few millimicrons of mercury of exchange gas in the inner jacket to conduct away the heat of magnetisation to the liquid helium bath. The exchange gas is gradually pumped off until the remaining gas exerts a pressure of only a few hundredths of a millimicron of mercury, the pump is switched off by a magnetic tap and the specimen demagnetised reducing the field over a period of about 1 minute. Both specimen and "getter" cool and the last traces of exchange gas are adsorbed onto their surfaces, thus further ensuring the isolation of the specimen.

The current having been reduced to zero and the circuit broken, the magnet is lowered so that the top provides a table for the counters. The counter plate has locating lugs so that the setting is quick and accurate, the whole procedure requiring only 10-15 seconds. Counts are taken for 20 or 40 second periods, using automatic timing, for a period of several minutes as the crystal warms up.

Measurements of the susceptibility are taken every half minute during this period, using a ballistic galvanometer.

On warming up, it is possible that temperature inhomogeneities may arise because the temperature of the interior of the crystal lags behind that of the surface because of the poor conductivity so counting is usually stopped after about 5 minutes and the crystal is warmed up artificially to 1°K. by passing a small current through a winding round

the "getter" pill. This causes the release of enough exchange gas to provide thermal contact with the helium bath and avoids the necessity of putting in more gas which only has to be pumped out next time.

Another set of counts are then taken and used to normalise the previous set since, at $1^{o}K$, $kT \gg A$ and the angular distribution will be isotropic. Hence $I(\theta) = \frac{N(\text{cold})}{N(1^{o}K)}$. Repeat demagnetisations from different initial values of H/T allow the whole range of temperature to be covered. If one run gives readings which overlap the next, forming a continuous curve, then no serious temperature inhomogeneities can have arisen. If inhomogeneities were present, then both the anisotropy and magnetic temperature observed will be averages over small temperature ranges. Although both ϵ and $\delta(T^{*})$ are functions of the absolute temperature their averages will not necessarily represent the same average value of $\frac{1}{T}$ because the dependence on $\frac{1}{T}$ is different in the two cases. The effect is particularly important if the warming up rate is too rapid and then the anisotropy at a given temperature depends on whether the point occurs at the beginning of one run or the end of another from a larger field.

Demagnetisations from very low fields (i.e. 50 amps current), when no cooling would be expected, serve as a check that drifts and fluctuations in the counting rate are not introducing a spurious effect since the counting rate should be isotropic throughout. Inspection of the "warm-readings" also checks the behaviour of the equipment since, within a run the warm readings should follow the statistical decay of the source, and any drift will show up as a change in the

mean value from run to run.

7. Treatment of data

Normally the first step is to find $I(\theta)$ by normalising the counting rates to those at 1°K but it may be necessary to make corrections to the raw data before this can be done.

7a. A Composite Spectrum

In many cases the photopeak of the observed gamma ray is superimposed on the Compton scattering spectrum of a gamma ray of higher energy. If this latter gamma ray has the same anisotropy as the other, then there is no correction to make. If the anisotropies are different then it is necessary to find the relative amount of each gamma ray in the counting channel and subtract those counts due to the high energy gamma ray before calculating $I(\theta)$.

Such a correction is made for Mn^{56} and Mn^{54} in the presence of Co^{60} and the details are dealt with in the respective chapters.

7b. Resolving time of apparatus

If high counting rates are used the resolving time of the scalers may reduce the observed effect. The number of counts lost is given by $N2\tau$ where N is the counting rate and τ the resolving time. The latter was found by the drop in counting rate when two separate sources were measured together compared with the sum of the independently measured counting rates from the same position. τ is of the order of 5μ s, and N was frequently of the order of 2,000 counts per sec. giving $2\tau N = 0.02$ a number which is quite negligible.

7c. Finite aperture of the counters

Because of the finite aperture of the counters $I(\theta)$ will be an average over a small range of θ . The correction necessary for this can be calculated for the counters used, which have axial symmetry, and has been considered by Rose (1953).

The true angular distribution is given by $I(\theta) = \sum_\nu A_\nu P_\nu(\cos\theta)$ and the counter geometry is as shown in figure 7 for a counter, i.e. NaI crystal, which is a right circular cylinder with its base oriented toward a point source. In general the observed intensity can be written $\overline{I(\theta)} = \sum_\nu g_\nu A_\nu P_\nu(\cos\theta)$ where g_ν is an attenuating factor which has to be found.

Rose considers the case where the absorption of the radiation by the counters depends on the angle α, i.e. on the path length in the crystal. He finds $g_\nu = 2\pi \int_0^\theta P_\nu(\cos\alpha)\,\epsilon(\alpha)\,d(\cos\alpha)$

where $\epsilon(\alpha) = 1 - \exp(-\gamma x(\alpha))$ is the detection "efficiency" and is the distance traversed by the radiation in the crystal at angle α . A good approximation is obtained if $\epsilon(\alpha)$ is taken to be uniform over the face of the crystal and putting $\tan\alpha = \frac{r}{l + t/2}$, then $\epsilon(\alpha) = 1 \quad \alpha \leq \alpha_0$
$= 0 \quad \alpha > \alpha_0$

so in fact $g_\nu = 2\pi \int_0^{\alpha_0} P_\nu(\cos\alpha)\,d(\cos\alpha)$

This integral is much simpler to evaluate and gives $g_0 = 2\pi(\cos\alpha_0 - 1)$; so redefining g_ν to give $g_0 = 1$ we have $g_\nu = \frac{\int_0^{\alpha} P_\nu(\cos\alpha)\,d(\cos\alpha)}{\int_0^{\alpha} d(\cos\alpha)}$ and

$$g_2 = \frac{\cos\alpha_0(1+\cos\alpha_0)}{2} \quad ; \quad g_4 = \frac{g_2}{4}(7\cos^2\alpha_0 - 3)$$

When making this correction it is better to find the theoretical

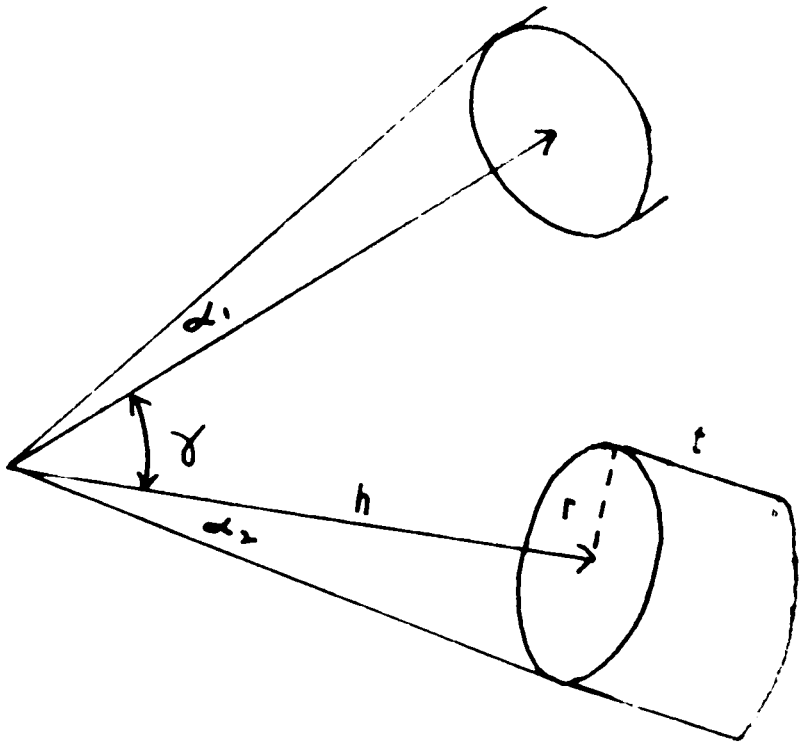
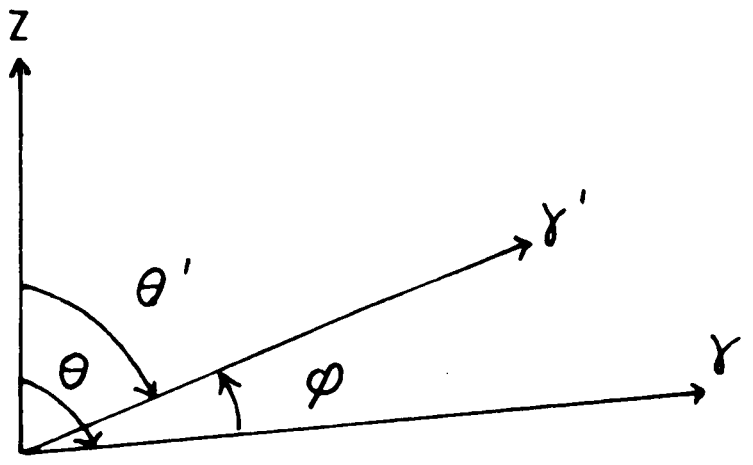


Figure 7



Counter Geometry for

Aperture and Scattering Corrections

Figure 8

distribution $I(\theta) = \sum_\nu g_\nu A_\nu P_\nu(\cos\theta)$ and compare it with that observed than to find A_ν from the observed values and recalculate $I(\theta)$ from the adjusted values of A_ν.

7d. Scattering

Since the radioactive source is enclosed in the cryogenic apparatus, it is possible for photons not originally emitted within the solid angle defined in the previous section to reach the counter by scattering in the walls of the apparatus. Attenuation coefficients can be obtained in a similar manner but one must first make some approximations in order to keep the problem within bounds.

In practice the various jackets of the apparatus form concentric cylinders about the source perpendicular to the plane of the counters. Let us assume that these can be replaced by a spherical scatterer of the same total thickness.

Now, if the scatterer is immediately in front of the counter the only effect would be a small edge effect. On the other hand, if the scatterer was immediately surrounding the source with the counter at a comparatively great distance, then we need only consider scattering of photons through such angles that they are parallel to the counter axis.

In this approximation the average intensity distribution outside the scatter can be split into two parts, the direct flux allowing for absorption and the scattered flux. Simple scattering is assumed. Thus $\overline{I(\Theta)} = I(\Theta)e^{-\mu t} + \int I(\theta')N\sigma(\theta'-\theta)d\Omega'$ where the angles are defined in

figure 8, N is the number of scattering centres and σ the cross-section for scattering per scattering centre.

Then $I(\theta') = \sum_\nu A_\nu P_\nu(\cos\theta')$

$= \sum_\nu A_\nu \sum_q Y_\nu^q(z) Y_\nu^q(\theta')^* \frac{4\pi}{2\nu+1}$

with respect to γ as the new z axis. $d\Omega' = d\psi \sin\phi\, d\phi$. ψ being azimuthal of γ' about γ. $\bar{I}_s = N \int I(\theta')\sigma(\phi)\, d\psi \sin\phi\, d\phi$

$= \frac{4\pi}{2\nu+1} \sum_{\nu q} N A_\nu Y_\nu^q(z) \int_{\phi=0}^{\phi=\phi_0} Y_\nu^{o}(\phi)^* \sigma(\phi) \sin\phi\, d\phi$. ϕ_0 being the maximum angle through which a photon can be scattered with corresponding energy degredation and still operate the discriminator. The properties of spherical harmonics then give

$\bar{I}_s = 2\pi N \sum A_\nu P_\nu(\cos\theta) \int_0^{\phi_0} P_\nu(\cos\phi)\sigma(\phi)\, d(\cos\phi)$

$= \sum k_\nu A_\nu P_\nu(\cos\theta)$ where $k_\nu = 2\pi N \int_0^{\phi_0} P_\nu(\cos\phi)\sigma(\phi)\, d(\cos\phi)$

Thus, $\overline{I(\theta)} = \sum_\nu \bar{A}_\nu P_\nu(\cos\theta)$ with $\bar{A}_\nu = \left[e^{-\mu t} + h_\nu\right] A_\nu$

$\overline{I(\theta)}$ is the actual intensity along θ outside the apparatus and observation averages this over the counter solid angle Ω_c about $\theta = \theta_0$.

Thus $\overline{\overline{I(\theta)}} = \int_{\Omega_c} \bar{I}(\theta)\epsilon(\theta)\, d\Omega_c = \sum_\nu \bar{\bar{g}}_\nu A_\nu P_\nu(\cos\theta_0)$

with $\epsilon(\theta)$ as the counter efficiency as in the previous section. We have now $\bar{\bar{g}}_\nu = \bar{g}_\nu\, g_\nu(\text{uniform})$

$= (e^{-\mu t} + h_\nu) \dfrac{\int_0^{\alpha_0} P_\nu(\cos\alpha)\, d(\cos\alpha)}{\int_0^{\alpha_0} d(\cos\alpha)}$

h_ν can be evaluated by putting $N = \frac{\rho t Z}{\bar{A}} L_0$ electrons/cm^2. where ρ = density of scatter, t = thickness of scatterer, Z = the atomic number and A the atomic weight of the scatterer and L_0 is Avogadros number. ϕ_0 is found from $E' = \frac{E}{1+\alpha(1-\cos\phi)}$, $\alpha = \frac{E}{m_0 c^2}$ where E is photon energy and

E′ the lower limit accepted by the discriminator. ϕ_0 is of the order of 30° for the gamma rays considered in this work and for this range $\sigma(\phi)$, which is essentially the Klein Nishina differential cross-section, can be approximated by the form a+b cosϕ where $a+b = \sigma_0 = 8 \times 10^{-26}$ cm^2/electron.

Calculation of h_ν for Mn^{54} with E = 0.840 Mev, $\phi_0 = 30°$ gives $h_0 = 0.0406$, $h_2 = 0.0331$, $h_4 = 0.0210$; $e^{-\mu t} = 0.834$ with $\mu = 0.526 \text{cm}^{-1}$ for copper and the wall thickness, t = 0.35 cms. Hence $g_0 = (0.834 + 0.0406) = 0.8756$ and as $g_0 = 1$, $\overline{\overline{g}}_0 = 0.8746$

With a further renormalisation to give $\overline{\overline{g}}_0 = 1$ we have

$$\overline{g}_2 = 0.8671, \quad \overline{\overline{g}}_2 = \frac{\overline{g}_2 g_2}{\overline{\overline{g}}_0} = \frac{0.8671 \times 0.95}{0.8764} = 0.942 = 0.992\, g_2$$

$$\overline{g}_4 = 0.855 \quad \overline{\overline{g}}_4 = 0.819 = 0.980 \quad \text{for } g_4 = 0.836.$$

For the experimental conditions where the source, scatterer and scatterer-counter distances are comparable the evaluation of the attenuation parameters becomes more difficult but these approximations indicate the order of magnitude of the effect. In most cases only the correction for finite aperture has been made since this will represent the conditions to within the experimental error.

7e. Counting rate drift

Should the counting rate drift the anisotropy observed will be different from the true effect. For instance, if the equatorial counting rate decreases with time then if I(90°) is greater than 1 the drift enhances the effect. A drift upward would lead to a reduced effect. Similarly a downward drift on the axial would reduce the effect and an upward drift increase it. Inspection of the isotropic

counting rate will show if there is a systematic effect outside the statistical fluctuation and corrections could be made by extrapolating the warm counting rate back to the time of the cold reading and normalising to the new value.

8. The deduction of information

8a. From the observed intensities

Having made the various corrections to the experimental data, one can proceed to compare it with calculated values in order to derive new information.

The observed quantities are the gamma ray intensities along the crystal axis $I(0^\circ)$ and in the equatorial plane $I(90^\circ)$. Theoretically these are given by

$$I(0^\circ) = 1 + B_2U_2F_2 + B_4U_4F_4$$

$$I(90^\circ) = 1 - \tfrac{1}{2}B_2U_2F_2 + \tfrac{3}{8}B_4U_4F_4$$ and as they are both observed simultaneously, they involve the same values of B_2 and B_4. It is useful, therefore, to plot $I(0^\circ)$ as a function of $I(90^\circ)$ since this does not require a knowledge of the temperature or any other measured parameter and it is not usually very sensitive to the magnetic moment because the orientation parameters are involved in both coordinates. If there are no terms in $P_4(\cos\theta)$, i.e. if $B_4U_4F_4=0$, then the graph will be a straight line with a slope 2:1. Hence if this is not the case the radiation must contain a quadrupole (or higher) component. The ~~mfk~~ fact that this curve is insensitive to the alignment parameters means that its shape is closely the same for all spin sequences for which $U_{22}F_{22}$ and $U_{44}F_{44}$ have the same sign and so will reveal defects in

timing, drift and general electronic defects which all cause displacement laterally from the calculated curve. If the agreement is reasonable and the value of A is known, one can deduce the temperature reached for a given point by its distance along the curve.

In the special case where the beta transition is of the type $I \rightarrow I$, and I is small, this plot is particularly sensitive to the Fermi ($j=0$); Gamow-Teller ($j=1$) mixture through the value of U_4 and can be used to find the ratio of the two components (Co^{58}). For Co^{58} $U_2(F) = 1.0$, $U_2(G\text{-}T) = 0.5$ and $U_4(F) = 1.0$ but $U_4(G\text{-}T) = -0.6665$ so that while $I(0^\circ)$ for a pure Fermi transition tends to zero, it never falls below 0.822 for pure Gamow-Teller. $I(90^\circ)$ is much less sensitive.

8b. <u>The anisotropy</u>

A more generally useful parameter is the anisotropy, $\epsilon = \frac{I(90^\circ) - I(0^\circ)}{I(90^\circ)}$, which can be plotted as a function of temperature. The anisotropy does not reveal the presence of $P_4(\cos\theta)$ terms but depends more strongly on the magnetic moment, through the orientation parameters B_2, B_4, and on the decay scheme. Its drawback is the need for a knowledge of the absolute temperature. The sign of ϵ is a guide to the multipolarity of the gamma transitions being positive for a pure quadrupole transition and negative for a pure dipole. Its saturation value, i.e. for $\frac{1}{T} \rightarrow \infty$, is independent of the magnetic moment since $B_\nu \rightarrow (2\nu+1)^{\frac{1}{2}} C^{II\nu}_{IL0}$ and depends only on the nuclear spin.

If the temperature scale and nuclear decay scheme are known the

magnetic moment of the parent nucleus can be found by fitting the experimental points to a series of theoretical curves based on the values of B_ν calculated for possible values of moment. When the decay scheme is not known completely, it is possible to eliminate some of the possible sequences from the sign and magnitude of the anisotropy but nuclear orientation is always dependent on the information provided by angular correlation and other studies.

8c. From the correlation parameters

Sometimes the analysis of the data to give the coefficients $A_\nu = B_\nu U_\nu F_\nu$ is useful. These can be found by solving $I(0^\circ)$ and $I(90^\circ)$ as simultaneous equations, thus $I(0^\circ) = 1 + A_2 + A_4$, $I(90^\circ) = 1 - \frac{1}{2}A_2 + \frac{3}{8}A_4$ giving, $A_2 = \frac{1}{7}\left[3I(0^\circ) - 8I(90^\circ) + 5\right]$, $A_4 = \frac{4}{7}\left[I(0^\circ) + 2I(90^\circ) - 3\right]$.

For a mixed gamma ray F_ν is a function of the mixing ratio, δ, so if $B_\nu U_\nu$ are known, δ can be found. On the other hand, if there are two gamma rays from the same nucleus, the parameters B_2, B_4 will be common factors so the ratio A (1):A (2) will be temperature independent, and depend only on the decay scheme. Thus it may be possible to deduce spins and multipolarities for the decay. These ratios may be sensitive functions of δ particularly if one gamma-ray is a pure transition and for this case it is possible to deduce δ without a knowledge of either temperature or nuclear moment (Mn^{56}).

8d. The derivation of a temperature scale

Usually the measured magnetic temperature T^* is correlated with the absolute temperature from the results of a separate thermodynamic measurement. However, for nickel-zinc fluosilicate such a correlation

is dependent on the Ni:Zn ratio and at present no applicable correlation is available. This has led to the use of a temperature scale deduced from a nuclear alignment experiment.

Consider a radioisotope such as Co^{58} or Co^{60} for which all the nuclear parameters are known. The magnetic properties of the Co^{++} ion in the fluosilicate are known so if these isotopes are aligned in this salt a temperature scale can be found by a comparison of the experimental and theoretical anisotropies.

Experimentally ϵ is measured as a function of the galvanometer deflection δ, while theoretically it is known as a function of $\frac{1}{T}$ so a $\delta, \frac{1}{T}$ relationship can be found directly. However, δ depends on minor experimental details and is valid only within a particular experiment but the value of H/T (initial) used is a measure of the entropy removed from a specimen of given shape and concentration. Heating up effects can be eliminated by plotting ϵ as a function of time, t, after demagnetisation and extrapolating the curve back to $t = 0$, giving a value of $\epsilon_{t=0}$ for each H/T(initial) used. From this a relation between H/T(initial) and $\frac{1}{T}$ can be obtained which is in effect a temperature scale for all similar crystals. Such a relation has been derived from the alignment of Co^{58} and used to interpret the other experiments described in this thesis.

8e. Other uses of nuclear alignment

So far we have only considered the possibility of obtaining nuclear information but it must be remembered that the orientation parameters depend on the properties of the crystal.

Deductions of the hyperfine couplings have been made for the case of Co^{60} aligned in cobalt metal (Scurlock 1957) and in Chapter 5 of this thesis it is briefly indicated how it may be possible to obtain information about the solid state through radiation damage and subsequent annealing.

CHAPTER 3

THE MAGNETIC MOMENT OF MANGANESE 54

1. The Introduction

The simple decay scheme of Mn^{54} and the magnetic properties of the Mn^{++} ion makes this isotope particularly suitable for study by the methods of the nuclear orientation.

It was first studied using these methods by Grace et al (1954) and Bishop et al (1954), who measured the anisotropy and the plane polarisation of the gamma rays respectively for both aligned and polarised nuclei. For these experiments manganese was included in a crystal of cerium magnesium nitrate. The dependence of the anisotropy on temperature for aligned nuclei differed markedly from what one would expect and although the dependence for polarised nuclei had more or less the expected shape, no complete fit to theory could be made. The sign and magnitude of the anisotropy and the direction of the plane polarisation of the gamma-ray for polarised nuclei led to the determination spin and parity sequence but it was not possible to deduce a value for the magnetic moment of the ground state of Mn^{54}. The unexpected behaviour of the anisotropy was believed to result from the nature of crystalline environment and this chapter describes a new attempt to measure the magnetic moment using nickel fluosilicate. Since fluosilicates had not been used previously for nuclear alignment experiments, this work also served as an investigation of the usefulness of this environment.

2. The decay scheme

Mn^{54} decays by electron capture to the first excited state of Cr^{54} (Deutsch & Elliott 1944), the half life being 291 days (Backofen & Herber 1955). A study of the X-rays (Deutsch & Elliott) emitted following the capture process indicate that the captured electrons are from the K-shell and coincidences between these and the gamma rays suggest that the lifetime of the excited state is less than 10^{-6} sec.; the resolving time of the equipment will be of this order and delay longer than this would mean that all coincidences observed were random. Transition probabilities calculated using the relations given by Mąkowski (1955) are shown in Table 1.

TABLE 1

Transition probabilities on a single particle model

$A = 54$, $E(\gamma) = 0.84$ Mev.

Transition	Probability sec^{-1}	Lifetime sec
E1	12.65×10^{14}	0.79×10^{-15}
M1	1.65×10^{13}	0.60×10^{-13}
E2	1.36×10^{10}	0.73×10^{-10}
M2	7.14×10^{8}	0.14×10^{-8}
E3	0.94×10^{5}	0.11×10^{-4}
M3	1.07×10^{4}	0.93×10^{-4}

It can be seen that the gamma ray must be either dipole or quadrupole. On the basis of its energy (0.5h Mev) and half-life, the beta transition has a log ft. value of 6.1 suggesting that it is

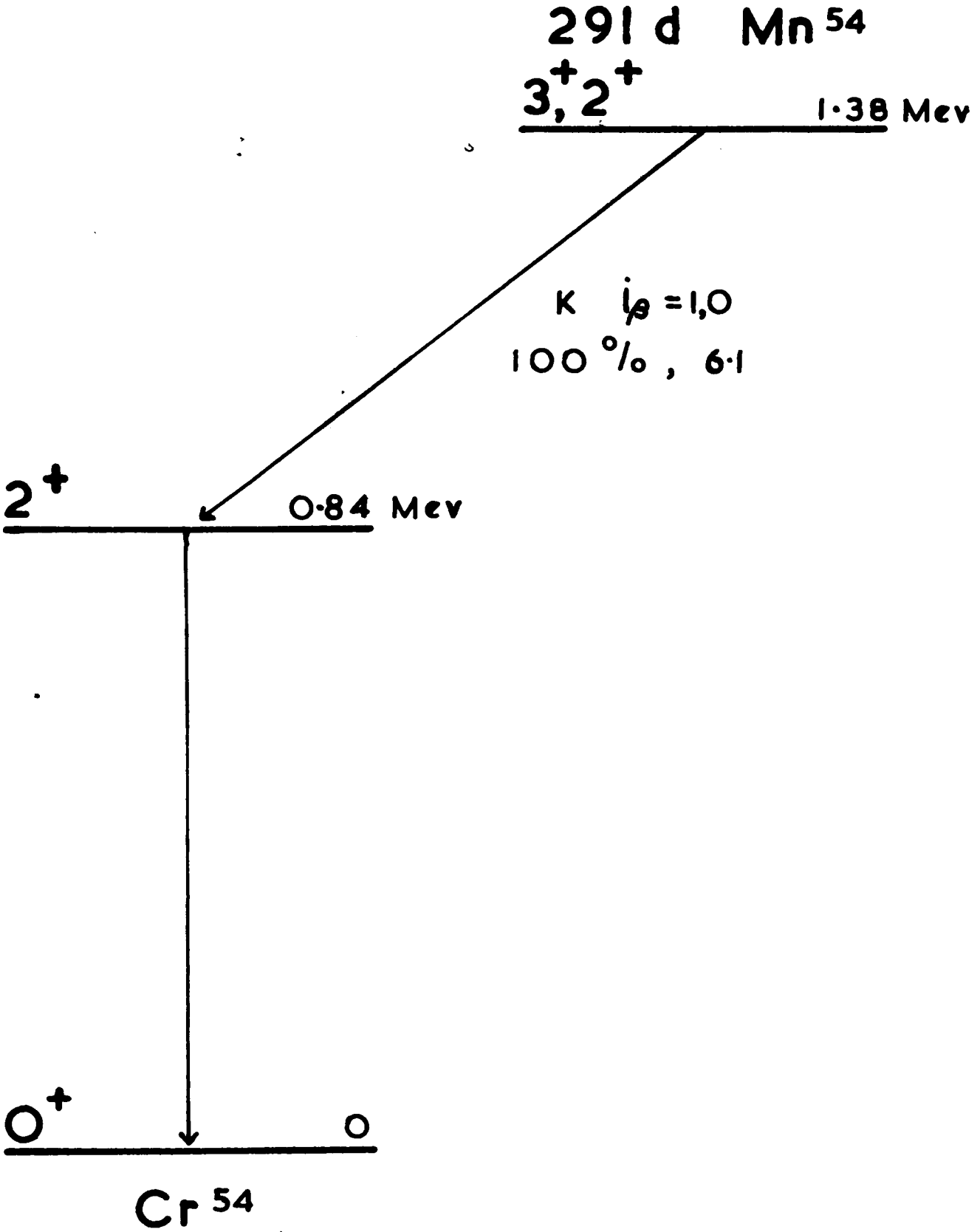


Figure 1

allowed or first forbidden involving a spin change of $\Delta I = 0$ or 1, (Nordheim, 1951). Since Cr^{54} is an even-even nucleus with spin 0 the excited state must have a spin of 1 or 2 and the ground state of Mn^{54} can be 1, 2 or 3.

The sign and magnitude of the anisotropy of the gamma ray from polarised Mn^{54} (Grace et al) shows that it cannot be dipole (see next section) since anisotropies of up to 90% were observed. The K-capture transition must introduce little or no disorientation, implying that $i_\beta = |I_1 - I_2|$. Thus if $I_1 = 3$, $i_\beta = 1$ and if $I_1 = 2$, $i_\beta = 0$. The plane polarisation of the gamma ray (Bishop et al) shows it to be an electric transition so the parity of all levels is even if the K-capture is allowed: if it is first forbidden the ground state of Mn^{54} has odd parity. On a simple shell model configuration one would expect the odd proton to be in an $f(7/2)^-$ state and the odd neutron to be probably $p(3/2)^-$ or $(f\,5/2)^-$ giving even parity to the complete wave function. This would rule out the possibility of a first forbidden Fermi type decay $3^-(1,yes)2^+$. The decay scheme is shown in figure 1.

3. The previous orientation experiments

The magnetic properties of Mn^{++} had been studied by paramagnetic resonance in three salts - Manganese fluosilicate, Manganese ammonium sulphate (a Tutton salt) and Manganese bismuth nitrate (Bleaney & Ingram 1951a; Trenam 1953). For all these the resonance spectrum

could be interpreted by a Spin Hamiltonian

$$\mathcal{H} = g\beta \underline{H}.\underline{S} + DS_z^2 + A\underline{S}.\underline{I} + F(a) \quad \text{with } S = 5/2.$$

D being >0 for the Tutton salt and <0 for the other two. If $D>0$, the lowest electronic level is $S_z = \pm\frac{1}{2}$, the separation of the hyperfine levels is small and none of the lowest levels are pure in M_I. This means that the degree of alignment at the same temperatures will be much less than for the case where $D<0$ and $S_z = \pm 5/2$ is lowest. The level pattern has been given by Mleaney and Ingram for stable Mn^{55} ($I = 5/2$).

Since no magnetic cooling experiments had at that time been done using the fluosilicates, Grace et al chose to use the double nitrate. It was known that cerium magnesium nitrate was suitable for adiabatic demagnetisation and a temperature scale for it had been established (Daniels & Robinson 1953).

The specimen was a single crystal of $Ce_2(NO_3)_6 Mg_3(NO_3)_6 .24H_2O$ with a trace of active manganese replacing some of the magnesium.

The results of alignment by the magnetic h.f.s. method differed both qualitatively and quantitatively from what would be expected. The anisotropy instead of increasing monotonically to a saturation maximum at very low temperatures, passed through a maximum of 28% at $\frac{1}{T^*} = 100$ and then decreased to 21% at $\frac{1}{T^*} = 300$. The general behaviour is similar to that found previously in the experiments on Ce60 in cobalt cerium nitrate (Ambler et al 1953, Johnson 1955) and more recently with Mn^{52} in cerium magnesium nitrate (Huiskamp et al 1956, 1957).

In these crystals the cerium ions are very close to the divalent

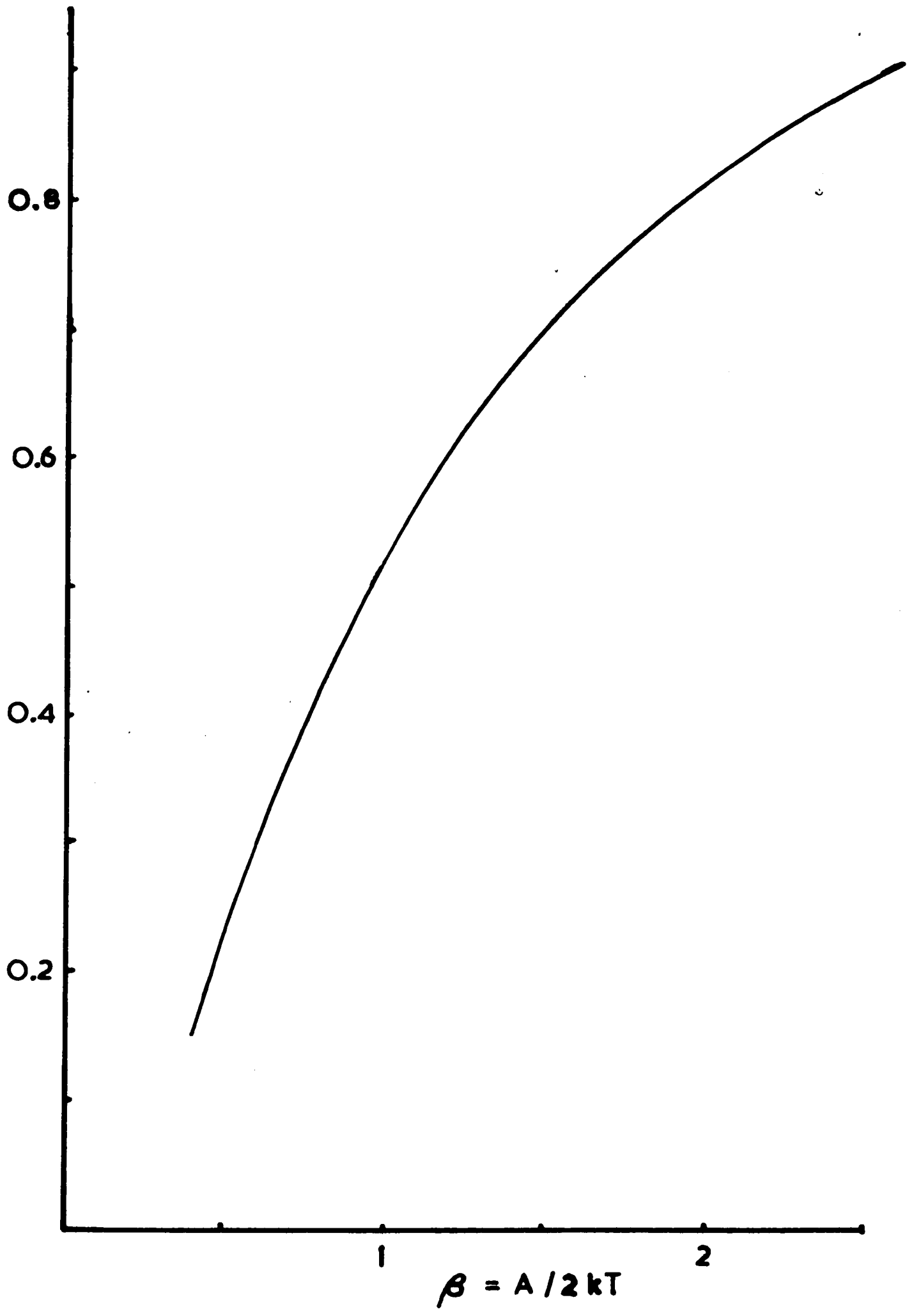
ions and it is possible that there is some interaction between the two which disturbs the alignment (Chapter 2, section 2b).

If this is the case, then polarisation of the nuclei in an external field (magnetic h.f.s. polarisation) should produce better results since a field of 1,000 gauss is large enough to swamp the effects of such interionic fields.

Grace et al did this and observed anisotropies up to 90% but although the experimental points followed the expected trend, no attempt was made to deduce a value for the magnetic moment. This was because of the uncertainty of the measurements of temperature (i.e. susceptibility) in the presence of a magnetic field. However, it has since been shown (Scurlock 1958) that if the polarising field is parallel to the crystal axis ($g_{||} = 0.25 \pm 0.05$, Cooke et al 1953) then $T^{\ominus}$ and T are very closely the same for the range $0 < \frac{1}{T} < 150$.

Making this assumption, $\epsilon v \frac{1}{T}$ can be calculated easily if the alignment occurs effectively through the $A.S_z.I_z$ term as will be for the case $g\beta\underline{H}.\underline{S} \gg AS_zI_z$. Population parameters have been tabulated for this simple case (Gray and Satchler 1955). The correction for $g\beta\underline{H}.\underline{S} \backslash AS_zI_z$ will only be of the order $B_2 = (1-\alpha^2)B_2(00)$ where and $B_2(00)$ is the value for the extreme case considered.

Since measurement $T^{\ominus}$ is difficult for large T and corrections due to interionic effects and for the approximations used will be most important for small T, the curve has been fitted for an intermediate value, viz. $\frac{1}{T} = 60$ and gives $\mu = 3.3$ nm for $I = 3$ (figure 2). In spite of the poor fit, this must be of the right order of magnitude



Mn 54 in $CeMgNO_3$

Figure 2

for the magnetic moment.

However, the possible spin sequences and corresponding saturation anisotropies were:

3(1)2(2)0 +1	2(0)2(2)0 +1	1(1)2(2)0 $+\frac{1}{3}$
	2(1)2(2)0 $+\frac{1}{3}$	1(1)1(1)0 $+\frac{1}{3}$
	2(1)1(1)0 -1	1(0)1(1)0 -1

It is seen that only the first two fit the experimental data showing that the beta transition is "stretched" and the gamma radiation is quadrupole. No distinction could be made between the two possibilities (2,3) for the spin of Mn^{54}.

4. The design of the present experiment

Nickel fluosilicate diluted with zinc has been found to be a suitable salt for cooling by adiabatic demagnetisation (Hill, Meyer & Milner 1959) and in view of the results of the alignment of Mn^{54} in the double nitrate, this salt was chosen as a new environment for the isotope.

With one ion per unit cell and a single axis of alignment, the experiment and its analysis is straightforward. It should be possible to find the magnetic moment by fitting a theoretical curve, for which the moment is a variable parameter, to the experimental results.

The immediate difficulty was that no $T-T^{*}$ correlation had been obtained for the fluosilicate when the experiment was first carried out. To overcome this deficiency Co^{60} was aligned in a similar crystal of the same salt. Now, the decay scheme of Co^{60} is well known and its

magnetic moment has been accurately measured by Dobrowolski et al (1956) so the parameters are known. The dependence of the gamma ray anisotropy on H/T initial can then be used to find a relation between H/T initial and T final (see Chapter 2) which will apply to all crystals of the same concentration. The final temperature depends on the Mn-Zn concentration of the crystal which in turn depends on the growing conditions. The alignment of Co^{58} can also be used to give a similar relationship (Chapter 6) so the latter isotope has also been used to give a temperature scale.

The fact that this method requires both crystals to have the same concentration led to a further experiment in which Mn^{54} and Co^{60} were included in the same crystal. This is possible because the gamma radiation of the two isotopes is readily resolved, so assuming there is no interference between the two ions affecting their alignment, the Mn^{54} anisotropy can be plotted against 1/T directly.

5. The alignment of Mn^{54}

5a. The experiments

In all, five experiments have been performed using three crystals (A,B,C) and two sets of apparatus. Three of the experiments were carried out on the first crystal (A) but, of these, two were carried out to test the functioning of the second apparatus and will not be considered separate from the first. The results of these two, however, show that the result for a given crystal is independent of the equipment used.

The fourth experiment was carried out with a new crystal (B)

while the last experiment involved the alignment of Mn^{54} and Co^{60} in the same crystal.

The first experiment, (A), was carried out with the crystal axis vertical, i.e. parallel to the magnetic field, because for this arrangement the measurement of the magnetic temperature is easier although the counter geometry is not symmetrical. The other experiments were made with crystal axis horizontal since it was then known that the T-T* correlation was not applicable and the measurement of δ was not important.

5b. The source material

Mn^{54} is produced by the Fe^{56} $(d,\alpha)Mn^{54}$ reaction in the Birmingham cyclotron, the targets being processed at the Radiochemical Centre, Amersham. The activity is supplied as Manganese chloride in aqueous solution with a specific activity of 10 mc/gm of manganese.

5c. The crystals

The crystals were grown from solutions of approximately (10% Ni, 90% Zn)$SiF_6 . 6H_2O$., and the final composition of the crystals has been given in Table 1, section 3 of Chapter 2. It is seen that the composition of crystal A was closely the same as that of the Co^{60} and Co^{58} crystals used to give the temperature scale. Both crystal B and C, however, contained about 2% more nickel than the others. Each crystal weighed about 2 gms. and contained approximately 10μc Mn^{54} (i.e. ~ $\frac{1}{2}$% of metallic ion is Mn). The mixed crystal had in addition between 5 and 10μc Co^{60} introduced to the growing solution as carrier-free cobalt chloride. The ratio of Co^{60} to Mn^{54} activities is not critical

but was intended to be such that both Co^{60} and Mn^{54} counting rates could be measured to 1% accuracy.

5d. The gamma-ray spectra

The pulse height spectrum for the Mn^{54}, (figure 3) showed a single gamma ray at 0.840 Mev with its associated Compton distribution. For the experiments with crystals A and B a discriminator was set in the trough below the Mn^{54} peak, i.e. at ~0.7 Mev and the anisotropy found for all pulses above this level. For the mixed crystal (C) two discrimination levels were set. The first at 0.7 Mev as before and the second between 0.9 and 1.0 Mev (figure 4). This places it well below the Co^{60} 1.17 Mev peak in a region where the counting rate is not varying too rapidly with energy but high enough for the number of Mn^{54} pulses above it to be neglected. This upper bias position then gives the Co^{60} counting rate directly while the Mn^{54} counting rate is found by a simple correction to the channel counting rate.

5e. The analysis of the composite spectrum

First of all a spectrum of the composite source was obtained under the experimental conditions, i.e. with the source inside the cryogenic apparatus, so that the effects of scattering and absorption are taken into account. Integral counting rates are found for the two bias positions together with one at about 1.05 Mev. A pure Co^{60} spectrum is then obtained under the same conditions using a source of similar strength to the Co^{60} component of the combined spectrum and integral counting rates taken at the same energies.

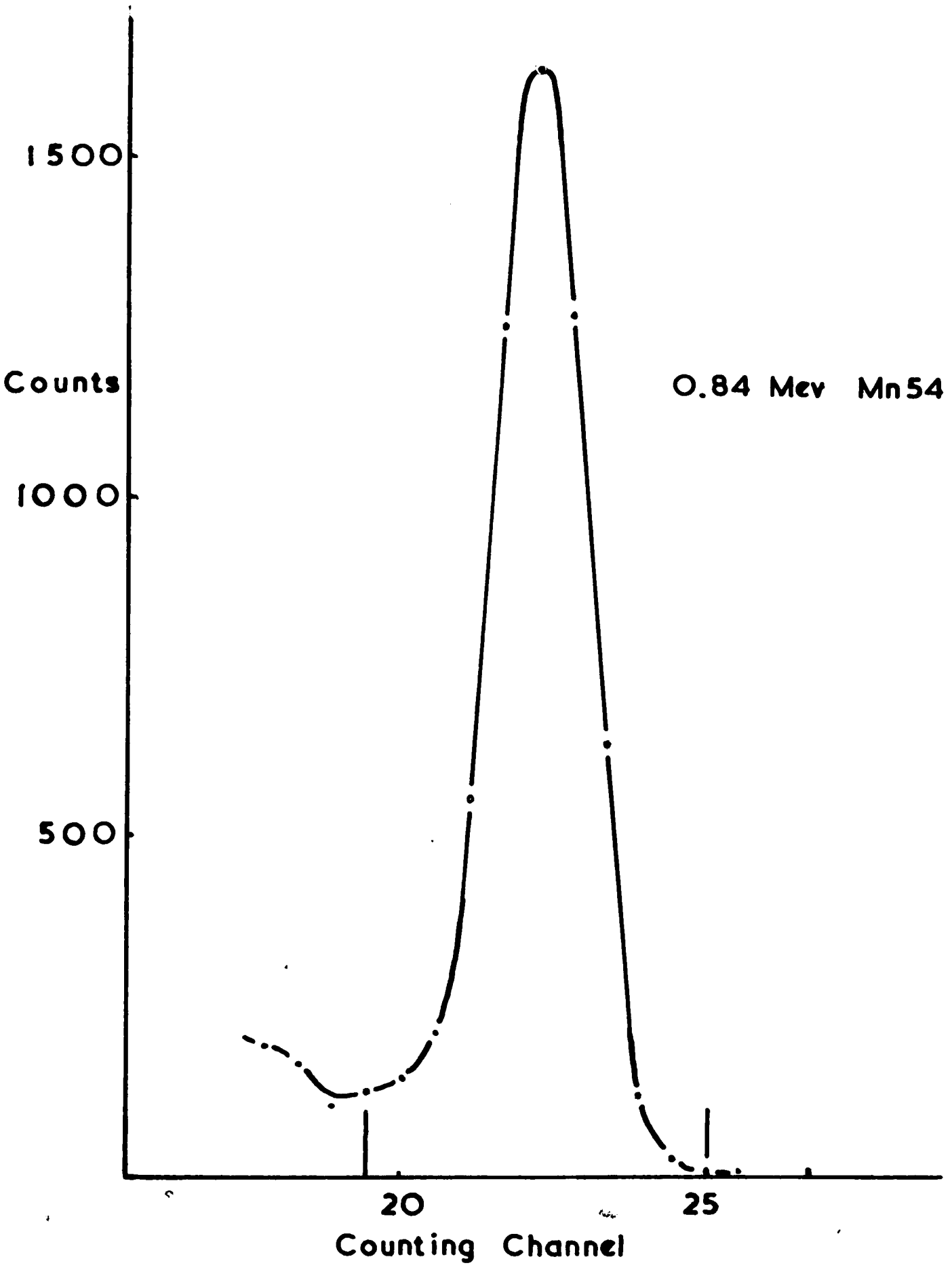


Figure 3

This spectrum was then fitted to the composite one at 1.05 Mev where it is certain that the Mn^{54} can be neglected. It was found that the integral counting rates at the high bias position (0.9-1.0 Mev) also agreed within the statistical error as had been assumed previously.

The number of counts between the two bias positions due to Co^{60} is then $C_L - C_H$ and this can be expressed as a fraction of the high bias counting rate C_H,

$$\text{i.e.} \quad f = \frac{C_L - C_H}{C_H}$$

The total number of counts in the channel is $N_L - N_H$ where N_L and N_H are the counting rates at the lower and upper bias positions. The number of counts due to Mn^{54} are then

$$M = (N_L - N_H) - (C_L - C_H)$$
$$= (N_L - N_H) - f.C_H$$

But it has already been seen that $N_H = C_H$ so that we have

$$M = N_L - N_H(1+f)$$

The correction factor (1+f) can be determined before the experiment and is valid at all temperatures so that it can be applied as a running correction during an experiment to give an immediate answer; f = 0.67 for the axial counter and 0.70 for the equatorial.

5f. Procedure

In all three experiments the gamma-ray intensities at 0° and 90° were measured after demagnetisation and as the crystal warmed up to 1°K. Recordings of a typical run for crystal B and crystal C are given in tables 2 and 3 respectively.

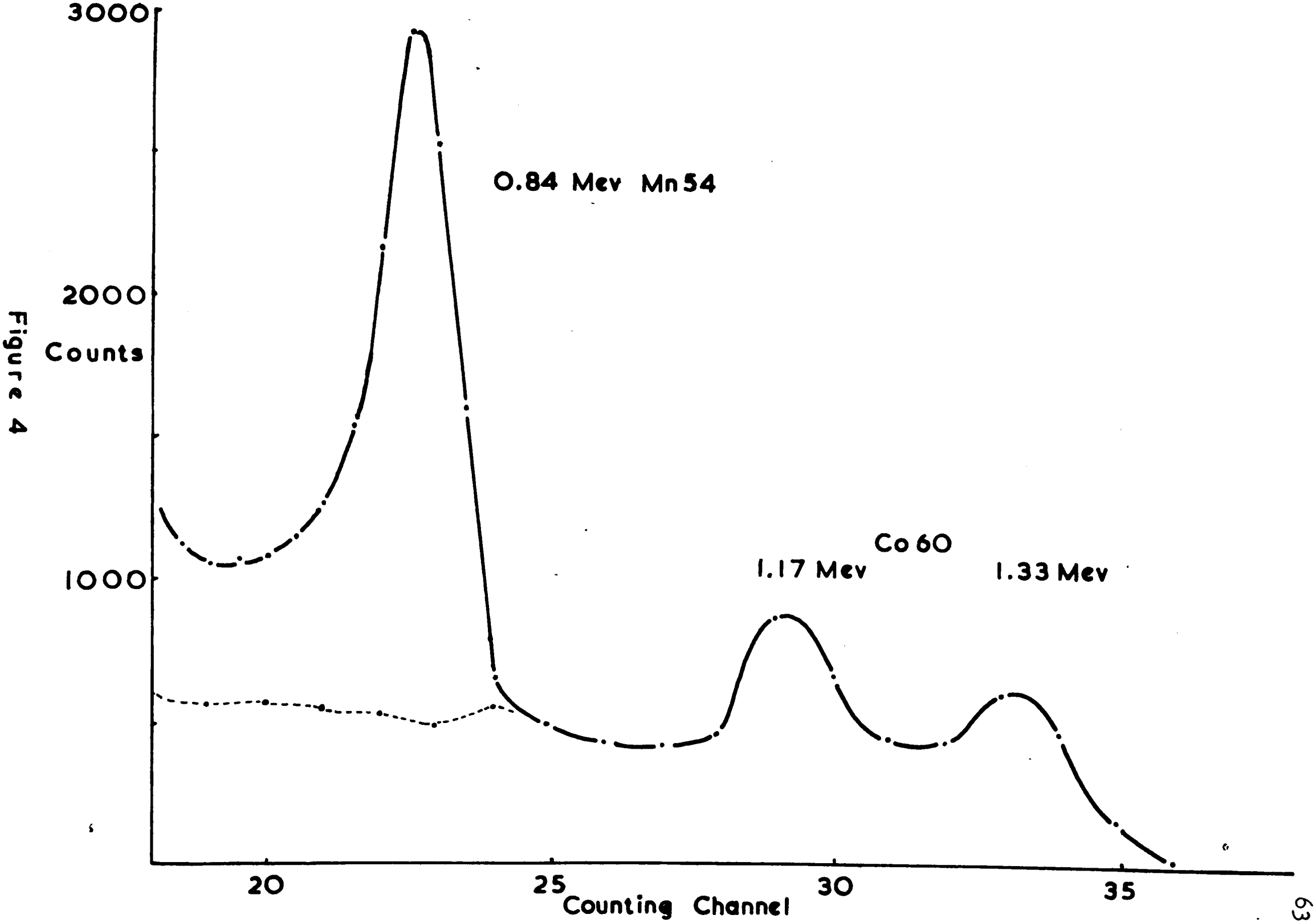

3000
2000
1000
Counts
0.84 Mev Mn54
Co 60
1.17 Mev
1.33 Mev
20
25
30
35
Counting Channel

Figure 4

TABLE 2

Mn^{54} in Ni-Zn $SiF_6.6H_2O$ - crystal B

Initial Field = 34.4 kilogauss (2000 amps); Counting interval = 40 seconds; source counter distance = 6.77 cms)

Time minutes & seconds	Galvanometer deflection cms.	Axial Counting Rate	$I(0^\circ)$	Equatorial Counting Rate	$I(90^\circ)$	ϵ
0-10	9.17	13451 ± 116	0.323 ± 0.003	49837 ± 223	1.207 ± 0.006	0.732 ± 0.007
1-05	8.85	16883	0.405	49096	1.190	0.660
1-51	8.64	19047	0.457	48672	1.178	0.612
2-45	8.53	20470	0.492	48256	1.169	0.579
3-37	8.30	21891	0.525	48002	1.161	0.548
4-33	8.17	22972	0.552	47530	1.150	0.520
		41317		41281		$\epsilon_{t=0} = 0.772 \pm 0.014$
		41608		41290		$T_i = 1^\circ K$
		41736		41579		$\frac{1}{T_f} = 110 \pm 10\ (^\circ K)^{-1}$
		41725		41205		
		41829		41334		
	mean value	41644 ± 91		41338 ± 91		

TABLE 3

Mn^{54} and Co^{60} in Ni-Zn SiF_6 .6 H_2O - crystal C.

Initial field = 34.4 kilogauss (2000 amps); counting interval = 40 seconds; source counter distance = 6.77 cms.

AXIAL COUNTER - Correction factor f = 1.67 ± 0.02

Time mins.-secs.	L.B. (Low Bias)	H.B. (High Bias)	fxH.B.	Δ = LB-fxHB	$I(0^0)$ Mn^{54}	$I(0^0)$ Co^{60}
11	37853 ± 195	15997 ± 126	26700 ± 320	11153 ± 107	.394 ± 0.004	0.484 ± 0.004
1-13	44941	19248	32150	12791	0.451	0.582
2-10	49695	21170	35300	14395	0.508	0.640
3-06	53887	22879	38200	15687	0.554	0.693
4-06	57003	23878	39500	17503	0.618	0.723
5-06	59202	25023	41950	17252	0.610	0.760
	83105	33060				
	83284	33069				
	83445	33060				
	83956	33054				
	83784	32920				
Mean value	83515 ± 130	33032 ± 81	55200 ± 660	28315 ± 170		

EQUATORIAL COUNTER - Correction factor f = 1.70 ± 0.02

L.B. (Low Bias)	H.B. (High Bias)	fxH.B.	Δ = LB-fxHB	$I(90^0)$ Mn^{54}	$I(90^0)$ Co^{60}	ϵ_Δ Mn^{54}	ϵ_{HB} Co^{60}
94595 ± 340	37404 ± 193	63580 ± 748	31000 ± 778	1.173 ± 0.010	1.183 ± 0.007	0.664 ± 0.015	0.592 ± 0.008
92809	36758	62300	30500	1.154	1.162	0.609	0.548
91388	35930	61000	30390	1.149	1.136	0.558	0.436
90631	35669	60700	29950	1.134	1.128	0.513	0.386
89761	34999	59500	30260	1.145	1.106	0.460	0.346
88931	34943	59400	29530	1.118	1.104	0.454	0.312
80211	31587						
80391	31856						
80303	31578						
80133	31628						
80208	31539						
80249 ± 126	31638 ± 80	53800 ± 632	26400 ± 1[illegible]				

$\epsilon_{t=0}$ = 0.705 ± 0.030 = 0.655 ± 0.016

$T_i \sim 1^0K$

$1/T_f$ = 155 ± 8 $(^0K)^{-1}$ Co^{60}

= 110 ± 10 $(^0K^{-1})$ Co^{58}

Demagnetisations were carried out from many different initial fields and the anisotropy plotted as a function of t, the time after the removal of the field. By extrapolation, the anisotropy and the instant of demagnetisation, $\epsilon_{t=0}$, was found. In most cases two or more runs were done for each field in order to confirm the individual results. These values of $\epsilon_{t=0}$ are tabulated in table 4 and have been plotted in figures 5, 6 and 7 against the values of $\frac{1}{T}$ derived from the Co^{58} experiment. Blocked values of $I(0^\circ)$ and $I(90^\circ)$ are given in table 5 and the dependence of $I(0^\circ)$ on $I(90^\circ)$ is shown in figures 8 and 9. The Mn^{54} anisotropies obtained from the mixed crystal were also correlated with the absolute temperature by comparing the associated Co^{60} anisotropy with the theoretically predicted values.

The consistency of these two temperature scales was tested by plotting the experimental Co^{60} anisotropies against the temperatures obtained from Co^{58} and comparing this curve with the theoretical one (figure 10). The curves agree well up to $\frac{1}{T} = 75$ and the divergence above this value does not exceed the experimental error for $\frac{1}{T} < 100$. The difference could be due in part to the difference in the concentrations of the crystals.

5g. <u>The theoretical curves</u>

Values for the population parameters B_2, B_4 have been obtained by solving the Spin Hamiltonian (see Appendix). Because of the difficulties and labour involved in solving high order polynomial equations this has only been done rigorously for the case of $I=3, \mu=3.5$ and then only

TABLE 4

Mn^{54} in Ni-Zn SiF_6, $6H_2O$

Anisotropy at instant of demagnetization, ϵ t = 0

Magnet calibration = 17.2 gauss/amp

H/T ($T_i = 1°K$) Amps	$1/T(Co^{58})$ $(°K)^{-1}$	A ±0.02	B ±0.02	C ±0.03	Co^{60} ±0.02	$1/T(Co^{60})$ $(°K)^{-1}$ (From Crystal 8)
2000	110 ±10	-	0.76	0.693	0.64	155 ± 10
1700	91 ±10	-	-	0.664	0.52	114 ± 6
1500	81 ±12	0.780	0.67	0.627	0.47	102 ± 5
1450	77 ±12	0.753	-	-	-	-
1310	70 ±10	0.706	-	-	-	-
1200	65 ± 9	0.690	0.56	0.513	0.310	63 ± 4
1160	58 ±10	0.626	-	-	-	-
1000	45 ± 5	-	0.43	0.372	0.210	48 ± 3
900	37 ± 3	0.445	0.340	0.288	0.15	36 ± 4
872	33 ± 3	0.453	-	-	-	-
750	25 ± 4	-	0.20	0.195	0.08	26 ± 4
727	24 ± 4	0.316	-	-	-	-
655	21 ± 4	0.235	-	-	-	-
600	18 ± 4	-	0.09	0.063	0.05	20 ± 4
570	16 ± 3	0.137	-	-	-	-
510	14 ± 3	0.072	-	-	-	-
500	14 ± 3	-	0.03	0.064	0.04	18 ± 4
436	~12	0.041	-	-	-	-
385	~11	0.017	-	-	-	-
364	~10	0.006	-	-	-	-
350	~10	0.017	-	-	-	-
290	~ 8	0.002	-	-	-	-
250	~ 7	-	-	0	0	1
218	~ 6	0.002	-	-	-	-
200	~ 5	-	0	-	-	-

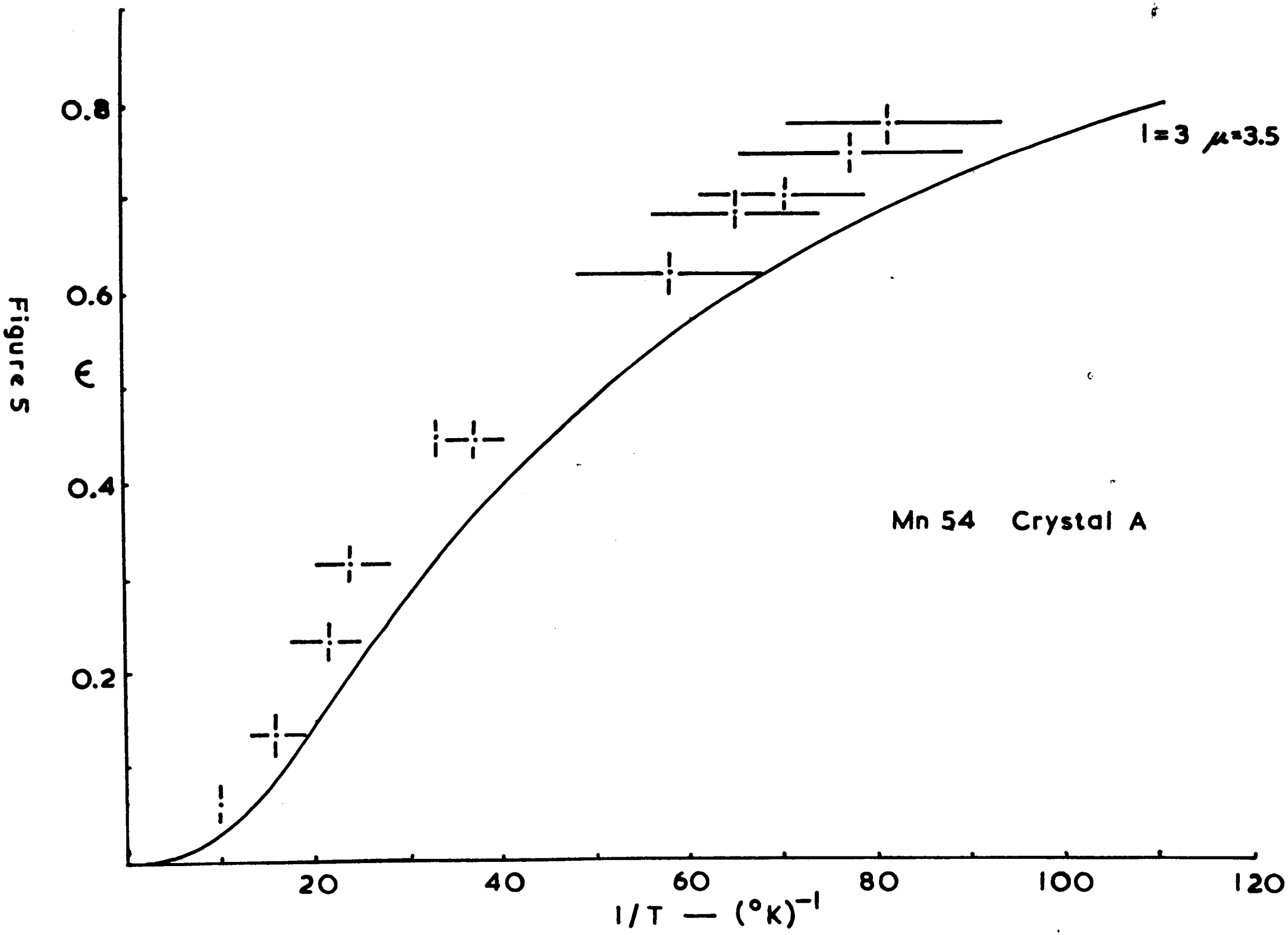


Figure 5

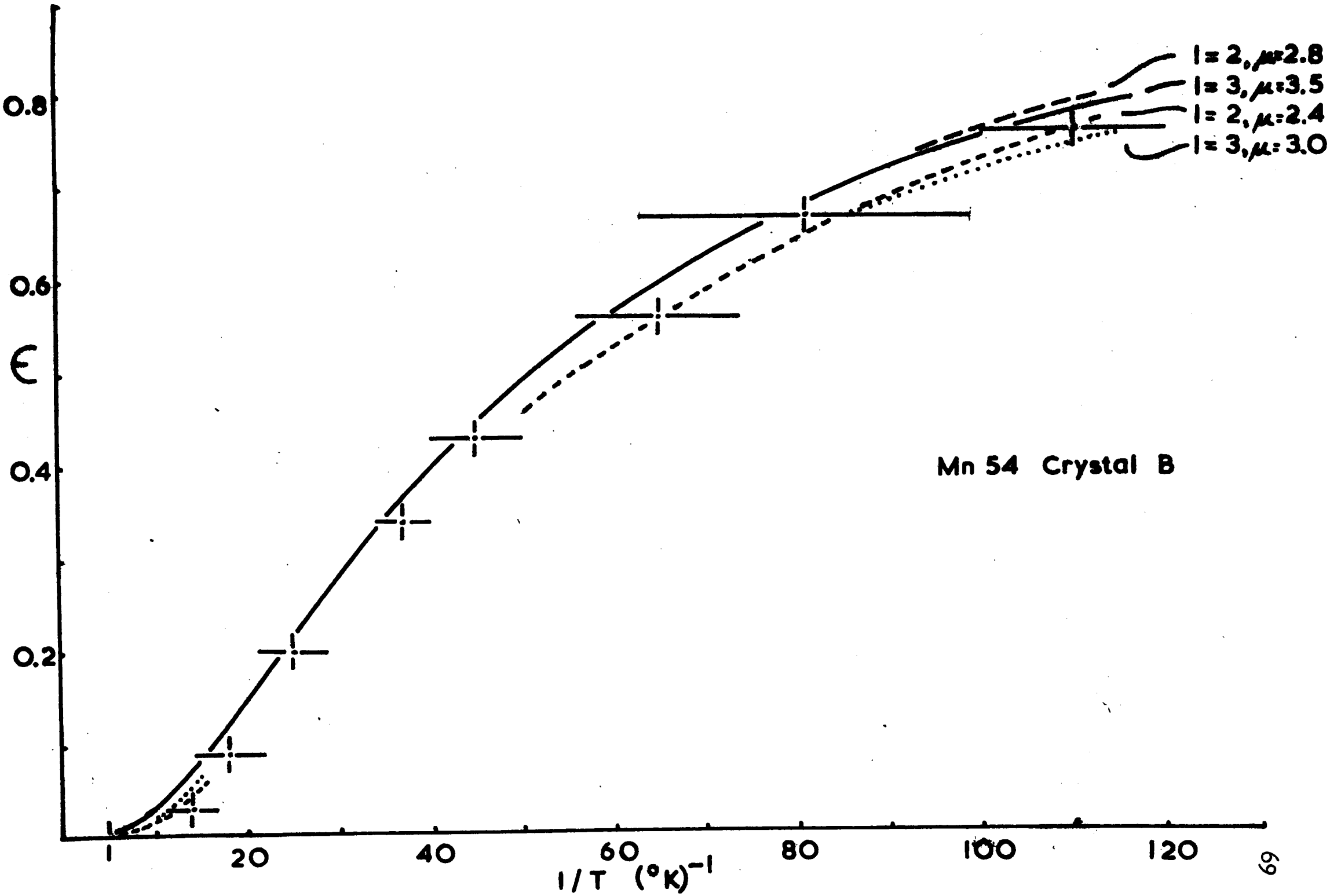

0.8
0.6
ε
0.4
0.2
1
20
40
60
80
100
120
1/T (°K)⁻¹
l = 2, μ=2.8
l = 3, μ=3.5
l = 2, μ=2.4
l = 3, μ=3.0
Mn 54 Crystal B

Figure 6

Figure 7

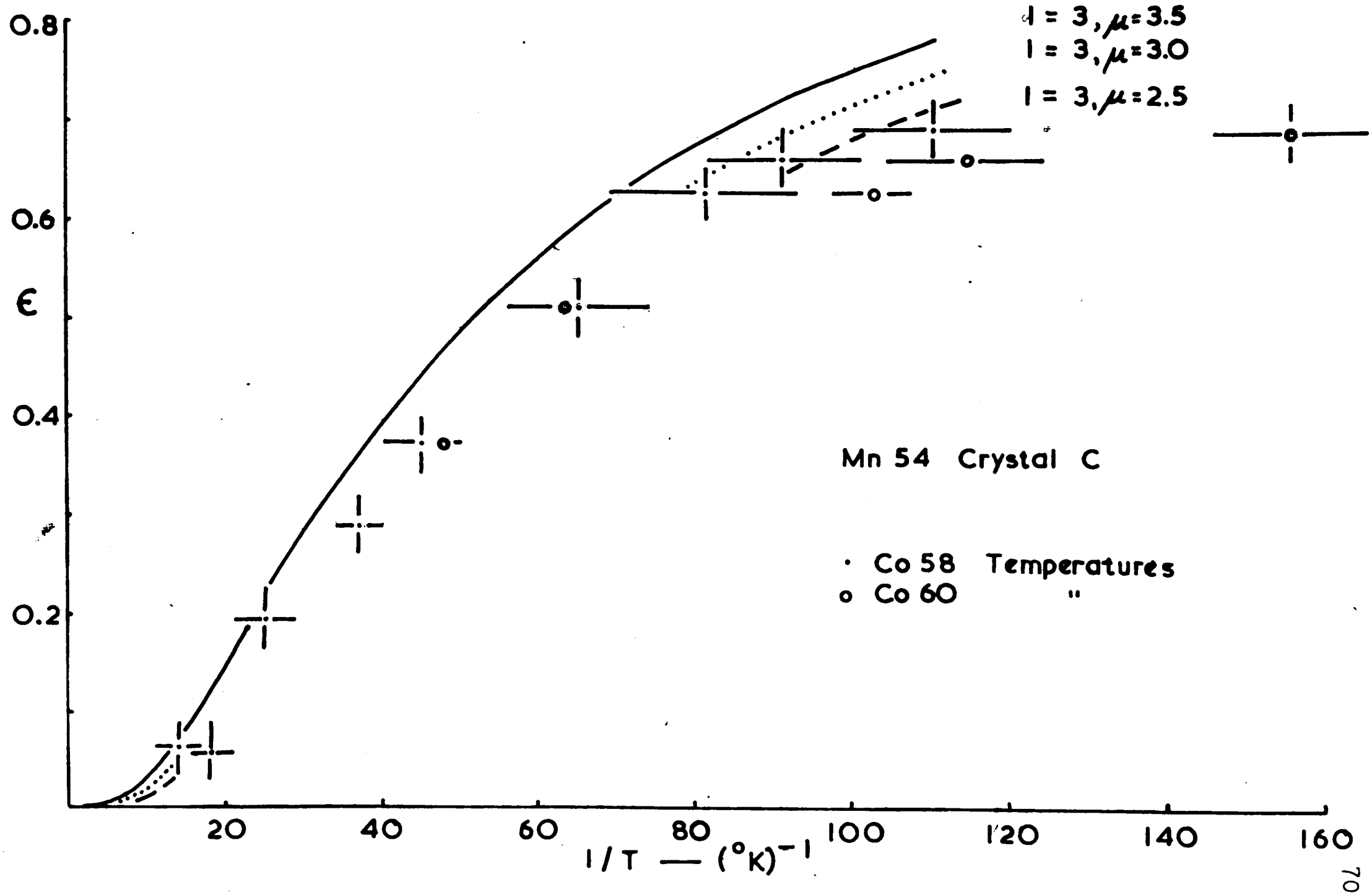

0.8
0.6
ε
0.4
0.2
20
40
60
80
100
120
140
160
1/T — (°K)⁻¹
l = 3, μ = 3.5
l = 3, μ = 3.0
l = 3, μ = 2.5
Mn 54 Crystal C
· Co 58 Temperatures
o Co 60 "

TABLE 5

Mn^{54} in Ni-Zn SiF_6, $6H_2O$

Normalised Intensities

A		B		C		Co^{60}-crystal C	
I(0°)	I(90°)	I(0°)	I(90°)	I(0°)	I(90°)	I(0°)	I(90°)
0.284 ± 0.004	1.226 ± 0.006	0.390 ± 0.003	1.195 ± 0.006	0.366 ± 0.002	1.1[illegible] ± 0.006	0.434 ± 0.002	1.200 ± 0.006
0.374	1.216	0.497	1.172	0.400 ± 0.004	1.190 ± 0.[illegible]	0.560 ± 0.004	1.166 ± 0.007
0.496 ± 0.005	1.173 ± 0.003	0.539	1.161	0.440	1.180	0.616	1.164
0.600	1.160	0.598	1.146	0.560	1.150	0.772	1.104
0.742 ± 0.003	1.111 ± 0.005	0.633	1.135	0.716	1.140	0.849	1.076
0.840 ± 0.005	1.060 ± 0.003	0.668	1.123	0.796	1.118	0.892	1.044
0.900	1.047	0.706	1.120	0.858	1.064	0.940	1.027
0.925	1.033	0.770	1.099	0.970	1.036	0.968	1.013
0.947	1.027	0.816	1.075	0.964	1.020	0.974	1.013
0.963 ± 0.004	1.015 ± 0.006	0.871	1.059	1.000	1.000	1.000	1.000
0.997 ± 0.002	1.000 ± 0.004	0.889	1.051				
		0.943	1.021				
		0.978	1.008				
		0.999	0.999				

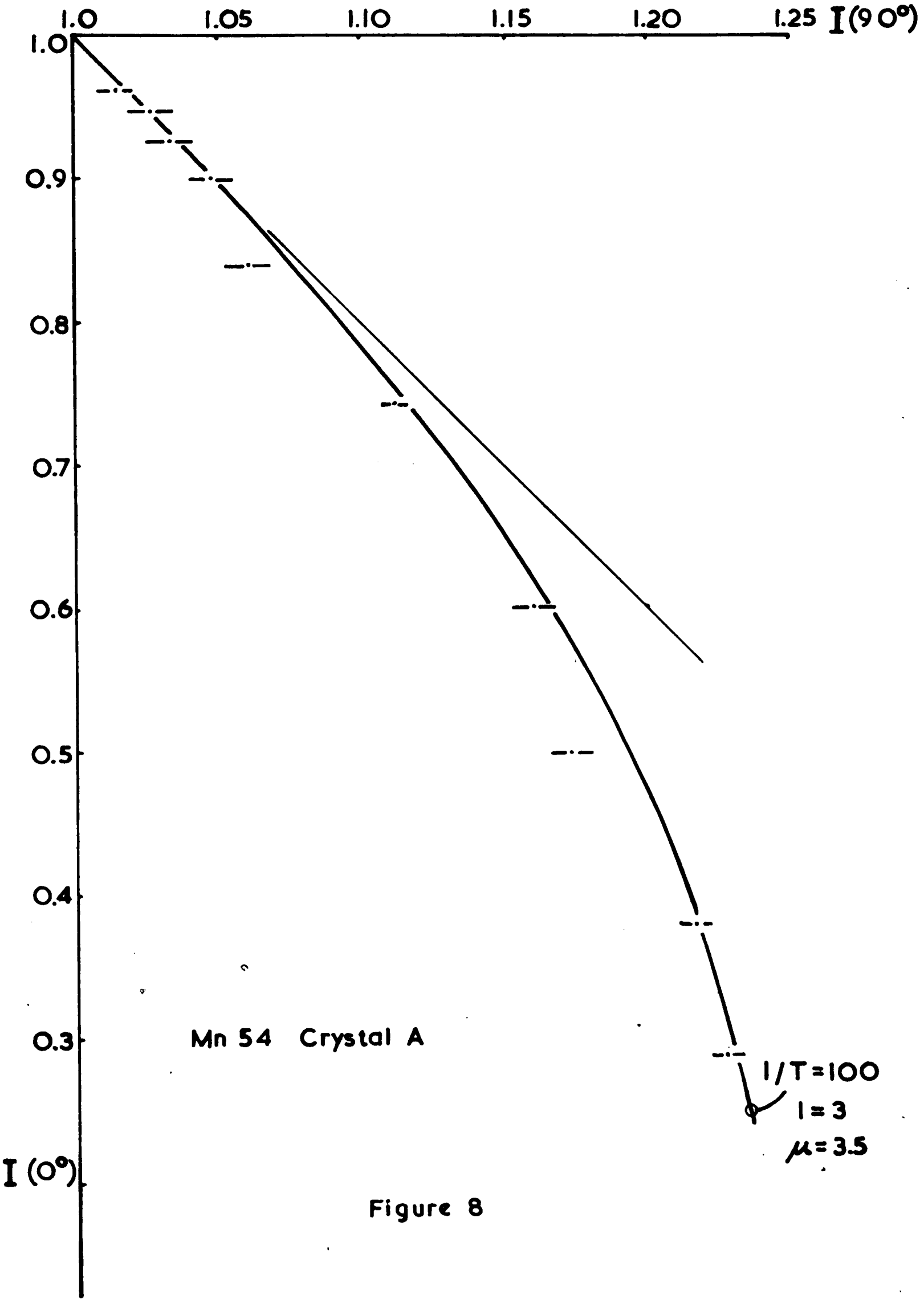

1.0
1.05
1.10
1.15
1.20
1.25
I(90°)
1.0
0.9
0.8
0.7
0.6
0.5
0.4
0.3
I (0°)
Mn 54 Crystal A
1/T=100
l=3
μ=3.5

Figure 8

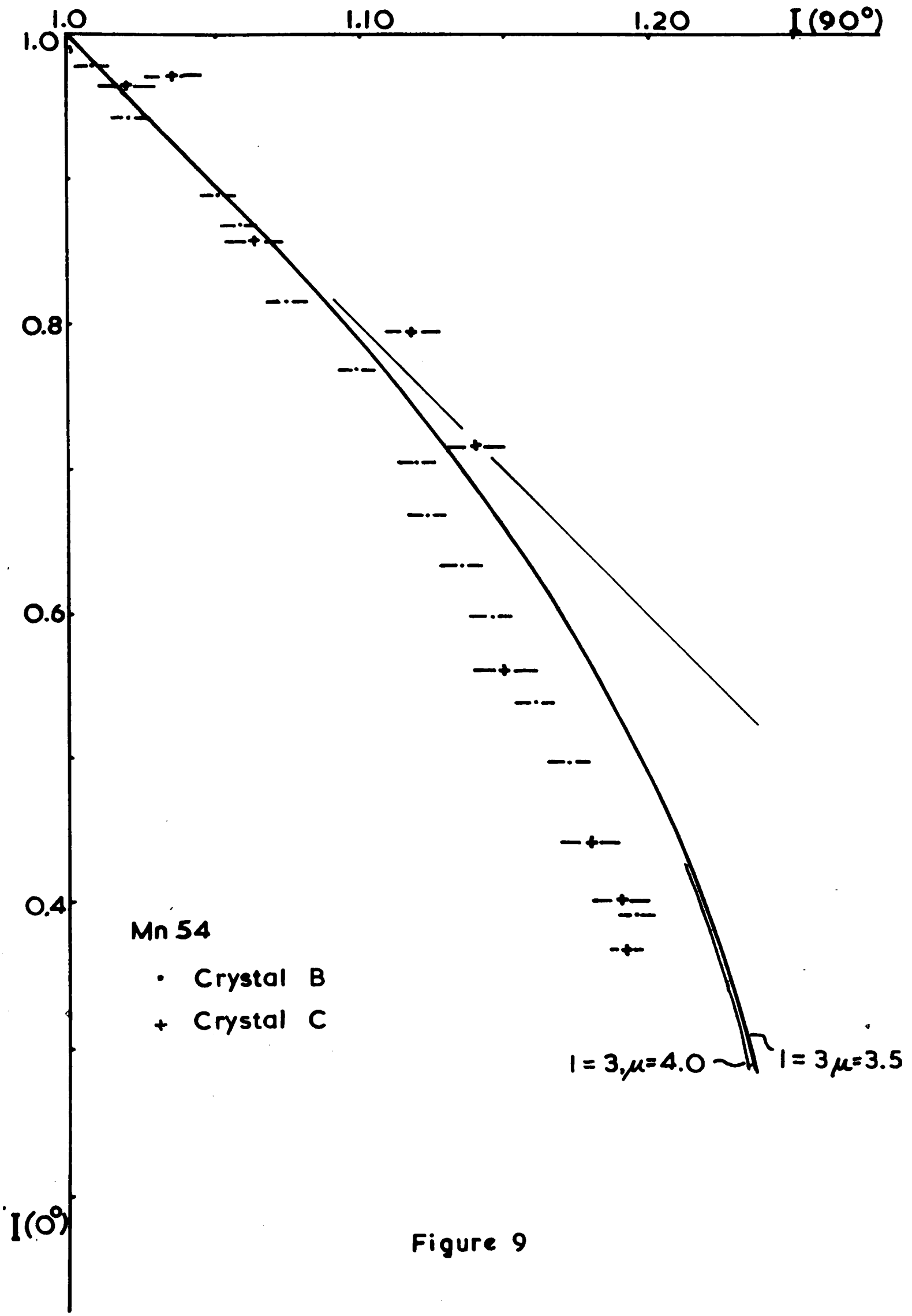

1.0
1.10
1.20
I (90°)
1.0
0.8
0.6
0.4
Mn 54
• Crystal B
+ Crystal C
I(0°)
I = 3, μ = 4.0
I = 3 μ = 3.5

Figure 9

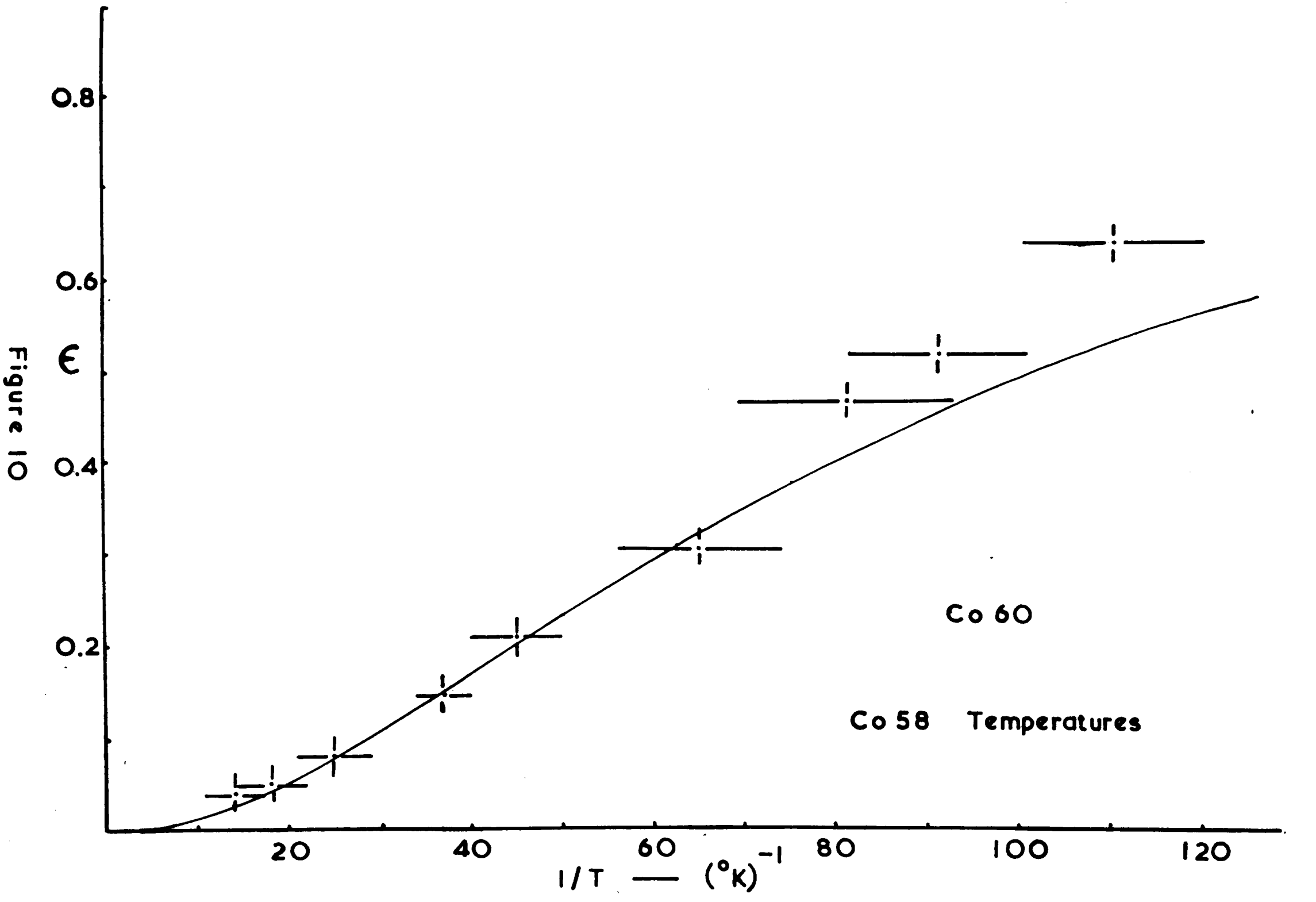


Figure 10

for the lowest six energy levels. For the other possibilities a perturbation theory calculation has been used to give B_2,B_4 by considering the lowest three energy levels only. These approximations should be valid for very low temperatures, viz. $\frac{1}{T} > 50$ for six levels and $\frac{1}{T} > 70$ for three levels respectively where the population of the lowest levels is predominant. In the first case, it is probably true for a greater range since the Boltzmann factor $\exp(-\Delta E/kT)$ for the sixth level is still only 0.13 at $\frac{1}{T}=20$. Thus ~82% of the ions are in these six levels.

A high temperature approximation gives B_2 in the range $\frac{1}{T} = 0$ to $\frac{1}{T} \sim 10$. Interpolation between these limits gives a good estimate for the complete curve for the six level calculation while the three level approximation can be interpolated by comparison with this.

5h. Corrections

The theoretical curves have been adjusted to take into account the averaging effect produced by a counter of finite aperture, using the results of paragraph 7c, Chapter 2.

For the experiment with Specimen A, 1" NaI crystals were used the half angle being $\alpha = 12\frac{1}{2}^0$ for the axial counter and $\alpha = 17^0$ for the equatorial counter, so we have

Axial	$g_2 = 0.96$	Equatorial	$g_2 = 0.93$
	$g_4 = 0.93$		$g_4 = 0.79$

2" crystals were used with specimens B and C and in both cases the counter arrangement was symmetrical with

$\alpha = 15^0$ $\quad g_2 = 0.95$ and $g_4 = 0.84$

If scattering is taken into account $g_2 = 0.94$, $g_4 = 0.82$ for the latter case but the difference is small compared with the experimental error.

5i. Results

These experiments have shown that Mn^{54} can be aligned in nickel-zinc fluosilicate and further, it is apparent from figures 5, 6 and 7 that the variation of ϵ with $\frac{1}{T}$ for Mn^{54} in the fluosilicate is monotonic in contrast to the results of the double nitrate experiments. Furthermore the experimental results closely follow the theoretical curves and confirm the proposed decay scheme of Mn^{54}. These facts demonstrate that nickel fluosilicate is a good environment for nuclear alignment using the magnetic h.f.s. method and its use for the experiments to be described (Chapters 4, 5 and 6) has given increased support for this conclusion.

It is very difficult from the results to make a choice between $I = 2$ or $I = 3$, but as is seen in figure 6, the general trend appears to favour $I = 3$, since this appears to give higher anisotropies in the intermediate temperature range and slightly lower ones as saturation is approached.

The marked difference between the results of A and those of B and C is probably due to the different orientation of the axes. The effective field H_{eff} acting on the ions will be different from the applied field H because of the demagnetising effect in the specimen. $H_{eff} = H + (\frac{4\pi}{3} - N)M$ where M is the magnetisation per unit volume and N is the demagnetising factor. N depends on the shape of the specimen

and its orientation with respect to the external field; it is difficult to calculate for an irregular specimen but for an ellipsoid $N = 0$ if the axis is parallel to the field and $N = 4\pi$ for the perpendicular orientation. This means N_{eff} is larger for crystal A than for the other two so that H/T(initial) is larger for the same field and lower temperatures will be reached. Thus the Co^{58} H/T, $1/T$ relationship is not really applicable and a correction to it would bring the experimental points for crystal A into closer agreement with the other two.

The value of the magnetic moment of Mn^{54} can be derived from figures 6 and 7. The values are

	B n.m.	C n.m.	Mean value n.m.
I = 3	3.2 ± 0.5	2.5 ± 0.5	2.85 ± 0.35
I = 2	2.5 ± 0.5	2.0 ± 0.5	2.25 ± 0.35

6. Alignment of Co^{60}

This experiment was carried out to provide a temperature scale for other experiments with fluosilicates and also provides further confirmation of the usefulness of these salts for nuclear orientation.

A crystal was grown with a weight of about 1 gm. and containing approximately 30μc of Co^{60}.

The crystal was aligned with a horizontal axis and demagnetisations carried out from a number of fields up to 25 kilogauss. Two discriminator levels were set for each counter, one at 1.0 Mev and the other at about 1.25 Mev so that the anisotropy of both gamma rays could be observed (figure 11).

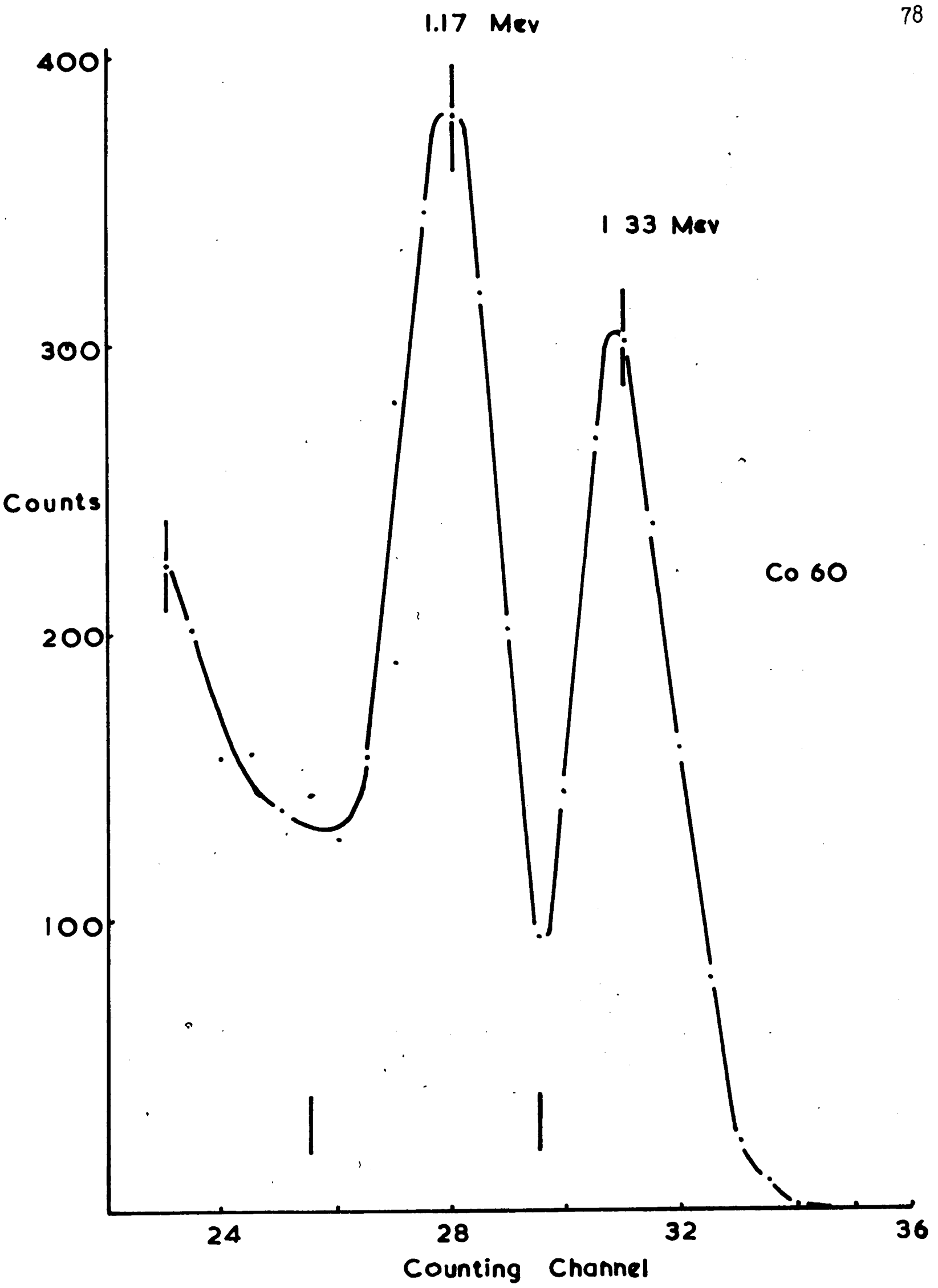

1.17 Mev
1 33 Mev
Co 60
400
300
200
100
Counts
24
28
32
36
Counting Channel

Figure 11

The recordings of a typical run are given in table 6. It is seen that within the experimental error, the anisotropy of the two gamma rays was the same, as expected for stretched cascade transitions, 4-2-0. The dependence of $I(0^{\circ})$ on $I(90^{\circ})$ (Table 7 and figure 12) did not quite agree with the theoretical curve and this could not be completely explained by a small drift on both counters. However, extrapolation of the anisotropy back to the instant of demagnetisation (Table 8) enabled the relation between H/T(initial) and $\frac{1}{T}$ to be obtained. This is shown in figure 9 of Chapter 6, where it is compared with a similar relationship obtained using Co^{58}. It is seen that the maximum value of $\frac{1}{T}$ reached using a field of 25 kilogauss at $1^{\circ}K$ is about 150. This result was a little surprising in view of the work of Hill, Meyer and Milner (1959) who reached $0.015^{\circ}K$ for 25 kilogauss with a 15% crystal. Milner (1957) shows that the final temperature should depend roughly on the square root of the concentration so for an 8% crystal one would expect to reach $0.011^{\circ}K$ or $\frac{1}{T} = 91$.

The experiment has been repeated on two subsequent occasions, using the same crystal, the agreement with the theoretical $I(0^{\circ})$, $I(90^{\circ})$ plot being quite good in each case. The first of these was carried out with magnetic fields of between 25 and 35 kilogauss, giving a range of temperature $70 < \frac{1}{T} < 105$ while the second was carried out with 25 kilogauss giving $\frac{1}{T} \sim 80$, both of which are in contrast with the earlier results but in accord with Milner's estimate.

In a later chapter, the alignment of Co^{58} is described. This

TABLE 6

Co^{60} in Ni-Zn Si $F_6.6H_2O$

Initial Field = 25 kilogauss; Counting interval = 20 secs.

time mins-secs.	Galv. defl. cms.	Axial Counter Low bias	$I(0^o)$ L.B.	Axial Counter High bias	$I(0^o)$ H.B.	Equatorial Counter Low bias	$I(90^o)$ L.B.	Equatorial Counter High Bias	$I(90^o)$ HB	ϵ_{LB}	ϵ_{HB}
0-30	2.00	11671±108	0.607±0.006	4770±69	0.601±0.01	30291±174	1.188±0.007	12061±110	1.207±0.011	0.490 ± 0.008	0.502 ± 0.013
1-0	1.88	12962	0.673	5310	0.669	29705	1.165	12011	1.202	0.423	0.443
1-2	1.84	13924	0.723	5788	0.728	29056	1.140	11426	1.143	0.366	0.362
1-55	1.79	14635	0.760	6107	0.769	28621	1.123	11275	1.128	0.328	0.318
2-20	1.75	15207	0.789	6198	0.781	27951	1.097	11037	1.104	0.281	0.293
2-5	1.71	15853	0.827	6467	0.814	27651	1.085	11066	1.107	0.242	0.264
3-25	1.69	16109	0.836	6634	0.836	27549	1.081	10864	1.087	0.227	0.231
3-45	1.66	16725	0.868	6825	0.861	27232	1.068	10835	1.084	0.187	0.207
4-15	1.65	17285	0.897	7040	0.881	27248	1.069	10948	1.095	0.161	0.190
4-45	1.62	17541	0.910	7180	0.904	26883	1.055	10634	1.064	0.137	0.150
		19266		**7975**		**25311**		9996		$\epsilon_{t=0} = 0.63 \pm 0.016$	
		19233		7897		**25495**		**10086**			
		19528		**7926**		**25335**		**9990**		$T_i = 1^oK$	
		19359		7910		**25648**		**10153**			
		19143		1907		**25416**		**10047**			
		19191		**7964**		**25539**		9882			
		19454		**7896**		**25615**		9992			
		19327		**7977**		**25561**		**9914**			
		19031		**7888**		**25481**		**9922**			
		19525		8045		**25608**		**10046**			
		19220		7960		**25359**		9951			
		19180		**8021**		**25496**		9983			
		19153		**7937**		**25362**		**9990**			
		19504		**7837**		**25493**		**10035**			
		19169		**7898**		**25609**		**9919**			
Mean values:		19269±36		7936±23		25437±41		9994±26			

TABLE 7

Co^{60} in Ni-Zn $SiF_6.6H_2O$

Normalised Intensities
(blocked values)

I(0°)	I(90°)
0.616 ± 0.004	1.169 ± 0.008
0.673 ± 0.006	1.165 ± 0.011
0.725 ± 0.003	1.140 ± 0.006
0.774 ± 0.002	1.106 ± 0.004
0.826 ± 0.002	1.094 ± 0.003
0.880 ± 0.002	1.070 ± 0.003
0.920 ± 0.001	1.046 ± 0.002
0.982 ± 0.001	1.011 ± 0.002
1.010 ± 0.001	1.012 ± 0.002

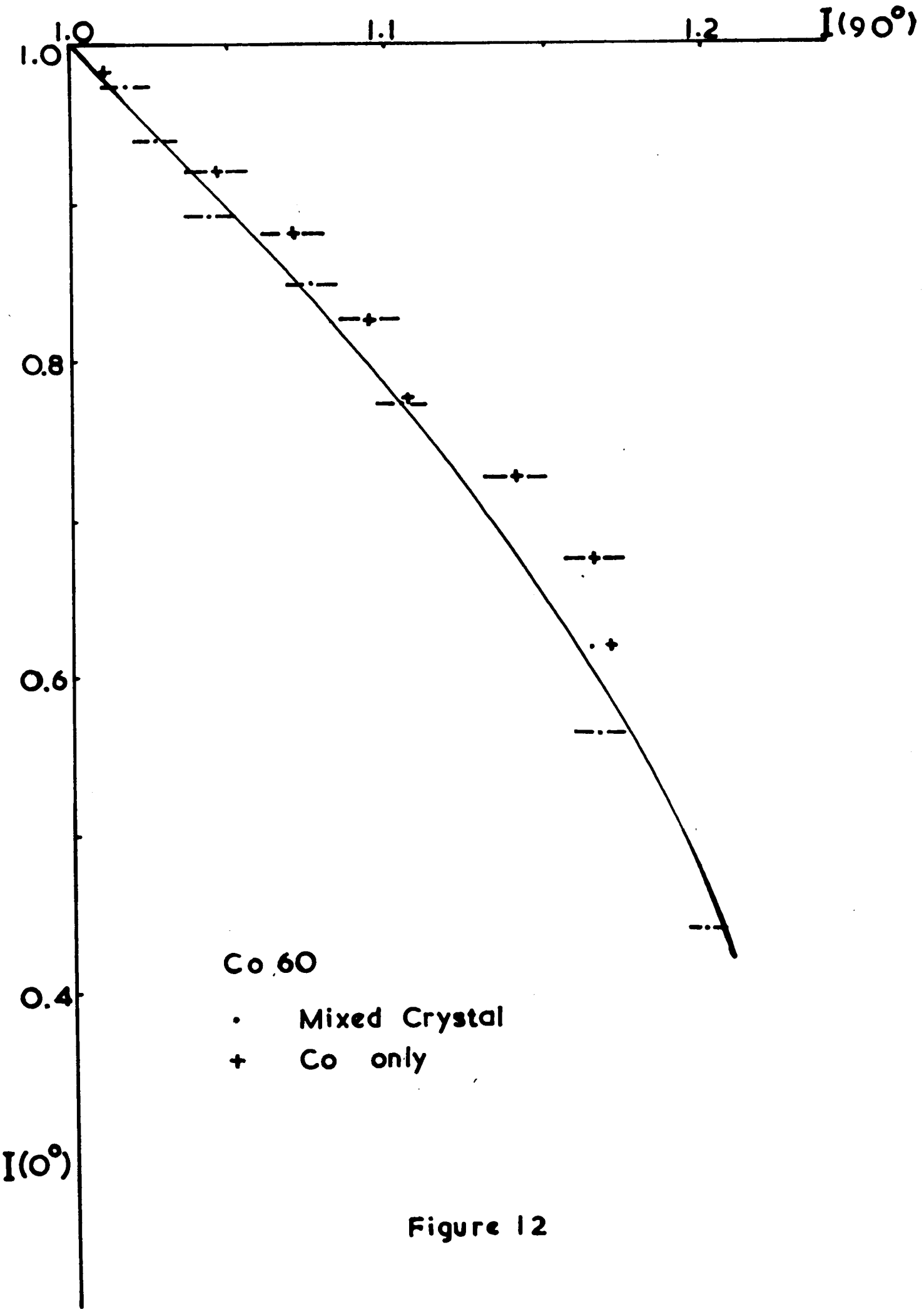


Figure 12

TABLE 8

Co^{60} in Ni-Zn $SiF_6 .6H_2O$

Anisotropy at instant of demagnetisation

Magnet Calibration = 17.2 gauss/amp

H/T ($T_i \sim 1^\circ K$) amps	$\epsilon_{t=0}$	$1/T$ $(^\circ K)^{-1}$
1450	0.635 ±0.016	144 ± 6.0
1160	0.430	86 ±3.0
870	0.237	50 ±3.0
530	0.065	22.5 ±2.5
436	0.040	17.5 ±3.0
292	0.025	14 ±3.0
145	0.010	10 ±4.0

experiment was carried out with great care and has also been used to provide a temperature scale. This is shown in figure 9 of Chapter 6. The crystal had the same concentration as that of the Co^{60} crystal (i.e. 8.6% Ni) but a temperature of $\frac{1}{T} = 80$ was obtained for 25 kilogauss and the lowest temperature reached was only $\frac{1}{T} = 115$ for H = 35 kilogauss. A further set of values has been obtained from the mixed Co^{60}-Mn^{54} crystal which had a concentration of 10.6% Ni. For this $\frac{1}{T} = 100$ for 25 kilogauss and $\frac{1}{T} = 150$ for 35 kilogauss, agreeing very closely with the Co^{58} scale for $\frac{1}{T} < 80$. In fact, it has already been seen (paragraph 5f) that the observed Co^{60} anisotropy for this crystal, when plotted as a function of the Co^{58} temperature scale, agrees well with the theoretical curve in this range.

Since the discrepancy between the Co^{58} scale and the first Co^{60} scale cannot be explained by different concentrations, and in view of the fact that the other scales are closely the same, the Co^{58} temperature scale has been used to interpret the experiments described in this thesis.

7. Discussion

The main difficulty in making a fit to the theoretical curve lies in the large errors inherent in the method of obtaining the temperature scale. Until an accurate thermodynamic temperature scale is obtained there is no merit in solving the Spin Hamiltonian more completely to give the population parameters for the whole range.

However, the present experiment gives a result similar to the

value estimated from the experiment of Grace et al (1954) and the results of a paramagnetic resonance experiment (Jaffries 1950, Kedzie 1958), using the method of dynamic nuclear polarisation, give $g = \frac{\mu}{I} = 1.10 \pm 0.02$ from the line spacings. The resonance spectrum is very complex because of the large number of lines and it is not possible to give a clear-cut value for the spin but I = 3 is favoured. If I = 3 $\mu = 3.30 \pm 0.06$ n.m; for I = 2 the moment would be $\mu = 2.20 \pm 0.04$ n.m.

For Mn^{54} one expects the odd proton and odd neutron to be in $f_{7/2}$ and $p_{3/2}$ states respectively, so that $j_p = 1 + \frac{1}{2}$; $j_n = 1 + \frac{1}{2}$ and a spin between 2 and 5 is expected on the basis of Nordheim's "weak" coupling rule. The Schmidt values for the magnetic moment are tabulated below with the values obtained from the empirical nuclear gyromagnetic ratios.

$g_n(3/2) = -0.334$ (Cr^{53} I = 3/2, $\mu = -0.5$)

$g_p(7/2) = 1.444$ (Mn^{53} I = 7/2, $\mu = 5.05$)

$g_p(5/2) = 1.385$ (Mn^{55} I = 5/2, $\mu = 3.46$)

	Schmidt	g_p (Mn^{53})	g_p (Mn^{55})
I = 3	4.95 n.m.	4.38	4.15
I = 2	5.22	4.65	4.49

None of these agree very well with the measured values but the discrepancy is much smaller for I = 3 than for I = 2 so that one might prefer to adopt the former value.

The disagreement between the experimental and theoretical values probably arises from an "anomalous" coupling of the nucleons outside

the closed shells. Such a coupling appears in the case of Mn^{55} which has a spin of $5/2$ rather than the expected value of $7/2$ as a result of an odd $f7/2$ proton.

The shell model configuration of Mn^{56} is the same as Mn^{54} but for the addition of two neutrons and the expected values for the magnetic moment will be identical. The spin and moment of Mn^{56} have been measured as $I = 3$ $\mu = 3.53 \pm 0.01$nm. (Childs, Goodman & Kieffer 1956) and these values are indeed similar to those found for Mn^{54}.

The deviation of the experimental points from the theoretical plot of $I(0^\circ)$ v $I(90^\circ)$ cannot be explained by difficulties with the temperature scale or by a different value of moment and it suggests that the Hamiltonian does not give a complete description of the ionic states. The effect is that of the ratio B_2/B_4 being smaller than predicted and hence there is a larger contribution from terms in $\cos^4\theta$ than expected.

The effect cannot be produced to any marked extent by changing the value of D and thereby taking into account the variation of D with temperature (Bleaney & Ingram 1951a; figure 2, Chapter 1). The curve for $D = -0.010$ cm^{-1} $A = -0.00766$ cm^{-1} is indistinguishable from that for $D = -0.0134$ cm^{-1} shown in figure 9. However, it suggests that the lowest level is separated from the other levels by a larger interval than given by the hyperfine coupling. This is consistent with the term $a(S_1^+ + S_2^+ + S_3^+)/6$, part of which mixes states $\left|+\frac{5}{2}, M\right\rangle$ and $\left|-\frac{1}{2}, M\right\rangle$ with the accompanying depression of the lower level but the measured value of a is too small to produce any noticeable effect.

CHAPTER 4

THE NUCLEAR ALIGNMENT OF Mn^{52}

1. Introduction

The main theme of the work described in this thesis is the investigation of the properties of nuclear levels by nuclear orientation and, further, to demonstrate that nickel fluosilicate crystals provide a suitable environment for isotopes of the iron transition group. At the outset of this work Mn^{52} had not been investigated by these methods so once the suitability of the environment had been established (i.e. with Mn^{54} and Co^{60}) Mn^{52} was incorporated in this salt. The results should enable the decay scheme to be verified and provide an estimate for the magnetic moment.

Before the experiments were completed an alignment experiment was reported (Huiskamp et al, 1956-57) and since then the moment has been determined by paramagnetic resonance (Abraham et al, 1957).

The results of the alignment experiment (Huiskamp) could not be entirely understood showing an approximately constant anisotropy for temperatures below $\frac{1}{T} = 100$. The manganese had been incorporated in cerium magnesium nitrate and it is believed that the peculiar form of the curves arises in the same way as has been already discussed for Mn^{54}. The present experiments give results in reasonable agreement with theoretical predictions and which verify the proposed decay scheme giving a value for the magnetic moment of 2.5 ± 0.5 n.m. ($I=6, i_\beta = 1$ or $I=7$) or 2.0 ± 0.5 n.m. ($I=6, i_\beta=0$), depending on the character of the

beta transition.

2. The decay scheme

A radioactive isotope, produced by the Fe(d,α)Mn reaction, with a half life of about 6 days was reported by Livingood and Seaborg (1938) and was attributed to Mn^{52}. The decay scheme is shown in figure 1. The ground state of Mn^{52} decays by positron emission and K-capture to an excited state of Cr^{52}. The branching ratio K/β^+ has been measured by several authors:

1.86 ± 0.17	Good et al (1946)
2.01 ± 0.22	Sehr (1954)
1.99 ± 0.06	Konijn et al (1958)[a]
2.05	Zweifel (1957) calculated.

It is seen that they agree well with the value calculated for an allowed transition on the basis of the measured end-point energy, (0.582 ± 0.015 Mev, Peacock & Deutsch, 1946; 0.575 ± 0.004, Konijn 1958[a]) and the atomic number, Z = 25. The shape of the positron spectrum and half-life (log ft. = 5.6) are also consistent with an allowed transition.

The beta-decay is followed by a cascade of three gamma rays 0.734 ± 0.015 Mev (0.741 ± 0.004 Mev - Konijn 1958[a]), 0.940 ± 0.02 Mev and 1.46 ± 0.03 Mev (Peacock & Deutsch 1946) for which the measured internal conversion coefficients, α_K, (Keister 1954) are compared in Table 1 with the calculated values (Rose 1958).

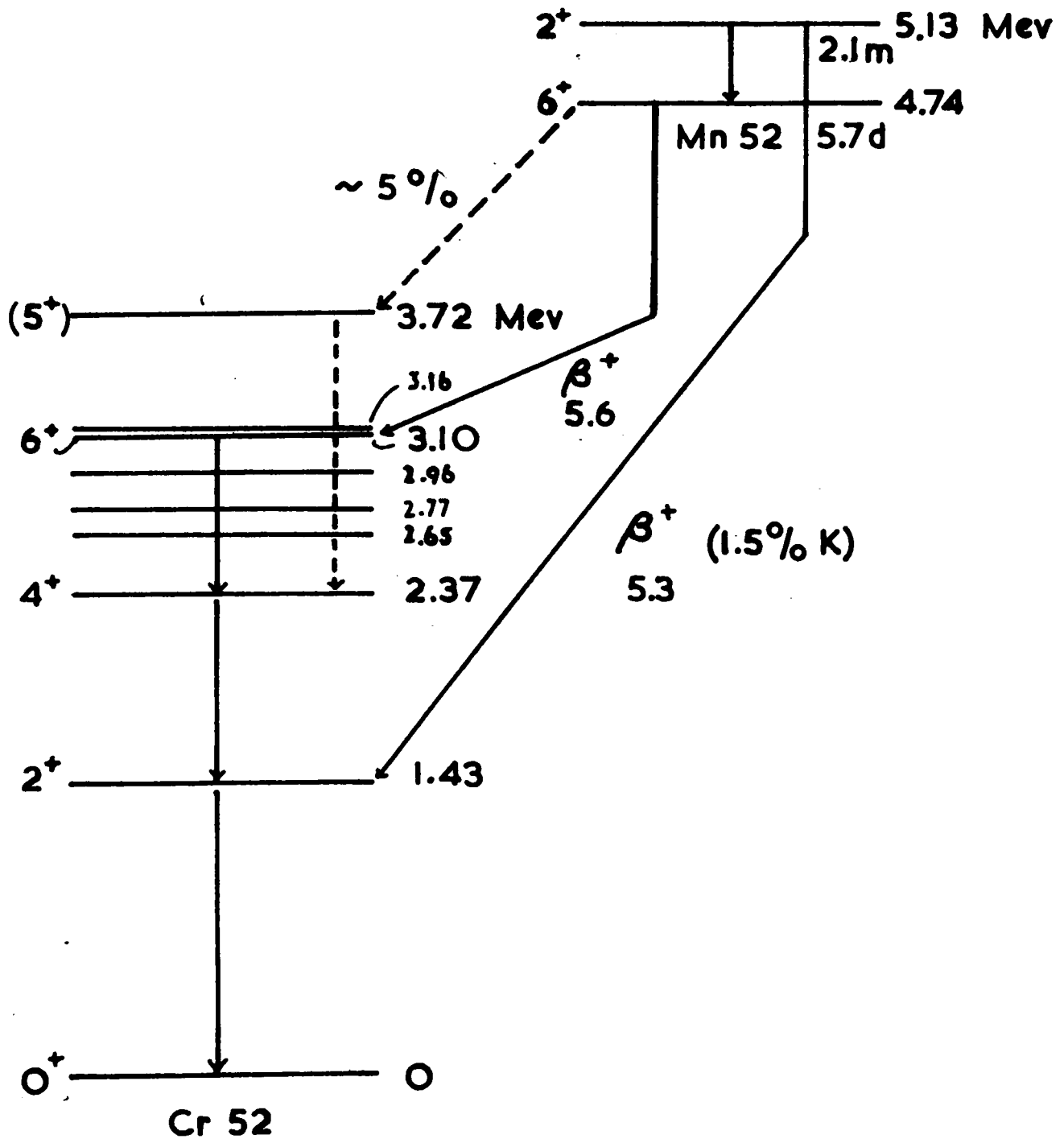

2+
5.13 Mev
2.1m
6+
4.74
Mn 52
5.7d
~ 5 %
(5+)
3.72 Mev
3.16
β+
5.6
6+
3.10
2.96
2.77
2.65
4+
2.37
β+
(1.5% K)
5.3
2+
1.43
0+
0
Cr 52

Figure 1

TABLE 1

Energy Mev	Measured	E1	M1 All x 10^{-4}	E2	M2
0.734	3.0	1.3	2.3	3.4	6
0.940	1.8	0.77	1.4	1.8	3.5
1.46	0.72	~0.35	~0.6	~0.7	~1.2

The measured values are all consistent with electric quadrupole transitions but M1 cannot be definitely excluded. However, E1 and M2 transitions can be definitely ruled out; the pure transitions are not consistent with the observed values while a mixture would require the intensity mixing ratio, δ^2, to be some 10^6 times the value based on single particle transition probabilities. Therefore the change of angular momentum is $\Delta I = 0$, 1 or 2 in each case with no change in parity. The angular correlations for all pairs (Slack 1955) briefly reported in nuclear data compilations are consistent with a spin sequence 6-4-2-0. No cross-over transitions have been observed.

According to the predictions of the Shell model, both the odd proton and odd neutron are in $(f^{7/2})^-$ states and Nordheim's "weak" coupling rule (Nordheim) predicts that $|J_p - J_n| < I < J_p + J_n$ with a preference for a high value, i.e. for 7, and the parity will be even. Such a high spin would be consistent with angular correlation and the fact that the ground state of Mn^{52} only decays to the highest level figuring in the gamma cascade.

The sequence of the gamma rays is determined as a result of inelastic proton (p,p') scattering experiments on Cr^{52} (Naumann 1952;

Masari 1957b) The latter authors have studied both the Mn^{55} (p,α) Cr^{52} and Cr^{52} (p,p') Cr^{52} reactions and find the energy levels given in the following table. The values found by Haussmann et al are also shown with doubtful assignments in brackets.

TABLE 2

Level	$Mn^{55}(p,\alpha)Cr^{52}$	$Cr^{52}(p,p')Cr^{52}$	N	$Cr^{52}(p,p')Cr^{52}$	N
0	0	0		0	
1	1.434	1.433	0.005	1.45	
2	2.368	2.368	0.005	2.43	
3	2.649	2.648	0.008	(2.69)	
4	2.769	2.767	0.008	(2.79)	
5	2.965	2.965	0.008	2.99	
6	——	3.161	0.008	3.20	

The fact that level 6 did not show up in the (p,α) reaction is believed to be due to the low intensity of these groups (Masari). It can be seen that if the cascade takes place between levels 6, 2, 1 and 0 with the order of the gamma rays 0.7h, 0.9h, 1.46 Mev, then their measured energies are in reasonable agreement with those of the levels. However, this would require that the gamma transition between levels 6 and 2 should be 0.793 ± 0.007 Mev in disagreement with measured value. Also if the decay was through level 6, then the end-point energies of the positron spectra from the ground state and isomeric state of Mn^{52}, 0.575 ± 0.00h Mev (Konijn 1958a) and 2.631 ± 0.015 Mev (Arbmann 1956) respectively, would require the

isomeric transition to be 0.32 Mev rather than 0.392 ± 0.008 Mev (Osborne & Deutsch 1947). A study of the beta- and gamma-ray energies (Konijn 1958) suggests that the 0.741 Mev gamma ray is single and comes from a level at 3.109 Mev which is different from the 3.161 ± 0.008 Mev level found by Kasari. The non-appearance of the 3.109 Mev level in the scattering experiments suggests that a large angular momentum change is required to excite this level in agreement with the supposition that the level has spin 6.

The presence of a weak (~5%) transition from the ground state of Mn^{52} to a state of spin 5^+ at about 3.7 Mev, which then decays to the 2.368 Mev level in Cr^{52} emitting a gamma ray of about 1.3 Mev, has been reported (Coleman 1958).

3. Experimental

3a. The production of Mn^{52}

The source material was produced by the Cr^{52} (p,n) Mn^{52} reaction in the Birmingham cyclotron, using 10 Mev protons. A small disc of chromium (Diam. ~0.7 cm. thickness ~0.15 cm.) was held onto the standard copper target by a copper frame screwed onto the target block. This enabled the chromium to be removed easily after bombardment while sufficiently good thermal contact was ensured by making the contact surfaces smooth and clean.

Hemmendinger (1940) reports a yield of 0.68×10^{-6} radioactive atoms per proton using 6.6 Mev protons. Hence $\frac{L\rho t}{A}.\sigma = 0.68 \times 10^{-6}$ radioactive atoms per proton where L=Avogadros number, A = atomic weight

and ρt is the effective range of the protons in units mg/cm^2, assuming that this is less than the target thickness and σ is the cross section. The range of 6.6 Mev protons in copper is $\rho t \sim 0.107$ gm per sq. cm. (Rich & Madey 1954). Assuming ρt for Cr^{52} to be ~ 0.1 gm/cm^2, then the cross section at 6.6 Mev is

$$\sigma = \frac{0.68 \times 10^{-6} \times 52}{6.02 \times 10^{23} \times 0.1} = 0.587 \times 10^{-27} cm^2$$

Thus if we take the cross section at 10 Mev as 1 millibarn, the yield should be

$$\frac{dN}{dt} = \lambda \frac{L \rho t}{A} n.\sigma$$

and with $\rho t = 0.2$ gm/cm^2 (Rich & Madey 1954) this gives 100μc per 505 watt hours.

To allow for the decay while the chemistry and crystal growing were being carried out, it was planned to obtain 200μc. This would require 1010 watt hours and this was most conveniently obtained by running the cyclotron at 500 watts for two hours.

An estimate of the source strength of the manganese activity, after chemical separation, was made from the number of counts in the 1.45 Mev photopeak using a 1" cube NaI crystal at 25 cms. This gave the source strength at the time of removal from the cyclotron as about 70μc., from which a cross section ~ 0.35 mb. can be derived. The difference between these figures arises from the errors in the measurement of source strength and in extrapolation from the results at low energy.

3b. The chemical separation

The chromium was detached from the target, dissolved in HCl and a trace of iron added. The solution was then treated with sodium peroxide and filtered, the filtrate being CrO_4. The residue, containing the manganese as an oxide together with iron and possible copper hydroxide, was re-dissolved in hydrochloric acid. This solution was treated with hydrogen peroxide in the presence of ammonia in order to separate out any copper which goes in the filtrate as $Cr(NH_3)_4$. To separate out the iron which has so far acted as carrier for the manganese, the residue is dissolved in 6N-HCl and shaken with ether. Most of the iron separates out into the ether layer, the manganese remaining in the water. This process was repeated two or three times and then the manganese chloride was evaporated to dryness to remove excess water and HCl. Some manganese activity remained with the iron portion.

3c. The crystal

The Manganese chloride was dissolved in a small quantity of water and added to a solution of 10 grams $(Ni-Zn)SiF_6, 6H_2O$ with a small excess of hydrofluosilicic acid. A crystal of about 2 gms was grown from this solution using an inactive seed of about 0.2 gms and at the time of the run there were about 2μs of activity. This is consistent with about 1/5 of the activity going into the crystal and the half life of the decay.

The crystal was mounted in the low temperature apparatus with its axis horizontal in the usual way.

3d. The gamma ray spectrum

Scintillation counters with 2" x 2" cylindrical NaI crystals were used and the pulse height distribution from the Mn^{52} is shown in figure 2. It can be understood as the composite spectrum for gamma rays of 1.45 Mev, 0.94 Mev and 0.73 Mev, together with the annihilation radiation associated with the positron emission. There is no evidence for a peak at 1.3 Mev (Coleman) or at 0.84 Mev from Mn^{54}, a certain amount of which will have been produced by $Cr^{54}(p,n)Mn^{54}$ reaction. When the 5.7 day Mn^{52} had decayed, a peak at 0.840 Mev was found. There were 35 counts per second in the photopeak using a 2" x 2" NaI crystal 2.5 cms from the source, i.e. a source strength of 4.7×10^{-2} μc. At the time of the experiment the Mn^{54} will have had a strength of $\sim 0.055\mu c$ or 2.7% of the Mn^{52} and its contribution to the counting rate will have been much less and has been neglected.

The cross section for Mn^{54} can be deduced from this measurement. Allowing for the decay there must have been $0.056\frac{5}{\mu c}$ Mn^{54} at the time of removal from the cyclotron. Thus, using the relationship for the yield given in Section 3a, we get 0.0156×10^{-27} cm^2 for natural chromium. The ratio of cross sections is $\sigma_{54} : \sigma_{52} :: 0.0156 : 0.35$ for the natural abundances of Cr^{54} and Cr^{52}, i.e. 2.6% and 83.5% respectively. Thus for equal abundance the ratio would be

$$\frac{0.0156}{2.6} : \frac{0.35}{83.5} \text{ or } 1 : 1.43$$

which is reasonable since although the Q of the reactions is somewhat different, the Coulomb barrier is the same.

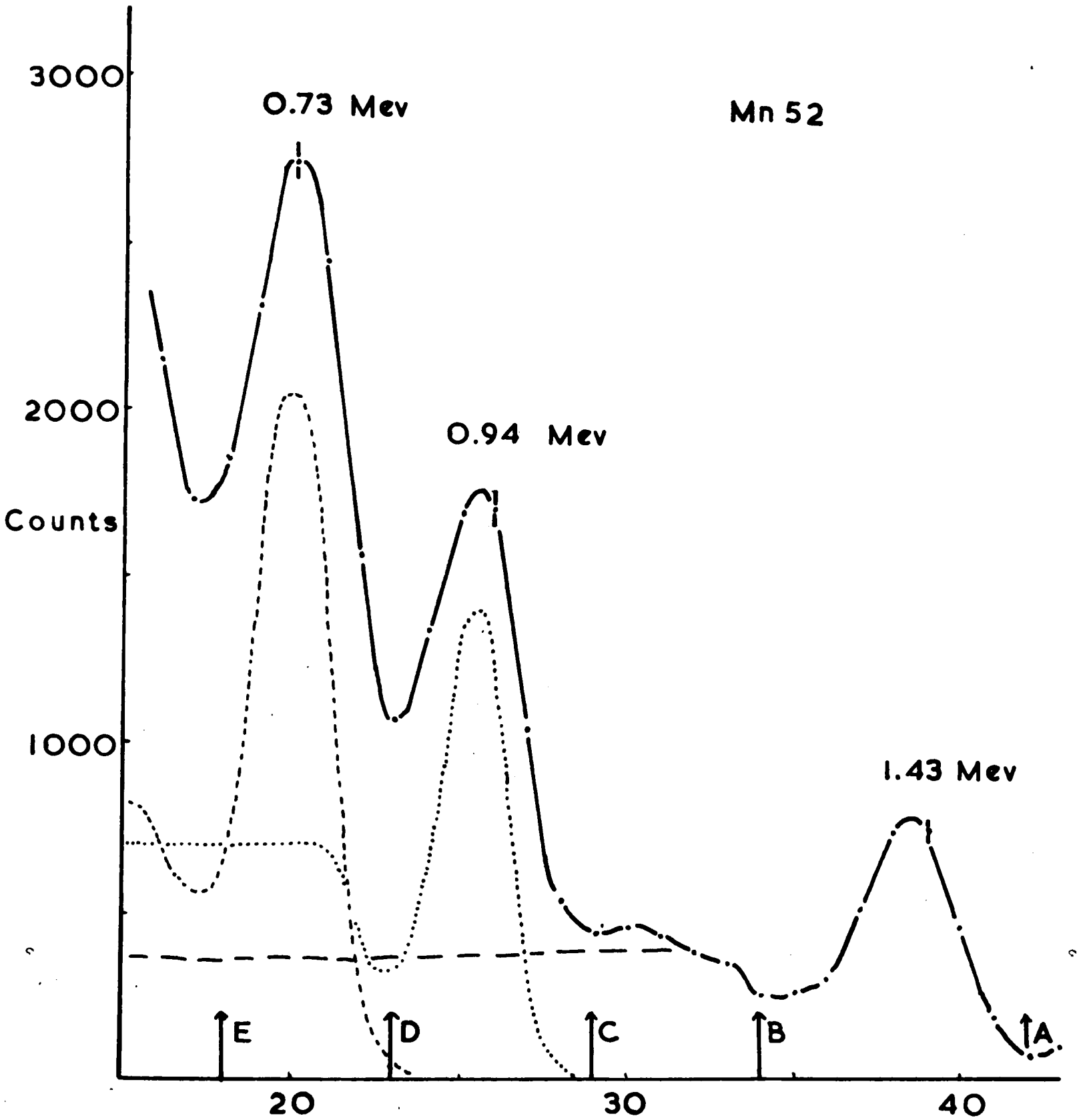

3000
2000
1000
Counts
0.73 Mev
0.94 Mev
1.43 Mev
Mn 52
E
D
C
B
A
20
30
40
Counting Channel

Figure 2

Discriminator levels were set at A(1.55 Mev), B(1.25 Mev), C(1.07 Mev), D(0.84 Mev) and E(0.65 Mev) (figure 2). Thus B - A formed a channel about the 1.45 Mev peak, D - C formed one about the 0.94 Mev peak and E - D about the 0.73 Mev peak.

3e. Procedure

A series of demagnetisations were carried out from initial fields of up to 25 kilogauss. Gamma-ray intensities were measured along the crystal axis and in the equatorial plane as the crystal warmed up and these were normalised to unity for the intensity at 1°K (Table 3).

The anisotropy for each channel (Table 4) was plotted as a function of the magnetic temperature (δ) (figure 3) and it was found that within experimental error (±0.014) each showed the same anisotropy. Now gamma rays which are Compton scattered in the detector show the same anisotropy as the photopeak, so pulses due to higher energy gamma rays lying under the lower energy peaks will have the same anisotropy as the true gamma ray giving rise to the peak so there is no need to make any correction for these pulses.

3f. Scattering and aperture corrections

The source counter distance was 4.97 cms. for the axial position and 3.97 cms. for the equatorial position giving angular apertures of $18\frac{1}{2}^{\circ}$ and $21\frac{1}{2}^{\circ}$ (half-angle) respectively, hence:-

$g_2 = 0.92$ axial	$g_2 = 0.90$ equatorial
$g_4 = 0.76$ "	$g_4 = 0.69$ "

No additional correction has been made for scattering because for the 1.45 Mev gamma ray, the change in the attenuation factors is negligible

TABLE 3

Mn^{52} in Ni-Zn Si $F_{6}.6N_2O$ - 1.45 Mev gamma ray

Initial Field = 25 kilogauss, Counting Interval = 20 secs., Source Counter Distance = 4 cms.

(Low bias counting rates only - corrected for background)

Time min-secs	Galv. defl. cms.	Axial Counter - bgd 56	mean	$I(0^\circ)$	Equatorial Counter - bgd 64	mean	$I(90^\circ)$	ϵ
0-15		2878			6289			
0-51	7.55	2989	2933 ± 38	0.685 ±0.010	6229	6259 ± 56	1.144 ±0.011	0.40 ± 0.014
1-20		2975			6149			
1-49	7.16	3041	3008	0.703	6269	6205	1.133	0.38
2-15		3115			6192			
2-45	6.93	3118	3117	0.728	6064	6128	1.120	0.35
3-14		3204			5909			
3-43	6.74	3322	3263	0.762	6101	6005	1.099	0.31
4-11		3184			6094			
4-40	6.60	3302	3243	0.757	6012	6053	1.108	0.32
		4338			5499			
		4343			5554			
		4312	4311		5277	5432		$\epsilon_{t=0} = 0.44 \pm 0.03$
		4262			5417			
		4299			5414			$T_1 \sim 1^\circ K$
		4344			5536			
		4162			5550			
		4213	4254		5453	5515		
		4186			5495			
		4365			5540			
			4282 ± 21			5474 ±23		

TABLE 4

Mn^{52} in Ni-Zn $SiF_6, 6H_2O$

Anisotropies for all gamma-rays -
(blocked values)

1.46 Mev		0.94 Mev		0.73 Mev	
ϵ %	δ	ϵ %	δ	ϵ %	δ
39.59	7.51	34.6	7.05	36.63	7.31
37.70	7.15	29.1	6.61	32.63	6.88
34.50	6.93	26.6	6.37	30.47	6.63
31.10	6.65	23.7	6.13	27.87	6.39
28.68	6.36	21.7	5.90	24.54	6.13
24.72	6.12	18.8	5.69	21.75	5.90
21.94	5.88	15.6	5.34	19.0	5.68
17.60	5.61	13.45	5.22	14.30	5.36
15.4	5.44	5.94	4.70	11.16	5.17
9.85	5.09	1.50	4.12	7.72	4.86
6.75	4.88	0.82	3.03	2.24	3.96
5.2	4.65				
2.57	3.97				
0.08	3.12				

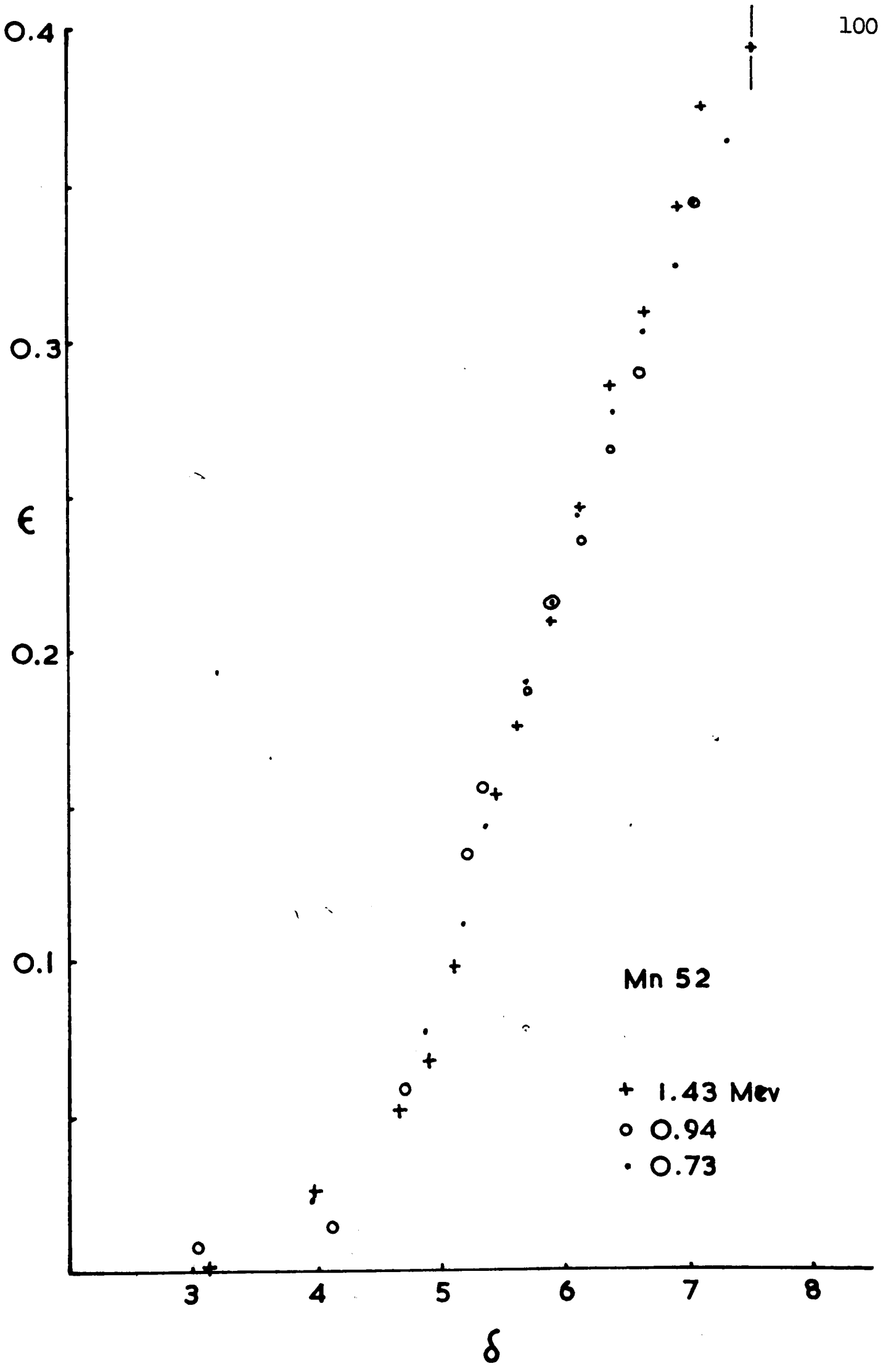


Figure 3

compared to the experimental error.

3g. Results

The anisotropy, ϵ, for each of the three gamma rays (Table 4) is plotted as a function of the magnetic temperature parameter δ in figure 3. It can be seen immediately that ϵ is very closely the same for each gamma ray and is positive. The normalised intensities $I(0^0)$ and $I(90^0)$ are given in Table 5 for the 1.45 transition. Their interdependence is shown in figure 4. The values for the other transitions follow the same curve which indicates the presence of P_4 terms, i.e. gamma-rays cannot be pure dipole transitions.

4. Conclusions

4a. The spin sequence

It is possible using this information to deduce the spins of the levels involved in the decay. First of all the observance of an anisotropy means that none of the excited states can have spin zero while the absence of ground state transitions from the levels at 3.109 Mev and 2.368 Mev suggests that these states have spins $\geqslant 3$.

The 1.45 Mev transition must be pure since the Cr^{52} ground state has spin zero and the presence of P_4 terms (figure 4) requires that it is a quadrupole transition. A dipole transition could give a positive anisotropy if the 0.94 Mev transition was mixed but this would mean that the three gamma rays would have different anisotropies. Thus $I_1 = 2$ and $I_2 = 1,2,3,4$. The absence of ground state transitions suggests 3, 4 are more likely than 1 or 2. 2 or 3 could only give

TABLE 5

Mn^{52} in Ni-Zn Si $F_6 . 6H_2O$

Normalised Intensities for 1.46 Mev Gamma ray
(blocked values)

I(0°)	I(90°)
0.678	1.129
0.697	1.130
0.715	1.127
0.738	1.119
0.759	1.111
0.776	1.100
0.798	1.092
0.823	1.079
0.842	1.073
0.862	1.058
0.882	1.066
0.896	1.062
0.918	1.064
0.945	1.033
0.962	1.018
0.980	1.016
1.000	1.005

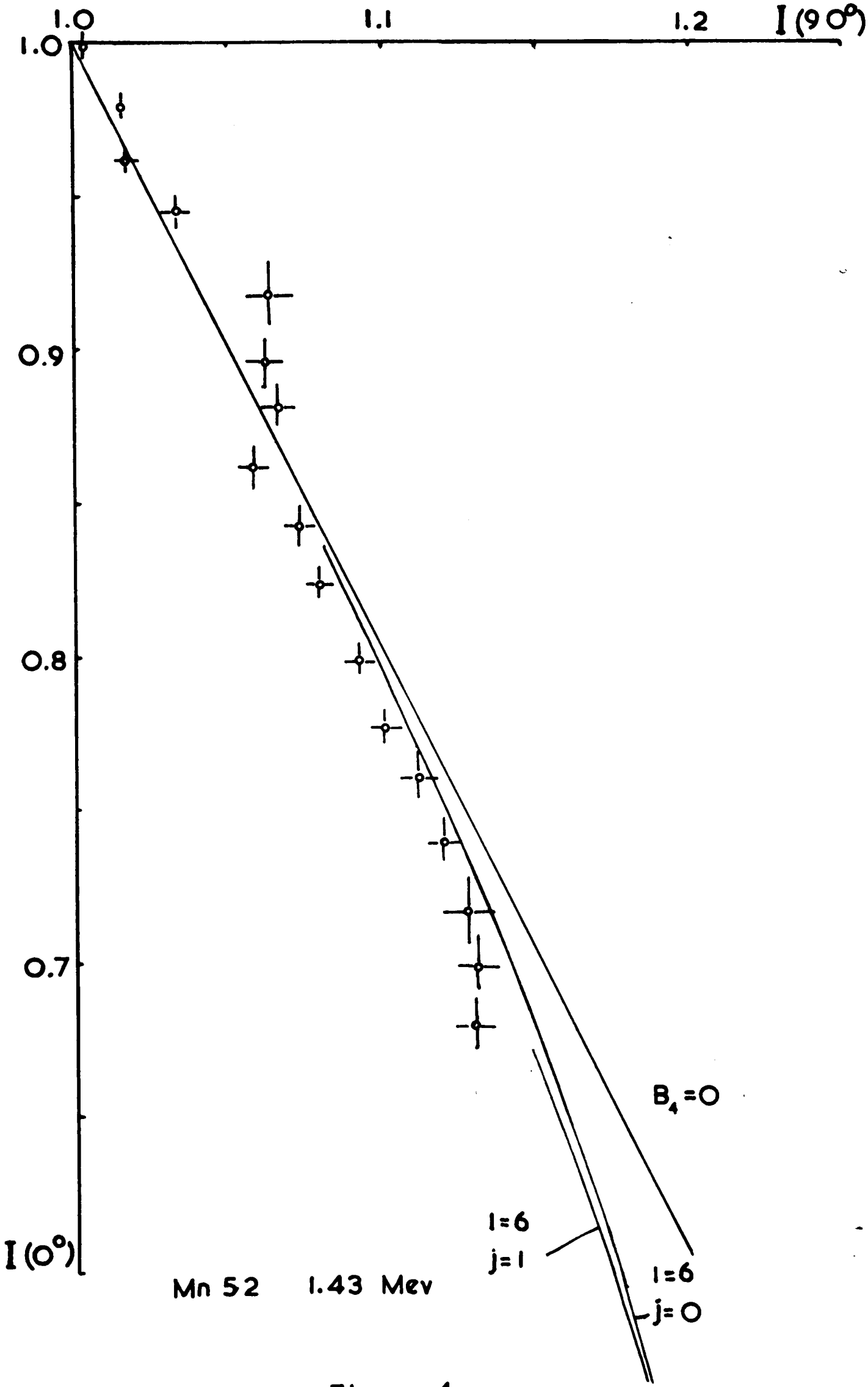


Figure 4

equal anisotropies for the two gamma rays if the 0.94 Mev gamma ray was a dipole-quadrupole mixture but this would not give anisotropies of the same magnitude for the three gamma rays. A spin sequence 4-2-0 gives the same positive anisotropy for the gamma rays and limits I_3 to 2,3,4,5 or 6. Values 2,3,4 would give transitions to the ground or first excited state while spin 5 does not allow the gamma rays to have equal anisotropies. The sequence $6^+ \rightarrow 4^+ \rightarrow 2^+ \rightarrow 0^+$ is consistent with the measured positive and equal anisotropies and the internal conversion results. The ground state of Mn^{52} is then either 6 or 7.

The 21 minute isomer of Mn^{52} decays by an allowed β^+-transition to the first excited state of Cr^{52} and by a 0.39 Mev gamma ray to Mn^{52} ground state. Both the ground state and isomeric state of Mn^{52} have even parities so the transition can only be M3, E4, M5 or E6, etc. The single particle half life (Moszkowski) for such a transition is ~38 minutes for E4, while the M3 half life is less than 1 second ($M4, T_{\frac{1}{2}} \sim 3.3$ hours) and M5, E6 gave much longer lived states.

Hence the isomeric level must have spin 1, 2, 3 but, as it only decays by β^+-emission to one level, 2 is most likely. The Mn^{52} ground state would then have spin 6.

4b. The angular distribution

Having deduced the decay scheme, the expected angular distribution can be calculated. We have three possibilities:-

$I(\theta)$ $1-0.4029\, g_2 B_2 P_2 - 0.2088\, g_4 B_4 P_4$, I=6, J=0,

$I(\theta)$ $1-0.3739\, g_2 B_2 P_2 - 0.1591\, g_4 B_4 P_4$, I=6, J=1

and $I(\theta)$ $1-0.3915\, g_2 B_2 P_2 - 0.1875\, g_4 B_4 P_4$, I=7, J=1.

Population functions B_2, B_4 have been calculated using the high and low temperature approximations and an interpolation made between these two regions to give the approximate form of the curve.

In figure 4 $I(0^\circ)$ is plotted against $I(90^\circ)$ for 1.46 Mev gamma ray and it is seen that the general agreement with the theoretical curve is quite good but no distinction can be made between the three possibilities.

4c. The magnetic moment

The anisotropy, ϵ, is plotted against temperature in figure 5 using the scale obtained from Co^{58} (Table 6). It is seen that the variation is monotonic although the experimental points tend to deviate slightly from the curve at lower temperatures. Values of the magnetic moment can be deduced for each of the possible distributions by taking the best fit curve.

$$\mu = 2.0 \pm 0.5 \quad I=6,\ j=0$$

$$\mu = 2.5 \pm 0.5 \quad I=6,\ j=1$$

$$\mu = 2.5 \pm 0.5 \quad I=7,\ j=1$$

5. Other experiments

5a. Gamma ray measurements with oriented nuclei

Huiskamp et al (1956, 1957) have carried out similar experiments in which the Mn^{52} was incorporated in crystals of cerium magnesium nitrate. Two sets of experiments were carried out with specimens consisting of 5 and 4 aligned single crystals respectively. The Mn^{52} nuclei were both aligned and polarised, measurements being made of

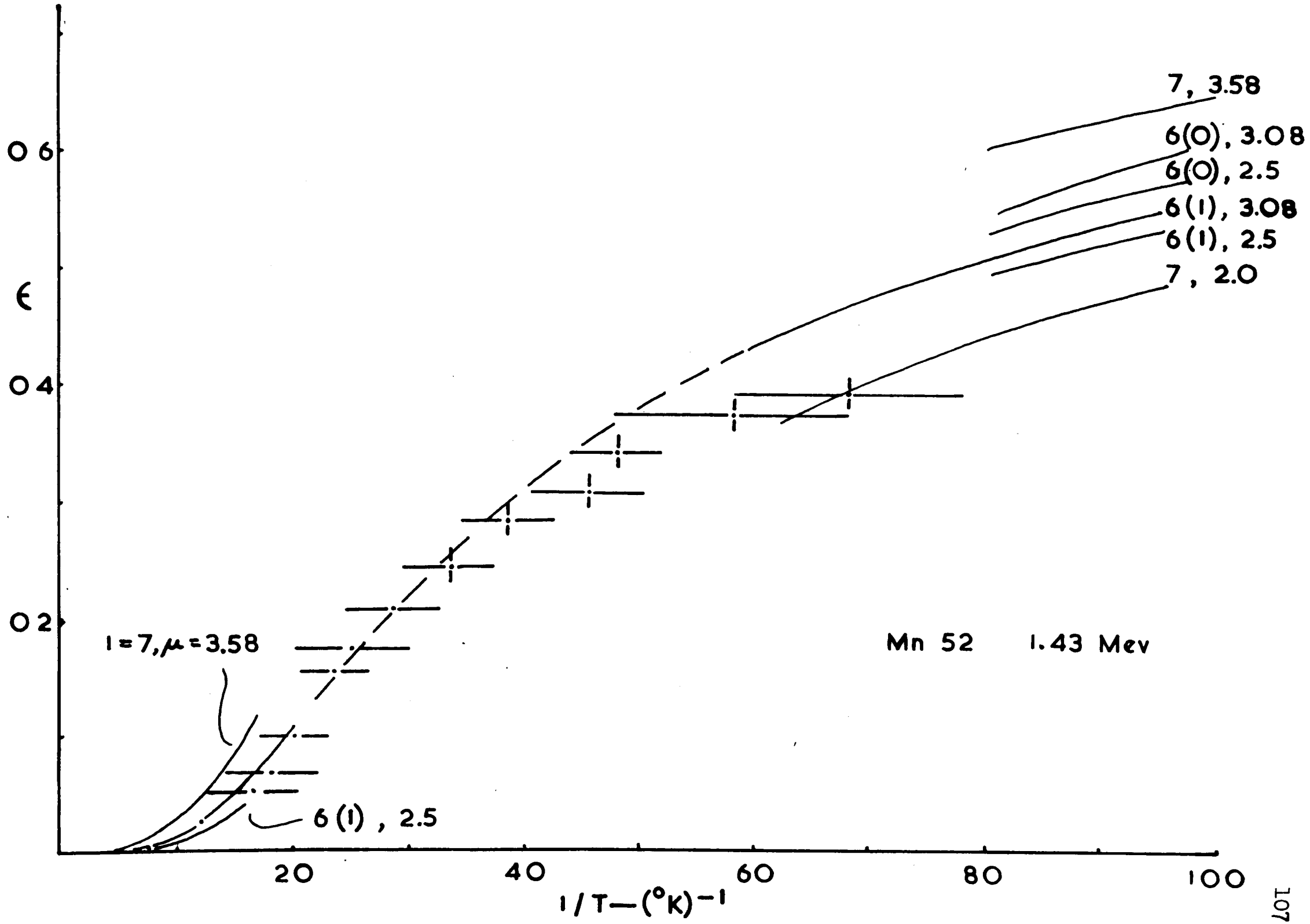
TABLE 6

Mn^{52} in Ni-Zn $SiF_6.6H_2O$

Anisotropy for 1.43 Mev transition
(blocked values)

ϵ	$\frac{1}{T}$
0.395 ± 0.014	68 ± 10
0.378	58 ± 10
0.345	48 ± 4
0.310	45 ± 5
0.286	38 ± 4
0.245	33 ± 4
0.210	28 ± 4
0.175	25 ± 5
0.155	23 ± 3
0.100	20 ± 3
0.070	18 ± 4
0.050	16.5 ± 4
0.025	~12
0.002	~7.5

Figure 5


0.6
ε
0.4
0.2
7, 3.58
6(0), 3.08
6(0), 2.5
6(1), 3.08
6(1), 2.5
7, 2.0
I=7, μ=3.58
6(1), 2.5
Mn 52 1.43 Mev
20
40
60
80
100
1/T—(°K)⁻¹

the angular distribution, the linear polarisation and circular polarisation of the three gamma rays.

The gamma ray anisotropy was found to be positive and closely the same for each transition in agreement with the present work. The linear polarisation measurements show that the gamma rays were polarised predominantly in a direction perpendicular to the nuclear spin indicating that the radiation is indeed electric in character. The circular polarisation requires the magnetic moment to be positive.

Although it was possible to draw these general conclusions the anisotropy from aligned nuclei showed marked deviations from that expected on the basis of the Spin Hamiltonian. It reached a maximum at $\frac{1}{T\Theta} = 100$ and then remained practically constant to the lowest temperatures reached ($\frac{1}{T\Theta} = 300$). This effect is very similar to that observed for Mn^{54} in the same environment (Grace et al 1954) which has been discussed earlier. The anisotropy from polarised nuclei showed a similar but smaller deviation from theory. The magnitude of the anisotropy was much larger in this case in spite of the fact that the temperatures reached were not as low (e.g. for alignment ϵ max = 0.20 at $\frac{1}{T\Theta} = 300$; for polarisation $\epsilon_{max} = 0.68$ at $\frac{1}{T\Theta} = 150$).

The experimental points could be fitted to a theoretical curve for $\frac{1}{T\Theta} < 80$ giving a magnetic moment $\mu = 2.8 \begin{smallmatrix} +0.8 \\ -0.5 \end{smallmatrix}$ for a pure Gamow-Teller transition $I = 6 \rightarrow I = 6$. The value for the other modes of beta transition differ by only a few percent.

No fit could be made for $\frac{1}{T\theta} > 80$ and this experiment emphasises the fact that the Spin Hamiltonian used does not describe completely the state of the Mn^{++} ion in cerium magnesium nitrate.

5b. Beta-ray measurements

Measurements of the beta-ray asymmetry and beta-gamma angular correlation from polarised Mn^{52} (Ambler et al 1958; Postma et al 1958) and of the circular polarisation correlation (Boehm 1958) show evidence for interference between Fermi and Gamow-Teller matrix elements. This interference can only occur if the ground state spin of Mn^{52} has spin 6.

However, the Fermi component is small (Ambler $0.0018 < \lambda < 0.022$; Postma, $\lambda \sim 0.0025$; Boehm, $\lambda = 0.05 \pm 0.03$). If I = 7 there would be no interference and the asymmetry parameter α' would be +1.0 compared with the measured value of 0.232 ± 0.010. A pure Gamow-Teller transition 6→6 would give $\alpha' = +0.1428$.

5c. The spin and magnetic moment from paramagnetic resonance

Measurement of the gyromagnetic ratio $g = \frac{\mu}{I}$ for the ground state of Mn^{52} has been made by the method of dynamic nuclear polarisation (Abraham 1957). It is found by comparison of the gamma ray anisotropy spectrum for Mn^{52} with the paramagnetic resonance absorption spectrum for stable Mn^{55}. They find $g = 0.514 \pm 0.02$ and spin 6 is favoured (i.e. $\mu = 3.08 \pm 0.12$). Although the value of $I = 7$ ($\mu = 3.598 \pm 0.14$) cannot be definitely excluded.

6. Discussion

The present experiment again shows that nickel fluosilicate is a useful salt for alignment and in this instance the proposed decay scheme 6^+ or 7^+ (β) 6^+ (E2) 4^+ (E2) 2^+(E2) 0^+ has been verified. Values of the nuclear magnetic moment for the 3 possible types of beta transition $6\rightarrow6$ $j=0$, 1 and $7\rightarrow6$ have been obtained. These are in agreement with the value found by Huiskamp but agreement with the value found by Abraham et al can only be obtained if $I=6$, a condition which is also required by the beta ray investigations. It is not possible to choose between the Fermi and Gamow-Teller modes or measure the possible admixture.

On the basis of the nuclear shell model, the odd proton and odd neutron states are both $f_{7/2}$ giving a nuclear moment $\mu=\frac{1}{2}(g_p+g_n)I$. If the free particle g values are used the Schmidt limit for the magnetic moment is $\mu=3.309$ if $I=6$ and 3.860 for $I=7$. Empirically we have

$g_n(7/2) = -0.314$ from Ti^{49} ($\mu=-1.102$, $I=7/2$)

$g_p(7/2) = 1.44$ Mn^{55} ($\mu=5.05$, $I=7/2$)

or $g_p(7/2) = 1.385$ Mn^{55} ($\mu=3.46$, $I=9/2$)

giving

Mn^{53}	Mn^{55}	
3.38 n.m.	3.21 n.m.	$I=6$
3.94 n.m.	3.75 n.m.	$I=7$

It has been noted that in the present experiment, the anisotropy

tends to be lower than the theoretical value for the lowest temperatures reached ($\frac{1}{T}=70$). This could be due in part to the difference in concentrations of the Mn^{52}(9.25%) and Co^{58}(8.6%) crystals but if the temperature varies as the square root of the concentration (Milner 1957) this will only give a difference of 3 in $\frac{1}{T}\sim 70$. This effect is very similar to that found by Huiskamp et al for aligned and polarised Mn^{52}. It is very interesting to ask whether the anisotropy for Mn^{52} aligned in nickel fluosilicate would show deviations for temperatures lower than $\frac{1}{T}=100$. It can be seen from the plots $I(0^{\circ})$ v $I(90^{\circ})$ for both Mn^{52} and Mn^{54} that there is a general tendency to lie to the left of the curve. These effects cannot be described in terms of the present Spin Hamiltonian but could perhaps be explained by some additional interaction between the ions.

CHAPTER 5

THE DECAY OF MANGANESE 56

1. Introduction

Manganese 56 decays by beta-emission to various excited states of iron-56. The latter falls in an interesting region of the periodic table; it is an even-even isotope with both neutron and proton numbers differing by two from those required for a closed shell. It is also in a region where collective phenomena appear, e.g. the vibrational levels of Fe^{58} and Ni^{60} (Wilets and Jean 1956; Scharff-Goldhaber and Weneser 1955) so that it might be expected that characteristics of both single particle and collective models should appear. A considerable amount of work has been done with Mn^{56} but there was still some ambiguity in the assignment of spins to the Mn^{56} ground state and the 2.98 Mev level of Fe^{56}. These uncertainties might be resolved by an alignment experiment.

The early work of Grace et al (1954) demonstrated that Manganese nuclei could be aligned using the method of Bleaney and earlier experiments in this series using Mn^{54}, Mn^{52} (Chapters 3, 4) showed that nickel fluosilicate was a suitable crystal for this purpose.

However, it would be very difficult to grow a crystal from active solution with such a short half-life and it is necessary to produce the activity by irradiation of a crystal containing Mn^{55}. This procedure immediately presents two difficulties. First of all, no other activity of comparable strength and similar energy must be produced by the irradiation and, secondly, the possible effects of

radiation damage must be considered.

The work reported in this chapter shows that nuclear data can be extracted from the results in spite of these difficulties and by combination with an angular correlation measurement unique assignments have been made for the level spins and gamma-ray multipolarities.

2. The decay scheme

The 2.58 hour Manganese seems to have been discovered first by Amaldi et al (1935) and many investigations of its decay have since been carried out. The levels of the daughter nucleus, Fe^{56}, are also excited in the decay of Co^{56}. This nucleus has been thoroughly investigated in alignment experiments of the Leiden group (Diddens 1958) and their conclusions are important for the understanding of the decay of Mn^{56}.

The decay scheme of figure 1 is based primarily on the work of Elliott and Deutsch (1943), Sakai (1955), Cook and Townsvee (1957) and Diddens; the level energies are also known from the proton inelastic scattering experiments of Masari et al (1957)[a] For clarity only the gamma-rays in the decay of Mn^{56} are shown and the spin assignments underlined are those obtained from the present experiments. The dotted levels are known from (p, p') experiments; those of full length being known also from the decay of Co^{56}.

Gamma rays 1-5 are firmly established and a good measure of agreement has been obtained for the relative intensities of the principal ones:- $\gamma_1 : \gamma_2 : \gamma_3 : \; : 100 : 30 : 20$. Different intensities

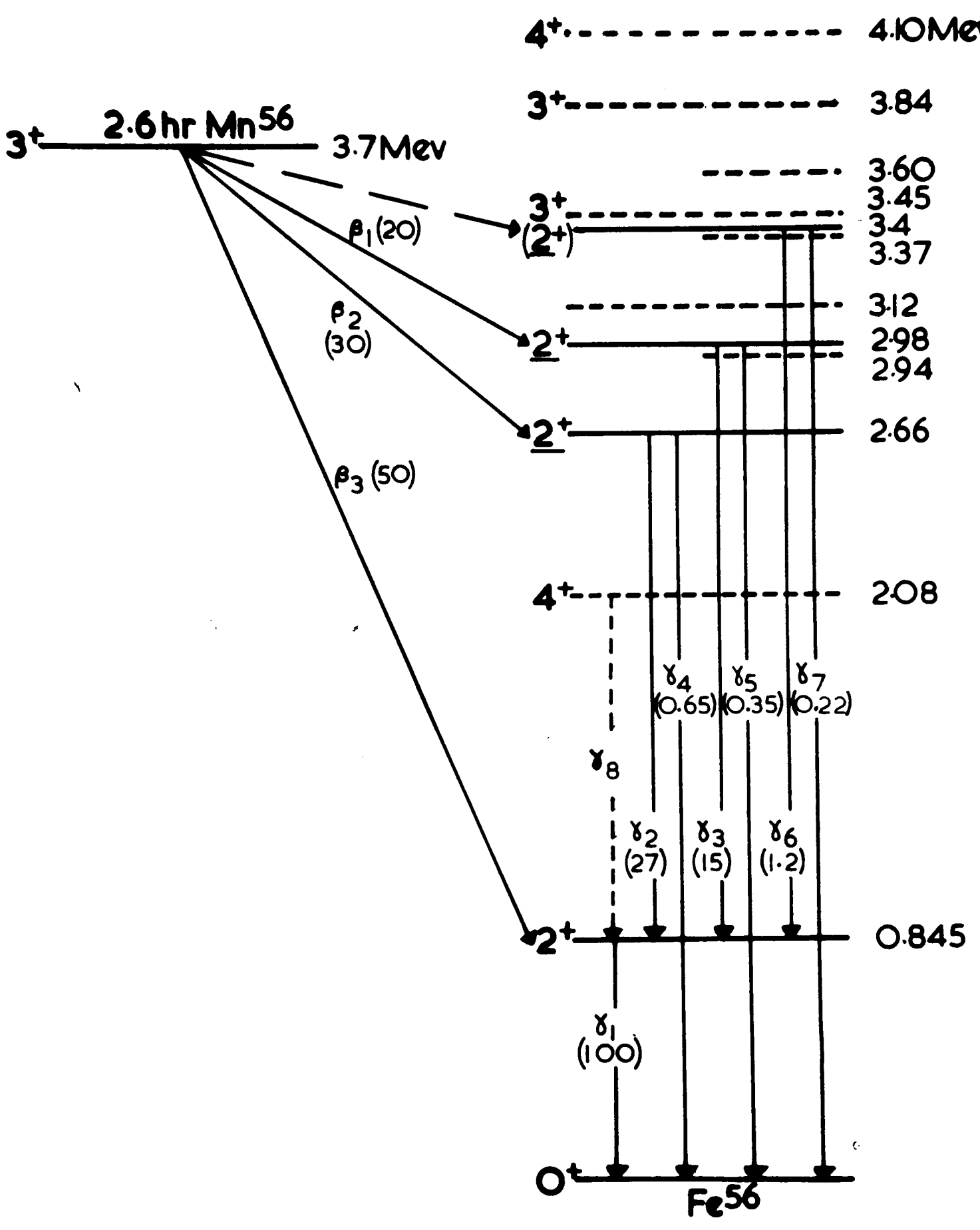

4+ 4.10Mev
3+ 3.84
3.60
3+ 3.45
(2+) 3.4
3.37
3.12
2+ 2.98
2.94
2+ 2.66
4+ 2.08
3+ 2.6hr Mn56 3.7Mev
β1 (20)
β2 (30)
β3 (50)
γ4 (0.65)
γ5 (0.35)
γ7 (0.22)
γ8
γ2 (27)
γ3 (15)
γ6 (1.2)
2+ 0.845
γ1 (100)
0+
Fe56

Figure 1

have been found for γ_4 and γ_5 by Bishop et al (1950), Russell et al (1948) and Cook and Tomnovec (1957). Namely:-

γ_4	γ_5		
0.1	0.2	per cent γ_1,	Bishop
1.0	1.0		Russell
0.72	0.38		Cook

Cook (1958) also reports gamma rays of 2.52 Mev (γ_6) (1.15%) and 3.39 Mev (γ_7) (0.21%). Slätis and Seigbahn (1952) have measured the internal pair conversion coefficients for γ_2 and γ_3 as 6×10^{-4} and 5×10^{-4} respectively and on this basis they suggest that γ_2 is predominantly an electric dipole (E1) transition and γ_3 an E2 gamma ray. The angular correlation measurements (Metzger & Todd 1953) for the $\gamma_2-\gamma_1$ and $\gamma_3-\gamma_1$ cascades show that both the gamma rays are a dipole-quadrupole mixture but they only consider the mixing ratio, δ, for the case of the dipole component being more intense than the quadrupole. The log ft. values for the beta-transitions feeding these levels are 5.2 (β_6) and 5.5 (β_2), showing that these are both allowed transitions with no parity change so that γ_2 and γ_3 must involve the same parity change as each other, i.e. both E2/M1 or both E1/M2.

The systematics of even-even nuclei, the evidence of coulomb excitation (Temmer & Heydenberg 1956) and the polarisation correlation experiments of Wood and Jastram (1955) show the 0.845 Mev level to have spin 2. The $\gamma - \gamma$ correlation results show that the spin of the

2.66 Mev state is 2 but were not sufficiently accurate to decide between the possibilities of 2 and 3 for the spin of the 2.98 Mev level.

Since the present work was begun, the ground state spin of Mn^{56} has been measured by Childs and Goodman and Kieffer (1958), using an atomic beam technique; the same authors find a value of 3.53 ± 0.01 n.m. for the magnetic moment.

3. Irradiation damage

Exploratory experiments using Cobalt in nickel fluosilicate and cerium in cerium magnesium double nitrate show that the full anisotropy will not be obtained for irradiated crystals.

If the damaged crystal is heated and another experiment is carried out, it has been found that the anisotropy increases and if annealing is repeated sufficiently it may be restored to a value very close to that obtained for the same isotope aligned in a crystal grown from active solution.

For Co^{60} the maximum anisotropy observed for a crystal irradiated at normal pile temperatures (~40°C) was about 10%. When the crystal was annealed for 24 hours at 60°C, the maximum effect was 29% and after annealing at 80°C a 33% effect was observed. An anisotropy of 36% was found for a similar crystal which had been grown from active solution.

A similar experiment was performed using Ce^{141} in cerium magnesium nitrate. A maximum anisotropy, after annealing, of 14.8% being found, compared with 16.5% found by Taylor (1957) for a crystal grown from active solution. These results clearly illustrate the effect of damage on the anisotropy and show how these effects can be partially removed by annealing.

The average energy required to displace an atom is about 25 ev (Kinchin & Pease 1955) and the threshold for displacement of an atom (A ~ 50) is 325 ev for neutrons, so the actual damage may be due to either "knocks on" by fast neutrons or recoil on the emission of a gamma ray following the capture of a thermal neutron. These gamma rays have energies between 5.5 and 7.3 Mev for Mn^{56} and will give the atoms a recoil energy of ~ 350 ev.

The cross-section for displacement by fast neutrons is simply the total neutron cross-section, σ_T (~3 barns for an average energy of 2.0 Mev). Each primary gives rise to ~1200 secondary displacements (Kinchin & Pease) so for a flux of ~5 x 10^{11} neutrons/sq.cm/sec. about 1 in 10^9 atoms will be displaced. Thus the chance of this affecting the environment of one of the radioactive atoms is very small. On the other hand, every activated atom will suffer some recoil which may knock the atom from its surrounding octahedron of water molecules or distort the octahedron in some way. The direction of recoil will be random and it seems reasonable to assume that little or no alignment will occur for displaced atoms and the average radiation

distribution from these will be isotropic. Thus if a fraction n of the atoms are displaced, the angular distribution can be written:

$$I(\theta) = n + (1-n)\{1 + A_2 P_2(\cos\theta) + A_4 P_4(\cos\theta)$$
$$= 1 + (1-n)\, A_2 P_2(\cos\theta) + (1-n)\, A_4 P_4(\cos\theta)$$
$$= 1 + A_2' P_2(\cos\theta) - A_4' P_4(\cos\theta)$$

and the effect is to introduce an attenuating factor, λ, into the A term, such that $A_\nu' = \lambda A_\nu$ and $\lambda = 1-n$.

The factor λ is explicitly required in order to make an estimate of the magnetic moment and it will be necessary to anneal the crystal at the highest possible temperature it can stand without deteriorating. This was found to be 80°C by a monitor experiment carried out with a separate crystal. The crystal was exposed to increasing temperatures and dehydration was first observed at about 82°C when the surface was reduced to a white powder.

4. The design of the experiment

The angular distribution can now be written:-

$$I(\theta) = 1 + A_2' P_2(\cos\theta) + A_4' P_4(\cos\theta)$$

where $A_\nu' = \lambda B_\nu U_\nu F_\nu$ (Chapter 1).

Values of A'_ν can be found from the experimentally measured values of $I(0°)$; $I(90°)$ and since the gamma rays result from the decay of the same nucleus λ and B_ν will be common factors. Thus the ratios

$$\frac{A_\nu'(2)}{A_\nu'(1)}, \quad \frac{A_\nu'(3)}{A_\nu'(1)}$$

will be independent of the temperature and radiation damage and it should be possible to evaluate some of the unknown

parameters, e.g. the mixing ratios for a given spin sequence,

$$\frac{A_\nu'(2)}{A_\nu'(1)} = \frac{\lambda B_\nu U_\nu(2) F_\nu(2)}{\lambda B_\nu U_\nu(1) F_\nu(1)} = \frac{U_\nu(2) F_\nu(2)}{U_\nu(1) F_\nu(1)}$$

$U_\nu(1)$ is a composite term containing contributions from the two gamma cascades and the direct beta-transition to the first excited state. However, $U_\nu(1)$ is not very sensitive to δ since it enters through a term $U_\nu = \frac{U_\nu(L) + \delta^2 U_\nu(L+1)}{1+\delta^2}$ and the small variations caused by the change of δ^2 for the gamma ray not entering in the numerator can be neglected. The ratio can then be treated as a function of $Q = \frac{\delta^2}{1+\delta^2}$ where δ is the dipole/quadrupole mixing ratio for the gamma-ray in the numerator. Ellipse-like curves, arising from the quadratic form of F_ν (Chapter 1), for the dependence of ratio on Q can be constructed (figures 12, 13) for each possible spin sequence. Comparison of the experimental values with these curves gives the two possible values of δ for each sequence.

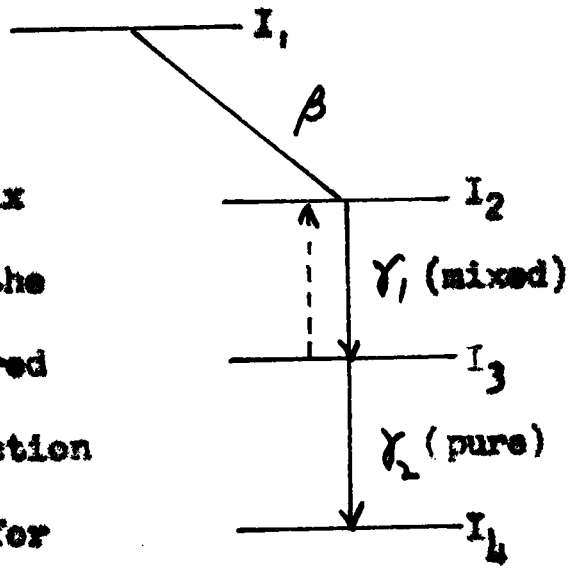
Such assignments will not give a unique decay scheme but it is possible by combining these results with those of an angular correlation of the same cascade to reduce the ambiguity. The information given by a correlation measurement is essentially similar but with one important difference, applicable in this case, if the mixed gamma-ray is the first of the correlation cascade.

For alignment of the mixed gamma-ray:

$$I(\theta) = \sum B_\nu U_\nu F_\nu P_\nu(\mathrm{Cos}\theta)$$

where $F_\nu = \dfrac{F_\nu(LI_2I_3) + \delta^2 F_\nu(L+1,\ I_2I_3) + 2\delta F_\nu(L, L+1,\ I_2I_3)}{1+\delta^2}$

and $\delta = \dfrac{\langle I_3|L+1|I_2\rangle}{\langle I_3|L|I_2\rangle}$



$\langle I_a|L|I_b\rangle$ being the reduced matrix elements for the components. In the correlation experiment the preferred direction is obtained by the detection of γ_2 so $B_\nu U_\nu$ is replaced by F_ν' for the transition $I_3 \rightarrow I_4$. For symmetry both gamma rays are considered to arise from the intermediate level so we have:

$$I(\theta) = \sum F_\nu' F_\nu^* P_\nu(\mathrm{Cos}\theta)$$

F_ν^* is a redefinition of F_ν and is given by

$$F_\nu^* = \frac{F_\nu(LI_3I_2) + \delta^{*2} F_\nu(L+1 I_2I_2) + 2\delta^* F_\nu(L, L+1; I_3I_2)}{1+\delta^{*2}}$$

with $\delta^* = \dfrac{\langle 2|L+1|3\rangle}{\langle 2|L|3\rangle}$

The reduced matrix elements are defined (seeBiedenharn & Rose 1953) such that $(2j+1)^{\frac{1}{2}}\langle j_1|L|j\rangle = (-1)^{j_1-j+L}(2j_1+1)^{\frac{1}{2}}\langle j|L|j_1\rangle$ so we have

$$\delta^* = (-1)^{|L-(L+1)|}\delta \quad \text{and} \quad F_\nu(LI_3I_2) \neq F_\nu(LI_2I_3)$$

This result in only one of the values of δ from the alignment equalling one of those from the correlation and thus eliminating the other two values.

Having found the spin sequence an estimate of the nuclear magnetic moment of Mn^{56} could be made from the dependence of the anisotropy on temperature provided it is known to what extent the radiation damage affects the anisotropy. If this is not known then a lower limit to its value can be found.

5. The angular correlation and scintillation spectrometer study

Since the angular correlation results of Metzger and Todd were subject to rather large errors and only one value for δ was given for each cascade a similar experiment was carried out in conjunction with this work by Gregory (see Dagley et al 1959).

The singles spectrum and spectrum in coincidence with γ_1 were displayed on a multichannel kicksorter and analysed in terms of both γ_2 and γ_3. In this way the errors have been reduced considerably. The results of the experiment are included in Table 7.

Measurements of the gamma-radiation were also made using a 4" x 4" NaI(Tl) crystal. The seven gamma-rays shown in the decay scheme were identified and their relative intensities measured (Table 1). The energies and intensities of γ_4 γ_5 γ_6 and γ_7 agree closely with those found by Cook and Tomnovec. Furthermore, γ_6 (2.52 Mev) was found to be in coincidence with γ_1, so that γ_6 and γ_7 (3.4 Mev) would appear to be transitions to the first excited state and ground state respectively from a level at about 3.4 Mev. Masari et al (1957) found three levels in this region and this is most probably the one at 3.386.

TABLE 1

Energies and intensities of gamma-rays observed in Mn^{56}

Gamma-ray	Adopted value of energy	Intensity
γ_1	0.845	100
γ_2	1.81	27 ± 3
γ_3	2.13	15 ± 3
γ_4	2.66	0.65 ± 0.1
γ_5	2.98	0.35 ± 0.1
γ_6	2.55	1.2 ± 0.2
γ_7	3.4	0.22 ± 0.05
γ_8	1.24	< 2

No 1.24 Mev gamma-ray was found limiting the transition via the 4^+ level at 2.08 Mev to be less than 2% of the decays.

6. Experimental

6a. The composition of the crystal

To minimise the radiation damage the irradiation should be as short as possible and therefore the maximum permissible amount of target element is required. However, the thermodynamic properties are determined by the nickel (10%) and in order that the basic internal environment of the crystal and its low temperature properties are not seriously affected, the quantity of Mn^{55} added was made not more than 1% of the cation, that is, 10% of the paramagnetic component. It was added to the growing solution in the form of manganese carbonate which rapidly dissociates in the acidic solution and avoids the introduction of other radicles.

6b. The irradiation parameters

The pile temperatures are not known accurately but a rough estimate by the Harwell Isotope Division for a typical stringer indicates that they increase with pile factor (i.e. neutron flux) and probably do not exceed 50°C for pile factors up to 10 (P.F.1=10^{11} neutrons/sq.cm/sec). The crystal itself could reach higher temperatures as a result of an exothermic reaction following neutron capture. Also as the fast neutron flux increases with the pile factor, low pile factors would be preferred in order to keep the risk of damaging the crystal both internally and as a whole to a minimum.

However, for such a short-lived isotope, it is more efficient to use a high pile factor with a very short irradiation time and this also reduces the possibility of producing long-lived isotopes (e.g. Zn^{65}).

A compromise of 15 minutes at pile factor 5 was eventually decided upon to give sufficient activity throughout an experiment. For a 2 gram crystal there will be about 440μc (see section 6c) on extraction from the pile, about 55μc at the time of the first run and only 3μc at the end of the experiment.

6c. The present of other activities

Isotopes of nickel and zinc (Ni^{63}, Ni^{65}, Zn^{65}, Zn^{69}) will also be produced by the irradiation but an estimate based on the thermal neutron absorption cross-sections suggested that none of these would interfere with the measurements proposed. The crystal contains 1% Mn, 10% Ni and 90% Zn so we may consider the ratio as 1:10:100 approximately,

and use the relationship: $S = \frac{0.6\,\phi\,\sigma}{3.7 \times 10^{10} A}\,(1 - e^{-\frac{.69t}{T}})$ for the rise of activity with time, where:

S = specific activity of product in curies/gm.

ϕ = neutron flux in neutrons/cm^2/sec.

σ = excitation cross-section in barns

A = atomic weight of bombarded element

t = irradiation time

T = half-life of the radioisotope (same units as t).

Putting $\phi = 5 \times 10^{11}$ and t = 0.25 hr., the activities can be computed as follows:

	Mn^{56}	Ni^{65}	Zn^{65}
σ (barns)	13.2	0.03	0.244
A	55	58.69	65.38
T	2.58 hr.	2.56 hr.	245 d
weight	1 mgn.	10 mgn.	100 mgn
exp(-0.69t/T)	0.0352	0.0352	$(1-2.93 \times 10^{-5})$
S_μ	126	2.665	0.089

Ni^{63} is a pure beta emitter and the 14-hour Zn^{69} isomer has one gamma-ray at 440 kev so none of the other isotopes should affect the results for Mn^{56}.

In order to check these conclusions, samples of manganese, nickel and zinc powders in the above ratio were irradiated under these conditions.

A pulse height spectrum (figure 2) of the composite source and

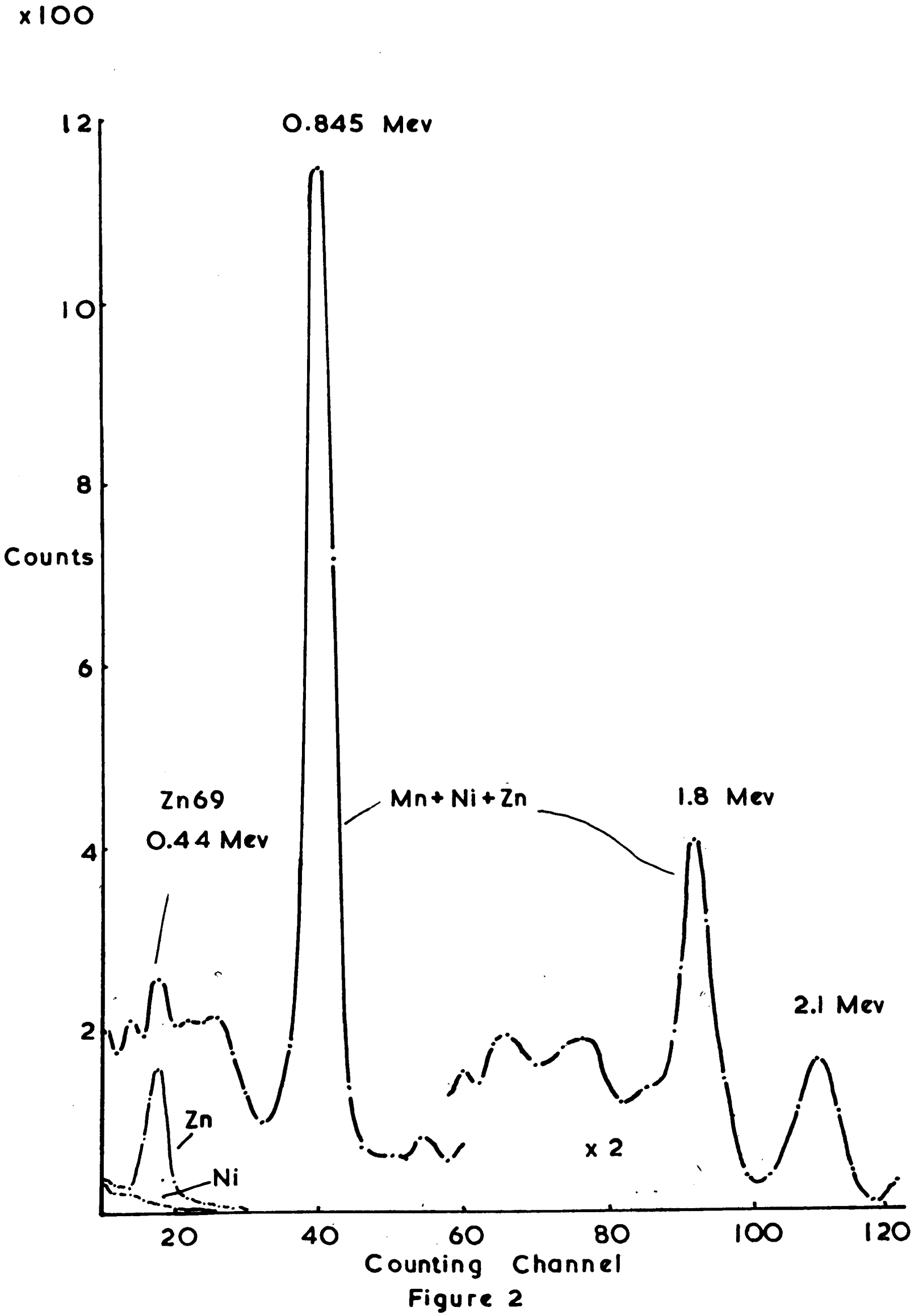

x100
12
10
8
6
4
2
Counts
0.845 Mev
Zn69
0.44 Mev
Mn + Ni + Zn
1.8 Mev
2.1 Mev
Zn
Ni
x 2
20
40
60
80
100
120
Counting Channel

Figure 2

of each one separately showed practically no trace of Ni^{65} (2.6 hours) and Zn^{65} (245 days) in agreement with the calculated activities, but when the Mn^{56} and Ni^{65} had decayed out, a small peak at 1.1 Mev due to the zinc became apparent. However, even at the end of the run the Zn^{65} activity was less than 10% of that of the Manganese and no correction for its presence was necessary.

6d. The alignment experiment

A crystal weighing 2.12 gms. was grown, irradiated in the Harwell pile and delivered to the laboratory within one hour of extraction from the pile. It was then quickly mounted in the perspex holder and fitted into the cryostat. By carrying out the cooling procedures as quickly as possible and leaving the susceptibility calibration until after the experiment it was possible to carry out the first demagnetisation about 5 hours after the receipt of the crystal.

While the low temperature apparatus was being assembled and cooling to helium temperatures carried out, the discriminators were set with the aid of an auxiliary source of Manganese powder. The gamma-ray spectrum of the crystal was also displayed on a Sunvic (Hutchinson-Scarrett) Multichannel Kicksorter in order to check that only gamma-rays from Mn^{56} were present.

In fact, peaks at approximately 2.7, 2.2, 1.8, 1.35 and 0.85 Mev (figure 3) were found and by monitoring the spectrum at intervals throughout the run, the contaminant was shown to be 15 hour sodium Na^{24} which has gamma-rays of 2.7 and 1.35 Mev, the former giving rise

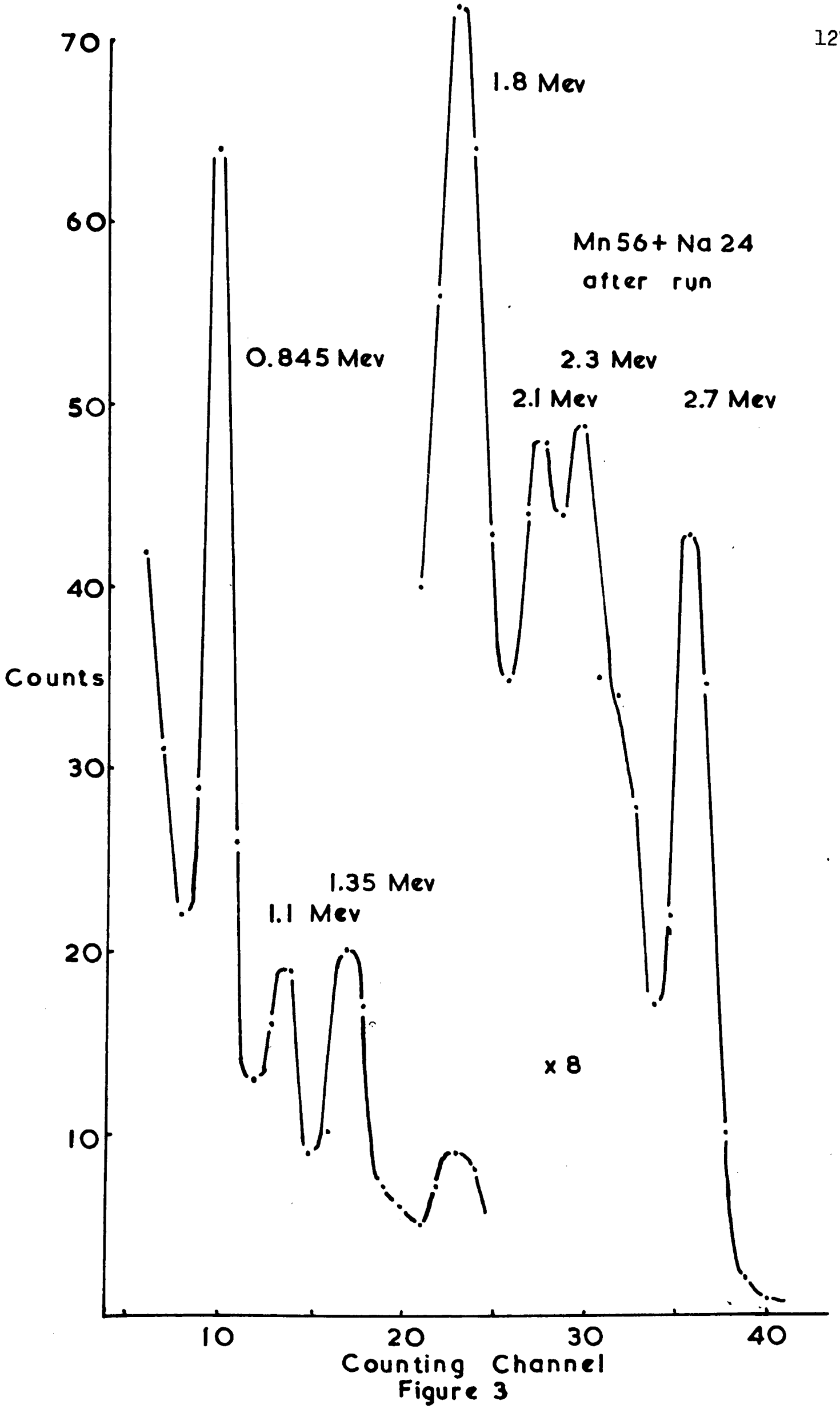

70
60
50
40
30
20
10
Counts
1.8 Mev
Mn 56 + Na 24
after run
0.845 Mev
2.3 Mev
2.1 Mev
2.7 Mev
1.35 Mev
1.1 Mev
x 8
10
20
30
40
Counting Channel

Figure 3

to pair -1 and pair -2 peaks at 2.3 and 1.7 Mev, thus broadening the Mn^{56} lines. The inclusion of sodium in the crystal was rather surprising since the fluosilicate of sodium, Na_2SiF_6, is anhydrous and not isomorphous with the $ZnSiF_6.6H_2O$ but it could perhaps be trapped in inclusions within the crystal. Analysis suggests that the amount of Na present varies roughly in direct proportion to the amount of nickel (approximately 1 gm Na per 10 gms Ni) and that the nickel fluosilicate used was contaminated, probably through an unexpected impurity in the chemicals used.

The counters had 2" x 2" Na(Tl) phosphors the front faces of which were 6.47 cms from the source and thus subtending an average angle of $15\frac{1}{2}^{\circ}$.

Runs were carried out for different initial fields and with the discriminators set on γ_3, γ_2 and γ_1 in turn. A repeat irradiation of the same crystal gave similar results.

Two more experiments were carried out in which after irradiation the crystal was annealed at 80°C for 2 hours before mounting in the cryostat. The anisotropies of γ_1 and γ_3 were observed and showed a marked increase over the unannealed values. γ_2 has not been observed under these conditions because of the greater delay, introduced by annealing, before demagnetisation makes the analysis of the small counting rate unprofitable.

7. Analysis of Results

7a. The temperature scale

The magnetic temperature parameter δ was plotted against time for each run and extrapolated back to the instant of demagnetisation (t=0). Graphs of $\delta . V^{H}/T$ (figure 4) and H/T v. $1/T$ derived from Co^{58} then allowed all the δ values to be converted into absolute temperature.

7b. Correction for sodium activity

Before the readings can be normalised in the usual way, correction must be made for the sodium. Let there be N counts in a particular counting channel for the isotropic distribution, i.e. the "warm readings", at time $t = 0$. Then $N_o = x+y$, where x counts are due to manganese and y to the sodium. At some later time, t, there will be N_t counts where $N_t = x \exp(\frac{-0.69t}{2.58}) + y \exp(\frac{-0.69t}{15})$ where t is measured in hours, and the exponential terms allow for the decay of the two isotopes with different half-lives.

Since N_o, N_t and t are known, two or more simultaneous equations can be set up to find x and y. The ratio of manganese to sodium is then given by: $f = \frac{x}{y} \frac{\exp(\frac{-0.69t}{2.58})}{\exp(\frac{-0.69t}{15})} = \frac{x}{y} \exp(-0.2215t)$ for any time t, and can be read from a graph of log f v t. (figure 5). The number of counts due to the sodium can then be found for each run and subtracted from the readings:

$$\text{i.e.} \quad N = Na + Mn = Na + Na \frac{Mn}{Na} = Na(1+f)$$

$$\text{and} \quad Na = \frac{N}{1+f}$$

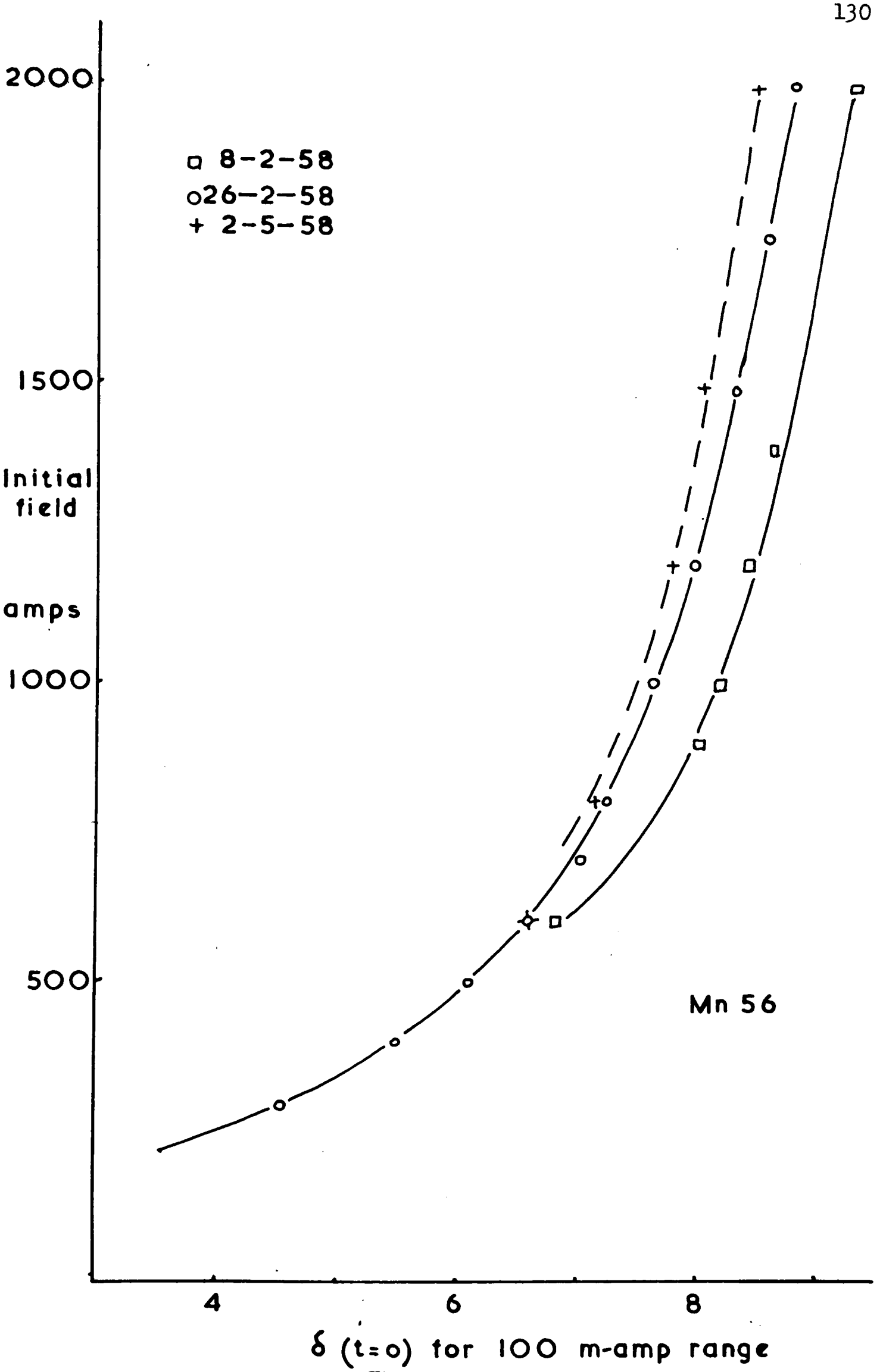
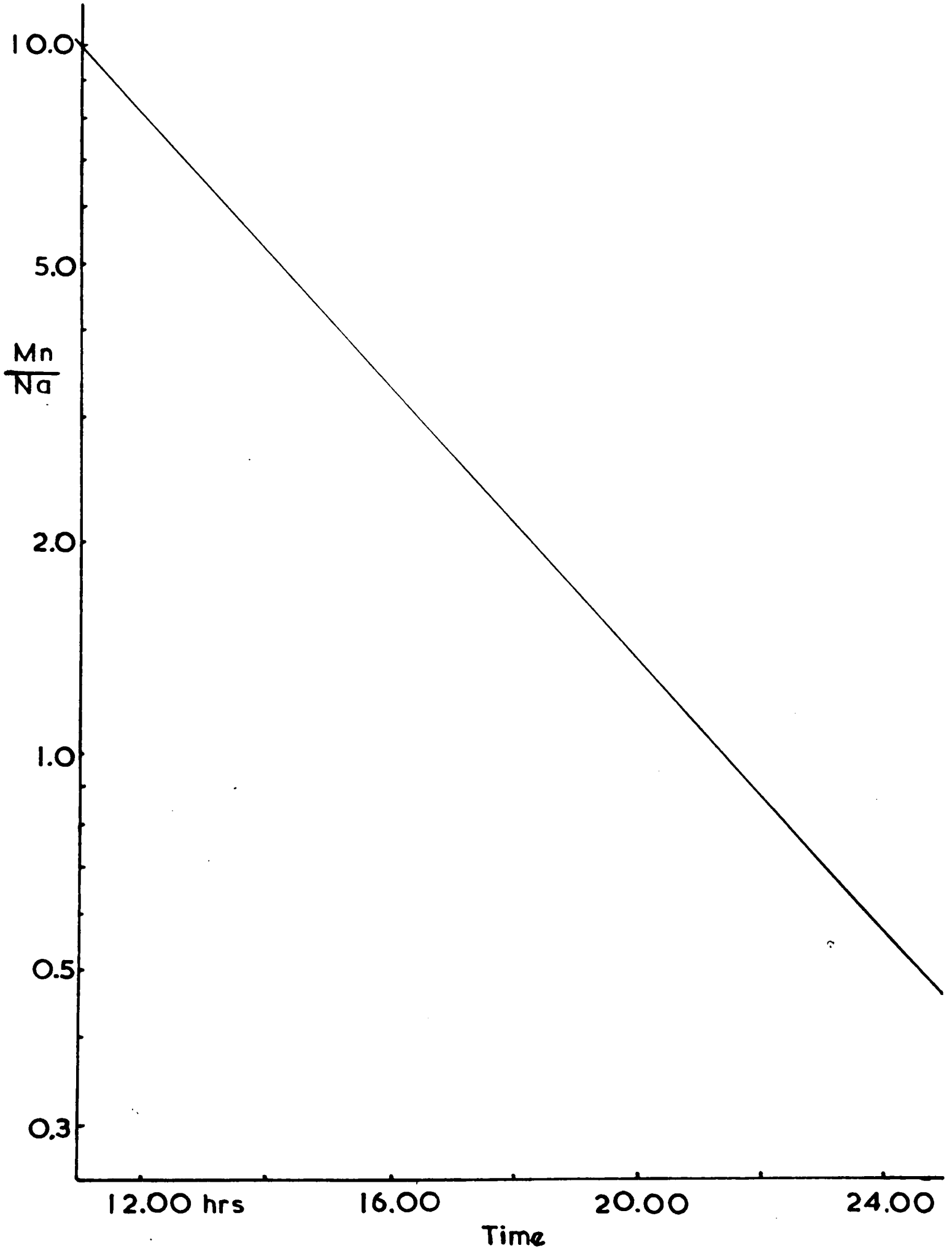

2000
1500
1000
500
Initial field amps
□ 8-2-58
○26-2-58
+ 2-5-58
Mn 56
4
6
8
δ (t=o) for 100 m-amp range

Figure 4



Manganese to Sodium ratio

Figure 5

This was calculated for the mean time of each run since it changes very little over the period of 5 - 10 minutes involved. The accuracy of the correction can be tested by plotting the decay of the corrected warm readings; this should have the slope appropriate to 2.58 hours half life which it did to within the experimental error.

7c. Decay correction

If $I(0^0)$ and $I(90^0)$ are used to find A_2, a correction is necessary to allow for the decay of the source. Let the counting rate when cold be Nc and that when warm be N_w. The apparent normalised intensity $I'(\theta) = \frac{Nc}{N_w}$. However, the true value for $I(\theta)$ is $I(\theta) = \frac{Nc}{N_w} \exp(\frac{-0.69t}{2.58})$

$$= I'(\theta)\, e(\frac{-0.69t}{2.58})$$

where t is the time interval in hours between the cold reading and the mean warm reading. A graph (figure 6) can be constructed of $\exp(\frac{-0.69t}{2.58})$ so that the correcting factor for any time interval is readily obtainable.

Since the anisotropy is defined as:

$$\epsilon = \frac{I(90^0) - I(0^0)}{I(90^0)} = 1 - \frac{I(0)}{I(90^0)}$$

this is unaffected by the decay since both axial and equatorial readings are taken at the same instant.

7d. Correction for other gamma-rays

The results for γ_3 can now be found but γ_2(1.8) presents a further difficulty. After the correction has been applied for the sodium, allowance had to be made for the degraded 2.1 Mev gamma rays lying under


1.0
Correction factor
0.98
0.96
Mn 56
Decay Correction
11
10
9
8
7
6
5
4
3
2
1
0
time interval between cold & warm readings - mins

Figure 6

the peak.

In order to find the shape of a 2.1 Mev pulse height spectrum a source of Arsenic 76 was obtained. This has no other gamma rays above 1.4 Mev, except one at 2.05 Mev. Gamma-ray spectra were measured for Mn^{56} and As^{76} using the experimental geometry (figure 7). The As^{76} spectrum was fitted to the 2.1 Mev peak of the Mn^{56} spectrum and the ratio of 2.1 to 1.8 gamma rays in the counting channel for calculated. It was found to be 44 ± 3.8 (2.1): 56 ± 3.8 (1.8). Since the two gamma rays have different anisotropies, the correction must be made to the normalised readings $I(\theta)$. First the $I(\theta)$ v $\frac{1}{T}$ curves are drawn for γ_3 and γ_2'(1.8+2.1) in order that $I(\theta)_{,}^{\gamma_3}$ $I(\theta)^{\gamma_2'}$ can be found for the same temperature.

Let the warm counting rate be: $N = N_2 + N_3 = xN + (1-x)N$ and expressing the intensity at angle θ by $1+\alpha$ then, when "cold", we have:

$$(1+\alpha)N = (1+\alpha_2)N_2 + (1+\alpha_3)N_3$$

$$= (1+\alpha_2)xN + (1+\alpha_3)(1-x)N$$

$$\alpha = \alpha_2 x + (1-x)\alpha_3$$

hence α_2 can be found since α_3, α and x are known. The method is illustrated in the following table (2). It can be seen that the analytical errors are large.

The correction for γ_1 can be made very simply since the effect of the zinc is negligible. For the last runs on γ_1 there was only about $3\mu s$ of Mn^{56} which all decays through γ_1, while only $\sim 0.35\mu s$ of Zn^{65} are present, only half of this decaying through the 1.1 Mev

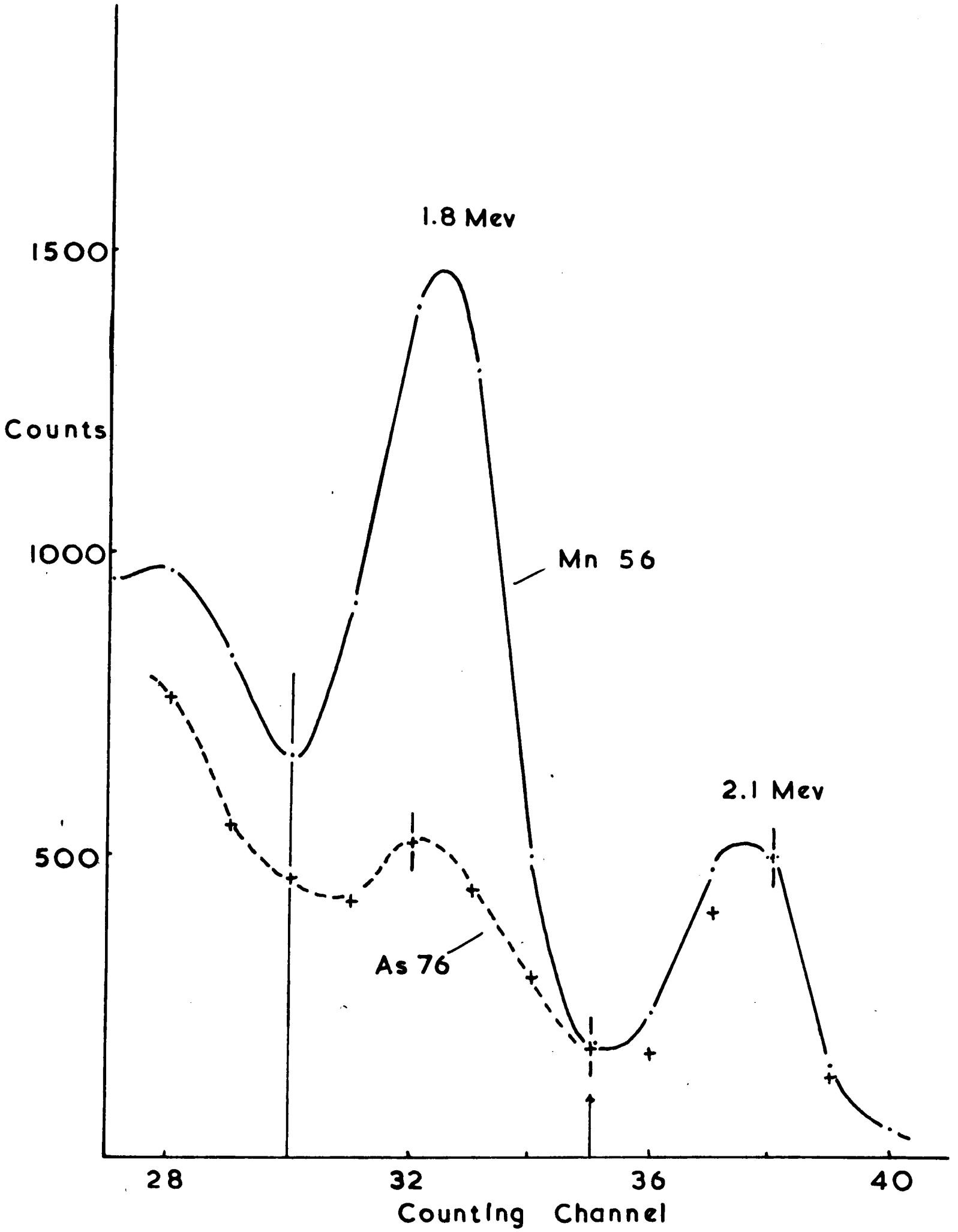

1.8 Mev
1500
Counts
1000
Mn 56
2.1 Mev
500
As 76
28
32
36
40
Counting Channel

Figure 7

TABLE 2

Mn^{56} in Ni Zn $SiF_6 .6H_2O$

1.8 Mev gamma ray - correction for 2.1 Mev contribution

$\frac{1}{T}$	MIXED $I(90^\circ)$ $I(0^\circ)$ $(1+\alpha)$		2.1 Mev $I(90^\circ)$ $I(0^\circ)$ $(1+\alpha')$		0.44 x 2.1 $I(90^\circ)$ $I(0^\circ)$ $(0.44\alpha')$		0.56 x 1.8 $I(90^\circ)$ $I(0^\circ)$ $(\alpha - 0.44\alpha')$		1.8 Mev corrected $I(90^\circ)$ $I(0^\circ)$ $(1+\alpha'')$		ϵ	A_2
80	1+0.089 ±0.011	1-0.193 ±0.011	1+0.145 ±0.011	1-0.316 ±0.011	0.064 ±0.038	-0.139 ±0.038	0.025 ±0.040	-0.054 ±0.040	1+0.045 ±0.089	1-0.096 ±0.089	0.135 ±0.120	-0.09 ±0.08
70	1+0.084	1-0.183	1+0.133	1-0.29	0.059	-0.128	0.026	-0.056	1+0.046	1-0.099	0.139	-0.10
60	1+0.077	1-0.169	1+0.118	1-0.260	0.052	-0.114	0.025	-0.055	1+0.045	1-0.098	0.136	-0.09
50	1+0.068	1-0.151	1+0.099	1-0.222	0.044	-0.098	0.025	-0.053	1+0.044	1-0.095	0.134	-0.09
40	1+0.058	1-0.127	1+0.073	1-0.170	0.032	-0.075	0.026	-0.052	1+0.046	1-0.093	0.131	-0.09
30	1+0.045	1-0.094	1+0.052	1-0.100	0.023	-0.044	0.022	-0.050	1+0.040	1-0.089	0.124	-0.08
20	1+0.028	1-0.040	1+0.032	1-0.052	0.014	-0.023	0.014	-0.017	1+0.025	1-0.036	0.054	-0.04

gamma-ray so the percentage in the counting channel is negligible.

Apart from zinc and sodium there is an almost flat distribution due to γ_2 and γ_3 as can be seen from figure 8 for the pure source and very good approximation can be made of the following procedure is carried out allowing the anisotropy to be calculated during the run.

If a "background" is allowed for, as in figure 8, then the number of counts above and below the peak are known and the "background" counts as a fraction of the high bias counting rate can be found, i.e. $B = bH$.

Then the low bias reading minus the high bias and background counts gives the counting rate due to γ_1 proper. Thus the channel counting rate is given by $L-(1+b)H$ rather than $L-H$. This can be applied to both "cold" and "warm" readings since the anisotropy of the background (γ_2 and γ_3) is automatically taken into account. This method relies for its accuracy on the fact that $\gamma 1$ is much more intense than the others and the amounts of Zn and Na are relatively small in this region. Again, its accuracy can be found by plotting the decay of the corrected warm readings.

7e. Results

Recordings made in a typical run on the 0.845 Mev gamma ray are shown in Table 3 and the anisotropies for all three gamma rays are given in Tables 4 and 5. The corrected curves $\epsilon v_T^{\frac{1}{2}}$ are shown in figure 9 for $\gamma_1 \gamma_2$ and γ_3 for the unannealed crystal and in figure 10 for the annealed experiments. No correction has been made for the

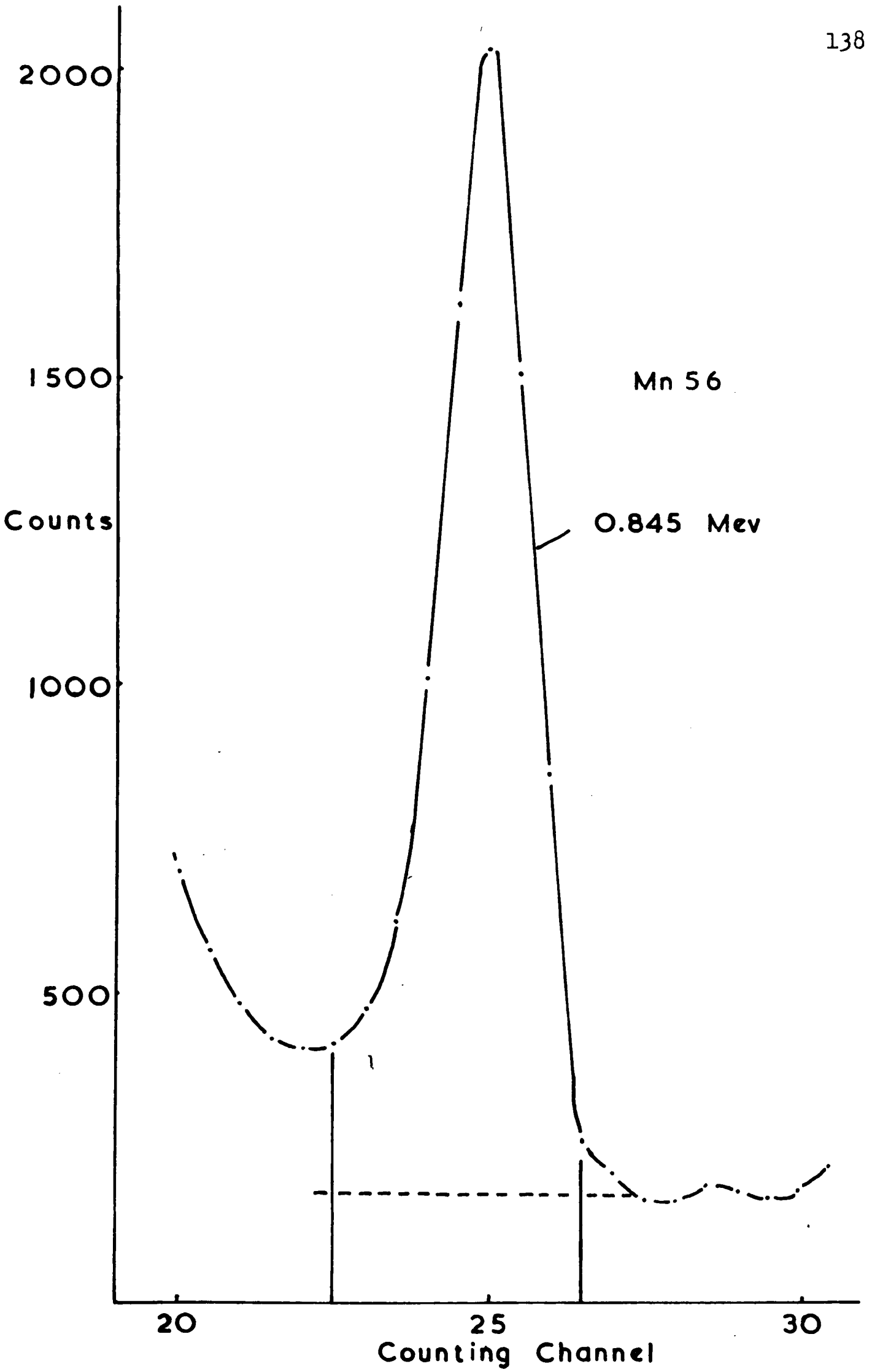

2000
1500
1000
500
Counts
Mn 56
0.845 Mev
20
25
30
Counting Channel

Figure 8

TABLE 3

Mn^{56} in Ni-Zn Si $F_6 . 6H_2O$

Typical run for 0.845 Mev gamma ray

Initial field = 34.4 kilogauss Source counter distan ce = 6.47 cms. Counting interval = 40 secs.

		Axial Counter $\epsilon f = 0.25 \pm 0.02$					I(0°)		Equatorial Counter $\epsilon f = 0.22 \pm 0.02$					I(90°)	
Time	Galv. defl.	Low bias	High bias	(1+f)HB	LB-(1+f) HB = Δ	raw	Decay corrected		Low bias	High bias	(1+f)HB	LB-(1+f) HB = Δ	raw	Decay corrected	∈
0-25	8.95	61333 ± 250	32131 ± 180	40150 ± 680	21183 ± 725	0.793 ± 0.035	0.767 ± 0.035		64139 ± 250	32115 ± 180	39200 ± 676	24993 ± 720	1.130 ± 0.044	1.093 ± 0.044	0.298 ± 0.051
1-18	8.80	62260	32358	40400	21860	0.819	0.795		63985	31920	38960	25085	1.131	1.098	0.276
2-11	8.68	63087	32555	40650	22437	0.841	0.820		63390	31946	39000	24390	1.102	1.075	0.236
3- 7	8.56	63407	32654	40750	22657	0.848	0.831		63092	31868	38900	24192	1.093	1.071	0.223
4- 0	8.46	63360	32623	40750	22610	0.847	0.832		62946	31504	38460	24486	1.108	1.087	0.233
4-52	8.39	63787	32545	40650	23137	0.866	0.854		62694	31443	38400	24294	1.098	1.082	0.210
		71149	35262						59376	30366					
		70343	35008						58790	29984					
8-03		70445	35056						59444	30587					
		70104	34897						58498	29973					
		69991	34696						58609	29965					
	Mean:	70406 ± 120	34994 ± 84	43700 ± 707	26700 ± 720				58943 ± 110	30175 ± 78	36800 ± 610	22143 ± 620			

TABLE 4

Mn^{56} in Ni-Zn $SiF_6.6H_2O$

Gamma-ray anisotropies for unannealed crystal
(blocked values)

0.845 Mev		1.8 Mev		2.1 Mev	
$\frac{1}{T}$	ϵ	$\frac{1}{T}$	ϵ	$\frac{1}{T}$	ϵ
80.5	0.272 ± 0.035	79.5	0.15 ± 0.10	72.5	0.38 ± 0.02
70.0	0.269	69.7	0.14	52.5	0.31
64.8	0.254	60.5	0.12	43.5	0.24
55.5	0.212	51.0	0.10	37.0	0.22
40.5	0.160	40.5	0.10	32.5	0.15
35.0	0.130	31.5	0.10	22.5	0.10
30.0	0.121	20.0	0.05	13.5	0.03
26.0	0.104				
17.0	0.039				

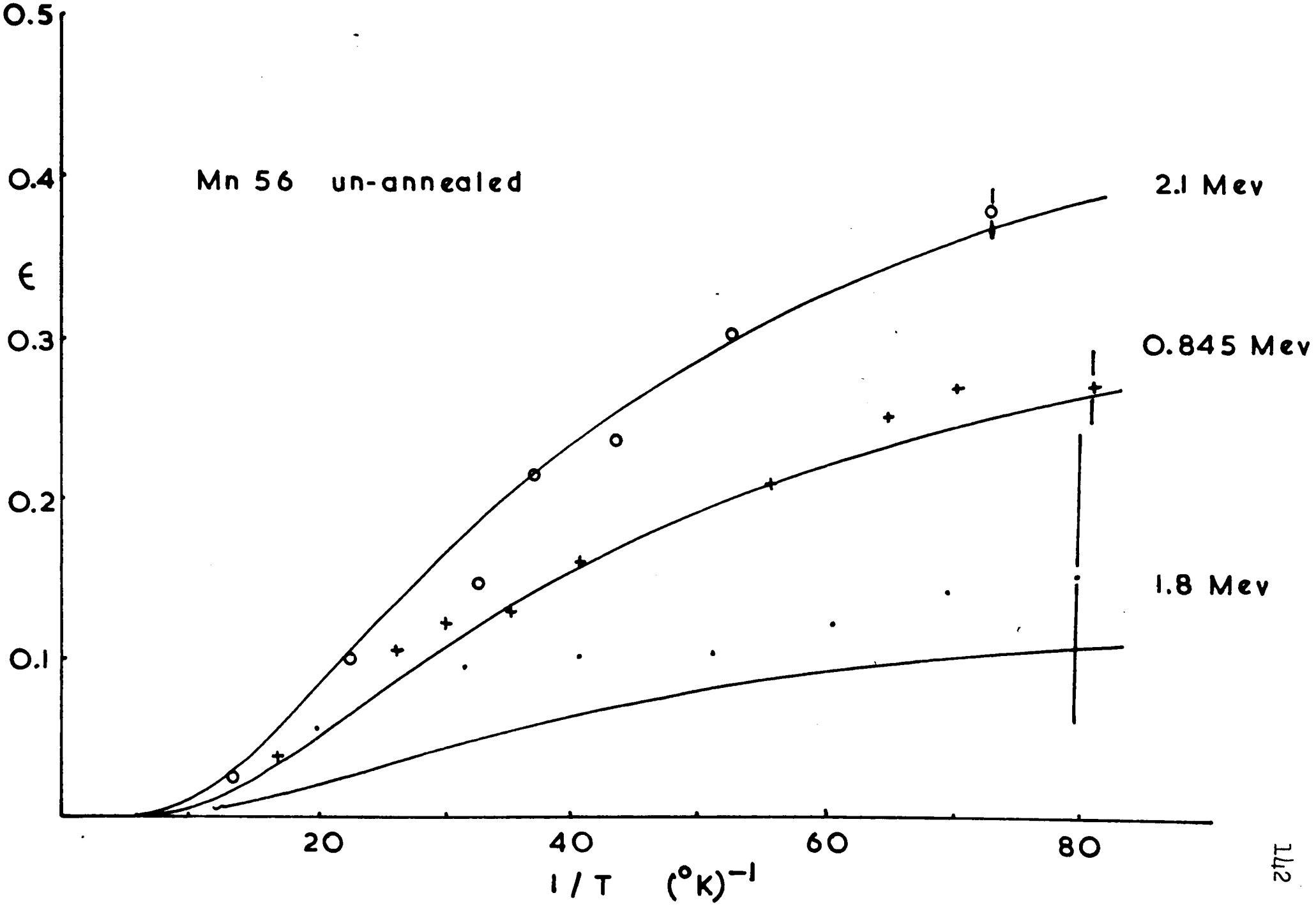
TABLE 5

Mn^{56} in Ni-Zn Si $F_6 . 6H_2O$

Gamma-ray anisotropies for annealed crystal
(blocked values)

0.845 Mev		2.1 Mev	
$\frac{1}{T}$	ϵ	$\frac{1}{T}$	ϵ
86.2	0.41 ± 0.04	78.5	0.50 ± 0.02
72.0	0.37	56.2	0.42
59.0	0.33	46.3	0.35
54.25	0.31	39.0	0.33
50.7	0.28	34.0	0.29
44.75	0.28	31.5	0.27
40.25	0.25		
35.7	0.21		
29.2	0.16		
23.0	0.09		
15.0	0.04		

Figure 9


0.5
0.4
0.3
0.2
0.1
ε
Mn 56 un-annealed
2.1 Mev
0.845 Mev
1.8 Mev
20
40
60
80
1 / T (°K)⁻¹

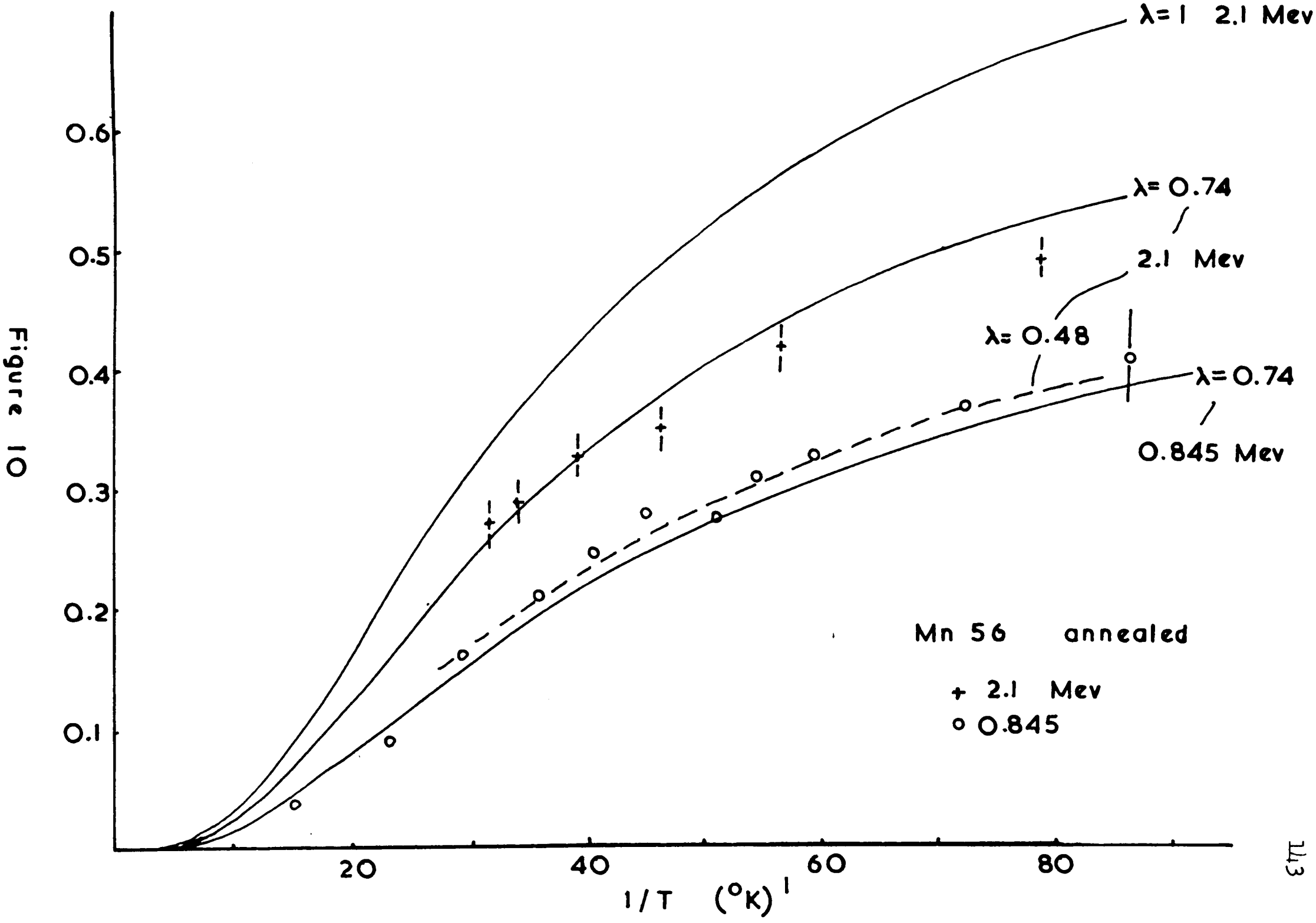

λ= 1 2.1 Mev
λ= 0.74
2.1 Mev
λ= 0.48
λ= 0.74
0.845 Mev
Mn 56 annealed
+ 2.1 Mev
o 0.845
0.6
0.5
0.4
0.3
0.2
0.1
20
40
60
80
1/T (°K)⁻¹

Figure 10

finite aperture of the counters. These results clearly show that alignment has been obtained for an irradiated crystal and that for Mn^{56} the anisotropy of all three gamma rays is positive.

8. Interpretation of Data

8a. Test of the angular distribution

We have $I(\theta) = 1+A_2' P_2(\cos\theta)+A_4' P_4(\cos\theta)$, so $I(0^\circ)=1+A_2'+A_4'$ and $I(90^\circ)=1-\frac{1}{2}A_2'+\frac{3}{8}A_4'$ giving $A_2'=\frac{1}{7}\left\{5+3I(0^\circ) - 8\, I(90^\circ)\right\}$

Thus, considering the blocked values of $I(0^\circ)$, $I(90^\circ)$ for the 0.845 Mev transition, we have:

$I(0^\circ)$	$I(90^\circ)$	$3I(0^\circ)$	$8I(90^\circ)$	A_2'
± 0.017	± 0.022			± 0.024
0.780	1.030	2.340	8.640	-0.185
0.789	1.080	2.367	8.640	-0.182
0.808	1.076	2.424	8.608	-0.169
0.847	1.064	2.541	8.512	-0.139
0.890	1.047	2.670	8.376	-0.101
0.898	1.033	2.694	8.254	-0.081

The values of A_2' derived in this way are plotted in figure 11 and values read from these curves are given in Table 6. In order to test whether the angular distribution from an irradiated crystal can be expressed in the form:

$$I(\theta) = 1+\lambda A_2 P_2(\cos\theta)+\lambda A_4 P_4(\cos\theta)$$

the ratio of $\dfrac{A_2' \text{ (annealed)}}{A_2' \text{ (unannealed)}} = \dfrac{\lambda a}{\lambda u}$, has been calculated for γ_1 and γ_3

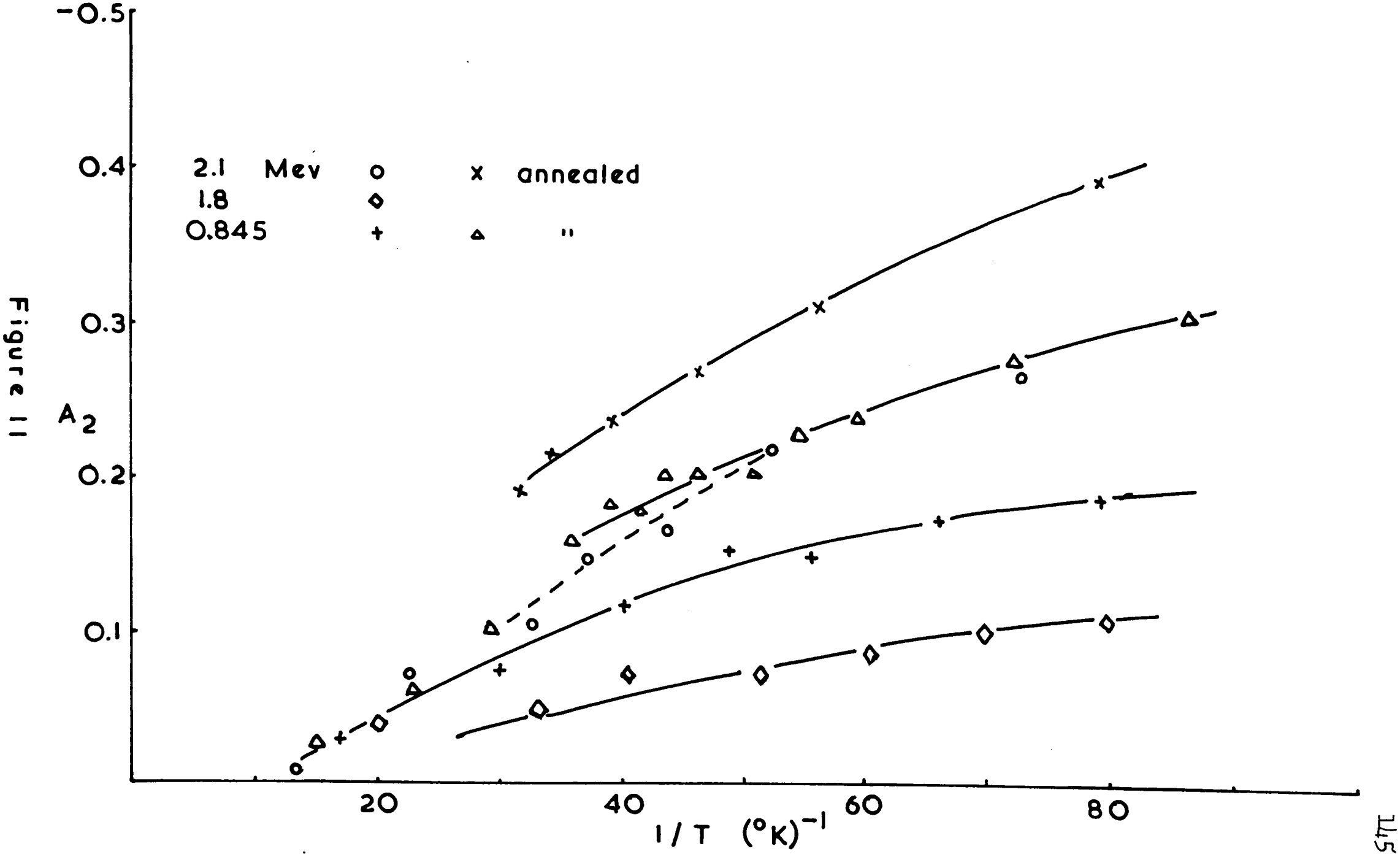


Figure 11

TABLE 6

$\frac{1}{T}$	A_2 - 2.1 Mev un-annealed	A_2 - 2.1 Mev annealed	$\frac{\lambda_a}{\lambda_u}$	A_2-1.8 Mev un-annealed	A_2 - 0.845 Mev un-annealed	A_2 - 0.845 Mev annealed	$\frac{\lambda_a}{\lambda_u}$	$\frac{A_1(2.1)}{A_2(0.8)}$ u	$\frac{A_1(2.1)}{A_2(0.8)}$ a	$\frac{A_2(1.8)}{A_2(0.8)}$
	± 0.014		± 0.09	± 0.09	± 0.024		± 0.24	± 0.2	± 0.12	± 0.44
80	-0.280	-0.400	1.43	-0.11	-0.186	-0.293	1.59	1.50	1.36	0.60
70	-0.270	-0.370	1.37	-0.10	-0.178	-0.270	1.52	1.52	1.37	0.56
60	-0.240	-0.330	1.37	-0.09	-0.160	-0.245	1.53	1.50	1.35	0.56
50	-0.210	-0.290	1.38	-0.07	-0.136	-0.208	1.53	1.54	1.39	0.51
40	-0.160	-0.240	1.50	-0.07	-0.105	-0.180	1.71	1.52	1.40	0.67
30	-0.100	-0.180	1.80	-0.06	-0.080	-0.105	1.31	1.25	1.37	0.75
20	-0.050	-	-	-0.04	-0.040	-0.048	1.20	1.04	-	1.00
Mean values for $\frac{1}{T} \geqslant 50$			1.39 ± 0.05				1.54 ± 0.12	1.52 ± 0.10	1.37 ± 0.06	0.56 ± 0.22

Then, independently of the decay scheme, aperture correction and extent of the damage, this ratio should be the same for both gamma rays and independent of temperature. The results of 1.39 ± 0.05 (γ_3) and 1.54 ± 0.12 (γ_1) are in reasonable agreement: the errors are based on the statistical counting errors. Because of the small anisotropy in the region of $\frac{1}{T} \ll 40$ the values obtained in this region are less reliable than those for lower temperatures and have been neglected in finding the average value.

8b. <u>The mixing ratios</u>

The anisotropy can be expressed in the form $\epsilon = \frac{-12A_2 - 5A_4}{8 - 4A_2 + 3A_4}$

and in the region where $A_2 \gg A_4$ (i.e. at high temperatures), a positive anisotropy requires A_2 to be negative. The sign of A_2 is determined by that of F_2 and one can say that for a 2-2-0 spin sequence δ must be less than +0.3 while for a 3-2-0 sequence $\delta < -0.175$ or $> +14.1$.

More definite values can be obtained from the ratios $\frac{A_2(3)}{A_2(1)}$ and $\frac{A_2(2)}{A_2(1)}$ which are given in Table 6. It is seen that the ratio is independent of temperature, the deviations for the high temperature region arising from the small values of anisotropy concerned. The values derived from the unannealed runs for $\frac{1}{T} \gg 40$ are $\frac{A_2(3)}{A_2(1)} = 1.52 \pm 0.12$ and $\frac{A_2(2)}{A_2(1)} = 0.56 \pm 0.22$. These have been compared with the theoretical curves (figure 12, 13) and the values of the mixing ratio, δ, deduced are given in Table 7 where they are compared with the angular correlation results. The sign of δ is that appropriate to the alignment (see section 4).

Figure 12

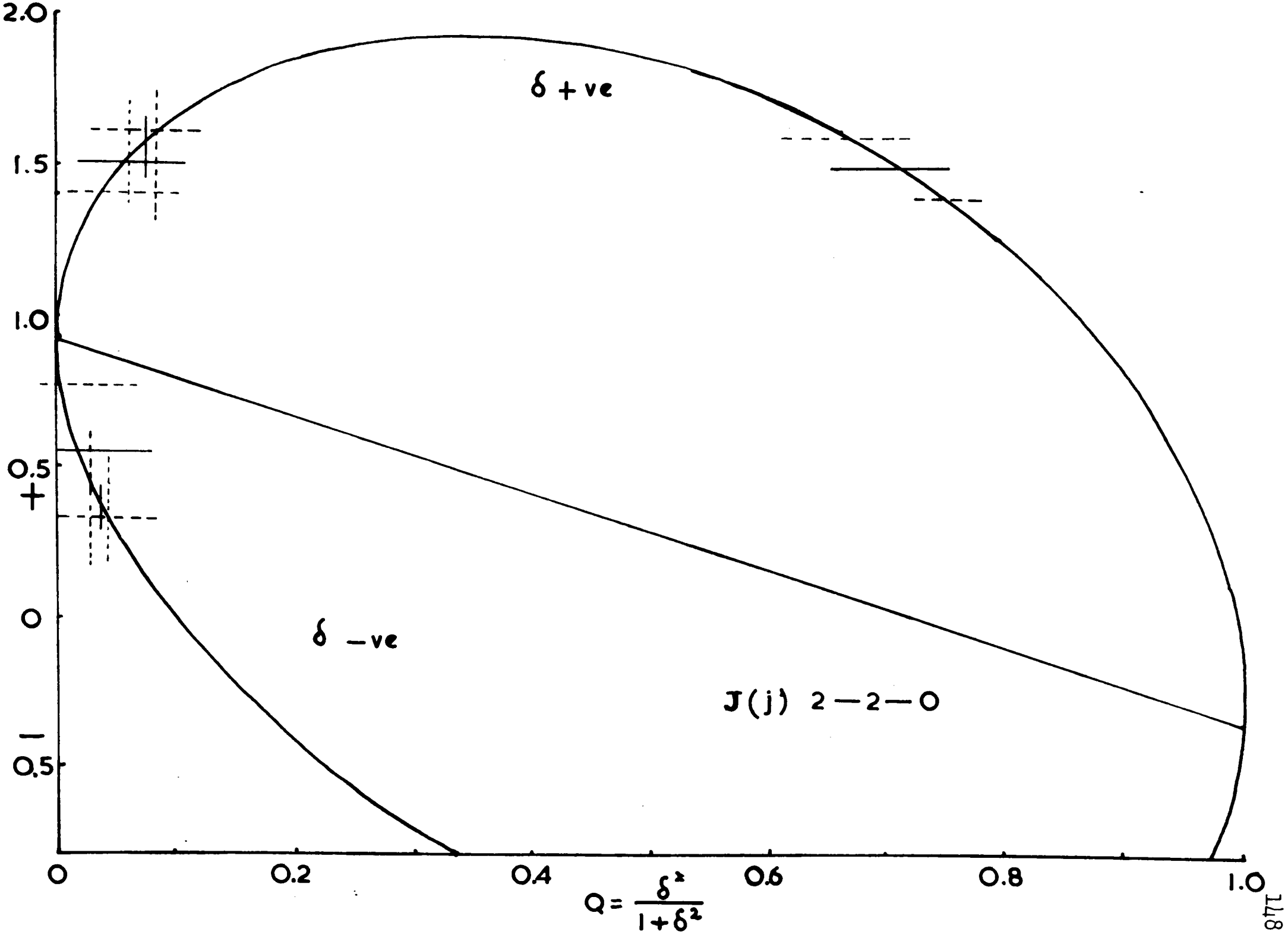
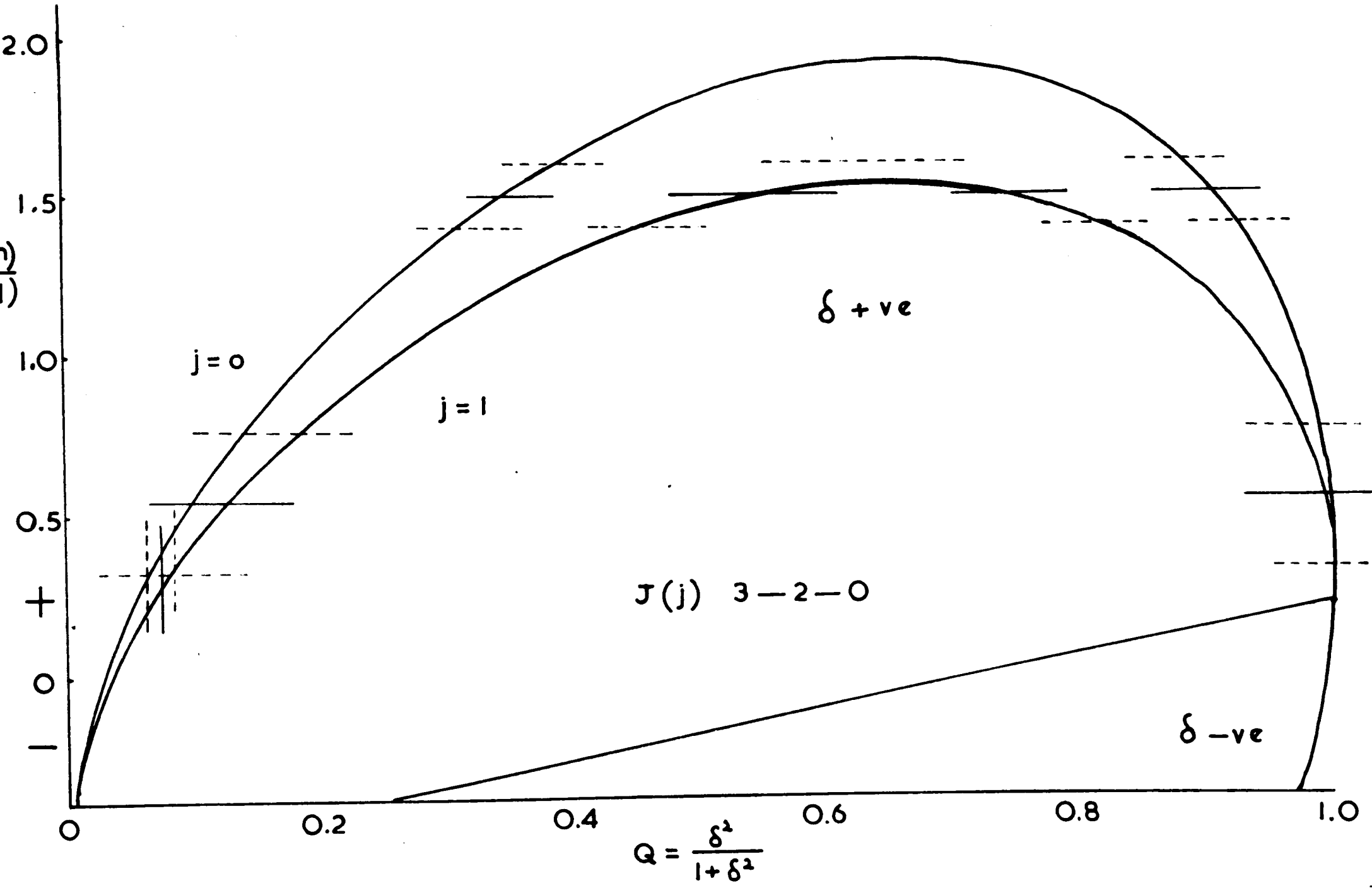

2.0
1.5
1.0
0.5
0
0.5
$\frac{A_2(n)}{A_2(1)}$
δ +ve
δ −ve
J(j) 2—2—0
0
0.2
0.4
0.6
0.8
1.0
$Q = \frac{\delta^2}{1+\delta^2}$

Figure 13



6TT

TABLE 7

Mixing ratios for the 1.8 and 2.1 Mev gamma rays
(sign appropriate to alignment)

γ_3 (2.1)

Sequence	Alignment	Gregory	Metager
3(0)3 - 2 - 0	+0.74 ±0.08 +3.0 ±0.5	+0.18 ±0.02 no large value possible	No values given
3(1)3 - 2 - 0 and 2 - 3 - 2 - 0	+1.08 −0.21 +0.28 +1.77 −0.41 +0.48	+0.18 ±0.02 no large value possible	
3 - 2 - 2 - 0 and 2 - 2 - 2 - 0	+0.24 +0.06 −0.05 +1.54 ±0.20	+0.28 ±0.02 −6.1 ±0.02	+0.28 no value given

γ_2 (1.8)

3(0)3 - 2 - 0	+0.33 ± 0.08 +18.2 + ∞ −10.0	not possible	doubtful
3(1)3 - 2 - 0 and 2 - 3 - 2 - 0	+0.39 ± 0.12 +9.95 −4.8 + ∞	(anisotropy greater than that given by 3 - 2 - 0)	
3 - 2 - 2 - 0 and 2 - 2 - 2 - 0	−0.13 ± 0.08 +3.64 −0.82 +2.04	−0.19 ±0.02 −1.42 ±0.02	−0.15 ± 0.07 no value given

Only one value of δ and spin sequence for the Fe^{56} levels fits all the experiments for each gamma ray:

i.e. 2.1 Mev, γ_3 $2 \rightarrow 2$ $\quad \delta = 0.28 \pm 0.02$

1.8 Mev, γ_1 $2 \rightarrow 2$ $\quad \delta = -0.19 \pm 0.02$

The results of these experiments still leave the spin assignment of Mn^{56} ground state ambiguous, i.e. 2 or 3.

8c. Possibility of spin 2 for Mn^{56}

Consider first γ_1 for which $\delta = -0.19$ then

$$I(\theta) = 1 - 0.175 \lambda g_2 B_2 U_2 P_2 - 0.0165 \lambda g_4 B_4 U_4 P_4$$

where $g_2 = 0.94$ and $g_4 = 0.82$ are the aperture correction factors. At saturation of the nuclear spins $B_2 = 1.1952$ and $B_4 = 0.2673$, so we have the following possible values for the anisotropy ϵ,

	$j=0$	$j=1$	exptl. maximum
$\lambda = 1$	0.271	0.1395	
$= 0.71$	0.2045	0.1043	
$= 0.48$	0.1414	0.0714	0.15 ± 0.10

The values of λ chosen in anticipation of section 8e.

For this gamma ray the experimental error is large but the Fermi $j=0$ beta-transition is favoured for a pure transition, otherwise one would require an admixture in which the Fermi component was prominent.

Similarly for γ_3 $\delta = +.28$ and we have

$$I(\theta) = 1 - 0.696 \lambda g_2 B_2 U_2 P_2 - 0.023 \lambda g_4 B_4 U_4 P_4$$

and the following values for the saturation anisotropy:-

	j = 0	j = 1	exptl. maximum
$\lambda = 1$	0.85	0.49	———
$= 0.71$	0.68	0.38	0.50 ± 0.02
$= 0.48$	0.49	0.267	0.40 ± 0.02

Bearing in mind that the calculated values are for $\frac{1}{T} = \infty$ while the experimental points refer to $\frac{1}{T} \sim 90$, a pure Gamow-Teller transition is ruled out and any mixture would have to be predominantly Fermi in character.

gives similar results, the possible values being:

	j= 0	j= 1	exptl. maximum
$\lambda = 1$	0.625	0.334	———
$= 0.71$	0.487	0.260	0.41 ± 0.03
$= 0.48$	0.345	0.184	0.28 ± 0.03

The three beta-transitions, if from a level of spin 2, would have to be pure Fermi or predominantly Fermi in an admixture.

Now, if T - the isotopic spin - is a good quantum number, then Fermi transitions only occur for $\Delta T = 0$, i.e. between states of the same isobaric multiplet (Skyrme 1950). The ground states of Mn^{56} and Fe^{56} have T = 3 and 2 respectively and the coulomb energy difference between neighbouring elements, $\frac{6e^2}{5R}(Z-1)$ in this region of the periodic table is very large (~19 Mev) so that the levels involved cannot be members of the same multiplet. Thus, if the Fermi mode is present it must be due to a coulomb mixture of the wave functions. Such mixing would have to be very large to give predominantly Fermi transitions and seems unlikely, so that the results of the present

experiment would favour spin 3 for Mn^{56}.

T may not be a good quantum number but in a later chapter it is shown that a similar 2→2 beta decay in Co^{58} must be pure Gamow-Teller and for Mn^{52} the results of the beta-ray experiments (Ambler) show that the Fermi matrix element is very small ($\lambda < 0.05$). However, a similar experiment by Ambler et al (1957) on the $4^+ \rightarrow 4^+$ beta decay from Co^{56} to the 2.08 level in Fe^{56} gives two possibilities for the admixture either 94.2% or 7×10^{-4}% Fermi. The latter seems to be favoured since the experimental result, $\alpha' = 0.221 \pm 0.021$, is within experimental error, that expected for a pure Gamow Teller interaction $\alpha' = \frac{+1}{J+1} = \frac{1}{5}$.

8d <u>The magnetic moment of Mn^{56}</u>

Now that the decay sequence is known, it should be possible to make an estimate for the magnetic moment of the ground state of Mn^{56}. This enters through the B_2 and B_4 terms and since there are three gamma-ray anisotropies depending on B_2 and B_4 i.e.

$$\epsilon = \frac{aB_2 + bB_4}{c + dB_2 + eB_4}$$

it should be possible to solve these simultaneously for B_2 and B_4. The ratio $\frac{B_2}{B_4}$ would eliminate the damage attenuation factor and allow an estimate of the moment. However, the A_4 term is small and the experimental and analytical errors involved in finding B_4 give meaningless results where B_4 is negative or greater than B_2.

Although the moment cannot be found a lower limit can be given for it from the value of B_2 by making the assumption that the anisotropy after annealing is the full effect, i.e. $\lambda = 1$.

Thus at $\frac{1}{T} = 80$ $\epsilon(\gamma_3) = 0.50 = \frac{6.46B_2 + 0.033B_4}{8 + 2.155B_2 - 0.020B_4}$

neglecting B_4 we have $B_2 = 0.744$. Using the approximate method for calculating B_2 given in the Appendix, it is found that for $\mu = 1.3$ n.m. $B_2 = 0.774$ for $\frac{1}{T} = 90$ and 0.722 for $\frac{1}{T} = 80$. These give an anisotropy at:

$$\frac{1}{T} = 90 \quad \text{of} \quad \epsilon = 0.52$$

$$\text{and } \frac{1}{T} = 80 \quad \text{of} \quad \epsilon = 0.49$$

in good agreement with the experimental value. Thus, the magnetic moment of Mn^{56} must be greater than 1.3 n.m.

8e. The damage factor

If use is now made of the reported value of 3.5 n.m. (Childs, Goodman & Kieffer 1958), the population parameters can be calculated as described in the Appendix and theoretical values for A_2, including the aperture correction, can be obtained. These are tabulated below (Table 8) together with the experimental values for γ_1, γ_3. The ratio of experiment to theory gives λ and theoretical curves can then be drawn. The good agreement between the experimental and calculated curves confirms that it is reasonable to account for the damage by such an attenuating factor.

8f. Summary of conclusions

These experiments have shown that it is feasible to align isotopes produced by the neutron irradiation of a crystal, and to derive useful nuclear information. It has also been shown that it is reasonable to introduce an attenuating factor into the angular distribution to describe the damage.

TABLE 8

The damage attenuation factor

$\frac{1}{T}$	γ_3					γ_1				
	Unannealed	Annealed	Theory	λ_u	λ_a	Unannealed	Annealed	Theory	λ_u	λ_a
80	± 0.014 -0.28	±0.014 -0.40	-0.574	± 0.024 0.49	±0.024 0.70	± 0.024 -0.186	±0.024 -0.293	-0.374	±0.065 0.50	±0.065 0.78
70	-0.27	-0.37	-0.542	0.50	0.68	-0.178	-0.270	-0.346	0.51	0.78
60	-0.24	-0.33	-0.481	0.49	0.68	-0.160	-0.245	-0.313	0.51	0.78
50	-0.21	-0.29	-0.421	0.50	0.69	-0.136	-0.208	-0.270	0.50	0.77
40	-0.16	-0.24	-0.338	0.47	0.71	-0.105	-0.180	-0.216	0.49	0.83
30	-0.10	-0.18	-0.236	0.42	0.76	-0.080	-0.105	-0.151	0.53	0.70
20	-0.05	-	-0.116	0.43	-	-0.040	-0.048	-0.075	0.53	0.64
		Mean values:-		0.47 ± 0.01	0.70 ±0.01				0.51 ± 0.02	0.75 ± 0.02

Weighted mean values: unannealed 0.48
annealed 0.71

From the present results taken together with the angular correlation, it is possible to conclude that the spin of both the 2.94 Mev and 2.66 Mev levels of Fe^{56} is 2 and each decays by a mixed gamma ray.

The quadrupole/dipole mixing ratio is $+0.28 \pm 0.002$ for γ_3 and -0.19 ± 0.02 for γ_2. A value of 3 for the ground state spin of Mn^{56} is shown to be favoured and the magnetic moment must be greater than 1.3 n.m.

Using the reported value of 3.53 n.m. (Childs, Goodman & Kieffer 1958) it is found that for the unannealed crystal the radiation damage left 50% of the ions in their correct lattice site, and on annealing at 80°C for 2 hours only ~30% remained displaced.

9. Discussion

The quadrupole dipole mixing ratios (δ^2) for γ_2 and γ_3 are compared below with those calculated on the basis of the single particle transition probabilities (Moszkowski 1955).

	experimental	E2 - M1	M2 - E1
γ_2	3.6×10^{-2}	5.6×10^{-3}	3.6×10^{-6}
γ_3	7.85×10^{-2}	4.0×10^{-3}	2.6×10^{-6}

It is seen that a M2-E1 mixture can be ruled out, showing that there is no parity change for either transition and all levels involved have even parity while the observed mixture is 10-20 times larger than the calculated value. The values of δ^2 together with the measured intensities (Table 1) show that the E2 constituents of the cascade transitions are 10-20 times faster than the cross-over transitions to the

ground state.

Mn^{56} is an odd-odd nucleus, the odd proton being $(f\,7/2)^-$ and the odd neutron $(p\,3/2)^-$ or perhaps $p\frac{3}{2}, f\frac{5}{2}$. The expected parity is even so that all the beta-transitions are of the $\Delta I = 1$, no type. In particular this implies that the decay to the 0.845 Mev level is allowed in spite of its log ft. value of 7.2. From the non-appearance of the 1.24 Mev gamma ray ($\gamma_\beta < 2\%$) the beta-transition to the 2.08 Mev level must have log ft. 7.6. The allowed decay of Co^{56} to the same 4^+ state also has a large log ft. value (8.1). The values for log ft. for the transitions to the 3.4, 2.98 and 2.66 Mev levels are all about 5.3. This enhancement of the E2 cascade transition and large log ft. values i.e. reduction of the matrix elements are typical of levels possessing some collective character (Scharff-Goldhaber & Weneser 1955; Kisslets & Jean 1956). Near the closed shells (e.g. 2d) collective motions frequently give rise to vibrational levels, e.g. $_{28}Ni^{60}_{32}$; $_{26}Fe^{52}_{32}$ and for such nuclei 1 phonon (2^+) and 2 phonon ($0^+\,2^+\,4^+$ triplet) excited states are built up on the ground state. The energy of the second excited state is roughly twice that of the first and E2 transition between these two levels are favoured for $2^+ \rightarrow 2^+$ decays with M1 forbidden. E2 transitions to the ground state from the second excited state must make a 2 phonon jump and are forbidden. These rules are relaxed by mixing of other phonon states and single particle levels.

Another feature of collective motions is the reduction in the lifetime, i.e. an increase in transition probability by a factor of

between 10 and 40 of the first excited state as has been revealed by coulomb excitation (Temmer & Heydenberg 1956). The transition probability of the 0.845 Mev gamma ray is in fact increased about 15 times the expected value.

$_{26}Fe^{56}_{30}$ is an even-even nucleus and shows some of these characteristics. The second excited state at 4^+ has 2.46 times the energy of the first excited state 2^+ and the E2 cascade transitions to the latter level are enhanced.

If the first excited state is really a vibrational level, its shell configuration will be the same as the ground state, i.e. $(f\,7/2)^-(p\,3/2)^-$. The allowed beta-decay from Mn^{56} will then involve "spin flip" as a $p\,3/2$ neutron decays into an $f\,7/2$ proton and such a transition has $\Delta l=2$ and will be 1-forbidden. The large log ft. value found for this decay is consistent with this argument.

A similar argument may apply to the unobserved transition to the 4^+ level but in this case one also has the possibility of it being a forbidden 2 phonon jump from the ground state (0^+) of Mn^{56} (Alaga 1955). However, in both cases the increase in log ft. is large, the transition probability being some 100 times less than expected for an allowed transition.

The small log ft. values for the other beta-transitions implies that their character is mainly of a single particle nature and so one would expect a mixing of single particle and collective characteristics which appears to be the case.

The work described in this chapter is to be published in the Proceedings of the Royal Society of London under the title:- "Nuclear Alignment of Manganese 56" by Dagley, P., Grace, M.A., Gregory, J.M., and Hill. J.S.

CHAPTER 6

THE BETA TRANSITION IN COBALT - 58

1. Introduction

Cobalt 58 was one of the first isotopes studied using the techniques of nuclear orientation. Measurements of the angular distribution (Daniels et al, 1952) of the gamma radiation led to the deduction of the spin sequence in the decay. It was found that the allowed beta-transition took place between nuclear levels of the same spin, and therefore satisfied both Fermi and Gamow-Teller selection rules, i.e. $\Delta I = 0$, $i_\beta = 0$ or 1.

The fraction, λ, of the transitions which obey Fermi selection rules $i_\beta = 0$ was measured to be about 10% in a similar experiment by Griffing and Wheatley (1956). However, the "parity" experiments of Ambler et al (1957) suggested that, on the basis of the two component theory of the neutrino, the transition only involved the Gamow-Teller interaction, $i_\beta = 1$.

It became important for the construction of the full theory of beta decay to know which of these results was correct and this chapter describes an experiment carried out to this end.

2. The decay scheme

A 72-hour positron activity from Cobalt was found by Livingood and Seaborg in 1941. Deutsch and Elliott (1944) and Good et al (1946) showed that the decay was predominantly by K-capture and that the value of the positron branching ratio, $K/\beta^+ = 5.9$ was consistent with a

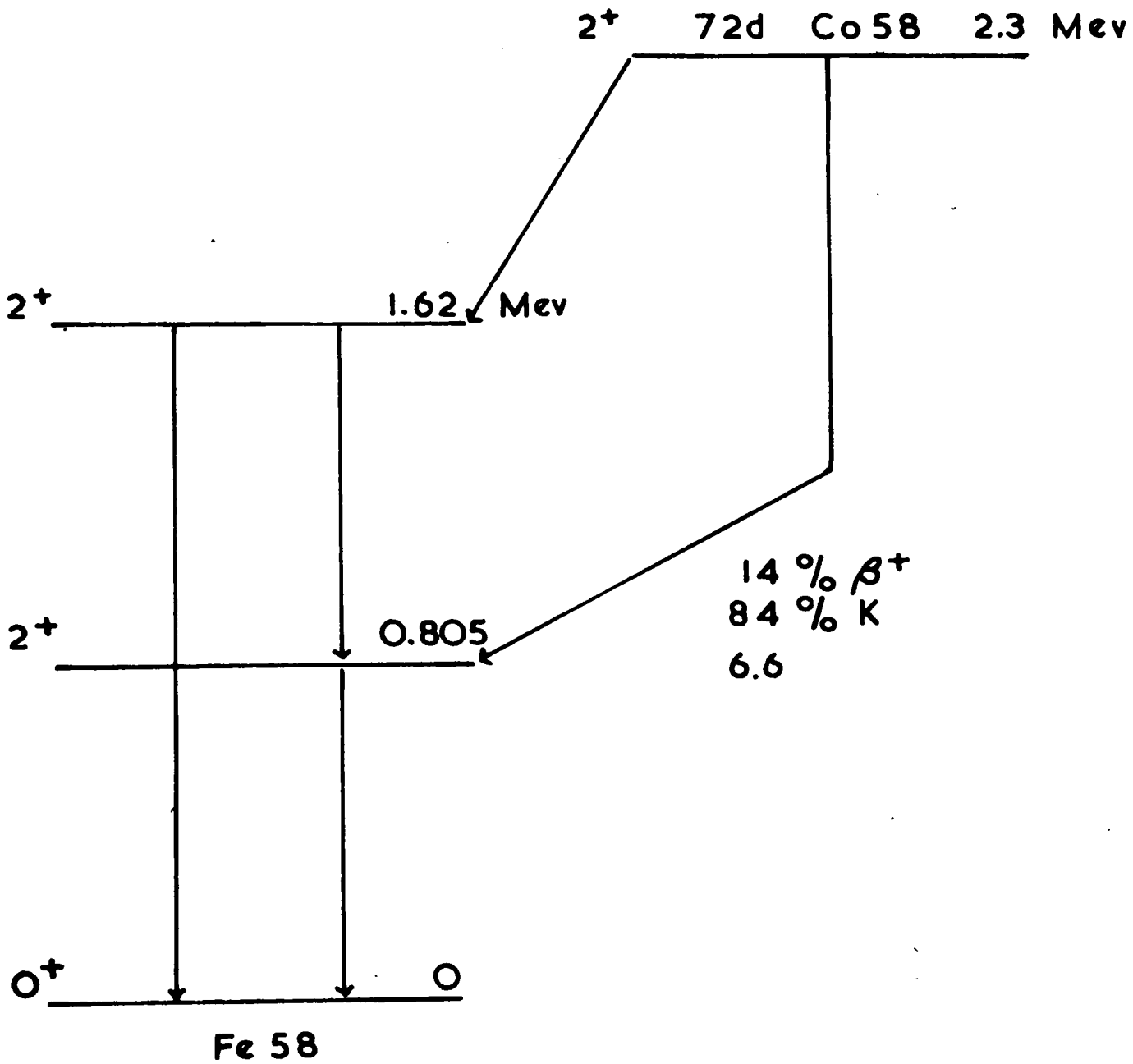


Figure 1

change in angular momentum of $\Delta I = 0$ or 1 but could be either allowed or first forbidden. The theoretical calculation of Zweifel (1958) gives $K/\beta^+ = 4.9$ for $Z = 27$, $W_0/m_0c^2 = 1.92$. A recent measurement of K/β^+ by Konijn (1958b) gives 5.67 ± 0.14 in good agreement with Zweifel when corrected for a contribution from the L shell. The positron spectrum has the allowed shape and the comparative half life, log ft. ~6.5, is also consistent with an allowed transition.

The measured value of $\alpha_K = 2.5 \times 10^{-4}$ (Strauch 1950) limits the gamma transition to be electric quadrupole ($\alpha_K = 2.65 \times 10^{-4}$; Rose 1958) or magnetic dipole ($\alpha_K = 1.9 \times 10^{-4}$). In view of the positive gamma ray anisotropy found by Daniels et al, the transition must be quadrupole.

This fixed the spin of the first excited state of Fe^{58} as 2^+ so that the possible sequences are

A $1 - (1) - 2 - (2) - 0$

B $2 - (1) - 2 - (2) - 0$

C $2 - (0) - 2 - (2) - 0$

D $3 - (1) - 2 - (2) - 0$

with the possibility of B and C occurring together.

The experimentally determined values of $I(0^0)$, $I(90^0)$, $I(45^0)$ were consistent only with the possibility B,C with the Gamow-Teller interaction predominating in the beta decay. The ground state spin of Co^{58} must be 2^+ and by fitting a theoretical curve to the experimental variation of $\epsilon v \frac{1}{\tau}$ they deduced a magnetic moment of 3.5 ± 0.3 n.m. for the Co^{58} ground state.

A paramagnetic resonance experiment (Debrov and Jeffries, 1957) confirmed the spin of Co^{58} to be 2 and gave the value of 4.052 ± 0.01 n.m. for the moment.

The decay through the 1.62 Mev level of Fe^{58} was discovered and studied by Frauenfelder et al (1956). They measured the relative intensities of the three gamma rays to be 100 (0.805 Mev); 1.6 (0.815 Mev) and 0.5 (1.62 Mev). From a gamma-gamma angular correlation experiment they showed that the second excited state of Fe^{58} also had a spin of 2, the transition to the first excited state being a dipole quadrupole mixture ($\delta = 2.2 \pm 0.3$).

With the spin sequence known, Griffing and Wheatley (1956) were able to use the measurements of the angular distribution of the gamma radiation from aligned Co^{58} to study the beta-transitions almost unambiguously (see section 4). Defining the fraction of disintegrations involving Fermi selection rules as $\lambda = \dfrac{C_F^2 |M_F|^2}{C_F^2 |M_F|^2 + C_{GT}^2 |M_{GT}|^2}$ (See Chapter 1), they found that for the principal branch $\lambda = 0.11 \pm 0.04$, while for the weak branch $\lambda = 0.45 \pm 0.11$.

A reanalysis of the experiments of Daniels et al showed that they were consistent with $\lambda = 0.1 \pm 0.1$.

3. The parity experiments

Following the suggestion of Lee and Yang (1956) that parity might not be conserved in beta-decay, Wu et al (1957) measured the asymmetry in the angular distribution of electrons from polarised Co^{60} nuclei.

The angular distribution for an allowed beta transition is given by $I(\theta) = 1 + \alpha \frac{v}{c} \cos\theta$. α is given by: (see Lee and Yang 1957)

$$\alpha = \left\{ \pm \left\langle \frac{I_M}{I} \right\rangle \lambda_{II'} \mathrm{Re}\left[(C_T C_T'^* - C_A C_A'^*) \pm \frac{iZe^2}{Rcp} (C_A C_T'^* - C_A' C_T^*) \right] |M_{GT}|^2 \right.$$

$$+ \delta_{II'} \left\langle \frac{I_M}{I} \right\rangle \frac{I}{\sqrt{I+1}} \mathrm{Re}\left[(C_T' C_S^* + C_T C_S'^* - C_A' C_V^* - C_A C_V'^*) \right.$$

$$\left. \left. \pm i \frac{Ze^2}{Rcp} (C_A' C_S^* + C_A C_S'^* - C_T' C_V^* - C_T C_V'^*) \right] |M_F| \, |M_{GT}| \right\} \frac{v}{c} \frac{2}{(\xi + \xi \, b/W)}$$

taking plus sign for β^- emission and minus sign for β^+ emission.

$$\lambda_{I'I} = \begin{cases} 1, & I \to I' = I - 1 \\ \frac{1}{I+1}, & I \to I' = I \\ \frac{-I}{I+1}, & I \to I' = I - 1 \end{cases}$$

$$\xi = |M_F|^2 (|C_S|^2 + |C_S'|^2 + |C_V|^2 + |C_V'|^2) + |M_{GT}|^2 (|C_T|^2 + |C_T'|^2 + |C_A|^2 + |C_A'|^2)$$

$$\xi b = 2\gamma \mathrm{Re}\left[|M_F|^2 (C_S C_V^* + C_S' C_V'^*) + |M_{GT}|^2 (C_T C_A^* + C_T' C_A'^*) \right]$$

$$\gamma = \sqrt{1 - \frac{Z\alpha^2}{R_0}}$$

We may write $\alpha = \alpha' \frac{v}{c} \left\langle \frac{I_M}{I} \right\rangle$ and the value of $\alpha' = -1$ found for Co^{60} is readily understood if the two component theory of the neutrino is valid. This theory gives $C_i = +C_i'$ and if absence of Fiers interference terms $C_S C_V$(Fermi); $C_T C_A$ (Gamow-Teller) is interpreted as implying that one of the coefficients for each mode is zero, i.e. ST, SA, VT, VA are the only possibilities, $\alpha' = -1$, for the pure Gamow-Teller decay of Co^{60} with an axial vector interaction. This implies that an electron is emitted with an antineutrino which has left-hand helicity and a

positron isassociated with a right-handed neutrino.

Thus for the positron decay of Co^{58} 2→2, we have

$$\alpha' = \frac{-1}{I+1}\alpha'(Co^{60}) = +\frac{1}{3}$$ if the interaction is purely Gamow-Teller; and Ambler et al (1957a) found $\alpha' = +0.325 \pm 0.047$.

The asymmetry is very sensitive to the Fermi:Gamow-Teller mixture and if the value found by Griffing and Wheatley is used, the expected value of α' varies greatly from that found. For instance, if the coupling involved vector axial vector (V,A) terms only, we have:

$$\lambda = \frac{C_V^2 |M_F|^2}{C_V^2 |M_F|^2 + C_A^2 |M_{GT}|^2} = 0.11 \pm 0.04$$

so that $\frac{C_V |M_F|^2}{C_A |M_{GT}|^2} = \pm(0.35 \begin{smallmatrix}+0.07\\-0.13\end{smallmatrix})$ and the calculated asymmetry would be

$$\alpha' = +0.041 \begin{smallmatrix}-0.049\\+0.060\end{smallmatrix} \text{ or } +.552 \begin{smallmatrix}-0.034\\+0.023\end{smallmatrix}$$

The result of Ambler et al was supported by the results of a similar experiment done at Leiden (Postma et al 1957) which gave $\alpha' = +0.23 \pm 0.06$ and the result of a beta-gamma ray circular polarisation correlation experiment of Boehm and Wapstra (1957). The latter authors found no evidence for Fermi:Gamow-Teller interference terms and suggests that the Fermi matrix element is smaller than about one quarter of the Gamow-Teller matrix element, i.e. $\lambda < 0.06$.

Ambler et al (1957b) pointed out that the discrepancy between the results of the gamma-ray and beta-ray experiments might arise from the Fermi:Gamow-Teller interference terms being largely imaginary in

the expression for the beta-ray asymmetry. They showed this hypothesis to be untenable from results of a beta-gamma correlation experiment. Here the direction of the gamma ray is considered as well as the directions of the beta ray and the nuclear spin, the angular distribution being of the form

$$I(\theta) = 1+k\,Im\left[C_S C_T'^* + C_S' C_T^* - C_V C_A'^* - C_V' C_A^* \pm \frac{iZ}{p}\left(C_S C_A'^* + C_S' C_A^* - C_V C_T'^* - C_V' C_T^*\right)\right] |M_F||M_{GT}| \frac{v}{c} \frac{2}{\left(\zeta + \frac{b}{w}\zeta\right)}$$

(Ambler, 1957b; Morita, 1957).

where k involves the alignment parameters and the angular terms $P_1(\cos\theta)$. It can be noted that here this expression involves the imaginary part of the interference term, the real part of which appeared in the beta-ray asymmetry. The measured correlation was not consistent with imaginary coupling constants for the mixing ratio found by Griffing and Wheatley.

Since the beta ray experiments gave self-consistent results but definitely excluded the value found by Griffing and Wheatley, it was decided to carry out an accurate measurement of the gamma ray angular distribution in order to establish or disprove the discrepancy. The techniques of this type of experiment are well known so that sources of error can be examined and their effect eliminated while the result can be found without a knowledge of $\frac{v}{c}$ or the absolute temperature.

4. The previous alignment experiments

For the early experiment Daniels et al used a biaxial Tutton salt and they did not in fact give a value for λ. However, an interpretation of the results in this way gives $\lambda = 0.1 \pm 0.1$ so that little

weight can be attached to the result. Griffing and Wheatley obtained a very good statistical accuracy in their counting rates but they also chose to incorporate the activity in a Tutton salt, (Tr Co, Cu, Zn) $K_2(SO_4)_2$, $6H_2O$. The drawbacks connected with these salts have already been discussed (Section 2, Chapter 2). For Co^{58}, it is the axial direction which is most sensitive to the admixture but with a Tutton salt this direction is not accessible for study.

Also they used an assembly of 19 single crystals. Although they took care in lining up the axes of the crystals parallel to one another, this is certain to increase the doubts about the correct orientation. Further, with such an assembly of crystals thermal equilibrium amongst the constituents is difficult to ensure and therefore the B term of the angular distribution $I(\theta) = \sum B_\nu U_\nu F_\nu P_\nu(\cos\theta)$ may need to be replaced by $\overline{B_\nu}$, where $\overline{B_\nu}$ is some average over the crystals. Such a change in the calculated B_ν could lead to erroneous values for λ.

In order to get round the difficulty of not knowing the exact location of the axes (see Chapter 2), Griffing and Wheatley used the results of a preliminary experiment to locate roughly the "0°" and "90°" positions, i.e. the bisector of the angle between the two axes and the common equatorial direction. They then made more accurate measurements at these positions and at an intermediate position in the same plane. Since $P_2(\cos\theta)$, $P_4(\cos\theta)$ vary very slowly for $\theta \sim 90^\circ$, the common equatorial direction, $I(90^\circ) = 1 - \frac{1}{2}B_2(\beta)U_2(\lambda)F_2 + \frac{3}{8}B_4(\beta)U_4(\lambda)F_4$ where $\beta = \frac{A}{2kT}$ and the measured intensity at a given instant will give

B_2, B_4 for a given value of λ since the other factors are known.

Then $I('0^{o}') = 1 + B_2 U_2 F_2 P_2(\mathrm{Cos}\alpha) + B_4 U_4 F_4 P_4(\mathrm{Cos}\alpha)$,

(where α is the half angle between the two axes) will give α as a function of β and λ.

The intermediate angle ϕ can then be found from the third set of data:

$$I(\phi) = 1 + B_2 U_2 F_2 P_2(\phi) + B_4 U_4 F_4 P_4(\phi)$$

$\mathrm{Cos}\,\phi = \mathrm{Cos}\,\Theta\ \mathrm{Cos}\,\alpha$, where $\mathrm{Cos}\,\Theta$ is the laboratory angle in the plane of the orthoganal counterpositions.

The values obtained for α and ϕ are functions of the parameter λ so that curves of $\alpha \vee \lambda$ and $\phi \vee \lambda$ could be plotted. Regardless of the magnetic temperature, and therefore β, the values of ϕ, α and λ must be the same so that the intersection of the curves for different values of β gives α, ϕ and λ.

Although the statistical accuracy of the counting was good, this method of treatment is iterative so that the propagation of errors is very complex, making the result rather uncertain. They give the final result as $\lambda = 0.11 \pm 0.04$.

5. Design of the present experiment

Nickel fluosilicate had already been used for some alignment experiments and with its single axis of alignment coincident with one of the crystal axes, it was seen to be a favourable salt in which to align Co^{58}. With a clear single crystal having well-defined edges, the problems of temperature homogeneity and location of the axis are

largely eliminated.

The h.f.s. data for Cobalt is known (Bleaney & Ingram, 1951b) so the population functions B_ν can be calculated (Appendix) and all quantities except λ are then known.

A family of curves, fig. 5 can be drawn showing the dependence of $I(0^\circ)$ on $I(90^\circ)$. Each member of the family corresponds to a single value of λ while each point on the curve corresponds to a different value of $\beta(\propto \frac{1}{T})$.

A number of curves are shown in the figure indicating the substantial differentiation between small values of λ which can be obtained by this method. The sensitivity to λ comes from the great difference in the gamma ray intensities along the axis for the two cases, which is due to the difference in sign of U_4. For the Fermi transition $U_4 = +1.0$ and the minimum value of $I(0^\circ)$ is 0.06, whereas for the Gamow-Teller transition with the consequent disorientation in a 2(1)2 transition $U_4 = -0.6665$ and $I(0^\circ)$ never falls below 0.822.

It should be pointed out that the derivation of λ in this way from a measurement of $I(0^\circ)$ and $I(90^\circ)$ uses the experimental values without further analysis and does not rely on any knowledge of the absolute temperature but only on the validity of the Spin Hamiltonian, the value of B/A and the sign of A. The validity of the Spin Hamiltonian is borne out by the many paramagnetic resonance and nuclear orientation experiments performed with Cobalt. The sign of A cannot be measured directly but, according to the theoretical

arguments of Abragam and Pryce (1951b) it should have the same sign as the magnetic moment which has been shown to be positive (Wheatley, Huiskamp et al 1955). The error in B/A is discussed later.

6. Experimental

6a. The source material

Co^{58} was produced by the $Ni^{58}(n,p)Co^{58}$ reaction, using the fast neutron flux of the AERE Harwell pile. Carrier free Cobalt (specific activity 100-1000μs/μgm Co) was separated chemically from the nickel by the Harwell Isotope Division, who estimated the amount of Co^{60} present to be less than 0.5%.

The Co^{60} is produced simultaneously by the $Ni^{60}(n,p)Co^{60}$ reaction and the low yield is in accord with that predicted by Hughes (1953). The mass differences Co^{58} - Ni^{58} and Co^{60} - Ni^{60} are equivalent to 0.16 Mev and 2.813 Mev respectively. The Q of the reactions is then given by :

$$Q = Ni^{58} - Co^{58} + n-p \quad \text{and} \quad Q = Ni^{60} - Co^{60} + n-p$$

$$= 0.622 \text{ Mev} \qquad = -2.031 \text{ Mev}$$

The threshold energy given by $E_T = \frac{-(A+1)}{A}$ is therefore -0.632 Mev for Co^{58} and 2.065 Mev for Co^{60}. Because of the shape of the fission neutron spectrum and the dependence of the penetrability of the nucleus on energy, cross sections can be calculated more readily in terms of an effective energy E_{eff} .. E_{eff} is such that all neutrons with greater energy take part in the reaction with equal penetrability and those with less energy do not contribute at all (Hughes 1953). The effective

energy is always greater than E_T but the difference $E_{eff} - E_T$ is independent of E_T. Hughes gives curves for the dependence of $E_{eff} - E_T$ on Z and the dependence of cross-section on E_{eff}. Using these it is found that:

$$E_{eff} - E_T(n,p) = 8.2 \text{ Mev for } Co^{58} \text{ and } 8.4 \text{ for } Co^{60}$$

$$E_{eff} = 7.568 \text{ Mev and } 10.465 \text{ Mev respectively,}$$

and the cross-sections $\frac{\bar{\sigma} 10}{A^{2/3}} \approx 0.57$ mb. for Co^{58} and ~ 0.06 for Co^{60}.

The activity produced is then given by $A = N\bar{\sigma} nv(1-e^{\frac{-0.69t}{\tau}})$, where

$$N = \frac{\text{mass bombarded x abundance of isotope x Avogadro's No.}}{\text{Atomic number}}$$

i.e. the total number of atoms available.

$\bar{\sigma}$ = the reaction cross section; nv = neutron flux. t is the bombardment time and τ the half life of the isotope produced. The ratio of the activities is then:

$$\frac{Co^{60}}{Co^{58}} = \frac{26.16 \times 0.06 \times (58)^{1/3} \times (1 - e^{\frac{-0.69t}{5.2 \times 365}})}{67.76 \times (60)^{1/3} \times 0.57 \times (1 - e^{\frac{-0.69t}{71}})}$$

since Ni^{58} and Ni^{60} have natural abundances of 67.76% and 26.16% respectively.

For an irradiation time of one week, the Co^{60} amounts to 0.2% of the Co^{58} activity and after 71 days would only be 0.24%. An analysis of the pulse height spectrum showed that the amount of Co^{60} present was in fact less than 0.25%.

6b. The spectrum

The pulse height spectrum corrected for background is shown in figure 2 . The relative areas of the 0.805 Mev, 1.17 Mev and 1.62 Mev photopeaks are 115: 19: 45 respectively. For the 2" crystals used at I28 I28 a source distance of about 10 cms. the photopeak efficiencies are approximately 0.14, 0.085 and 0.06 (Bell, 1955) respectively relative to the total spectra for each energy.

Then the activities are in the ratio given by:

$$\frac{N_{1.6} \times 0.06}{N_{0.8} \times 0.14} = \frac{45}{128} \times \frac{1}{115}$$

Therefore $\frac{N_{1.6}}{N_{0.8}} = \frac{0.7}{100}$, which is in reasonable agreement with reported value of 0.5/100.

For the Co^{60}, we have: $\frac{N^{60} \times 0.086}{N_{0.8} \times 0.144} = \frac{19}{128} \times \frac{1}{115}$

Therefore $\frac{N^{60}}{N^{58}} = \frac{0.2}{100}$, in agreement with the value expected from the previous section.

The high energy part of the spectrum has been analysed figure 2a. using the 1.28 Mev gamma ray peak from Na^{22} to estimate the shape of the 1.6 Mev Compton distribution. The remainder of the spectrum can be satisfactorily broken down into the tail of the 0.805 Mev gamma ray (estimated using a source of Mn^{54} (0.845 Mev)) and a Co^{60} distribution. On this scale, the areas of the 0.805 peak, which lies between 0.7 and 0.9 Mev is 5850 units relative to 12.5 units for the 1.62 Mev. Since the 0.805 Mev channel is 5 cms. wide, lying between 0.78 and 0.9 Mev, and the 1.62 distribution ~ 2 cms. high, the contribution of

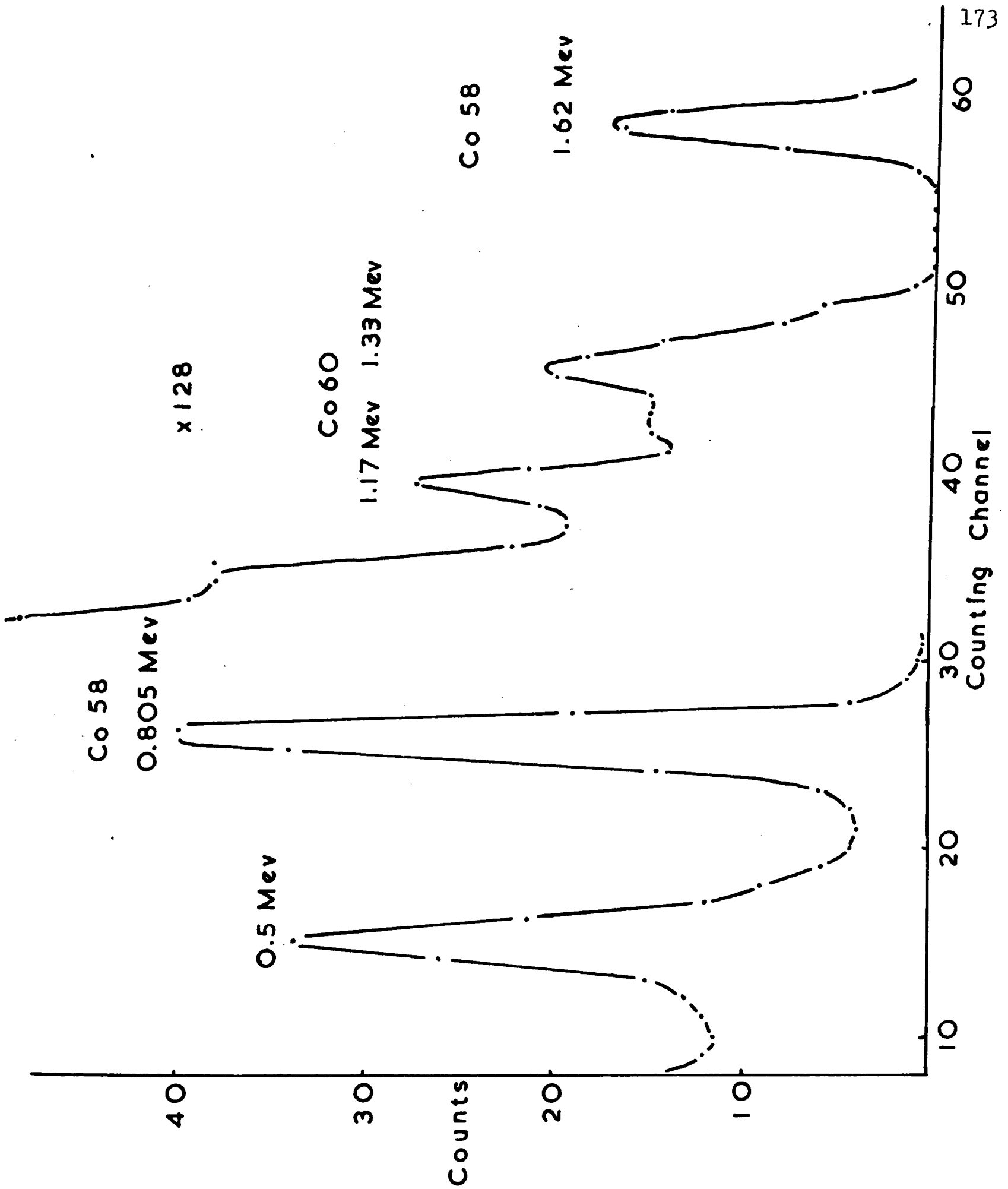

Co 58
0.805 Mev
x 128
Co 60
1.17 Mev 1.33 Mev
Co 58
1.62 Mev
0.5 Mev
Counts
Counting Channel
10
20
30
40
50
60
40
30
20
10

Figure 2

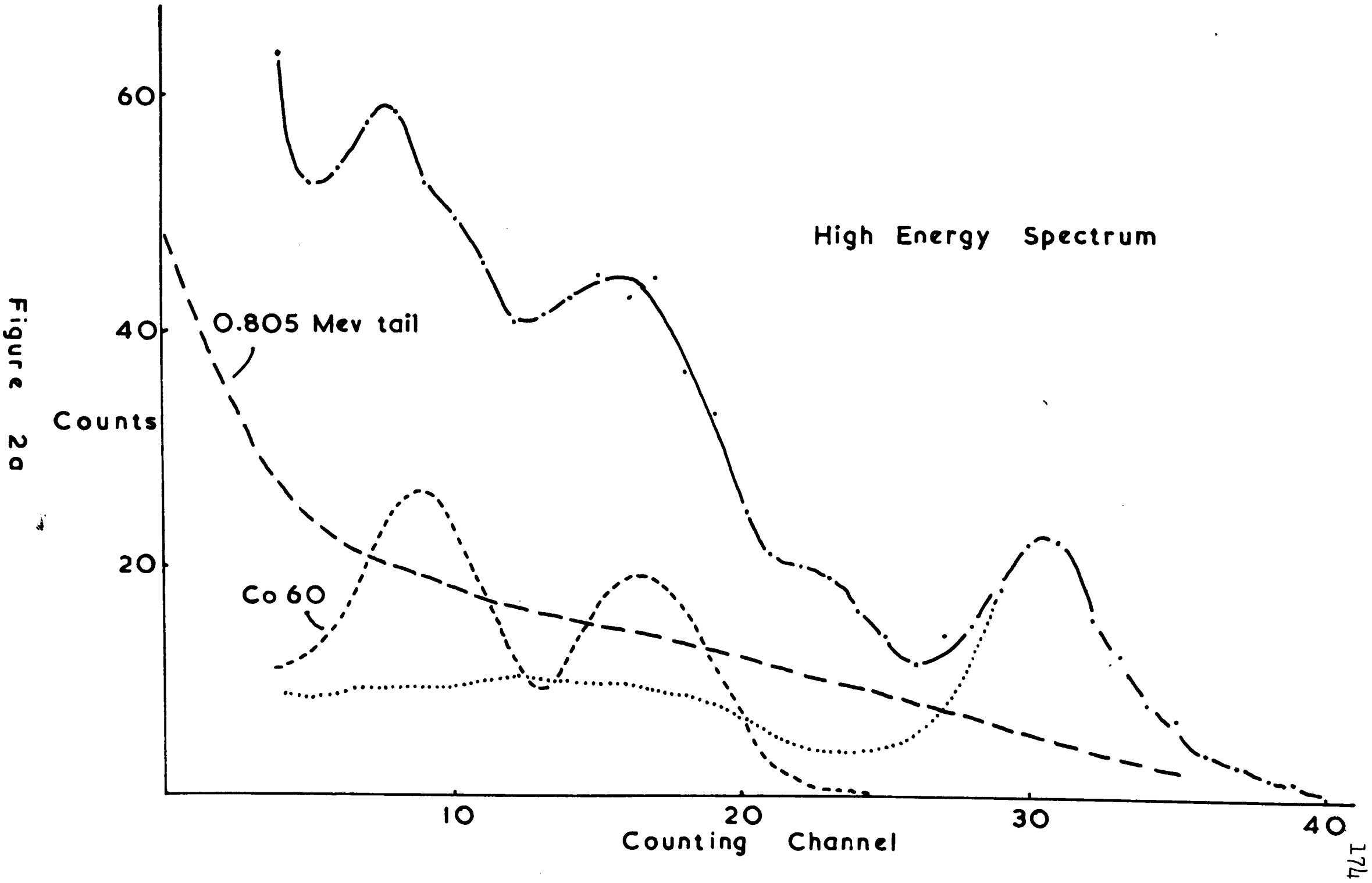

60
40
20
Counts
0.805 Mev tail
Co 60
High Energy Spectrum
10
20
30
40
Counting Channel

Figure 2a

the 1.62 Mev gamma ray to the counting channel is $\frac{2}{1170}$ or 0.17%. Similarly, the Co^{60} contributed $\frac{3}{1170}$ or 0.26% of the counts in this channel. These contributions are considered in Section 7.

6c. The crystal

A single crystal weighing 3.1 gms. and containing about 70μc of Co^{58} was grown from an active solution of $(10\%Ni, 90\%Zn)SiF_6, 6H_2O$. The surfaces of the crystal were clean and its axis could be located accurately. This was mounted with its axis horizontal in a standard perspex holder and placed in the cryostat in the usual way (Chapter 2), care being taken to line it up accurately with respect to the counter position. Three methods were used by several observers. First of all the crystal was aligned simply by eye and then this was checked by lining up the top edge of the crystal with two pins placed along the counter reference plate. Another check was made by using one of the plane faces of the perspex crystal holder as a plane mirror and shining a narrow beam of light along the equatorial direction. The alignment of the crystal was then adjusted until object and image coincided and the final position was considered to be correct within 1^0.

6d. The counters

The counters were the normal scintillation counters with 2" x 2" cylindrical Harshaw phosphors as described earlier. Their energy resolution was tested before the experiment and found to be 8% for the 660 kev gamma radiation of Cs^{137} and the phosphors subtended a

half-angle of 9° at the crystal, the effect of which is considered in Chapter 2.

A pair of discriminators was set above and below the 0.805 Mev photopeak (figure 3). In this way account could be taken of the effect of the higher energy radiation from Co^{58} and from the Co^{60} contamination on the counting rate in the channel.

6e. Precautions

(i) Temperature homogeneity: The counting rates for any given value of the magnetic temperature were independent of whether this temperature was reached by direct demagnetisation or by demagnetising to a lower temperature and allowing the crystal to warm up. This is illustrated in figure 4 and shows that the temperature was sensibly homogeneous within the crystal over the measuring period of 5 minutes.

(ii) Drifts and instability: Before the experiment was started, a long series of stability tests were carried out. These showed that there were no long term drifts in counting rate and that the statistical variations gave the largest contribution to the standard deviation.

Frequent tests throughout the series of runs were carried out which showed no systematic trends, due, for instance, to instability or fatigue of the counters produced by moving them to and away from the source. These tests took the form of demagnetisations from small fields (i.e. 860 oersted or ~ 50 amps excitation current) in which case no cooling is produced and the isotropic distribution should be obtained. This was found to be the case within the statistical error $\pm$ 0.0016,

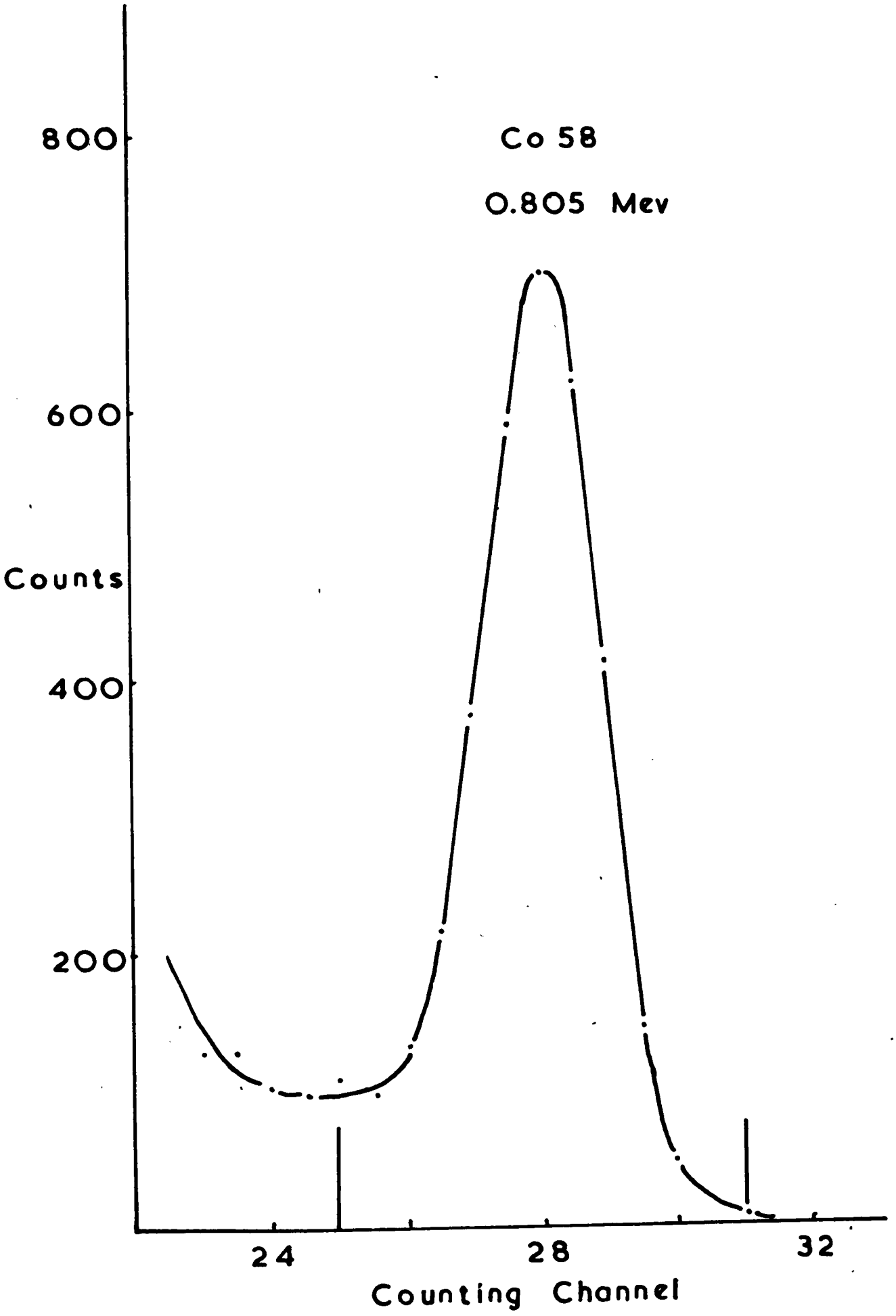

Co 58
0.805 Mev
800
600
400
200
Counts
24
28
32
Counting Channel

Figure 3

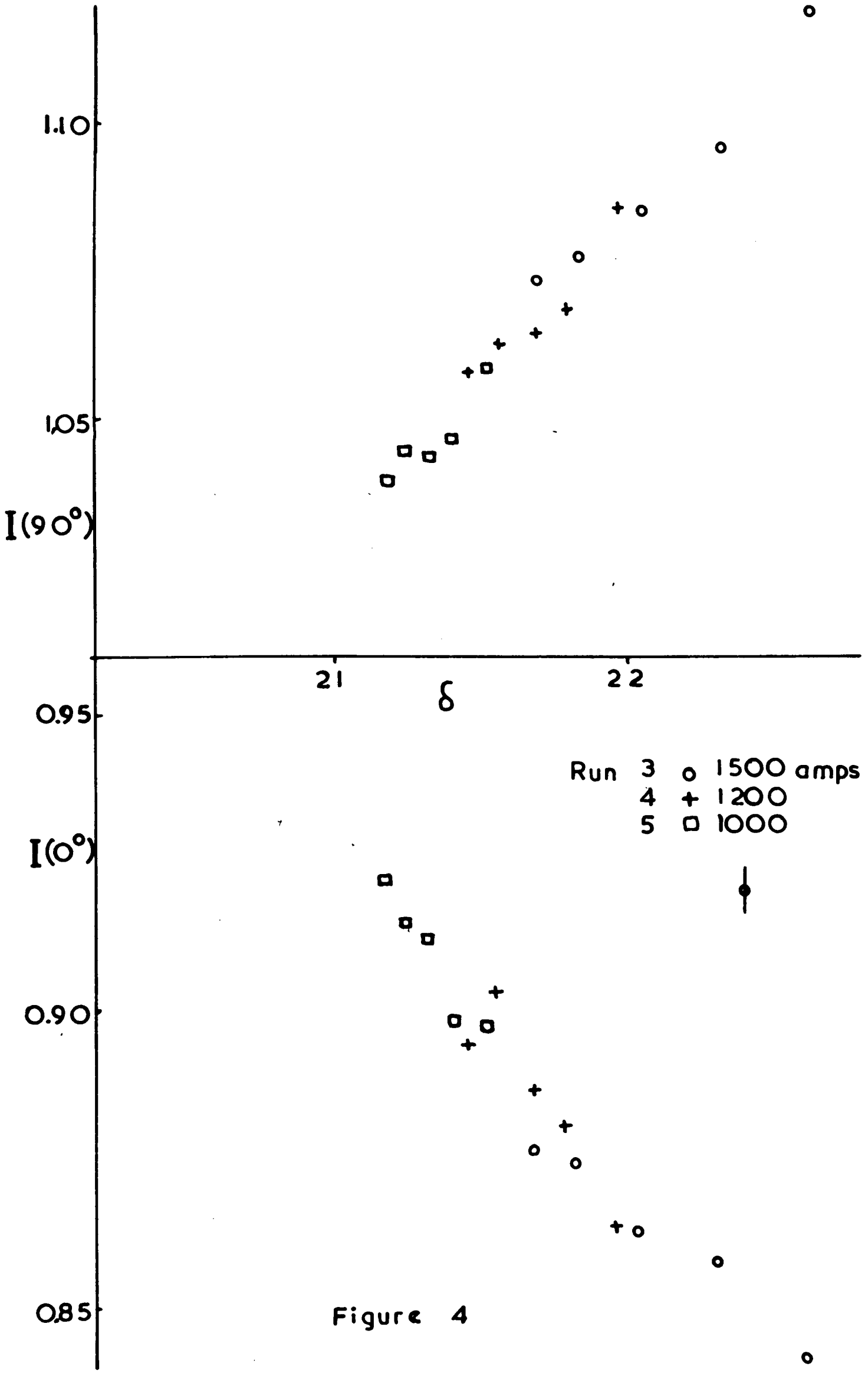


Figure 4

the mean of these runs gives $I(0^{\circ}) = 0.999$, $I(90^{\circ}) = 1.000$. The readings taken during a typical run are shown in Table 1.

6f. Results

Since all the points were consistent, they were blocked in 21 equal sets of 8 and one set of 9 points each covering a small range of values (Table 2). It is seen that these uncorrected points agree closely with the $\lambda = 0$ curve, (figure 5). The results were then treated quantitatively in the following way.

Each experimental point can be considered as a measurement of the value of λ with a probable error and hence a weight arising from the counting statistics. Each counting interval was 40 seconds with about 1500 counts/sec. so the statistical error, $\sqrt{N}$, gives rise to an error approximately $\pm 0.00\frac{1}{2}5$ for each point and hence to an error of approximately $\pm \frac{0.00\frac{1}{2}5}{\sqrt{8}} = \pm 0.0016$ in the blocked values of $I(\theta)$. This error is the same for all points but because of the form of the curve it covers a different range of λ ($\triangle\lambda$) for each point; those points obtained for the lower temperatures are much more sensitive to λ.

A large scale plot (figure 6) was made and the value of λ and $\triangle\lambda$ found for each point. These were then given a weight $w = \frac{1}{(\triangle\lambda)^2}$ and the mean value of λ, $\bar{\lambda} = \frac{\sum w.\lambda}{\sum w}$ was found to be $+0.003$ (Table 3).

The standard (r.m.s.) error was then determined from the scatter of the points about this mean value, i.e.

$$\sigma_{\bar{\lambda}} = \sqrt{\frac{\sum w(\bar{\lambda}-\lambda)^2}{n\sum w}} = \pm 0.00\frac{1}{2}4$$

TABLE 1

Co^{58} in Ni-$ZnSiF_6$ $5H_2O$

Initial Field = 34.4 kilogauss Source-Counter distance = 13.37 Counting interval 20 - secs.

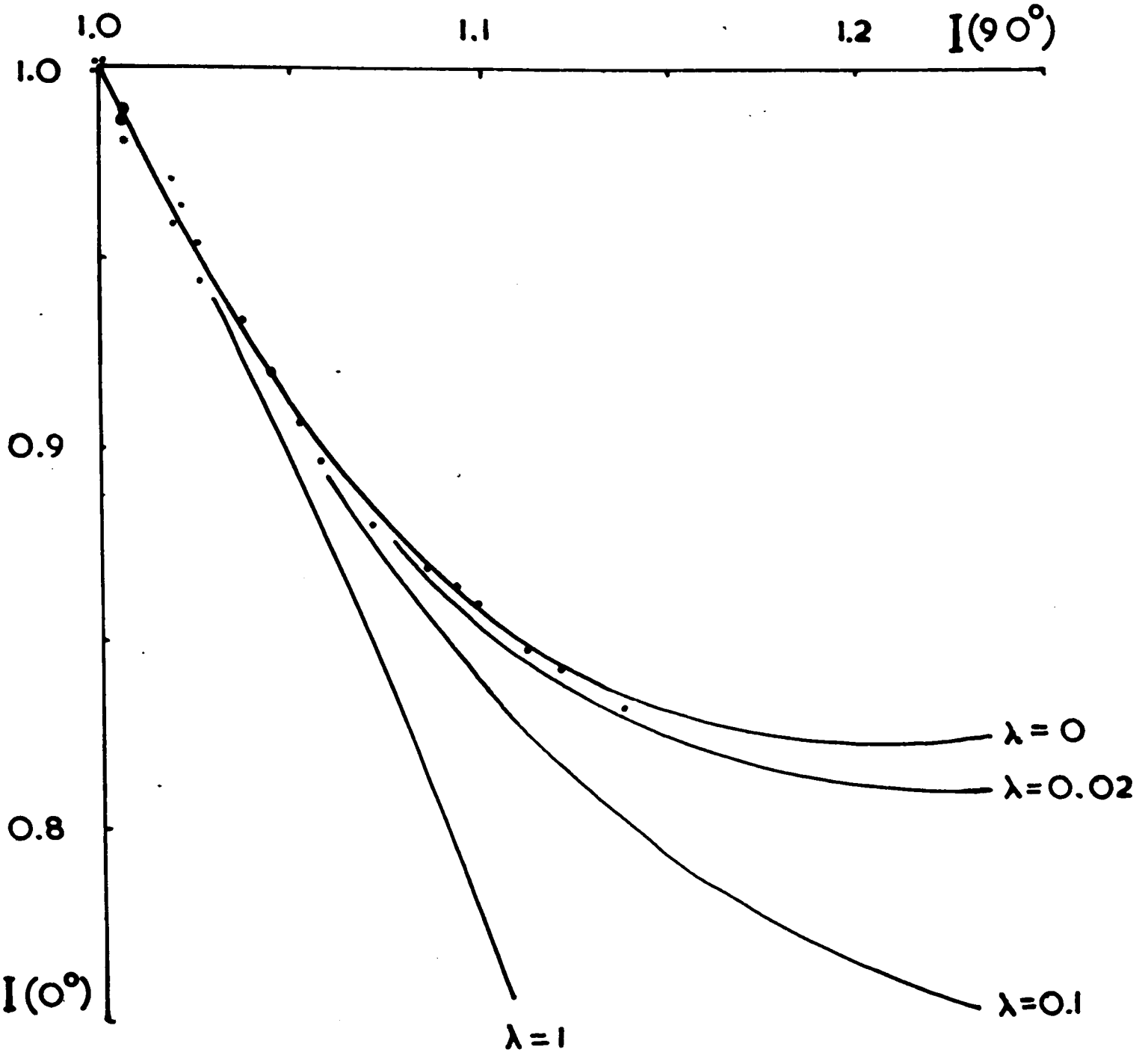
Time Mins. secs.	Galvanometer Defln. cms.	Axial Counter Low bias	Mean	High bias	Mean	LB-HB	I(0°)	Equatorial Counter Low bias	Mean	High bias	Mean	LB-HB	I(90°)	∈
0-11 / 0-45	23.75	28961 / 29035	28998	874 / 944	909	28089 ± 119	0.832 ±0.004	38046 / 37471	37739	1936 / 1880	1908	35831 ±135	1.144 ± 0.005	0.272 ±0.007
1-15 / 1-46	23.22	29342 / 29166	29254	906 / 908	907	28347	0.839	36776 / 36789	36838	1969 / 1846	1907	34931	1.118	0.250
2-13 / 2-44	22.88	29305 / 29659	29482	888 / 947	917	28565	0.845	36767 / 36152	36459	1906 / 1886	1896	34563	1.104	0.235
3-16 / 3-45	22.59	29853 / 29883	29868	970 / 931	950	28918	0.856	36105 / 36312	36208	1877 / 1819	1858	34350	1.097	0.217
4-12 / 4-47	22.38	30009 / 30333	30171	943 / 950	946	29225	0.866	35923 / 35808	35864	1882 / 1875	1878	33986	1.083	0.201
		34789		1162				33041		1672				$\epsilon_{t=0}$ = 0.290
		34858		1197				33094		1691				± 0.020
		34976	34870	1189	1169			32753	32974	1634	1650			
		34907		1136				33187		1677				
		34819		1152				32799		1574				
		34811		1149				33037		1697				
		35260		1071				33148		1584				
		34789	34953	1178	1132			32894	32916	1606	1620			
		34958		1099				32747		1643				
		34949		1162				32749		1571				
Mean			34911		1150	33761 ± 58			32945		1635	31310 ± 56		

TABLE 2

Co^{58} in Ni-Zn $SiF_6 \cdot 6H_2O$

Normalised Intensities
(blocked points)

I(0°)	I(90°)
0.830 ± 0.0016	1.136 ± 0.0016
0.841	1.120
0.846	1.111
0.858	1.098
0.863	1.093
0.868	1.085
0.879	1.071
0.897	1.057
0.907	1.052
0.920	1.044
0.933	1.036
0.945	1.026
0.953	1.025
0.959	1.019
0.963	1.021
0.970	1.018
0.981	1.006
0.985	1.007
0.988	1.006
0.995	0.998
0.999	1.002
1.005	1.000



Co 58

Figure 5

TABLE 3

Calculation of λ

pt	λ	$\Delta\lambda$	$\omega = \frac{1}{(\Delta\lambda)^2}$	$\omega\lambda$	$\lvert\bar{\lambda}-\lambda\rvert$	$(\bar{\lambda}-\lambda)^2$	$\omega(\bar{\lambda}-\lambda)^2$
1	0.75	0.4	6.25	4.68	0.432	0.186	1.16
2	-0.36	0.64	2.44	-0.88	0.678	0.46	1.12
3	-0.01	0.85	1.39	-0.01	0.328	0.10	0.14
4	-2.0	1.5	0.44	-0.88	2.318	5.4	2.38
5	-2.8	1.8	0.31	-0.87	3.118	9.7	3.00
6	-0.1	2.0	0.25	-0.02	0.418	0.17	0.04
7	4.5	2.3	0.19	0.85	4.182	17.5	3.32
8	8.0	4.0	0.06	0.48	7.682	59.0	3.54
9	4.5	5.0	0.04	0.18	4.182	17.5	0.70
10	2.5	7.5	0.02	0.05	2.182	4.75	0.095
11	4.0	20	0.002	0.01	3.682	13.6	0.027
12	140	65	0.0002	0.03	139.6	19600	3.92
13	0	82.5	0.00017	0	0.3	0.09	0
14	169	108	0.00008	0.0135	169	28600	2.29
15	-125	117	0.00007	-0.00875	125	15600	1.10
16	-200	140	0.00005	-0.010	200	40000	2.00
17	700	300	0.000011	0.0077	700	490000	5.40
18	200	350	0.000008	0.0016	200	40000	0.30
19	50	466	0.000005	0.00025	50	2500	0.01
20	These	∞	0	0	-	-	0
21	points	∞	0	0	-	-	0
22	at origin within exptl. error	∞	0	0	-	-	0
	$n = 22$		$\sum w = 11.393$	$\sum w\lambda = 3.624$			$\sum w(\bar{\lambda}-\lambda)^2 = 30.542$

$$\bar{\lambda} = \frac{3.624}{11.393} = 0.318; \quad \sigma^2 = \frac{30.542}{22 \times 11.3986} = 0.1219, \quad \sigma_\lambda = 0.349$$

7. Corrections

This value of λ now requires to be corrected for the various systematic effects present and allowance made in the error for two sources of uncertainty. In order to find the effect of the corrections, the theoretical curve was adjusted and using a large-scale plot the change in λ for the point $\lambda=0, \beta=2$ was found. For this point $I(0^\circ)= 0.828\ 17$, $I(90^\circ)=1.14775$.

7a. The finite aperture of the counters

The half angle subtended by the counters at the crystal was 9° and using the relationships of section 7, chapter 2, $g_2= 0.98161$, $g_4= 0.93957$; thus the anisotropy expected theoretically is reduced, improving slightly the agreement with the experimental point.

Quantitatively $I(0^\circ) = 1-g_2(0.24251)+ g_4(0.07068)= 0.828438$

and $I(90^\circ) = 1+g_2(0.12125)+ g_4(0.02650)= 1.143924$

and the correction is equivalent to a change in λ of -0.0025.

7b. The effect of the 0.815 Mev and 1.62 Mev gamma rays

The presence of pulses due to the 0.815 Mev and 1.62 Mev gamma rays lying within the 0.805 Mev channel causes a correction which depends on the Fermi: Gamow-Teller admixture described by λ' in the weak low energy beta-transition leading to the second excited state of Fe^{58}.

(1) If $\lambda'=0$, the 1.62 Mev gamma ray contribution involves no correction since the spin sequence is identical with that for the 0.805 Mev transition. However, for the 0.815 Mev gamma ray (1.6%) which is a mixed transition ($\delta=2.2\pm 0.3$) $I(0^\circ)=0.81005$ $I(90^\circ)= 1.08034$, so

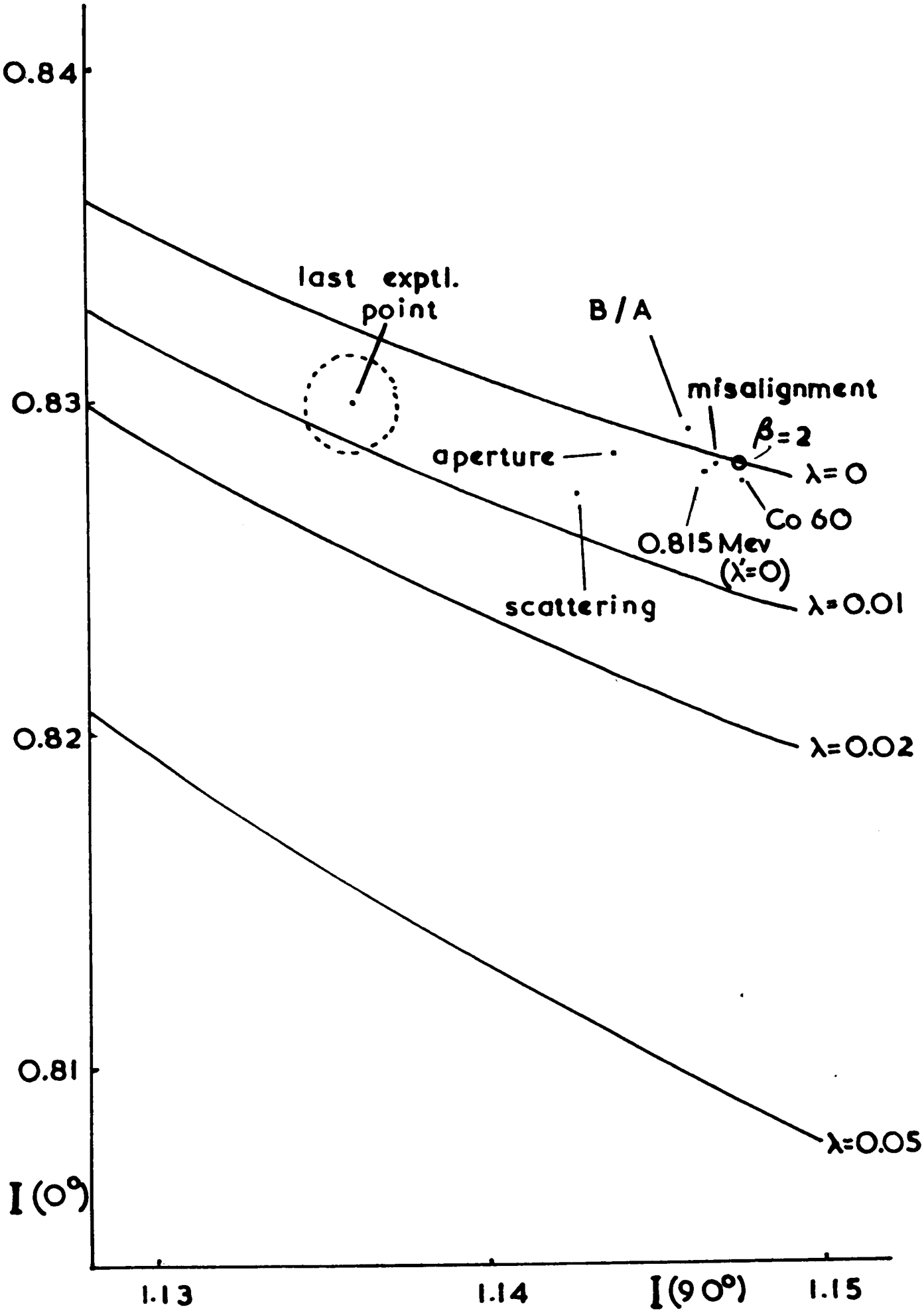

0.84
0.83
0.82
0.81
I (0°)
last expt.
point
B / A
misalignment
β=2
aperture
λ=0
Co 60
0.815 Mev
(λ'=0)
scattering
λ=0.01
λ=0.02
λ=0.05
1.13
1.14
I (90°)
1.15

Figure 6

giving 0.827885, 1.146688 for $\beta=2$, this reduces λ by 0.0019.

(ii) If λ' is not zero but about 0.45 as suggested by the measurements of Griffing and Wheatley, then the 0.815 Mev gamma ray gives $I(0^0)=0.75092$, $I(90^0)=1.12637$ and makes the final theoretical curve pass through $I(0^0)=0.826953$, $I(90^0)=1.1474133$, corresponding to a change in λ of -0.0035.

The number of pulses due to the 1.62 Mev gamma ray in the channel (Sec. 6.b) is estimated to be 0.17% from the pulse height spectrum and for these counts $I(0^0)=0.63953$, $I(90^0)=1.17250$ for $\beta=2$ and reduce the overall values to 0.8278493 and 1.1479205 and change λ by -0.0008.

The measurement of λ' is extremely difficult because of the very low intensity of the 1.62 Mev gamma ray and the presence of chance coincidences of two 0.805 Mev pulses having a large anisotropy, but a measurement of the gamma ray anisotropy (Grace & Sowter 1958) shows that it is closely the same as the anisotropy of the 0.805 Mev radiation. This result confirms the hypothesis the λ' is about zero and is incompatible with a value of λ' greater than 0.2. For the final result quoted here, λ' has been taken to be zero.

7e. <u>The Co^{60} contamination</u>

The presence of Co^{60} in the source is responsible for 0.2% of the counts in the 0.805 Mev channel. The plot of $I(0^0)$ v $I(90^0)$ for Co^{60} has the same form as that for Co^{58} with a pure Fermi interaction so the presence of Co^{60} tends to give an enlarged value of λ.

Now $\beta = \frac{A}{227}$, so when $\beta = 2.0$ for Co^{58}, for Co^{60} we have:

$$\beta = 2 \times \frac{\mu(60)}{I(60)} \times \frac{I(58)}{\mu(58)}$$

$$= 2 \times \frac{3.8}{5} \times \frac{2}{4.052}$$

$$= 0.75$$

For this value the Co^{60} point is $I(0^\circ) = 0.59611033$, $I(90^\circ) = 1.1646175$ and modifies the theoretical curve for the 0.805 Mev so that it passes through 0.8277058, 1.1477837, giving a value of λ 0.001 less than that previously deduced.

7d. Scattering

The total thickness of the glass and metal of the low temperature cryostat through which the gamma radiation had to pass was equivalent to a vertical cylinder of brass 0.35 cm. thick which caused some scattering of the radiation. The discrimination level of the counters, i.e. about 0.700 Mev, was such that it could not detect 0.805 Mev gamma radiation which had been single scattered through angles greater than 25° with the corresponding degradation of energy. It is difficult to calculate for these precise conditions but an approximate relationship has been obtained (Chapter 2) on the basis of a point source, spherical scatterer and a counter at an infinite distance.

This gives $\bar{g}_2 = 0.995\ g_2^\circ$, $\bar{g}_4 = 0.962\ g_4^\circ$

$= 0.976$ $= 0.904$

which makes: $I(0^\circ) = 0.8273$

$I(90^\circ) = 1.1427$

giving $\Delta\lambda = -0.0062$ for the combined scattering and

aperture corrections.

7e. Uncertainties

(i) The Spin Hamiltonian is believed to give an accurate description of the ionic energy levels because of the success with which it has been used in the past. The sign of A is taken to be positive (Abragam & Pryce 1951) and the values of A and B have been determined by Bleaney and Ingram (1951) for stable cobalt.

$A_{59} = 0.0184 \pm 0.0004$; $B_{59} = 0.0047 \pm 0.0001$ cm^{-1}

The value of B/A, necessary for the calculation of the theoretical curves, is a constant for all isotopes of cobalt and is 0.2554358 $\pm$ 0.0077699.

Using the upper limit B/A = 0.2632057, B_2 and B_4 have been calculated for $\beta = 2$ and this point is then I(0°) = 0.8292296, I(90°) = 1.1461910. Thus the uncertainty in λ is $\pm$ 0.0016.

(ii) The alignment of the crystal with respect to the counter positions was checked both before and after the experiments by several observers and its position was considered to be correct within 1°. However, allowing a possible misalignment of 2°, we have I(2°) = 0.828166 and I(92°) = 1.1469871. This leads to an error in λ of $\pm$0.0006, since whichever way the crystal was displaced the anisotropy would be reduced.

8. Conclusion

In this experiment a single uniaxial crystal has been used rather than several crystals of a biaxial Tutton salt, as had been used previously. In this way greater sensitivity to λ has been obtained

and some possible sources of error, i.e. temperature in homogeneity and the location of the axes, present in the experiments of Daniels et al (1952) and Griffing and Wheatley (1956) have been eliminated.

Combining all the corrections, the result is $\lambda = -0.006 \pm 0.005$ an allowance having been made in the error for the uncertainty of the corrections themselves. This value, which is in agreement with the results of the "parity" type of experiment (Ambler et al 1957), is consistent with the complete absence of Fermi admixture and makes it unlikely that it exceeds 0.005.

9. Discussion

The present result demonstrates that nuclear orientation can be used to make accurate measurements, particularly if the salt used has only one ion per unit cell. It shows ~~think~~ the measurement of Griffing and Wheatley to be incorrect and it seems certain that the discrepancy must arise through the difficulties with the Tutton salt. The difficulty in locating the axes and complicated analysis has already been discussed. It has been shown how B_2, B_4 are obtained from the equatorial counting rate. This, however, will require the calculation of a whole family of curves for the interdependence of $I(\theta)$, δ and λ and if interpolation between curves is used, serious discrepancies may arise, particularly since the values of B_γ were calculated for the cases $B = 0$ and for $A/B = 4$ (Griffing and Wheatley 1956 and Griffing 1956), although in fact $A/B = 3.92 \pm 0.12$. Systematic errors were not considered since it was felt that these would average themselves out

over several runs and misalignment of the crystal composing the specimen may have been underestimated.

The present result is consistent with the shell model configurations of Co^{58} and Fe^{58}. The former has one proton less than a closed shell $f_{7/2}$ and 3 neutrons outside the shell probably in a $p_{3/2}$ state. Fe^{58} has two vacancies in the proton, $f_{7/2}$ shell with 4 neutrons in $p_{3/2}$ or $f_{5/2}$ states.

Decay by positron emission requires an $f_{7/2}$ proton to decay to a $p_{3/2}$ neutron on an elementary picture, which means that $\Delta l = 2$ and the transition is l-forbidden in accord with the log ft. value of 6.5. Also a Fermi transition, which would require $p[f_{7/2}] \rightarrow n[f_{7/2}]$, cannot take place without a neutron being raised to a higher level and is therefore much less probable than the Gamow-Teller mode.

Similarly the isotopic spin of Co^{58} ground state is 2 while that for the first excited state of Fe^{58} must be equal to or greater than 3. Fermi transitions can only occur for $\Delta T = 0$ if T is a good quantum number and this would involve mixing of $T = 2$ and $T = 3$ states in Co^{58}. Such mixing is expected to be small in view of the coulomb energy difference between the nuclei of ~19 Mev.

This demonstration of the absence of Fermi transitions shows that the results of Ambler et al (1957) for the beta-ray asymmetry can be explained by the two component theory of the neutrino. The earlier measurements of the asymmetry for Co^{60} can be explained by this theory which requires that either C_T or C_A vanishes; this, in

turn, means that the Fiera terms for the Gamow-Teller mode are identically zero.

10. Corollary:- The derivation of a temperature scale

It has been already pointed out that the deduction of λ by the method described did not depend on a knowledge of absolute temperature. The theoretical dependence of the gamma-ray anisotropy:

$$\epsilon = \frac{I(90^\circ) - I(0^\circ)}{I(90^\circ)}$$

can therefore be calculated using the measured value of λ which for this purpose is taken to be zero (figure 7).

The experimental information gives ϵ as a function of time (t) for each value of H/Ti used where H is the magnetising field and Ti the initial temperature (i.e. temperature of the helium bath). If curves of ϵvt are extrapolated back to t = 0 (the first reading coming at t = 30 secs) then ϵ(t=0) is found for each value of H/Ti (figure 8). Combining the theoretical and experimental information, a curve can be constructed giving the final absolute temperature reached from a given H/Ti (Table 4) figure 9. The curves are plotted in terms of the magnetising current which for a given magnet is proportional to H/T.

For crystals of the same shape and composition H/Ti is a measure of the entropy removed independent of the size of the actual specimen provided the field is in the same direction relative to the crystal axis. This relationship, therefore, can be used as a temperature scale for all similar crystals avoiding some of the difficulties of deriving and using a $T - T^*$ correlation and has been employed to

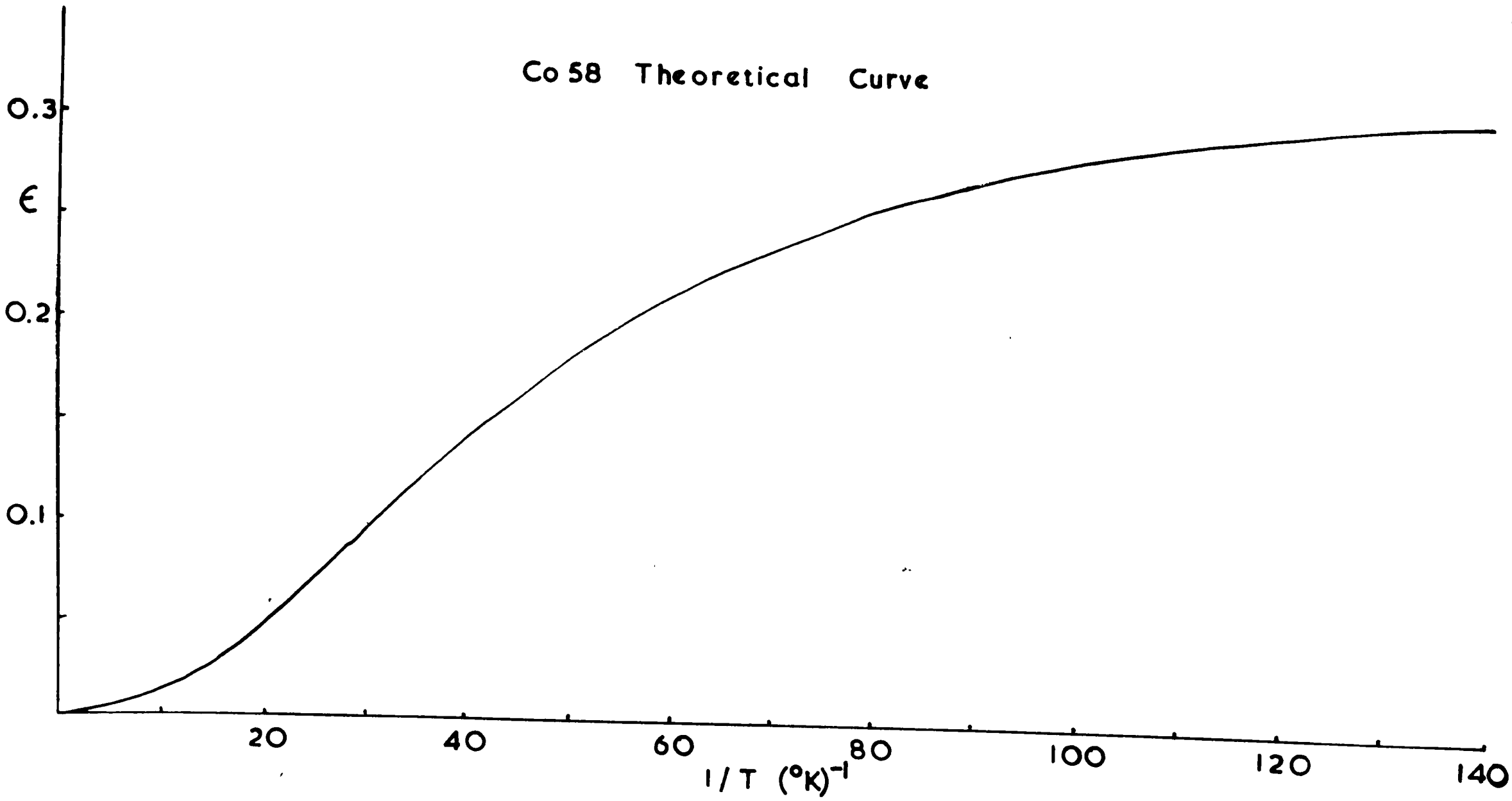
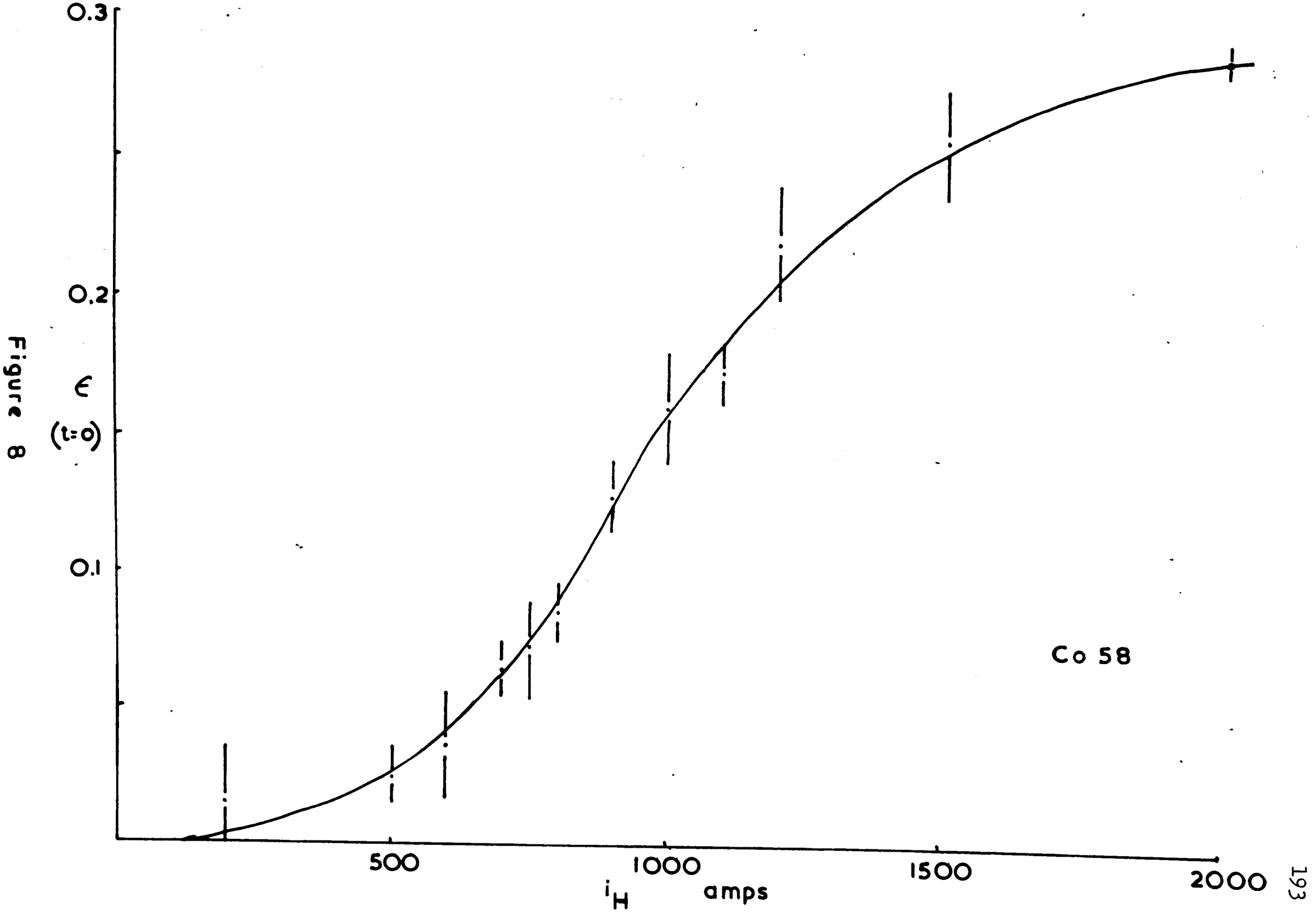


Figure 7



Figure

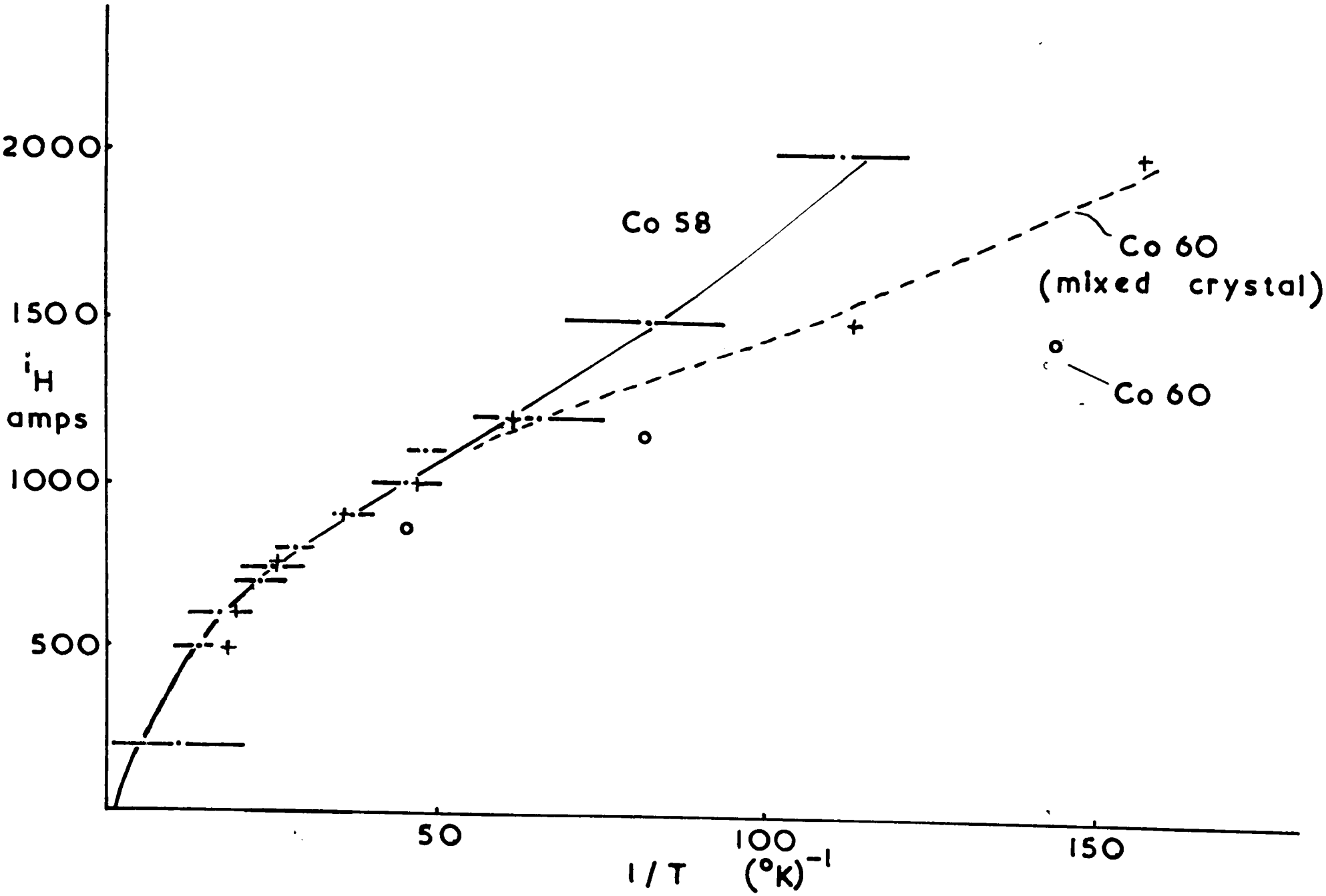
TABLE 4

Co^{58} in Ni-$ZnSiF_6 .6H_2O$

Extrapolated anisotropies
(blocked values)

H/Ti (Ti~1°K) amps	$\epsilon_{t=0}$	I/T $(°K)^{-1}$
2000	0.286 ± 0.007	110 ±10
1500	0.256 ± 0.020	81 ±12
1200	0.220 ± 0.020	65 ± 9
1100	0.178 ± 0.011	48 ± 3
1000	0.160 ± 0.020	45 ± 5
900	0.127 ± 0.014	37 ± 3
800	0.086 ± 0.011	27.5 ± 2.5
750	0.072 ± 0.020	25 ± 4
700	0.064 ± 0.011	23 ± 2.5
600	0.036 ± 0.020	18 ± 4
500	0.025 ± 0.011	14 ± 3
200	0.016 ± 0.020	11 + 6 -11

Figure 9


2000
1500
1000
500
i_H
amps
Co 58
Co 60
(mixed crystal)
Co 60
50
100
150
1/T (°K)$^{-1}$

interpret the results of the experiments on Mn^{56}, Mn^{54}, Mn^{52}.

The work described in this chapter has been published in The Philosophical Magazine (Phil. Mag 3, 489; 1958) under the title of: "Nuclear Alignment and the Beta-Transition in Cobalt-58'" by Dagley, I., Grace, M.A., Hill, J.S. and Sowter, A.V.

APPENDIX

The evaluation of the orientation parameters from the Spin Hamiltonian

1. The Problem

a. Introduction

The four principal methods of low temperature nuclear orientation have been discussed in terms of the Spin Hamiltonian which describes the energy levels of an ion in a paramagnetic crystal. The parameters D,A,B etc. of the Hamiltonian can be measured from paramagnetic resonance absorption spectra and in order to find the parameters, B , which describe the degree of alignment it is necessary to find the ionic energy levels and wave functions. The energy levels are the eigen values of the problem

$$\mathcal{H}|\psi\rangle = E|\psi\rangle$$

where $|\psi\rangle$ represents the wave function of a level and $\mathcal{H}$ is the operator represented by the Hamiltonian.

Some steps in the calculation are discussed in this appendix and results for Co^{58}, Co^{60} and Mn^{54} are given.

b. The eigen functions

In a strong field parallel to the z-axis, the axis of quantisation, the Spin states are characterised by the total magnetic quantum number, M_s. The eigen functions are written in the form $|M_s\rangle$ giving 2S+1 states $|S\rangle\ |S-1\rangle \cdots |-S\rangle$. If there are zero field splittings between levels then, with a weak magnetic field parallel to z, each state is in

general of the form

$$|\psi\rangle = a\,|S\rangle + b\,|S-1\rangle \cdots \text{ where } a^2+b^2 \cdots = 1$$

For the case where there is a hyperfine interaction ($I \neq 0$), each effective spin state $|M_s\rangle$ has $2I+1$ component states which are written in the form $|M_s, M_I\rangle$. In most cases the total magnetic quantum number is a constant of the motion so that only levels with the same $M_F = M_s + M_I$ mix, giving:

$$|\psi\rangle = a\,|M_s, M_I\rangle + b|M_s+1, M_I - 1\rangle \text{ etc.}$$

c. <u>The rules for using the spin operators</u>

The spin operators S, I can be considered in terms of three cartesian components S_x, S_y, S_z; I_x, I_y, I_z governed by the following rules:

(i) $S_z|M\rangle = M|M\rangle$; $I_z|m\rangle = m|m\rangle$

(ii) S_x and S_y, I_x and I_y are simplest to use in the form

$S_+ = S_x + iS_y$, $S_- = S_x - iS_y$

then $S_+\,|M\rangle = \left\{S(S+1) - M(M+1)\right\}^{\frac{1}{2}} |M+1\rangle$

and $S_-\,|M\rangle = \left\{S(S+1) - M(M-1)\right\}^{\frac{1}{2}} |M-1\rangle$

and similarly for I_+ and I_-.

(iii) The terms in S_i^4 occurring in the manganese Hamiltonian refer to the axes of the cubic crystal field, the alignment (trigonal) axis being the 111 direction relative to these. Operator equivalents for S^4 in terms of S_z, S_+ and S_- have been given by Stevens (1952) and Judd (1955). The crystal field represented by $\frac{a}{6}(S_1^4 + S_2^4 + S_3^4)$ is equivalent to one given

$$\text{by } -\frac{a}{180}\Big[35S_z^4 - 30S(S+1)S_z^2 + 25S_z^2 - 6S(S+1) + 3S^2(S+1)^2 - \frac{20\sqrt{2}}{4}\left\{S_z(S_+^3 + S_-^3) + (S_+^3 + S_-^3)S_z\right\}\Big]$$

d. The energy matrix:

The energy matrix is set up by operating on each state $|M,m\rangle$ and setting the elements in rows and columns so that those with the same value of M + m are adjacent. Levels with the same $M_p = M+m$ can have the same energy and, except for the case where $a \neq 0$ for Mn^{++}, the matrix consists of a number of submatrices arranged along the main diagonal and those elements other than the diagonal and one-off each way are zero.

In zero field a state $|+M, -m\rangle$ has the same energy as $|-M, m\rangle$ so although there are (2S+1)(2I+1) levels they are doubly degenerate in ± M so only half the number of rows and columns need be considered. Each submatrix may be taken separately and solved as a secular determinant, for instance:-

$$\begin{vmatrix} H_{11} & H_{12} \\ H_{21} & H_{22} \end{vmatrix} |\psi\rangle = E|\psi\rangle$$

or

$$\begin{vmatrix} H_{11}-E & H_{12} \\ H_{21} & H_{22}-E \end{vmatrix} |\psi\rangle = 0 \quad \text{and } H_{12} = H_{21}$$

so that:

$$E^2 - E(H_{11} + H_{22}) - H_{12}^2 = 0$$

The eigen vectors are then given by:

$$a_1 H_{11} + b_1 H_{12} = a_1 E_1$$

$$a_1 H_{21} + b_1 H_{22} = b_1 E_1$$

$$a_1^2 + b_1^2 = 1$$

e. <u>The orientation parameters</u>

Ions with a particular value of $m = I_z$ are distributed amongst the levels so that the relative numbers of ions with a particular m is dependent on temperature and is described by a series of Boltzmann terms, viz:

$$w(m) = a_1^2 \exp\left\{\frac{-E_1}{kT}\right\} + b_2^2 \exp\left\{\frac{-E_2}{kT}\right\} \quad \text{etc.}$$

where the energies are measured from the lowest level. The orientation parameters $B_\nu(I,T)$, (a measure of $\langle M^\nu \rangle_{av}$) are then defined (Gray & Satchler 1955) in terms of Clebsch-Gordon coefficients, thus:

$$B_\nu(I,T) = \sum_M (2I+1)^{\frac{1}{2}} w(M)(-1)^{I-M}(IIM - M \mid I\ I\ \nu\ 0)$$

which can be rewritten as:

$$B_\nu(I,T) = \frac{\sum_M \sqrt{2\nu+1}\ C^{II\nu}_{MM0}\ w(M)}{\sum_M w(M)}$$

f. <u>Clebsch-Gordon coefficients</u>

The coefficients $C^{CAB}_{\gamma\alpha\beta} = (A\ B\ \alpha\beta \mid A\ B\ C\ \gamma)$ describe the addition of states of angular momentum A, B with z-components α, β to form a single state with angular momentum C, z-component γ (Condon and Shortley, 1935). For the present purpose, we are asking how we can form a state I, M from a state I, M; ν, o so we require:-

$$C^{II\nu}_{M0} = \sqrt{\frac{2I+1}{2\nu+1}}\; C^{\nu II}_{0M-M}$$

$$= \sqrt{\frac{2I+1}{2\nu+1}}\; (I\ I\ M-M \mid I\ I\ \nu\ 0)$$

The coefficients needed for the present calculations have been obtained from the numerical tabulations of Simon (1954) for small values of I and from the calculations of Gauvin (1957) for some large values of I. However, neither of these sources give the values for I = 7 required for Mn^{52}. C^{II2}_{M0} can easily be found from the relationship:

$$C^{II2}_{M0} = \frac{3M^2 - I(I+1)}{I(I+1)(2I-1)(2I+3)}\ ;$$

this is a Legendre polynomial where Cos θ has been replaced by $\frac{M}{\sqrt{I(I+1)}}$ and normalised to give $\sum_M |C|^2 = \frac{2I+1}{2\nu+1}$

A similar transformation can be used for C^{II4}_{M0} but the commutating properties of the angular momentum vectors give some further terms (Stevens 1952) and the expression is the same as the operator equivalent of section C(iii) i.e.:

$$35M^4 - 30I(I+1)M^2 + 25M^2 - 6I(I+1) + 3I^2(I+1)^2$$

Normalisation is found from $\sum_M \left| C^{II\nu}_{M0} \right|^2 = \frac{2I+1}{2\nu+1}$ and the values for $C^{II\nu}_{000}$, $C^{II\nu}_{II0}$ and $C^{II\nu}_{I-I-10}$ can be checked against the special relationships:-

$$C^{II\nu}_{000} = \sqrt{2I+1}\ (-)^{\frac{2I+\nu}{2}}\ \frac{(I+\frac{\nu}{2})!\ \nu!}{(\frac{\nu}{2})!\ (\frac{\nu}{2})!\ (I-\frac{\nu}{2})!} \sqrt{\frac{(2I-\nu)!}{(2I+\nu+1)!}}$$

$$C^{II\nu}_{II0} = (2I)!\ \sqrt{\frac{2I+1}{(2I+\nu+1)!\,(2I-\nu)!}}$$

$$C^{IIv}_{I-1\,I-1\,0} = \left\{ \frac{2I - \nu(\nu+1)}{2I} \right\} C^{IIv}_{II0}$$

All the coefficients used in this work are given in Table 1.

2. The orientation parameters for Cobalt in $ZnSiF_6.6H_2O$

For Co^{++} $S_{eff} = \frac{1}{2}$ so that each submatrix is quadradiatic and the solution is straightforward. A general expression for the level populations has been obtained by Steenberg (1953):

$$W_M = W_{-M} = D \exp\{\gamma(1+q)\} + D' \exp\{\gamma(1-q')\} + E \exp\{\gamma(1-q)\} + E' \exp\{\gamma(1+q')\}$$

where $D(M) = \frac{q+2m-1}{4q}$, $D'(M) = D(M+1)$

$$E(M) = \frac{x^2(I+M)(I-M+1)}{q(q+2M-1)} , \quad E'(M) = E(M+1)$$

$$q(M) = \left[(2M-1)^2 + 4\, x^2(I+M)(I-M+1)\right]^{\frac{1}{2}} , \quad q'(M) = Q(M+1)$$

$$x = \frac{B}{A} \quad \text{and} \quad \gamma = \frac{A}{4kT} = \frac{\beta}{2}$$

but since $W(M) = W(-M)$, $W(M) = \frac{1}{2}\{W(M)+W(-M)\}$ and the relationship can be further reduced to:

$$W(M) = D(M) \exp\{\gamma(1+q)\} + E(M) \exp\{\gamma(1-q)\}$$

with $D(M) = 1 + \frac{2M-1}{q}$, $D(-M) = E(M+1)$; $E(-M) = D(M+1)$

$$q(M) = \left[(2M-1)^2 + 4\, x^2(I+M)(I-M+1)\right]^{\frac{1}{2}}$$

$$q(-M) = q(M+1)$$

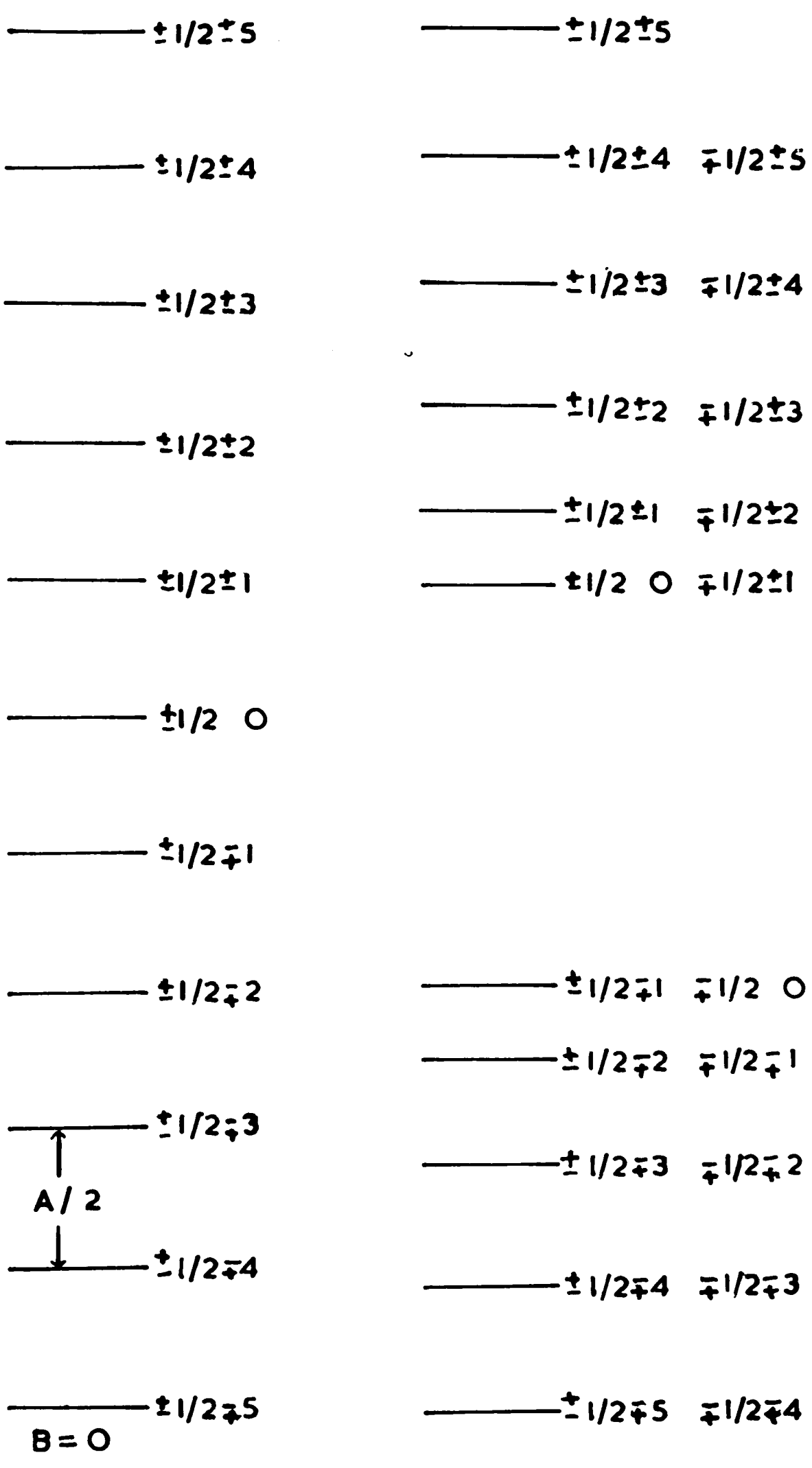
$$\gamma = \frac{A}{4kT} = \frac{\beta}{2} \quad \text{and} \quad x = \frac{B}{A} ; \quad A_{59} = 0.018 \pm 0.0004\ cm^{-1};$$

$$B_{59} = 0.0047 \pm 0.0002\ cm^{-1}$$

TABLE 1

Some Clebsch-Gordon coefficients

I	M	$5\,C^{II2}_{M0}$	$9\,C^{II4}_{M0}$
2	2	1.195	0.2673
	1	-0.5976	-1.069
	0	-1.195	1.064
3	3	1.443	0.640
	2	0	-1.495
	1	-0.866	0.213
	0	-1.155	1.280
5	5	1.698	1.177
	4	0.679	-1.177
	3	-0.113	-1.177
	2	-0.679	-0.196
	1	-1.019	0.785
	0	-1.132	1.177
6	6	1.773	1.368
	5	0.887	-0.912
	4	0.161	-1.356
	3	-0.403	-0.746
	2	-0.806	0.152
	1	-1.048	0.885
	0	-1.129	1.160
7	7	1.830	1.524
	6	1.045	-0.653
	5	0.382	-1.320
	4	-0.161	-1.071
	3	-0.534	-0.379
	2	-0.885	0.382
	1	-1.067	0.9435
	0	-1.128	1.152



Energy Levels for Co^{++} in $ZnSiF_6.6H_2O$
(S=1/2 , I=5)

Figure 1

The level energies are given by $E = \frac{A}{4}\left[-1 \pm q(M)\right]$ and are drawn for Co^{60} in figure 1.

Curves of B_2, B_4 as functions of $1/T$ for Co^{60} and Co^{58} are shown in figures 2, 3. A is taken to be positive (Abragam and Pryce, 1951) which means that the lowest level is not pure in M_I, So:

$$B_\nu(\infty) = \sqrt{2\nu+1}\left[D\, C^{II\nu}_{II0} + E^{II\nu}_{I-1I+0}\right]/(D+E)$$

$$= \sqrt{2\nu+1}\quad C^{II\nu}_{II0}\left[D + E\left(1 - \frac{\nu(\nu+1)}{2I}\right)\right]/(D+E)$$

$$1 - \frac{\nu(\nu+1)}{4I}\left\{1 - \frac{1}{\left[1 + \frac{81x^2}{(2I-1)^2}\right]^{\frac{1}{2}}}\right\}$$

3. Manganese in $ZnSiF_6.6H_2O$

This problem is more difficult because the submatrices (Table 2) cannot in general be factorised. However, the energy levels have been found for the case: $I = 3, \mu = 3.5$, $A = -0.00766 \pm 0.00084\ cm^{-1}$, $D = -0.0134 \pm 0.0003\ cm^{-1}$ $a = 0$

and are drawn out in figure 4. The eigen factors have been calculated for the lowest 6 levels only by the method described in section 1d. The solution of the higher order polynomials was found by successive approximations based on the positions of the pure states. Population parameters obtained using only these levels have been calculated for $\frac{1}{T} = 100 \rightarrow \frac{1}{T} = 20$. The accuracy decreases with $\frac{1}{T}$ but in this case at $\frac{1}{T} = 20 \sim 82\%$ of the ions are in these lowest 6 levels so that the approximation should be quite good. For small values of $\frac{1}{T}$ $B_4 = 0$ while an expression for B_2, found by using the methods of Simon,

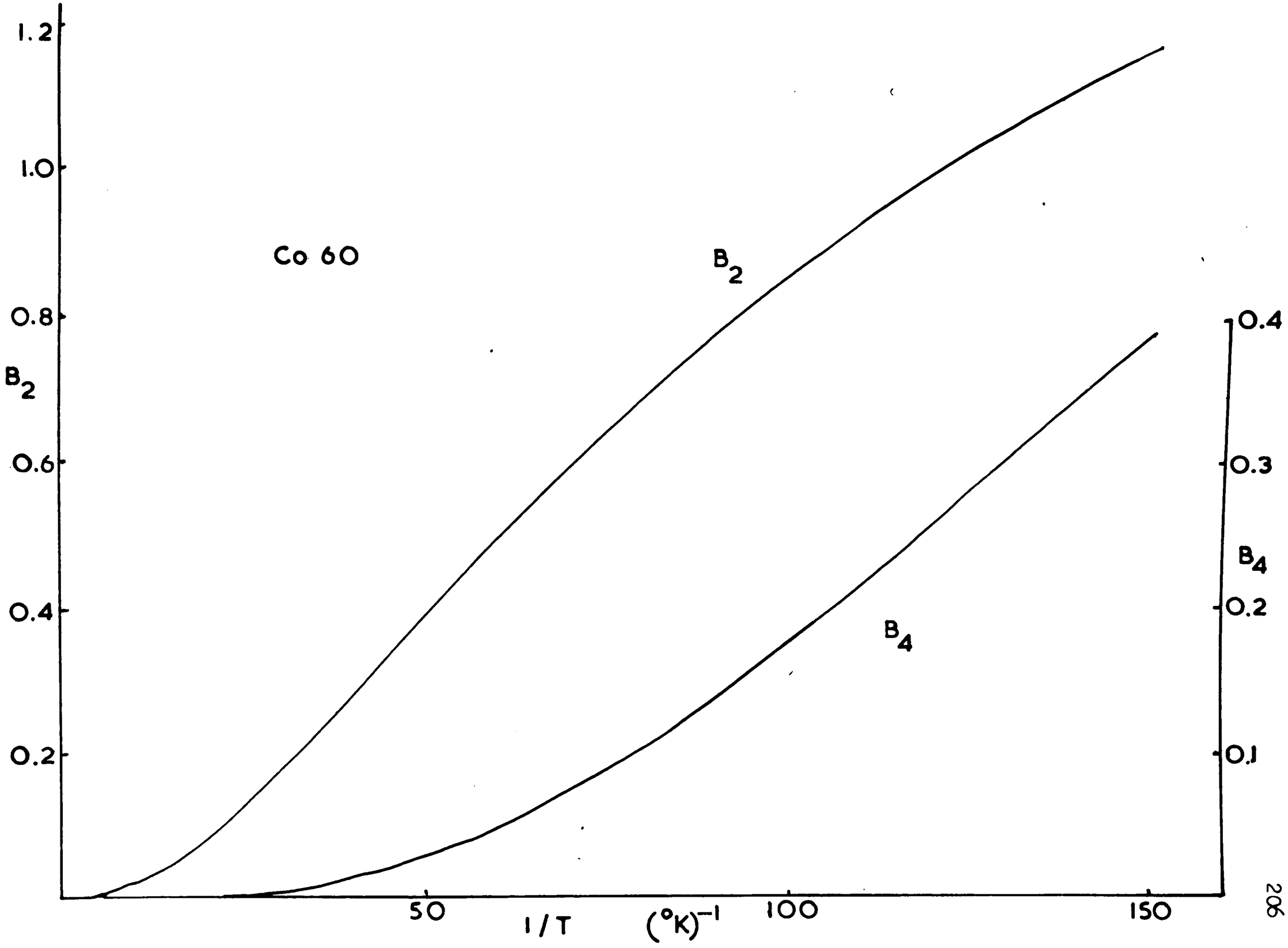
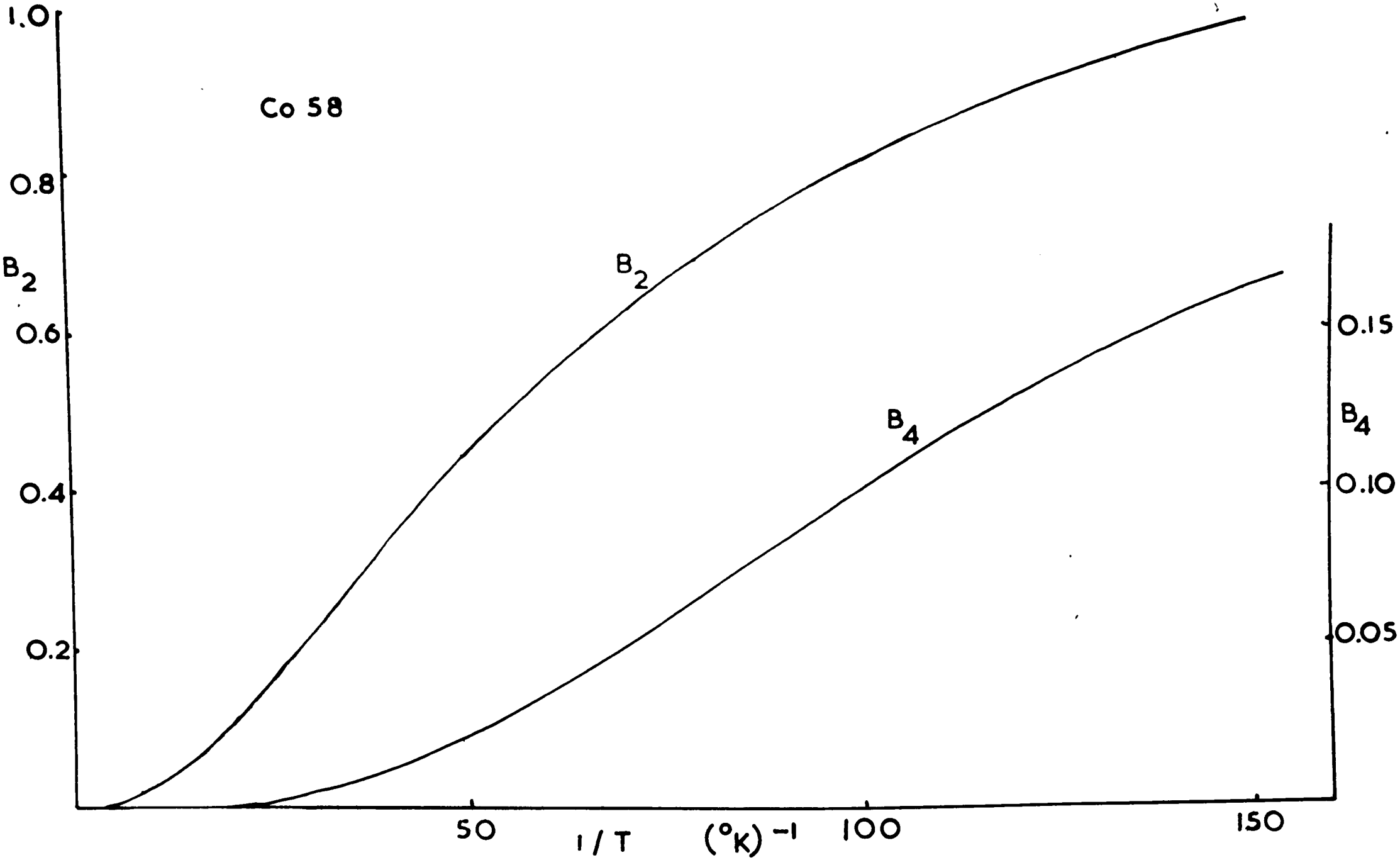


Figure 2

Figure 3



Rose and Jauch (1951) has been given by Blin Stoyle and Grace (1957).

$$B_2 = \frac{2}{9}\beta^2 S(S+1)\sqrt{\frac{11}{5}(I+1)(2I-1)(2I+3)}\left[1-x^2-\frac{(2+x^2)(2S-1)(2S+3)D}{30kT}\right]$$

where $\beta = A/2kT$ and $D/kT \ll 1$ $\qquad X = B/A$

If $X=1$, $B_2 = \frac{-2}{225}S(S+1)(2S-1)(2S+3)\frac{\beta^3 D}{A}\sqrt{5I(I+1)(2I-1)(2I+3)}$

a further term has been obtained by Grace (1956) so that :

$$B_2 = \frac{-2}{225}S(S+1)(2S-1)(2S+3)\frac{\beta^3 D}{A}\sqrt{5I(I+1)(2I-1)(2I+3)}\left\{1-\frac{(2S+5)(2S-3)D}{42kT}\right\}$$

This can be used for values of $\frac{1}{T}$ up to $\sim 1\frac{1}{4}$ and a smooth interpolation can be made to give the complete curve.

For other values of spin and moment, the energy levels and eigen vectors can be found using expressions given by Satchler (1958) where the level mixing produced by the B term has been treated as a perturbation:

$$\mathcal{H} = DS_z^2 + AS_zI_z + B/2\ (S_+I_- + S_-I_+).$$

Then to second order, the energy levels are given by:

$$E(M_S M_I) = DM_S^2 + AM_SM_I + \frac{B^2}{4}\left\{\frac{(S-M_S)(S+M_S+1)(I+M_I)(I-M_I+1)}{A[M_S-M_I+1]-D[1+2M_S]} + \frac{(S+M_S)(S-M_S+1)(I-M_I)(I+M_I+1)}{A[M_I-M_S+1]-D[1-2M_S]}\right\}$$

and for $M_S = S$, this reduces to:

$$E(SM_I) = DS^2 + ASM_I + \frac{\frac{1}{2}B\ S(I-M)(I+M_I+1)}{A[M_I+1-S]+D[2S-1]}$$

with $|M_SM_I\rangle = a|SM_I\rangle + b|S-1;\ M_I+1\rangle + c|S-2;\ M_I+2\rangle$ etc.

where $b = \frac{-\frac{1}{2}B\sqrt{2S(I-M)(I+M+1)}}{A[S-1-M_I]-D[2S-1]}$ and $c = \frac{\frac{1}{2}B\ S(2S-1)(I-M_I-1)(I+M_I+1)(I+M_I+2)}{[A(S-2-M_I)-2D(S-1)][A(S-1-M_I)-D(2S-1)]}$

and $a^2+b^2+c^2 = 1$.

$\lvert \pm 5/2 \pm 3 \rangle$
$\frac{25D}{4} + \frac{15A}{2}$

$\lvert \pm 5/2 \pm 2 \rangle$	$\lvert \pm 3/2 \pm 3 \rangle$
$\frac{25D}{4} + 5A$	$\sqrt{30}\ \frac{A}{2}$
$\sqrt{30}\ \frac{A}{2}$	$\frac{9D}{4} + \frac{9A}{2}$

$\lvert \pm 5/2 \pm 1 \rangle$	$\lvert \pm 3/2 \pm 2 \rangle$	$\lvert \pm \frac{1}{2} \pm 3 \rangle$
$\frac{25D}{4} + \frac{5A}{2}$	$5\sqrt{2}\ \frac{A}{2}$	0
$5\sqrt{2}\ \frac{A}{2}$	$\frac{9D}{4} + 3A$	$4\sqrt{3}\ \frac{A}{2}$
0	$4\sqrt{3}\ \frac{A}{2}$	$\frac{D}{4} + \frac{3A}{2}$

$\lvert \pm 5/2 \quad 0 \rangle$	$\lvert \pm 3/2 \pm 1 \rangle$	$\lvert \pm \frac{1}{2} \pm 2 \rangle$	$\lvert \mp \frac{1}{2} \pm 3 \rangle$
$\frac{25D}{4}$	$2\sqrt{15}\ \frac{A}{2}$	0	0
$2\sqrt{15}\ \frac{A}{2}$	$\frac{9D}{4} + \frac{3A}{2}$	$4\sqrt{5}\ \frac{A}{2}$	0
0	$4\sqrt{5}\ \frac{A}{2}$	$\frac{D}{4} + A$	$3\sqrt{6}\ \frac{A}{2}$
0	0	$3\sqrt{6}\ \frac{A}{2}$	$\frac{D}{4} - \frac{3A}{2}$

$\lvert \pm 5/2 \mp 1 \rangle$	$\lvert \pm 3/2 \quad 0 \rangle$	$\lvert \pm \frac{1}{2} \pm 1 \rangle$	$\lvert \mp \frac{1}{2} \pm 2 \rangle$	$\lvert \mp 3/2 \pm 3 \rangle$
$\frac{25D}{4} - \frac{5A}{2}$	$5\sqrt{2}\ \frac{A}{2}$	0	0	0
$5\sqrt{2}\ \frac{A}{2}$	$\frac{9D}{4}$	$4\sqrt{6}\ \frac{A}{2}$	0	0
0	$4\sqrt{6}\ \frac{A}{2}$	$\frac{D}{4} + \frac{A}{2}$	$3\sqrt{10}\ \frac{A}{2}$	0
0	0	$3\sqrt{10}\ \frac{A}{2}$	$\frac{D}{4} - A$	$4\sqrt{3}\ \frac{A}{2}$
0	0	0	$4\sqrt{3}\ \frac{A}{2}$	$\frac{9D}{4} - \frac{9A}{2}$

Sub-matrices of Hamiltonian Operator

for Mn^{++} $S = 5/2$ $I = 3$

TABLE 2

$\lvert \pm 5/2 \mp 2 \rangle$	$\lvert \pm 3/2 \mp 1 \rangle$	$\lvert \pm \frac{1}{2}\ 0 \rangle$	$\lvert \mp \frac{1}{2} \pm 1 \rangle$	$\lvert \mp 3/2 \pm 2 \rangle$	$\lvert \mp 5/2 \pm 3 \rangle$
$\frac{25D}{4} - 5A$	$5\sqrt{2}\ \frac{A}{2}$	0	0	0	0
$5\sqrt{2}\ \frac{A}{2}$	$\frac{9D}{4} - \frac{3A}{2}$	$4\sqrt{6}\ \frac{A}{2}$	0	0	0
0	$4\sqrt{6}\ \frac{A}{2}$	$\frac{D}{4}$	$6\sqrt{3}\ \frac{A}{2}$	0	0
0	0	$6\sqrt{3}\ \frac{A}{2}$	$\frac{D}{4} - \frac{A}{2}$	$4\sqrt{5}\ \frac{A}{2}$	0
0	0	0	$4\sqrt{5}\ \frac{A}{2}$	$\frac{9D}{4} - 3A$	$\sqrt{30}\ \frac{A}{2}$
0	0	0	0	$\sqrt{30}\ \frac{A}{2}$	$\frac{25D}{4} - \frac{15A}{2}$

Sub-matrices of Hamiltonian Operator

for Mn^{++} $S = 5/2$ $I = 3$ (continued)

Energy Levels for Mn^{++} in $ZnSiF_6.6H_2O$
(S=5/2, I=3)

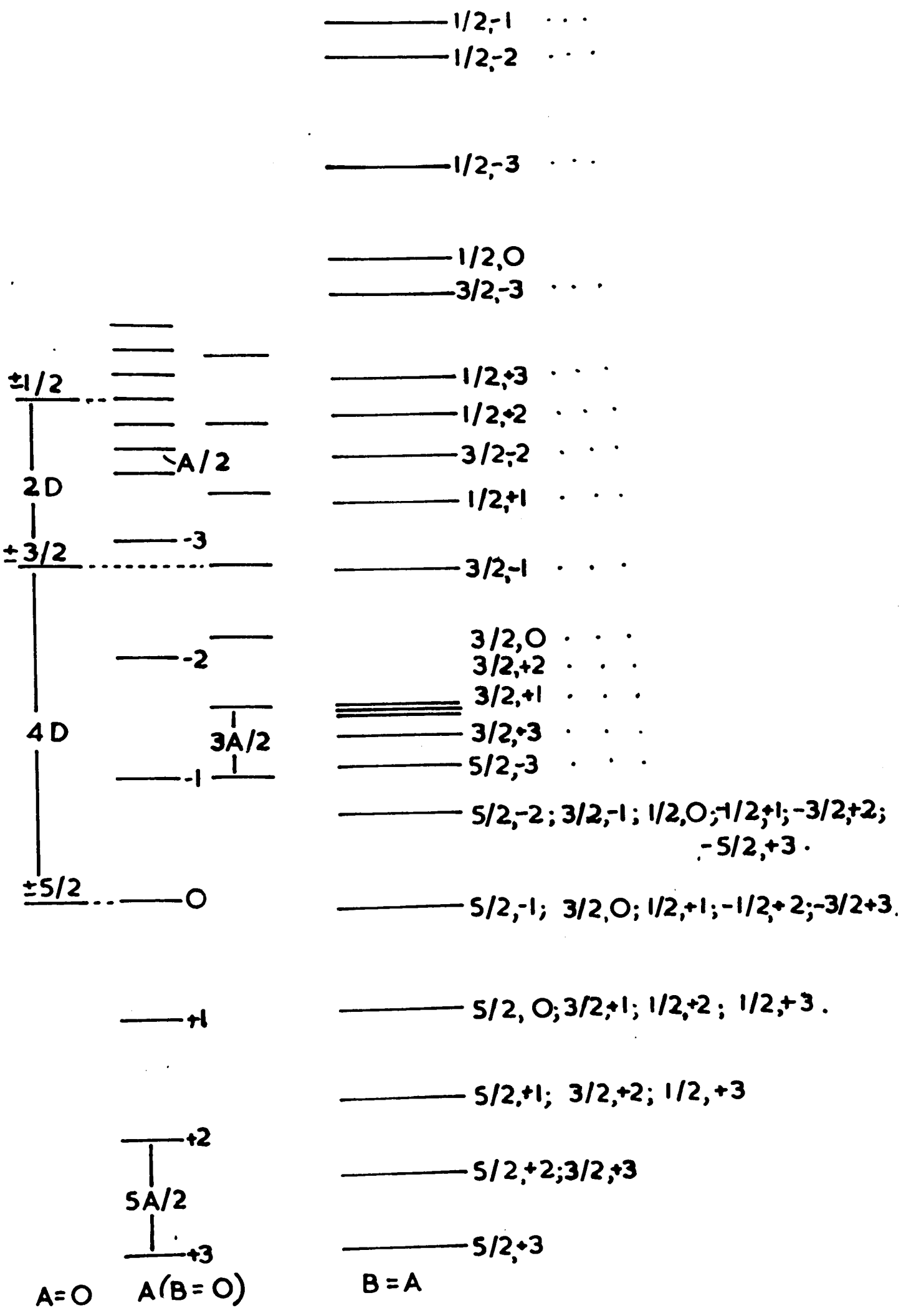


Figure 4

The dependence of B_2 and B_4 on temperature for $I=3, \mu=3.5$ is given in figure 5. For the other values of spin and moment, where the low temperature approximation has been used, the values of $\frac{1}{2}B_4$ are given in Table 3.

The term $\frac{a}{6}(S_1^4+S_2^4-S_3^4)$ of the Spin Hamiltonian slightly alters the relative position of the three manifolds. The separation between $S=\pm\frac{5}{2}$ and $S=\pm\frac{1}{2}$ is still 6D but the $\pm\frac{5}{2};\pm\frac{3}{2}$ separation changes from 4D to $4D+\frac{2a}{3}$ and the $\pm\frac{3}{2};\pm\frac{1}{2}$ separation becomes $2D-\frac{2a}{3}$.

Since $D=-0.0134\pm0.0003$ cm^{-1} and $a=+0.0009\pm0.0002$, this difference of 1.1% for the lower separation and 2.2% for the upper will give a negligible change in the calculated values of B_ν.

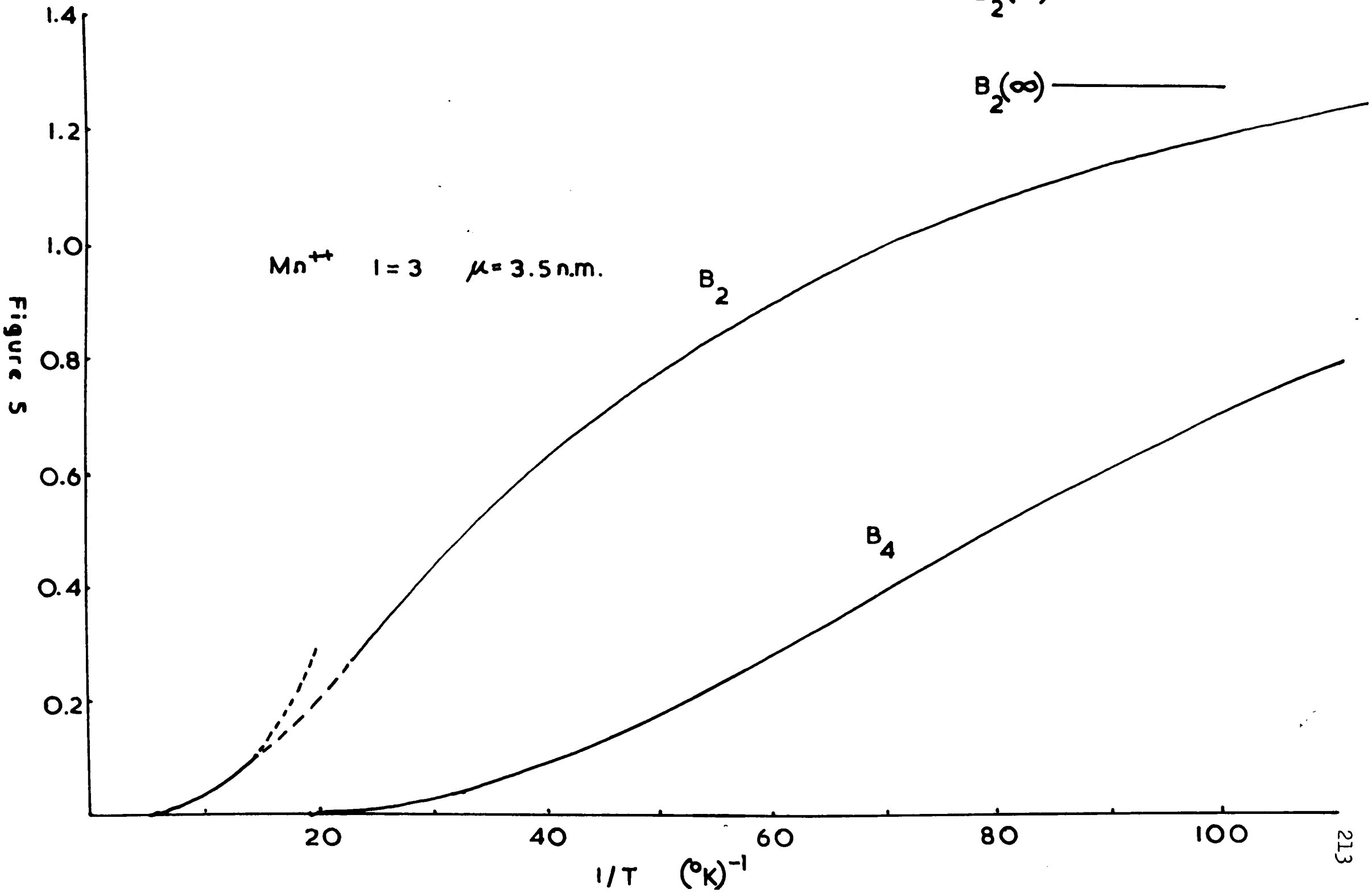

$B_2(\infty)$
$B_2(\infty)$
Mn^{++} I = 3 μ = 3.5 n.m.
B_2
B_4
1.4
1.2
1.0
0.8
0.6
0.4
0.2
20
40
60
80
100
1/T (°K)$^{-1}$

Figure 5

TABLE 3

Mn^{++} in $ZnSiF_6 \cdot 6H_2O$

Orientation parameters

														$D = -0.010\ cm^{-1}$
	I	7	7	6	6	6	3	3	3	3	2	2	2	3
	μ	3.598	2.0	3.5	3.08	2.5	4.0	3.5	3.0	2.5	2.8	2.4	2.0	3.5
	$\frac{1}{T}$													
B	100	1.38	1.066	1.33	1.259	1.215	1.213	1.201	1.158	1.097	1.007	0.970	0.905	1.090
	90	1.34	1.007	1.28	1.200	1.169	1.167	1.149	1.108	1.044	0.965	0.920	0.840	-
	80	1.29	0.944	1.23	1.134	1.118	1.111	1.088	1.049	0.984	-	0.860	0.78	0.968
B	100	0.534	0.209	0.475	0.402	0.316	0.348	0.351	0.297	0.239	0.143	-	0.108	0.222
	90	0.458	0.152	0.399	0.340	0.247	0.300	0.304	0.248	0.192	0.119	-	-	-
	80	0.375	0.094	0.318	0.262	0.176	0.246	0.253	0.194	0.141	-	-	-	0.114

REFERENCES

Abraham, A. and Pryce, M.H.L., 1951a Proc. Roy. Soc. A 205, 135

Abragam, A. and Pryce, M.H.L., 1951b. Proc. Roy. Soc. A 206, 173

Abraham, M., Jeffries, C.D., Kedzie, R.W. and Liefson, O.S., 1957
Bull. Am. Phys. Soc. 2, 382

Alaga, G., Alder, K., Bohr, A. and Mottleson, B.R. 1955,
Dan. mat. fys. Med. 29, Nr.9

Amaldi, E., D'Agostino, O., Fermi, E., Pontecorvo, B., Rasetti, F., and
Segre, E., 1935, Proc. Roy. Soc. A, 149, 522

Ambler, E., Grace, M.A., Halban, H., Kurti, N., Durand, H., Johnson, C.E.,
and Lemmer, H.R., 1953, Phil. Mag. 44, 216

Ambler, E. and Hudson, R.P., 1955, Rep. Prog. Phys. 18, 251

Ambler, E., Hayward, R.W., Hoppes, D.D., Hudson, R.P. and Wu, C.S.,
1957a. Phys. Rev. 106, 1361

Ambler, E., Hayward, R.W., Hoppes, D.D. and Hudson, R.P., 1957b,
Phys. Rev. 108, 503

Ambler, E., Hayward, R.W., Hoppes, D.D., and Hudson,R.R., 1958
Phys. Rev. 110, 787

Arbman, E. and Svartholm, N., 1956, Arkiv. Fysik., 10, 1

Backofen, E.W. and Herber, R.H., 1955, Phys. Rev. 97, 743

Bernstein, S., Roberts, L.D., Stanford, C.P., Dabbs, J.W.T., and
Stephenson, T.E., 1954, Phys. Rev. 94, 1243

Ball, P.R., 1955, Beta- and Gamma-ray Spectroscopy, North Holland Publishing Company, Amsterdam, p. 132

Bensie, R.J., and Cooke, A.H., 1950 Proc. Phys. Soc.A, 63, 213

Biedenharn, L.C., Blatt, J.M., and Rose, M.E., 1952, Rev. Mod. Phys. 24, 294

Biedenharn, L.C. and Rose, M.E., 1953, Rev. Mod. Phys. 25, 729

Bishop, G.R., Wilson, R., and Halban, H., 1950, Phys. Rev. 77, 416

Bishop, G.R., Daniels, J.M., Durand, H., Johnson, C.E., and Perez y Jorba, J., 1954, Phil. Mag. 45, 1197

Blatt, J. and Weiskopf, V. 1952, "Theoretical Nuclear Physics," John Wiley and Sons, Inc., New York

Bleaney, B., 1951 Proc. Phys. Soc. 64, 315

Bleaney, B. and Ingram, D.J.E., 1951a, Proc. Roy. Soc. A. 205, 336

Bleaney, B., and Ingram, D.J.E., 1951b. Proc. Roy. Soc. A, 208, 143

Blin-Stoyle, R.J. and Grace, M.A., 1957, Handbuch der Physik, 42, 555

Boehm, F. and Wapstra, A.H., 1957, Phys. Rev. 107, 1462.

Boehm, F., 1958, Phys. Rev. 109, 1018

Bohr, A. and Mottleson, B.R., 1955, Beta- and Gamma-ray Spectroscopy, North Holland Publishing Company, Amsterdam, p.414

Bowers, K.D. and Owen, J., 1955, Rep. Prog. Phys. 28, 304

Childs, W.J., Goodman, L.S., and Kieffer, L.J., 1956, Phys. Rev. Letters, 1, 296

Coleman, C.F., 1958, Nuclear Physics Conference, Cambridge, April 1958, Verbal report - unpublished.

Condon, E.U. and Shortley, G.H., 1935, Theory of Atomic Spectra, Cambridge

Cook, C.S., 1958, Nuclear Physics, 7, 481; Nuclear Data Sheets, N.R.C. 1958.

Cook, C.S. and Tomnovec, F.M., 1957, Bull. Am. Phys. Soc., 2, 24

Cooke, A.H., Duffus, H.J., and Wolf, W.P., 1953, Phil. Mag, 44, 623

Dabbs, J.W.T., Roberts, L.D. and Bernstein, S., 1955, Phys. Rev. 98, 1512

Dabbs, J.W.T., Roberts, L.D. and Parker, G.W. 1956, Bull. Am. Phys. Soc. 1, 207

Dagley, P., Grace, M.A., Hill, J.S., and Sowter, C.V., 1958, Phil. Mag. 3, 489

Dagley, P., Grace, M.A., Gregory, J.M. and Hill, J.S., 1959, Proc. Roy. Soc. - to be published.

Daniels, J.M., Grace, M.A., Halban, K., Kurti, N., and Robinson, F.N.H. 1952, Phil. Mag. 43, 1297

Daniels, J.M., and Robinson, F.N.H., 1953, Phil. Mag. 44, 630

Deutsch, M., and Elliott, L.G., 1944, Phys. Rev. 65, 211

Diddens, A.N., Huiskamp, W.J., Severiens, J.C., Miedema, A.R. and Steenland, M.J., 1958, Nuclear Physics, 5, 58

Dobrov, W. and Jeffries, C.D., 1957, Phys. Rev. 108, 60

Dobrowolski, W., Jones, R.V., and Jeffries, C.D., 1956, Phys. Rev. 101, 1001

Elliott, L.G., and Deutsch, M., 1943, Phys. Rev. 63, 321; 64, 321

Ferentz, M. and Rosenweig, N., Table of F Coefficients ANL - 5324

Frauenfelder, H., Levine, M., Rossi, A. and Singer, S., 1956, Phys. Rev. 103, 352

Gager, W.B., Jastram, P.S., and Daunt, J.G., 1958, Phys. Rev. Letters, 1, 83

Gauvin, J.N.L., 1957. D. Phil. Thesis, Oxford University.

Gorter, C.J., 1948, Physica, 14, 504

Good, W.M., Pearlee, D. and Deutsch, M., 1946, Phys. Rev. 69, 313, 673

Grace, M.A., Johnson, C.E., Kurti, N., Lemmer, H.R. and Robinson, F.N.H. 1952, Phil. Mag. 45, 1192

Grace, M.A., Johnson, C.E., Kurti, N., Scurlock, R.G. and Taylor, R.T., 1955, Comm. conf. Basses Temperatures, Paris

Grace, M.A., 1956, Private communication

Grace, M.A. and Souter, C.V., 1958, Private communication

Gray, T.P. and Satchler, G.R., 1955, Proc. Phys. Soc., A, 68, 349

Griffing, D.F., 1956, D. Phil. Thesis, University of Illinois, U.S.A.

Griffing, D.F. and Wheatley, J.C., 1956, Phys. Rev. 104, 389

Haussmann, H.J., Allen, A.J., Arthur, J.S., Bender, R.S., and McDole, C.J. 1952, Phys. Rev. 88, 1296

Hemmendinger, A., 1940, Phys. Rev. 58, 929

Hill, J.S., Mayer, H. and Milner, J., 1959, To be published

Hughes, D.J., 1953, Pile Neutron Research, Addison-Wesley Publishing Company Inc., Cambridge, Mass. U.S.A.

Huiskamp, W.J., Steenland, M.J., Miedema, A.R., Tolhoek, H.A. and Gorter, C.J., 1956, Physica 22, 587

Huiskamp, W.J., Diddens, A.N., Severiens, J.C., Miedema, A.R., and Steenland, M.J., 1957, Physica 23, 605

Jensen, J.H.D., 1955, Beta- and Gamma-ray Spectroscopy, North Holland Publishing Company, Amsterdam, p. 414

Jeffries, C.D., 1958, Private communication

Johnson, C.E., 1955, D. Phil. Thesis, Oxford University

Judd, B.R., 1955, Proc. Roy. Soc., A, 227, 552

Kedzie, R.W., and Jeffries, C.D., 1958, Bull. Am. Phys. Soc. 3, 415

Keister, O.L., 1954, Phys. Rev., 96, 855A

Kinchin, G.H., and Pease, R.S., 1955 Rep. Prog. Phys., 18, 1

Konijn, J., Van Nooijen, B. and Hagedoorn, H.L., 1958a, Physica 24, 377

Konijn, J., Hagedoorn, H.L., Van Krugten, H., and Stobben, J., 1958b. Physica 24, 931

Lee, T.D. and Yang, C.N., 1956 Phys. Rev. 104, 254

Lee, T.D. and Yang, C.N., 1957 Elementary Particles and Weak Interactions, B.N.L. 443

Livingood, J.J. and Seaborg, G.T., 1938, Phys. Rev. 54, 391

Livingood, J.J. and Seaborg, G.T., 1941, Phys. Rev. 60, 913

Mazari, M., Sperduto, A. and Buechner, W.W., 1957a Phys. Rev. 107, 365

Mazari, M., Buechner, W.W. and Sperduto, A., 1957b, Phys. Rev. 107, 1383

Metzger, F.R. and Todd, W.B., 1953, Phys. Rev. 92, 904

Meyer, J.W., 1957 Low Temperature Physics and Chemistry, University of Wisconsin Press, Madison, 1958,- p. 531

Milner, J. 1957 D. Phil. Thesis, Oxford University.

Morita, M. and Morita, R.S. 1957 Phys. Rev. 107, 1317

Moszkowski, S., 1955 Beta- and Gamma-ray Spectroscopy, North Holland Publishing Company, Amsterdam, p. 373

Nordheim, L.W., 1951 Rev. Mod. Phys. 23, 322

Osborne, L., and Deutsch, M., 1947 Phys. Rev. 72, 467 A.

Peacock, W.C. and Deutsch, M., 1946 Phys. Rev. 69, 306

Penrose, R.P. and Stevens, K.W.H., 1949 Proc. Phys. Soc. A, 63, 36

Postma, H., Huiskamp, W.J., Miedema, A.R., Steenland, M.J., Tolhoek, H.A. and Gorter, C.J., 1957, Physica 23, 259

Postma, H., Huiskamp, W.J., Miedema, A.R., Steenland, M.J., Tolhoek, H.A. and Gorter, C.J., 1958, Physica 24, 157

Pound, R.V., 1949 Phys. Rev. 76, 1410

Pryce, M.H.L., 1950 Phys. Rev. 80, 1107

Rich, M., and Madey, R., 1954 Range-Energy Tables, U.C.R.L. 2301

Rose, M.E., 1949 Phys. Rev. 75, 213

Rose, M.E., 1953 Phys. Rev. 91, 610

Rose, M.E., 1958 Internal Conversion Coefficients, North Holland Publishing Company, Amsterdam.

Russell, B., Sachs, R., Wattenberg, A. and Fields, R., 1948, Phys. Rev., 73, 545

Sakai, M., 1955 Phys. Soc., Japan, 10, 729

Satchler, G.R., 1953 Proc. Phys. Soc. A, 66, 1081

Satchler, G.R., 1954 Phys. Rev. 94, 1304

Satchler, G.R., 1958 Private communication

Scharff-Goldhaber, G. and Weneser, J., 1955, Phys. Rev. 98, 212

Scurlock, R.G. 1957, D. Phil. Thesis, Oxford University

Scurlock, R.G., 1958, Private communication

Sehr, R., 1954, Z. Phys., 137, 523

Simon, A., 1954 Numerical tables of Clebsch-Gordon coefficients, O.R.N.L. 1718

Simon, A., Vander Sluis, J.H., and Biedenharn, L.C., 1954 Numerical tables of Racah coefficients, O.R.N.L. 1679

Simon, A., Rose, M.E., and Jauch, J.M., 1951 Phys. Rev., 84, 1155

Skyrme, T.H.R., 1950 Progress in Nuclear Physics I, p. 115

Slack, L., 1955, see Nuclear Level Schemes A 40 A 92 USAEC, TID 5300

Sliätis, H., and Seigbahn, K., 1952 Arkiv. Fysik., 4, 485

Spiers, J.A., 1948 Nature, London, 161, 807

Spiers, J.A., 1949 Directional Effects in Radioactivity, N.R.C.C. publication

Steenberg, N.R., 1951 Phys. Rev., 84, 1051

Steenberg, N.R., 1952 Proc. Phys. Soc. A, 65, 791

Steenberg, N.R., 1953a Proc. Phys. Soc. A, 66, 399

Steenberg, N.R., 1953b Proc. Phys. Soc. A, 66, 391

Steenberg, N.R., 1953c D. Phil. Thesis, Oxford University

Stevens, K.W.H., 1952, Proc. Phys. Soc. A, 65, 209

Strauch, K., 1950 Phys. Rev. 79, 487

Taylor, R.T., 1957 D. Phil. Thesis, Oxford University

Temmer, G.M. and Heydenberg, N.P., 1956 Phys. Rev. 104, 967

Trenam, R.S., 1953 Proc. Phys. Soc. A, 66, 118

Wheatley, J.C., Huiskamp, W.J., Diddens, A.N., Steenland, M.J., and Tolhoek, H.A., 1955, Physica 21, 841

Wilets, L. and Jean, M., 1956, Phys. Rev. 102, 788

Wood, C.T., and Jastram, P.S., 1955 Phys. Rev. 98, 1187

Wu, C.S., Ambler, E., Hayward, R.W., Hoppes, D.D. and Hudson, R.P., 1957 Phys. Rev. 105, 1413

Wycoff, R.W., 1951 Crystal Structures, Interscience Publishers Inc. New York, Vol. II, Chapter X.

Zweifel, P.F., 1957, Phys. Rev. 107, 329